



Pico-Inside



Pico-Inside

Report

Computing inside a
single molecule using
atomic scale technologies



Pico-Inside Report

Computing inside a single molecule
using atomic scale technologies

Coordinators

Correia, Antonio (Phantoms Foundation, Spain)
Joachim, Christian (CEMES-CNRS, France)

Design and layout

Chacón, Carmen (Phantoms Foundation, Spain)
Fernández, Maite (Phantoms Foundation, Spain)
Narros, Concepción (Phantoms Foundation, Spain)
Serrano, Soraya (Phantoms Foundation, Spain)

Authors

Alemanni, Micol (Frei Universität Berlin, Germany)
Amijs, Catelijne H. M. (Institute of Chemical Research of Catalonia, Spain)
Ample, Francisco (CEMES-CNRS, France)
Baratoff, Alexis (Universitaet Basel, Switzerland)
Barattin, Regis (CEMES-CNRS, France)
Bechstein, Ralf (Universität Osnabrück, Germany)
Bellec, Amandine (LPM-CNRS / Université Paris-Sud, France)
Benjalal, Youness (CEMES-CNRS, France / Univ. Hassan II-Mohammédia, Morocco)
Bennewitz, Ronald (McGill University, Canada)
Besenbacher, Flemming (University of Aarhus, Denmark)
Bettac, Andreas (Omicron Nanotechnology GmbH, Germany)
Bombis, Christian (Freie Universität Berlin, Germany)
Bouju, Xavier (CEMES-CNRS, France)
Budzioch, Janusz (Jagiellonian University, Poland)
Chiaravalloti, Franco (LPM-CNRS / Université Paris-Sud, France)
De Mendoza, Paula (Institute of Chemical Research of Catalonia, Spain)
Dujardin, Gerald (LPM-CNRS, France)
Echavarren, Antonio M. (Institute of Chemical Research of Catalonia, Spain)
Feltz, Albrecht (Omicron Nanotechnology GmbH, Germany)
Gauthier, Sébastien (CEMES-CNRS, France)
Glatzel, Thilo (Universitaet Basel, Switzerland)
Gnecco, Enrico (Universitaet Basel, Switzerland)
Godlewski, Szymon (Jagiellonian University, Poland)
Goryl, Grzegorz (Jagiellonian University, Poland)
Goryl, Maria (Jagiellonian University, Poland)
Gourdon, André (CEMES-CNRS, France)
Grill, Leonhard (Frei Universität Berlin, Germany)
Hecht, Stefan (Humboldt-Universität zu Berlin, Germany)
Hirth, Sabine (Universität Osnabrück, Germany)
Hliwa, Mohamed (CEMES-CNRS, France / Univ. Hassan II-Mohammédia, Morocco)
Joachim, Christian (CEMES-CNRS, France)
Kantorovich, Lev (University College London, United Kingdom)
Kawai, Shigeki (Universitaet Basel, Switzerland)
Köble, Jürgen (Omicron Nanotechnology GmbH, Germany)
Kolodziej, Jacek J. (Jagiellonian University, Poland)

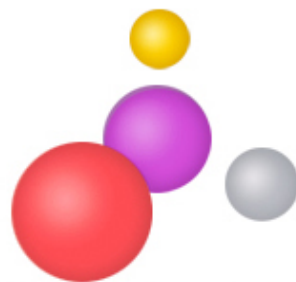
Krok, Franciszek (Jagiellonian University, Poland)
Kühnle, Angelika (Universität Osnabrück, Germany)
Lægsgaard, Erik (University of Aarhus, Denmark)
Lafferentz, Leif (Freie Universität Berlin, Germany)
Linderoth, Trolle R. (University of Aarhus, Denmark)
Maier, Markus (Omicron Nanotechnology GmbH, Germany)
Maier, Sabine (Universitaet Basel, Switzerland)
Mannsberger, Michael (Freie Universität Berlin, Germany)
Martrou, David (GNS/CEMES-CNRS, France)
Meyer, Ernst (Universitaet Basel, Switzerland)
Mielke, Johannes (Freie Universität Berlin, Germany)
Moresco, Francesca (Frei Universität Berlin, Germany)
Mosseri, Rémy (LPTMC-CNRS, France)
Nimmrich, Markus (Universität Osnabrück, Germany)
Nony, Laurent (Université Paul Cézanne Aix-Marseille III, France)
Ostendorf, Frank (Universität Osnabrück, Germany)
Peters, Maik V. (Humboldt-Universität zu Berlin, Germany)
Pfeiffer, Oliver (Universitaet Basel, Switzerland)
Piatkowski, Piotr (Jagiellonian University, Poland)
Prauzner-Bechcicki, Jakub S. (Jagiellonian University, Poland)
Rahe, Philipp (Universität Osnabrück, Germany)
Reichling, Michael (Universität Osnabrück, Germany)
Renaud, Nicolas (CEMES, France)
Riedel, Damien (LPM-CNRS / Université Paris-Sud, France)
Rieder, Karl-Heinz (Frei Universität Berlin, Germany)
Schütte, Jens (Universität Osnabrück, Germany)
Shluger, Alexander (University College London, United Kingdom)
Socoliuc, Anisoara (Universitaet Basel, Switzerland)
Solinas, Paolo (LPTMC-CNRS and UPMC, France)
Stara, Irena G. (Institute of Organic Chemistry and Biochemistry, Czech Republic)
Stensgaard, Ivan (University of Aarhus, Denmark)
Stojkovic, Sladjana (CEMES-CNRS, France)
Such, Bartosz (Jagiellonian University, Poland)
Sushko, Maria L. (University College London, United Kingdom)
Szymonski, Marek (Jagiellonian University, Poland)
Tekiel, Antoni (Jagiellonian University, Poland)
Trevethan, Thomas (University College London, United Kingdom)
Villagomez Ojeda, Carlos Javier (CEMES-CNRS, France)
Watkins, Matthew (University College London, United Kingdom)
Xu, Wei (University of Aarhus, Denmark)
Yu, Miao (University of Aarhus, Denmark)
Zambelli, Tomaso (ETH Zurich, Switzerland)
Zimmerli, Lars (Universitaet Basel, Switzerland)

Contents

1. Introduction	9
2. Hardware nano-architecture	23
2a. Classical	24
▪ Molecular switches: Isomerization of single azobenzene derivative	
▪ Nano-architecture by covalent assembly of molecular building blocks	
▪ Picometer-scale control of charge injection inside a single molecule	
2b. Semi-classical	34
▪ Semi-classical OR, AND, XOR molecule logic gate circuits	
2c. Quantum (qubits and QHC)	42
▪ Geometrical approach of quantum hamiltonian computer	
3. Nano-hardware	55
3a. Introduction: Constructing but preserving atom precision	56
▪ Chemistry towards intramolecular computing	
3b. Chemistry	62
▪ Design of new polyarenes	
▪ Helicenes as intriguing objects for chemical and physical studies	
▪ Molecular moulding	
3c. Surface selection and preparation, launching, imaging and assembling on a surface and manipulation	70
Metal	70
▪ STM investigations of molecular moulds on metal surfaces	
Insulator on metal	82
▪ Nanostructuring of an ultrathin insulating film of NaCl on Cu(111)	
▪ STM imaging of molecules on a thin insulating film	
▪ Scanning Probe Microscopy of adsorbates on insulating films	
Semiconductor	96
▪ STM study of organic molecules adsorbed on semiconductor surfaces	
Insulators on semiconductor	104
▪ Insulators on semiconductor	
▪ Thin insulating KBr layers deposited on InSb as a tool to study properties of organic molecules	

Insulators / NC-AFM instruments	116
<ul style="list-style-type: none"> ▪ Atomic resolution AFM on NaCl at 5 K using the QPlus sensor ▪ Dielectric substrates for anchoring organic molecules ▪ Immobilization of organic molecules on insulators ▪ Non-contact AFM as indispensable tool for investigation of patterned insulators ▪ PTCDA molecules adsorbed on rutile TiO₂(011)-(2x1): STM and nc-AFM studies 	
3d. Understanding the construction process (image interpretation & adsorption theory)	146
STM image cal.	146
<ul style="list-style-type: none"> ▪ Theory and numerical simulations for the Pico-Inside project 	
STM image + adsorption	152
<ul style="list-style-type: none"> ▪ Imaging and manipulation of molecules on reactive surfaces 	
AFM image cal.	156
<ul style="list-style-type: none"> ▪ Virtual Atomic Force Microscopy for modelling NC-AFM imaging on insulators 	
Adsorption on insulators	160
<ul style="list-style-type: none"> ▪ Theory of the adsorption of organic molecules on insulating surfaces 	
4. Planar multiple interconnect Atom Technology	167
4a. Introduction	168
4b. Number of interconnection steps & interconnection strategies	172
<ul style="list-style-type: none"> ▪ How to exchange information with a single molecule 	
4c. From the molecule to the nano-pads on a semi-conductor surface	176
<ul style="list-style-type: none"> ▪ Constructing interconnection nanostructure on the MoS₂ surface ▪ Gold-alloy nanowires: a high resolution STM imaging 	
4d. Optic navigation and interconnection	186
<ul style="list-style-type: none"> ▪ Nano level to macro level interconnects through static and nanostencil techniques 	
5. Conclusion	193

1. Introduction



Hybrid and Mono Molecular Electronics

Pico-Inside IST-FET European Integrated Project Christian Joachim (Coordinator)

*Nanoscience Group CEMES-CNRS 29, Rue J. Marvig BP94347 31055
Toulouse, France*

The 1974 seminal Aviram-Ratner paper had created a bridge between electronic circuits for computers and molecules. Ten years before, the relation between cybernetic and biomacromolecules was used by J. Monod in explaining the genetic machinery. The bridge between conducting materials and macromolecules was indicated by StGyorgi 30 years before. We have to appreciate the insight of A. Aviram and M. Ratner in their way to obtain a rectifier with a minimum number of atoms and 2 electrodes. Molecular Electronics was born from the idea that a single molecule will perform the same way a solid state device does with the advantage of its size. 30 years later, Molecular Electronics matures because of the invention of new tools to access electronically a single molecule (and always the same) during the measurement. This had created an explosion of sub-fields in Molecular Electronics from plastic electronics to quantum computing in a single molecule.

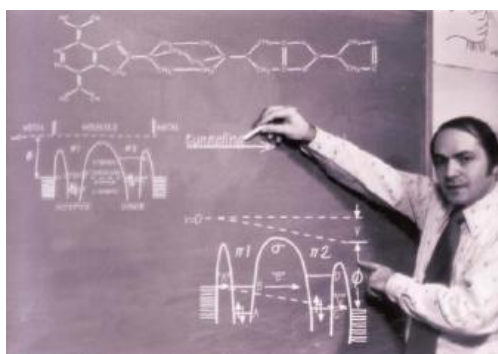


Figure 1: At the origin of molecular electronics: Ari Aviram and its molecular rectifier in the 70's

Following up the development of each Molecular Electronics sub-field, the initial concept of A. Aviram and M. Ratner can be pushed at the limits by asking a simple question: What is the minimum number of atoms required to embody a computer? Of course, the same question arises for mechanics machines, for transducer devices and also for communication machineries. But we will limit our analysis to computers. This question calls for a new approach designated by "monumentalization" and opposed to the miniaturization approach of the micro-electronics industry. With miniaturization, the game is clearly to keep an industry growing

with production plan and products. Physics, material sciences and technologies will follow. With monumentalization, the game is first to built up epistemological machines at the nanoscale not for sale but for the sake of understanding where are the physical, chemistry and technological limits of a machine like a computer. This is an up limit and not a down limit.

There are many possibilities to embody a computer with molecule(s). (1) to take benefit of the quantum response of a single molecule prepared in a non-stationary state to perform a computation. (2) to force a molecule to have the shape of an electrical circuit. (3) to attribute a particular electronic function to a single molecule and interconnect each function (each molecule) with metallic nanowires. (4) to attribute a particular electronic function to a macromolecule and interconnect them too. (5) instead of one molecule per electronic function, to fabricate a small film or crystal of such molecules and interconnect each device made of those molecular materials to shape the electronic circuit. (6) to create a crystal or a plastic and print the electronic circuit on this material as an equivalent to solid state micro-electronics.

All those possibilities have their advantages in term of technology, material science and performances. We will restrict our description to (1), (2) and (3) which are in direct lineage with the Aviram-Ratner molecular rectifier. Macromolecular electronics (4) with for example carbon nanotubes or semi-conductor nanowires are leading to fantastic devices. But they are too close to the actual solid-state nano-electronics transistor technology to be a valid candidate for exploring monumentalization. The integrated project NODE of the European Commission was selected to explore this branch of technology. The 2005 Pico-Inside integrated project launched in parallel to NODE under the Emerging Nanoelectronics priority of the IST-FET program started from (1) (www.PicoInside.org and www.node-project.com). It has explored how monumentalization can lead not only to a simple uni-molecular device embarked on a molecule but to a possible large complex computing machine embodies in a single molecule.

An atomic scale technology

At the laboratory scale and common to (1), (2) and (3), there was an urgent technological problem to be solved by Pico-Inside before asking for complexes architectures and production of molecular chips: how to interconnect a molecule to metallic electrodes in a planar technology? A related problem is the cleanness and precision of the connections. The rush in fabricating coplanar metallic electrodes with a separation below 10 nm starts in the early 90's culminating with the nanofabrication of 2 nm junctions 10 years later in the BUN IST-FET project of the fifth framework program. This was obtained by pushing e-beam nanolithography to the limit while in the mid 90's alternative solutions like the breaking of a metallic wire or the electro-migration techniques started to be explored.

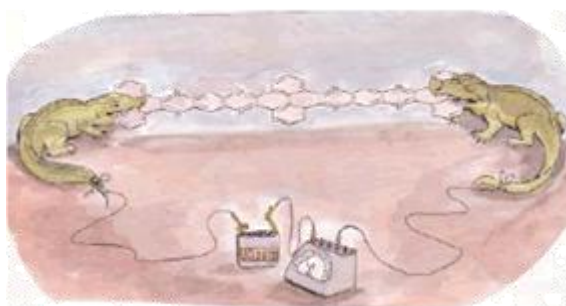


Figure 2: At the origin of the alligator clip in molecular electronics: the artistic view of the interconnection problem painted by C. Coudret from CEMES-CNRS in the 90's

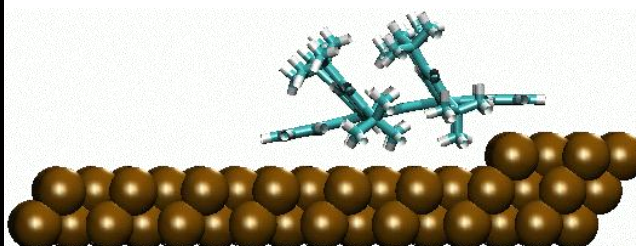
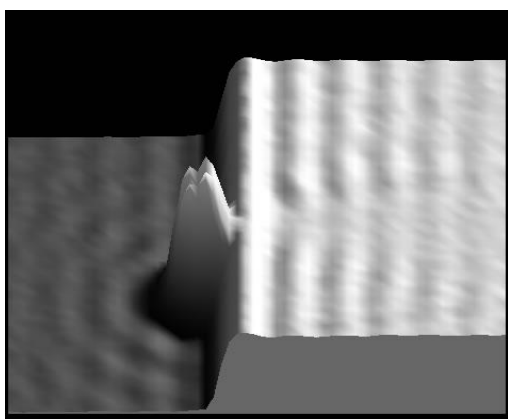


Figure 3: Interconnecting a molecular wire supported by 4 legs to a mono-atomic step edge on Cu(111). Left, LT UHV-STM image of the molecule at contact. Right: determined conformation of this Lander molecule from the experimental left image. (ref: F. Moresco et al., Phys. Rev. Lett., 91, 036601 (2003)).

But connecting a molecule to $N = 2$ or more metallic electrodes means creating an electronic interaction between well determined parts of the molecule and the end surface of the metal electrodes. Therefore, from a surface science point of view, any

change of the detail atomic ordering at the surface-end of the electrodes or any change in the adsorption site of the molecule in interaction with the metal will modify the orbital mixing between the metal surface and the molecule. Then, the conductance of the device will change. This is the explanation of so many different results published in the 90's and at the beginning of this century on planar metal-molecule-metal junctions and why, in the best case, statistical analysis of such experiments are needed. Clearly, the solutions for molecular interconnects explored in the 90's were not adapted to the ultra clean demand of the beginning of this century. In the mid 90's, this point of view was enforced by the first use of UHV-STM to image and contact a single atom and a single molecule in a very reproducible way. As a consequence both the atomic organization of the electrodes and the adsorption site must be mastered with a precision better than 0.05 nm. There is no technology ready yet to achieve such a precision. In PICO-INSIDE, one goal was to explore the possible developments of a new technology called "Atom based technology" for laboratory electrical experiments on a single molecule in a fully planar technology. Ingredients of such a technology are known.

First, the atomic structure and ordering of the surface end of the contact metallic wire must be known. This forbid the use of any resist lithography technique and even of the break junction technology for $N = 2$. For this "pico to nano" interconnection step, an atomic scale technology does not exist in the actual clean rooms and the new nanostencil technique is not clean enough in this prospect. In Pico-Inside, one solution was the growth of mesa ultra flat metallic nano-cluster. Furthermore, certain well designed molecules can manipulate surface metallic atoms by themselves and will be used to assemble very short atomic wires.

Second, an imaging technique is required to determine the atomic ordering at the interconnections. Scanning tunnelling microscope in the UHV (UHV-STM) is very capable of such a characterization for semi-conductor surface and the non-contact Atomic force microscope for plain insulator. An intermediate step is the use of an ultra thin insulating layer on a metal surface. The ultra low feedback loop tunneling current set-up of certain low temperature UHV-STM will help in understanding surface science at the atomic scale on insulating surface with a mixture of metallic cluster and organic molecules adsorbates.

Third, after this first step of atomic scale fabrication, the wiring fabrication technique for the "nano to meso" interconnection step must also be ultra clean. Again, this forbids the use of resist-like nanolithography. This point out the nanostencil technique where a mastering of the lateral diffusion through the stencil is necessary to limit the spreading of metal atom around.

Fourth, similar to the millipede technology, the "meso to micron scale" interconnection step may be deported on a second surface independent of the active atomic scale precision one. This second floor of interconnect opens the possibility to use standard nano and microlithography technique and to ultra-clean the device before performing the interconnection step. The relative positioning between the "ground" atomic floor and micro-technology floor is a very interesting technology which really needs to be developed

Digital logic in a molecule without circuits

Integrating a full electronic circuit inside a single conjugated molecule with the goal to reduce the fabrication costs and increase reliability was first proposed by F.L. Carter in

the 80's. Similarly to the "tyrannies of numbers" met in the 50's by those attempting to wire thousand of electronic devices together, F.L. Carter foresees at the end of the seventies that it will not be possible to wire together millions of discrete molecular devices to assemble a molecular circuit. Then, he proposed to shape the conjugate molecule itself like an electronic circuit. In our days, there are at least 2 possibilities to embody a logic function inside a molecule: (1) the use of intramolecular quantum time-dependent processes occurring when a molecule is prepared in a non-stationary state (with or without a structuration of the molecule in qubits) and (2) to force the molecule to have the shape of a standard electronic circuit as proposed by F. L. Carter.

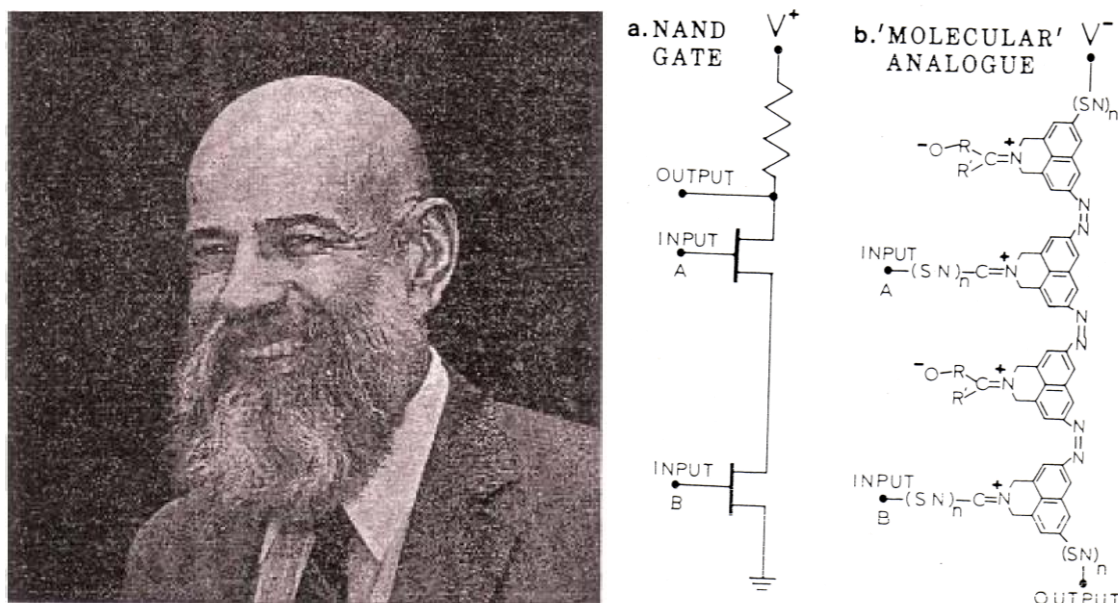


Figure 4: Going away from Hybrid molecular electronics: F. L. Carter in the 80's and its mono-molecular analogue to a Nand gate

For (1), the goal is to prepare the molecule in a non-stationary state and to optimize the molecular chemical composition in such a way that during the quantum time dependent evolution of this non-stationary state, the quantum trajectory of the molecule in its state space reaches well specified target states according to the initial preparation or to specific conformations of some specific chemical groups distributed along the molecule. This distinction between different initial preparations points out different kind of quantum computing. When the data are defining the initial quantum state, the molecule is structured in qubits and one recovers the initial 1984 proposal of R. P. Feynman. When the data are input on the molecule by changing for example the conformation of some small lateral groups, a quantum Hamiltonian computing is implemented. In both cases, the very difficult part of an experimental implementation is the fast intramolecular decoherence of the initial state because of the numerous quantum states weakly coupled to the ones in charge of performing the computation inside the molecule. On the top of that, intramolecular relaxations occur. In such a situation, one has to be fast enough to measure the result or to refresh the initial non-stationary state a lot of time to stabilize the result. This is the quantum Hamiltonian computing (QHC) scheme which was studied in Pico-Inside following the fifth framework IST project CHIC (Consortium for Hamiltonian Intramolecular Computing). Spontaneously, a tunnel junction is preparing billions of electron transfer events per second between the electrodes. The data are input on the molecule by changing the conformation of well positioned lateral group around a conjugated board. AND, OR, XOR, NAND and half adder molecules have already been optimized and are ready to be tested experimentally according to the above discussion on progresses of an Atom based technology. One advantage of QHC over a qubit like quantum computer

approach is that only one molecule is active and the statistic is provided by the quantum measurement performed natively by the tunnel junction. For an NMR like qubit molecular quantum computer approach, the statistic is dependent on the large number of active molecules present in solution.

For (2), the molecule must have the real shape of an electrical circuit with all the node and meshes required integrated in a single molecule. In this case, specific intramolecular circuit laws are needed because they are different from the standard Kirchhoff node and mesh laws used to describe the behaviour of an electrical circuit. In the past, a few monumental molecules have been proposed integrating mainly molecular rectifiers groups along the intramolecular circuit. None have been designed according to the specific intramolecular circuit laws. Following those laws, OR-molecules and an AND-molecule have been designed in the BUN IST-FET project. The architecture problem in Pico-Inside was the very fast native decay of the electronic transparency of a molecular wire group as soon as it is elongated. Tunnel current intensity of the order of a femto-ampere had been calculated for the AND-molecule interconnected between $N = 4$ electrodes. This opens a large field of research on how to optimize the architecture of an intramolecular circuit to compensate this secular property. One has to invent chemical groups able to compensate this phenomenon providing some kind of intramolecular gain. At present, all the intramolecular circuits more complicated than the AND-molecule lead to impracticable tunnel current intensity well below the atto-ampere when calculated using the N-ESQC routine developed in BUN.

Molecular board and molecular equipments

The molecular boards supporting the logic function are essentially polyaromatic like molecules. For (1), qubits separation can be triggered from inside the molecule. For (1), the QHC approach is requiring a full polyaromaticity to benefit from a very fast computation time and to use the different symmetry of n molecular levels to play with intramolecular time interferences. For (2), some saturated bonds are required for circuit design purpose to compensate for the exponential decay of the electron transfer rate with an increase of the length of the wire groups required along the intramolecular circuit.

Molecular equipments are the chemical groups required to port the molecular board in a given environment, to protect the digital logic function embarked on the board and to ease the nano-communication between the user and the molecule. Molecular legs are very popular on a metal surface to separate the conjugated board from the surface. But other separating groups are needed on insulating surfaces and started to be explored in Pico-Inside. Input/output groups can be specific end groups to increase the electronic interaction between a molecular wire and metallic pads or rotating group to define the logic digital input mechanically.

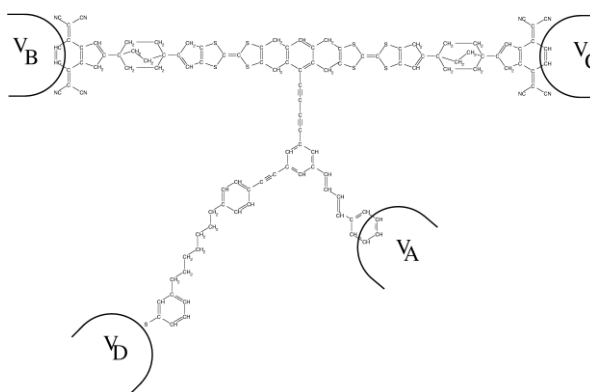


Figure 5: A mono-molecular AND gate integrating 2 Aviram Ratner molecular rectifiers groups and a few molecular wire groups to form an intramolecular circuit. The logic response of the molecule was optimized using the N-ESQC code (Ref: S. Ami et al, Chem. Phys. Lett., 367, 662(2003))

Molecular devices

Substituting each of the solid state devices integrated on the surface of a semiconductor by a molecule is leading to the hybrid molecular approach (3) mentioned above, in direct lineage with the Aviram-Ratner 1974 seminal paper. Adding one grid electrode to a single molecule properly interconnected between 2 metallic electrodes may lead to a transistor like behavior. There are many possible parameters to be controlled to obtain a molecular device presenting a power gain: the electronic coupling between the molecule and the source-drain electrodes, the homo-lumo gap of the molecule or the position of the energy level of the molecule relative to the electrode Fermi level. Shifting a few molecular levels by a lateral electric field applied via the grid electrode had long been advocated. But the range of electric field where a power gain can show up is not yet accessible experimentally: the electric field required is so large for the molecule design up to now that the breakdown limit of the metal-molecule-metal junction is reached before gain. Of course, a lot of 3 electrodes structure with a molecule in the nanojunction have been proposed and experimented. But their transconductance is so low that no gain will result while loading the device to an external resistor. A variant of this set-up is to perform an electrochemical experiment where the molecular levels are controlled relative to a reference electrode using an electrolyte. Here, the grid is macroscopic and no more on scale with the molecule.

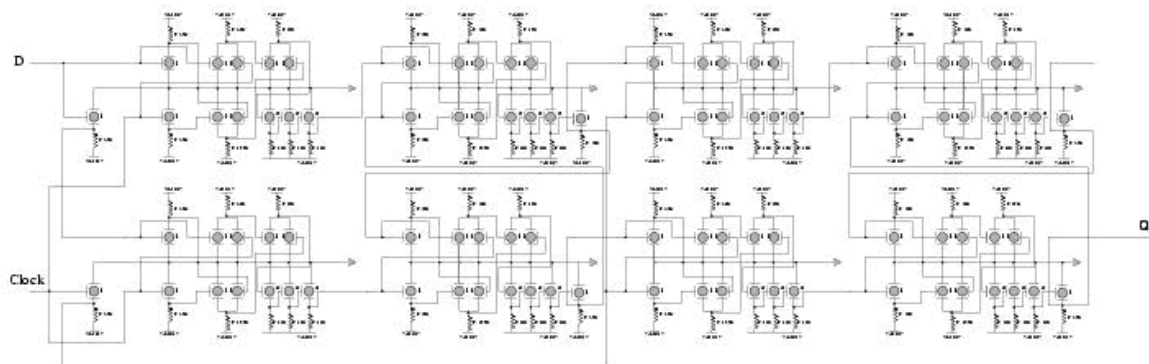


Figure 6: A full D latch hybrid molecular electronic circuit using 94 single molecule C60 transistors in a coplanar configuration whose time-dependant response had been simulated using SPICE (R. Staddler et al, *Nanotechnology*, 12, 350 (2001)).

One solution to this problem was to control the closure of the homo-lumo gap of a molecule positioned between the source and the drain of a tunnel junction by a mechanical deformation. The original experiment was performed in 1997 on a single C60 molecule trapped in the tunnelling junction of an STM. A small deformation of the C60 cage provides a large variation of the metal-C60-metal junction conductance leading to power gain. This was a proof of concept that a single molecule-device can provide gain by using the intrinsic electronic property of a single molecule. For C60, the 5 fold degeneracy of its Homo and 3-fold of its lumo are creating a nice destructive interference effect whose matching is cancelled by a compression of the molecule cage by the tip of the STM. This is a perfect example of a pure intramolecular electron transfer quantum phenomenon converted in a measurable tunnel current by the interaction of the molecule with the electrodes. A full planar version of this device had been proposed and its performance simulated in BUN. A full electrical circuit was established and included in a SPICE circuit simulator to evaluate the performances of a complete ALU up to 1000 C60 transistors. Aside from the real difficulties to find a

technology to fabricate such a molecular circuit, the gain in miniaturization is not exceptional since each C60 transistor need a minimum separation distance of a few ten of nanometer for the Kirchhoff electrical circuit node and mesh laws to be applicable. In comparison to the gigantic progress of solid state nanoelectronics, the future progress margin of hybrid molecular electronics is not very clear. This is the explanation why Pico-Inside was organized to intentionnaly remain away from this Hybrid approach.

Starting Pico-Inside

Pico-Inside was a 3.5 years FP6-IST-FET integrated project whose partnership is explained in the E-nano Newsletter n° 2 (2005):

www.phantomsnet.net/Foundation/Enano_newsletter02.php

This project decided to explore the monumentalization of a calculating unit up to the limits imposed by physics, chemistry and technology. Atomic scale technology is a very challenging path to be explored. But architecture, surface science (both experimental and theoretical) and chemistry were also included on the agenda. Pico-Inside challenge was to determine if a single unique molecule can compute and communicate its results to the macroscopic level.

Further reading

- BUN IST-FET final Report:
www.phantomsnet.net/Enano/euprojectreports.php
- CHIC IST-FET Project:
www.cemes.fr/chic/
- Pico-Inside IST-FET project:
www.picoinside.org
- C. Joachim, J. K. Gimzewski and A. Aviram, Nature, 408, 541 (2000)
- Molecular Electronics, Special issue of the Proceeding National Academy of Science, USA, 102 n° 25, June 21 (2005)

More Relevant Pico-Inside publications

A local view on Hyperconjugation

C. Villagomez, T. Zambelli, S. Gauthier, A. Gourdon, C. Barthes, S. Stojkovic and C. Joachim
Chem. Phys. Lett., 450, 107 (2007)

A NOR-AND quantum running molecule logic gate

N. Renaud, M. Ito, W. Yen, M. Hliwa, M. Seays and C. Joachim
Chem. Phys. Lett., 472, 74 (2009)

Study and manipulation of single functionalized molecules by low temperature STM

L. Grill, M. Alemani, K.-H. Rieder, F. Moresco, G. Rapenne, C. Joachim, M. V. Peters, and S. Hecht
J. Scan. Probe Microsc. 2, 19 (2007)

Adsorption and Switching Properties of Azobenzene Derivatives on Different Noble Metal Surfaces: Au(111), Cu(111), and Au(100)

M. Alemani, S. Selvanathan, F. Ample, M. V. Peters, K. H. Rieder, F. Moresco, C. Joachim, S. Hecht and L. Grill

Journal of Physical Chemistry C 112, 10509 (2008)

Conductance of a Single Conjugated Polymer as a Continuous Function of its Length

L. Lafferentz, F. Ample, H. Yu, S. Hecht, C. Joachim and L. Grill

Science 323, 1193 (2009)

Scanning Force Microscopies for Imaging and Characterisation of Nanostructured Materials

B. Such, F. Krok and M. Szymonski

Nanotechnology for Electronic Materials and Devices, eds. A. Korkin, E. Gusev, J.K. Labanowski, S. Luryi and Springer, Berlin 2007, p.223

How flat is an air-cleaved mica surface?

F. Ostendorf, C. Schuntz, S. Hirth, A. Kuehnle, J. J. Kolodziej and M. Reichling
Nanotechnology 19, 305705 (2008)

STM manipulation of molecular moulds on metal surfaces

M. Yu, W. Xu, Y. Ben Jalal, R. Barattin, E. Lægsgaard, I. Stensgaard, M. Hliwa, X. Bouju, A. Gourdon, C. Joachim, T. R. Linderoth, and F. Besenbacher

Nano Research, 2, 254 (2009)

Scanning tunneling microscopy and spectroscopy studies of individual larder molecules anchored on a copper oxide nanotemplate

Y. Naitoh, F. Rosei, A. Gourdon, E. Lægsgaard, I. Stensgaard, C. Joachim and F. Besenbacher

J. Phys. Chem. C 112 (2008) 16118-16122

Elementary structural motifs in a random network of cytosine adsorbed on a gold (111) surface

R. Otero, M. Lukas, R. E.A Kelly, W. Xu, E. Lægsgaard, I. Stensgaard, L. N. Kantorovich and F. Besenbacher

Science 319 (2008) 312-315

Dihydride dimer structures on the Si(100):H surface studied by low-temperature scanning tunneling microscopy

A. Bellec, D. Riedel, D. Dujardin, N. Rompotis and L. Kantorovich

Phys. Rev. B, v. 78, No. 165302 (2008)

Imaging molecular orbitals by scanning tunnelling microscopy on a passivated semiconductor

A. Bellec, F. Ample, D. Riedel, G. Dujardin and C. Joachim

Nano Lett. 9, 144 (2009)

Cyclodehydrogenation of hetero-oligophenylenes

S. Nagarajan, C. Barthes and A. Gourdon

Tetrahedron, on line (2009)

Nano-architectures by covalent assembly of molecular building blocks

L. Grill, M. Dyer, L. Lafferentz, M. Persson, M. V. Peters and S. Hecht

Nature Nanotechnology 2, 687 (2007)

High resolution LT-STM imaging of PTCDA molecules assembled on InSb(001) c(8x2) surface

G. Goryl, S. Godlewski, J.J. Kolodziej and M. Szymonski
Nanotechnology 19 (2008) 185708

Nanofabrication of PTCDA molecular chains on rutile TiO₂ (011)-(2x1) surfaces

A. Tekiel, S. Godlewski, J. Budzioch and M. Szymonski
Nanotechnology 19 (2008) 495304

Growth of ordered C₆₀ islands on TiO₂(110)

F. Loske, R. Bechstein, J. Schütte, F. Ostendorf, M. Reichling and A. Kühnle
Nanotechnology 20 (2009) 065606

Contrast inversion in NC-AFM imaging of C₆₀ molecules

F. Loske, P. Rahe and A. Kühnle
Nanotechnology, in print (2009)

Molecular assemblies grown between metallic contacts on insulating surfaces

Th. Glatzel, L. Zimmerli, S. Koch, S. Kawai and E. Meyer
Appl. Phys. Lett. 94 (2009) 1

Nanoscale Engineering of Molecular Porphyrin Wires on Insulating Surfaces

S. Maier, L. Fendt, L. Zimmerli, T. Glatzel, O. Pfeiffer, F. Diederich and E. Meyer
Small, 4, (8), (2008), 1115

Generalised Langevin Equation for solids: II. Stochastic Boundary Conditions for non-equilibrium molecular dynamics simulations

L. Kantorovich and N. Rompotis
Phys. Rev. B, v. 78, No. 094305 (2008)

Building blocks for molecular devices: Organic molecules on the MgO (001) surface

T. Trevethan and A. L. Shluger
J. Phys. Chem. C 111 (42), pp.15375-15381 (2007)

Designing molecular architecture to control diffusion and adsorption on insulating surfaces

M. Watkins, T. Trevethan, M. L. Sushko and A. L. Shluger
J. Phys. Chem. C 112 (11), pp. 4226-4231 (2008)

The role of dopant in silicon on the dynamics of a single adsorbed molecule

M. Lastapis, M. Martin, D. Riedel and G. Dujardin
Phys. Rev. B 77, 125316 (2008)

STM induced modifications of the trima molecule chemisorbed on Si(100)

M. Mamatkulov, L. Stauffer, Ph. Sonnet, A. J. Mayne, G. Comtet and G. Dujardin
J. Chem. Phys. 129, 1 (2008)

A straightforward route to helically chiral N-Heteroaromatic compounds: Practical synthesis of racemic 1,14-Diaza[5]helicene and optically Pure 1- and 2-Aza[6]helicenes

J. Misek, F. Těplý, I. Stara, M. Tichý, D. Saman, I. Cisarova, P. Vojtisek and I. Stary
Angew. Chem. Int. Ed. 2008, 47, 3188–3191

Pico-Inside: Summary and Objectives

Computing inside a Single Molecule using Atomic Scale Technologies (Pico-Inside) was one of the Integrated Projects funded within the 6th Framework programme IST-FET (Nano proactive initiative: www.cordis.lu/ist/fet/nid.htm).

Below are detailed a summary of the project objectives (more info available at www.picoinside.org).

During the last 4 years, Pico-Inside objectives were to develop:

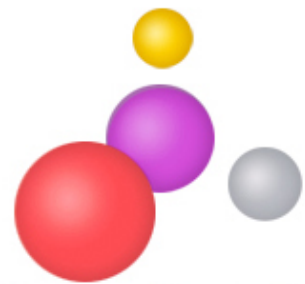
- (1) The architecture,
- (2) The atomic scale technology and
- (3) The chemistry to explore and quantify intramolecular resources for integrating much more than a single logic gate inside a single molecule.

Five very recent breakthroughs were fully exploited by Pico-Inside partners.

- (1) The theoretical demonstration that intramolecular quantum evolution based on the nonstationary mixing of large molecule quantum states can perform digital operations.
- (2) The new intramolecular mesh and node circuit rules for large molecules whose internal chemical structure is similar to a standard electronic circuit architecture.
- (3) The experimental demonstration that the electronic contact between a single molecular wire and its contacting atomic pad requires 0.05 nm precision.
- (4) The atomic resolution now obtained by a non-contact UHV-AFM on insulating surfaces and by low temperature UHV-STM on insulator on metal systems.
- (5) The progresses of organic chemists to design and synthesise large multi-functional molecules adapted to surface performances at the atomic scale.

Pico-Inside integrated the necessary groups to explore new architecture concepts with Fujitsu Europe. LT-UHV-STM and NC-UHV AFM offered a complete and true access to the atomic scale for interconnects with Omicron. This included nano-stencil contact experiments, the necessary chemistry labs task force and the required theoretical group to support the architecture, the molecular design and the analysis of Pico-Inside nanoscale experiments. This integration was completed by dissemination activities that created and diffused original roadmaps to a large community around Pico-Inside towards mono-molecular computing and atomic scale technologies.

2. Hardware nano-architecture



2a. Classical

Molecular switches: Isomerization of single azobenzene derivative

M. Alemani¹, K.-H. Rieder¹, F. Moresco¹, M. V. Peters², S. Hecht² and L. Grill¹

¹*Institut für Experimentalphysik, Freie Universität Berlin, 14195 Berlin, Germany*

²*Institut für Chemie, Humboldt-Universität zu Berlin, 12489 Berlin, Germany*

Keywords: Azobenzene, Adsorption, Scanning tunneling microscopy, Single molecule chemistry

The investigation of single molecules has become an important and well-established research field in the last years, driven by the prospect for fundamental electronic and mechanical device miniaturization [1]. Understanding and controlling conformational changes of single molecules is very important in this regard. For this purpose, the scanning tunneling microscope (STM) at low temperature constitutes a powerful tool, as it not only allows precise sub-molecular imaging of single molecules but also permits the manipulation of atoms and molecules [2, 3]. Looking for molecules suitable for application in molecular electronics, the current research interest is focusing on molecular switches [4, 5]. A molecular switch undergoes a reversible transformation between at least two distinct stable switching states, associated with different physicochemical properties [4]. The azobenzene molecule, based on a *trans-cis* isomerization mechanism, represents a very interesting example of such a molecular switch [6].

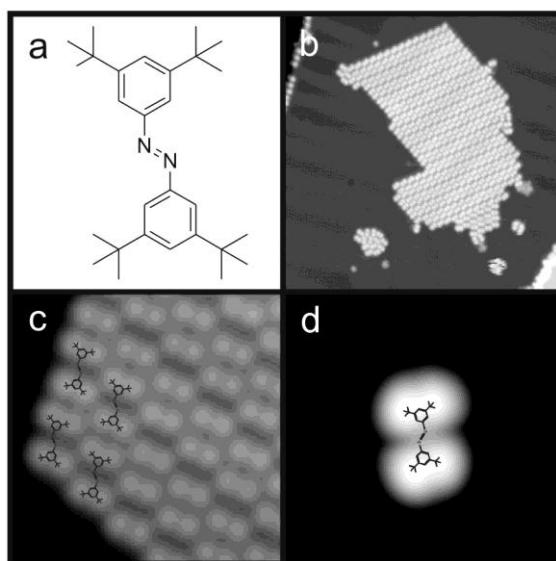


Figure 1: (a) TBA molecule. (b) STM image ($40 \times 40 \text{ nm}^2$) of a molecular island on Au(111). (c) Corner of an island in an enlarged STM image, the molecular structure is indicated. (d) Shows the STM image of a single TBA molecule.

The aim of the presented work is to switch single molecules on a metal surface in a controlled way. Figure 1a shows the investigated molecule: 3,3',5,5'-tetra-*tert*-butyl-azobenzene, called TBA [7]. The experiments were performed under ultrahigh vacuum conditions at a temperature of 5 K using a home built STM. An overview STM image of TBA molecules on Au(111) after deposition is shown in Figure 1b. The molecules are mobile after adsorption, as they cover step edges and form islands. The position and orientation of individual molecules inside these islands is shown in Figure 1c: the molecules form parallel rows indenting with each other. Each molecule appears as four lobes with an apparent height of $2.7 \pm 0.1 \text{ \AA}$ arranged in a rhombic shape (Figure 1d). According to the dimensions of the molecule in the gas phase, the lobes can be assigned to the *tert*-butyl groups while the central azobenzene part is not visible. All observed molecules are in the same planar configuration that we assign to the *trans* isomer (Figure 1a).

To induce the isomerization, voltage pulses of 2 V were applied with the STM tip positioned above an island. After these pulses, many molecules have changed appearance, showing a larger height of $4.1 \pm 0.3 \text{ \AA}$. These bright molecules are stable and to let them precisely restore their initial appearance we have to apply a further

pulse, as shown in Figure 2. As one can see in Figure 2a, the isomerization process has no consequence on the neighboring *trans* molecules, which remain unchanged. The *cis* form appears with a bright central intensity maximum, while three lateral lobes in an approximately triangular shape can be resolved, completely different from the planar *trans* conformation [8]. This shows that, in contrast to the *trans* isomer, the *cis* isomer is not planar, in agreement with the molecular conformation in the gas phase [6].

Such switching experiments can be reproduced several hundred times allowing us to conclude that the observed changes are due to the isomerization of single molecules

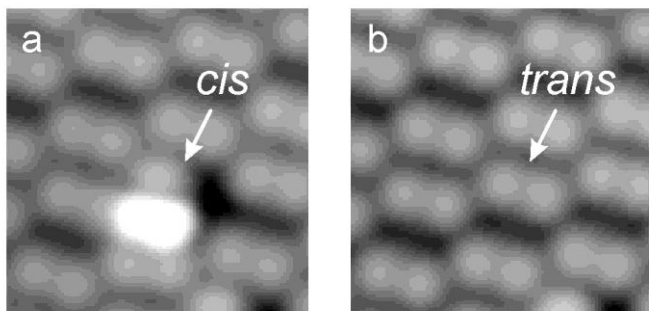


Figure 2: Isomerization process from *cis* to *trans*. (a) and (b) show STM images (both 3.5 nm x 3.5 nm) before and after the isomerization. The bright molecule in (a) is in the *cis* state and exactly returns to the *trans* state in (b), where all visible molecules are *trans* isomers, after applying a voltage pulse.

from the *trans* form to the *cis* form, and back to the *trans* form [7, 8]. The reversibility of the experiment and its high reproducibility exclude molecular dissociation or the presence of any contamination as cause for the observed change of the molecular appearance. The switching of an isolated molecule is very rare because, under the effect of a voltage pulse, the molecule can move or rotate. This effect is avoided in the islands when the molecules are stabilized by each other.

References

- [1] J. K. Gimzewski and C. Joachim, *Science* 1999, 283, 1683.
- [2] J. A. Stroscio and D. M. Eigler, *Science* 1991, 254, 1319.
- [3] L. Grill, *J. Phys.: Condens. Matter* 2008, 20, 053001.
- [4] B. L. Feringa, *Molecular Switches* (Wiley-VCH, Weinheim, 2001).
- [5] Z. J. Donhauser et al., *Science* 2001, 292, 2303.
- [6] H. Rau, *Photochromism - Molecules and Systems* (Elsevier, Amsterdam, 2003), p. 165.
- [7] M. Alemani et al., *J. Am. Chem. Soc.* 2006, 128, 14446-14447.
- [8] M. Alemani et al., *J. Phys. Chem. C* 2008, 112, 10509-10514.

Nano-architecture by covalent assembly of molecular building blocks

L. Lafferentz¹, M. V. Peters², S. Hecht² and L. Grill¹

¹*Institut für Experimentalphysik, Freie Universität Berlin, 14195 Berlin, Germany*

²*Institut für Chemie, Humboldt-Universität zu Berlin, 12489 Berlin, Germany*

Keywords: Scanning tunneling microscopy, Covalent bonding, Molecular architectures

The construction of electronic devices from single molecular building blocks, which inherit certain functions - such as switching or rectifying - and are connected by atomic scale wires on a supporting surface, is an essential goal of molecular electronics [1]. A key challenge in this regard is the controlled assembly of molecules into desired architectures by strong, i.e. covalent, intermolecular connections [2], enabling efficient electron transport [3] between the molecules and providing high stability [4]. Such large networks are difficult to be manufactured by traditional repetitive chemical synthesis and can hardly be deposited onto surfaces.

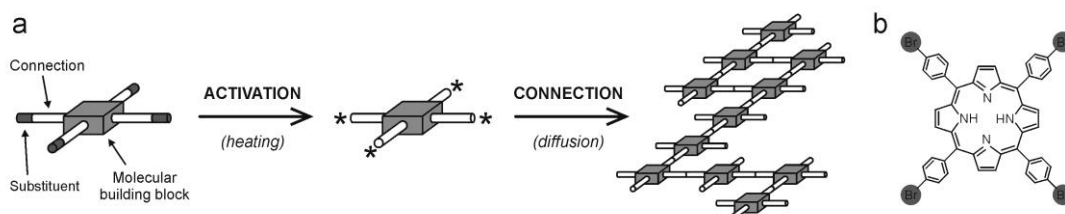


Figure 1: (a) Concept of the formation of covalently bound networks by connecting activated molecular building blocks. (b) Chemical structure of the Br4TPP (tetra(4-bromophenyl)porphyrin) molecule. From [5].

We have developed a method that overcomes this problem and creates covalently bound nano-architectures, i.e. macromolecular structures with controlled shape and size [5]. Our approach is based on small molecular building blocks with reactive side groups - "legs" - that form permanent chemical bonds at predefined connection points. This concept is illustrated in Figure 1a: A chemically stable, central molecular unit, is equipped with several legs. After dissociation of the substituent atoms in the first step by heating, the monomer building blocks are connected with each other through the activated legs directly on the surface upon thermal diffusion. The design of suitable molecules requires the incorporation of legs that can be activated selectively, without breaking the other bonds. For this purpose, carbon-halogen bonds were chosen. After selective thermal dissociation either on the surface or in the evaporator, the resulting activated fragments connect. Considering these requirements, we have chosen a porphyrin with four phenyl legs as a central building block (Figure 1b). At each leg, bromine was used as the labile substituent atom to be dissociated in a controlled manner.

The imaging and characterization of the molecular nanostructures were carried out with an STM at 7 K. The molecules were deposited onto clean Au(111), kept at room temperature during deposition. If the evaporator temperature was 550 K or below during the deposition of the Br4TPP molecules, large, highly ordered islands of intact molecules in a close-packed structure were found. The behaviour of the molecules changes fundamentally if the evaporator temperature is raised to at least 590 K: Most of the molecules become "activated" with the loss of several Br atoms in the evaporator. Upon thermal diffusion, these activated molecules react with each other to form intermolecular chemical bonds, thereby building macromolecular nanostructures of various shapes on the surface. The intermolecular bonds turn out to be relatively

strong, causing the entire molecular nanostructures to follow the pathway of the tip without fragmentation upon pulling on one end. Another signature of the covalent nature of the intermolecular bonds is revealed from spectroscopy measurements [5].

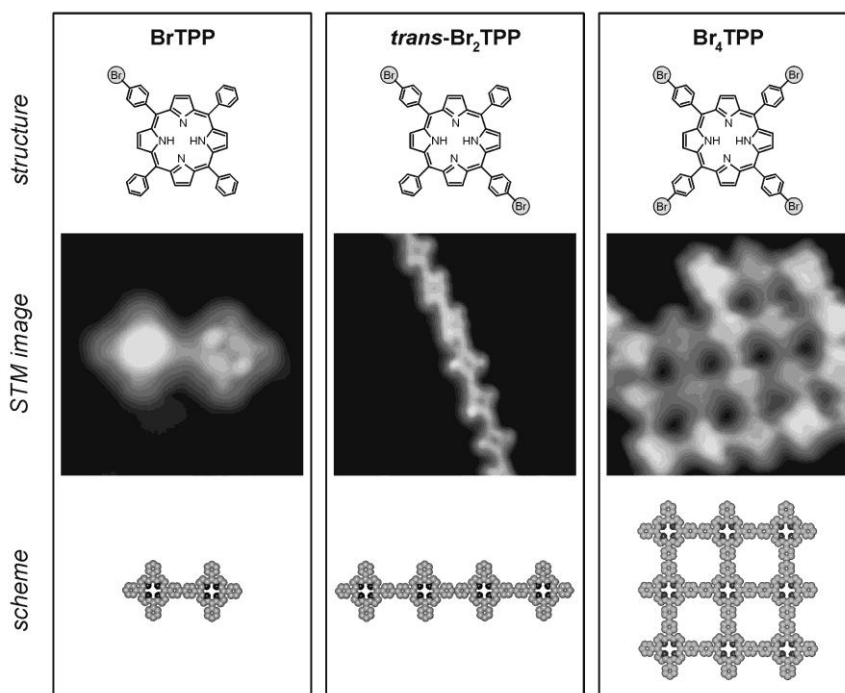


Figure 2: Results of different monomer building blocks with one (left panel), two (medium panel) and four (right panel) Br substituents, causing the formation of dimers, chains and networks, respectively. From [5].

In order to show the ability of controlling the nano-architecture of the macromolecular structures, we have synthesized different TPP-based molecules with one, two or four Br substituents (Figure 2). In the case of sufficient heating, characteristic molecular arrays are found on the surface. The topology of these nanostructures precisely corresponds to the molecular design (Figure 2): If only one Br substituent is used, exclusively dimers are observed, because each building block provides only one reactive site. Accordingly, porphyrin building blocks with two Br atoms in a linear geometry lead to the formation of linear chains. Finally, the use of four Br substituents enables the construction of two-dimensional networks. Hence, these results clearly show that the architecture of the nanostructures can be precisely controlled via the position of active end groups in the chemical structure of the molecular building blocks.

References

- [1] C. Joachim, J. K. Gimzewski, and A. Aviram, *Nature* 2000, 408, 541-548.
- [2] J. R. Heath, and M. A. Ratner, *Physics Today* 2003, 56, 43-49.
- [3] A. Nitzan, and M. A. Ratner, *Science* 2003, 300, 1384-1389.
- [4] A. P. Cote et al., *Science* 2005, 310, 1166-1170.
- [5] L. Grill et al., *Nature Nanotech.* 2007, 2, 687-691.

Picometer-scale control of charge injection inside a single molecule

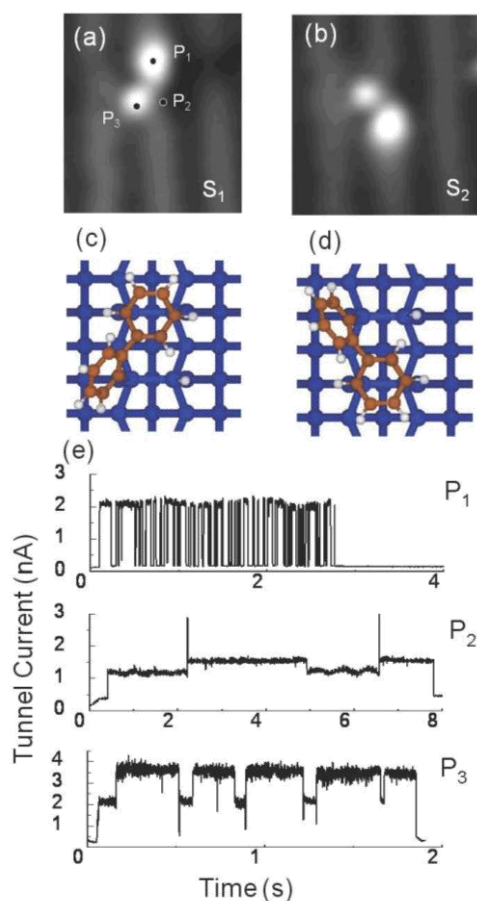
A. Bellec, F. Chiaravalloti, D. Riedel and G. Dujardin

Bâtiment 210, Université Paris-Sud 91405, Orsay, France

Introduction

Several techniques, such as nano-gap junctions [1] and break junctions [2,3], have been used in an effort to study electronic conduction through single molecules. However, the contacts between the molecules and the electrodes are poorly defined and there is increasing evidence that the molecular contacts need to be controlled with an atomic-scale precision. When calculating the electron transfer through a single benzene 1,4-dithiol molecule connected to two gold electrodes, Di Ventura et al. [4] have shown that adding just one gold atom between the molecule and one of the electrodes could change the conductance by two orders of magnitudes. This demonstrates that the contact between the molecule and the electrode needs to be defined with an atomic scale precision. Another important problem is the localization of the contact inside the molecule. Recently, it has been demonstrated that the localization of charge injection can be controlled with a picometer-scale precision inside a single molecule [5]. Different molecular dynamics have been activated when injecting charges at different positions inside the molecule. This suggests that the precise location of the atomic-scale electronic contacts inside the molecule can influence the whole properties (electron transfer, dynamics) of the molecule.

Picometer-scale electronic control of molecular dynamics inside a single molecule



A single biphenyl molecule adsorbed at room temperature on a Si(100) surface behaves as a bistable molecule at low temperature (5K) [5]. In its bistable configuration, the biphenyl molecule has two equivalent stable positions, S_1 and S_2 , as shown in the STM topographies of Figure 1. The biphenyl molecule is seen as a pair of bright features representing the two phenyl rings of the molecule. This bistable adsorption configuration consists of one phenyl ring lying parallel to the surface and attached to a silicon dimer in the so called "butterfly" configuration through two C-Si chemical bonds [6]. This phenyl ring is centered over the silicon dimer row. The second phenyl ring, perpendicular to the surface, is attached to a silicon atom through a single C-Si chemical bond. This is the result of a dissociative adsorption of the second phenyl ring where one hydrogen atom of the phenyl ring is adsorbed into the Si atom of the dimer as shown in Figure 1.

Figure 1: (a) (23 \AA by 23 \AA) topography of a single biphenyl molecule in the stable configuration S_1 . The dots indicate the STM tip position (P_1 , P_2 and P_3) where the negative bias pulse is applied. (b) Same as (a) after the surface pulse. The molecule has switched to its second stable configuration S_2 . (c) to (e) Three typical tunnel current curves recorded during negative bias pulses ($V_s = -3V$) at P_1 , P_2 and P_3 give insight into the dynamics of the molecular switch.

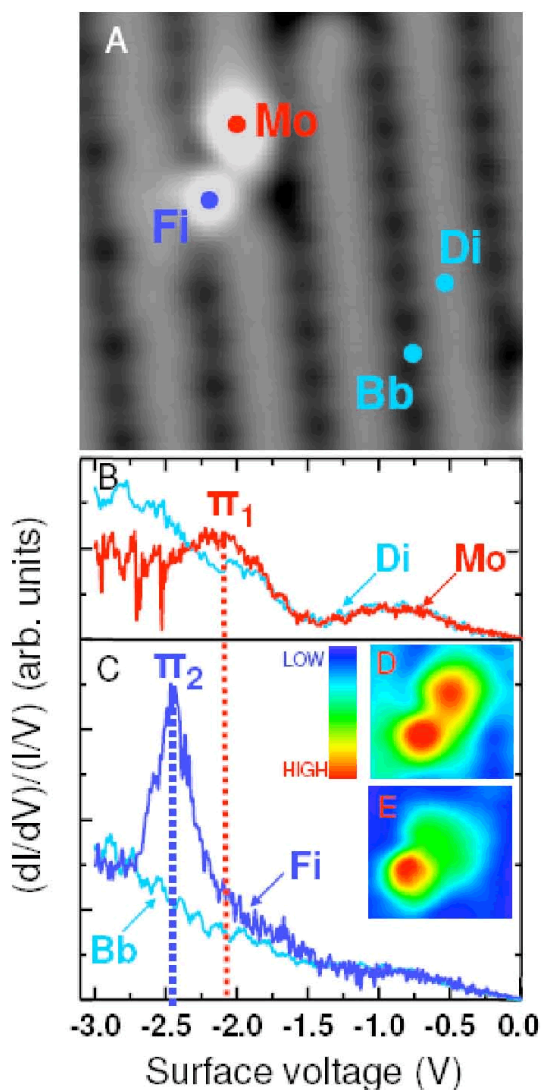


Figure 2: (A) Tunneling spectra have been recorded at the centers of the mobile (Mo) and fixed (Fi) phenyl rings of a biphenyl molecule and at the corresponding locations, Di (dangling bonds) and Bb (backbonds) of the clean Si(100) surface. (B) and (C) dI/dV curves have been recorded with a lock-in amplifier (frequency 930 Hz, voltage modulation 40mV) when recording the tunnel current I as a function of the surface voltage from 0 to -3.0 V. From this, $(dI/dV)/(I/V)$ has been calculated numerically. The narrow peaks in the $(dI/dV)/(I/V)$ curve of (B) for surface voltages smaller than -2.5 V are due to molecule motion. The π_1 resonance at -2.1 V and the π_2 resonance at -2.5 V are seen in the Mo and Fi curves respectively. (D) STM topography of a biphenyl molecule ($V_s = -2.5$ V, $I = 0.12$ nA). (E) Topography of the dI/dV signal recorded with the lock-in amplifier at $V_s = -2.5$ V, $I = 0.12$ nA showing the localisation of the π_2 resonance at -2.5 V.

The ability of the low-temperature STM to perform experiments with picometer-scale spatial resolution enables the investigation of both the electronic excitation processes and the ensuing molecular dynamics within a molecule. As previously reported [5], the reversible switching of the molecule from S_1 to S_2 can be activated through resonant electronic excitation by positioning the STM tip at different positions inside the molecule (for example positions P_1 , P_2 and P_3 in Figure 1) and applying a pulse voltage ($V_s = -2.5$ V) on the surface. The $S_1 \rightarrow S_2$ switching requires one of the molecular phenyl rings (called the mobile phenyl ring) to break two

Si-C bonds in its butterfly position, to move over the Si-H bond and to make two new Si-C. Recording the tunnel current during the pulse voltage enables a detailed investigation of the dynamics of the molecule as a function of the time of excitation. Step features in the time dependence of the tunnel current measured at three different locations inside the biphenyl molecule (Figure 1) correspond to the reversible switching of the molecule between the two S_1 and S_2 stable configurations. The molecule has switched 1, 3, and 9 times when the STM tip is in position P_1 , P_2 and P_3 respectively. From the distribution of the time of excitation before switching, the switching yield has been derived at each position for $V_s = -2.5$ V; $Y_{S_1 \rightarrow S_2}(P_1) = 2.7 \pm 0.5 \cdot 10^{-12}$, $Y_{S_1 \rightarrow S_2}(P_2) = 2.5 \pm 0.3 \cdot 10^{-13}$ and $Y_{S_1 \rightarrow S_2}(P_3) = 5.0 \pm 0.6 \cdot 10^{-11}$. This result shows that the switching yield varies by more than two orders of magnitude simply by moving the STM tip only 4 Å inside the molecule (from P_2 to P_3). Quite surprisingly, the switching yield is maximum when exciting the less mobile part of the molecule (location P_3). There are additional features in the tunnel current curves of Figure 1 consisting of narrow peaks that are far more scarce in curves P_2 and P_3 as compared to P_1 . We assign the narrow features to the movement of the molecule into a transient state (T) located between the two stable states (S_1 and S_2) of the bistable molecule. Transient states can be observed only if their lifetime is longer than ~ 1 ms because the frequency bandpass of our tunnel current detection is limited to about 1.3 KHz.

The markedly different molecular dynamics and switching yields at positions P_1 and P_3 inside the biphenyl molecule have been assigned [5] to injection of charges (injection

of holes, i.e. removal of electrons) into localized π_1 and π_2 molecular orbitals. Indeed, as seen in the dI/dV STM spectroscopy (Figure 2), the π_1 and π_2 molecular orbitals are localized at the positions of the mobile and fixed phenyl rings respectively. This localization of the molecular orbitals probably reflects the relatively weak coupling between the two phenyl groups of the molecule, which interact more strongly with the silicon surface. Thus, depending on the precise location of the STM tip inside the molecule, different electronically excited states (π_1 and π_2 resonances) of the molecular system can be produced, each associated with a specific molecular movement.

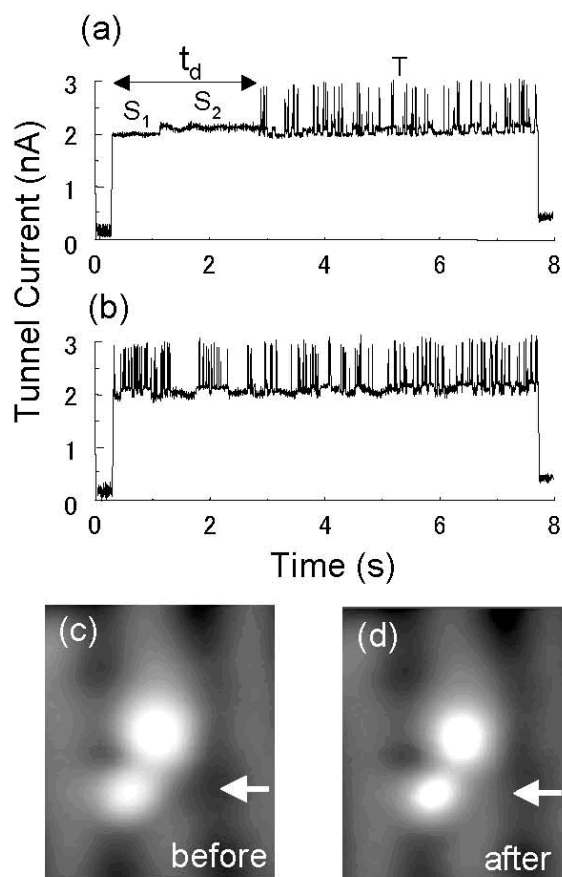


Figure 3: (a) Tunnel current during a negative bias pulse at P_2 ($V_s = -4V$, $t = 8s$). Desorption of the hydrogen atom occurs at time t_d . (b) Tunnel current during a negative bias pulse ($V_s = -4V$, $t = 8s$) after hydrogen desorption. (c) and (d) 20 \AA by 20 \AA STM topographies of the biphenyl molecule before and after the hydrogen desorption. The arrow indicates the area where the hydrogen atom has been removed leading to a slightly higher local density of states.

site. In the meantime, the other molecular phenyl ring (called the fixed phenyl ring) is expected to rotate around its single Si–C bond. It follows that the Si–H bond behaves as an obstacle to the operation of the bistable molecule since a part of the molecule has to pass over the hydrogen atom for switching to occur. Therefore, we decided to desorb this hydrogen atom with the STM tip in order to explore the resulting dynamics of the molecule. The desorption of hydrogen has been performed by using a negative surface voltage $V_s = -4 \text{ V}$ with the STM tip on top of the hydrogen atom (position P_2 in Figure 1). The desorption of the hydrogen atom after an excitation time t_d is clearly evidenced in the tunnel current curve of Figure 3. Indeed, before time t_d , the molecule switches only once from S_1 to S_2 . After a time t_d , the molecule has a completely different behaviour. It switches much more often between the S_1 , S_2 and T states. We

Compared to other molecular quantum control methods based on the use of photon absorption selection or coherent control rules [7], the real space picometer-scale control method described here has the advantage of working with single molecules and of dealing with a completely different concept based on the selection of a specific electronically excited state through the spatial localisation of the excitation inside the molecule. We emphasize that in this particular case of the bistable biphenyl, the picometer-scale electronic control is associated to the localization of initial molecular electronic states. However, similar effects can also occur in the case of fully delocalized initial molecular electronic states provided the charged excited electronic states are localized enough.

Mastering the molecular dynamics of a single molecule by single atom manipulation

We have seen in the previous part that the $S_1 \rightarrow S_2$ switching requires one of the molecular phenyl rings (called the mobile phenyl ring) to break two Si–C bonds in its butterfly position, to move over the Si–H bond and to make two new Si–C bonds to recover its butterfly position at the second silicon dimer

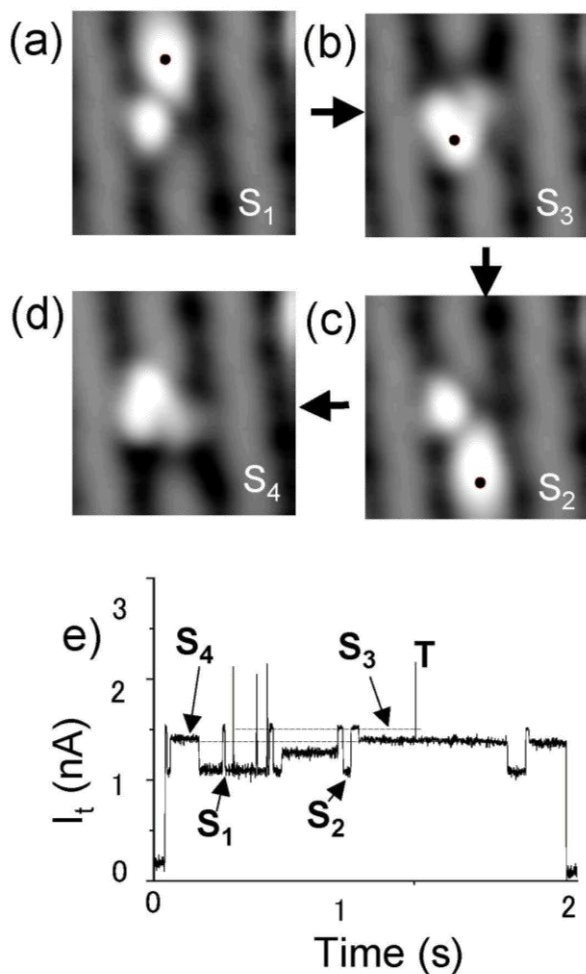


Figure 4: (23 Å by 23 Å) STM topographies of the four stable configurations of the biphenyl molecule after its H atom desorption. (a) and (c) depict the S_1 and S_2 configurations respectively. (b) and (d) show the two new stable S_3 and S_4 configurations. The series a) to d) (following the arrows) is a succession of molecular manipulations of the multistable molecule using negative surface pulses ($V_s = -3.0$ V) applied at the indicated black dots.

have found that the switching yields for excitation pulses of -3.5 V are increased after hydrogen desorption by a factor 3 to 50 depending on the excitation position and the molecular movement ($S_1 \rightarrow S_2$ or $S_1 \rightarrow T$). Another interesting consequence of the hydrogen desorption is that the molecule can now be switched (by applying a pulse voltage ($V_s = -3.5$ V)) into any of the four molecular configurations imaged in Figure 4. The S_1 and S_2 states are the same as before hydrogen desorption, whereas two new states (S_3 and S_4) of the molecule can be imaged with the STM. The occurrence of the four stable states (S_1 to S_4) and the transient states (T) can be seen in the tunnel curve (Figure 4e). Compared to the operation of the bistable molecule, where the biphenyl molecule could be switched only between two stable states (S_1 and S_2), the operation of the multistable molecule after hydrogen desorption is much more complicated since it can now be switched between four stable positions (S_1 , S_2 , S_3 and S_4) [8]. So far, we have found the switching of the multistable molecule to be random. A sequence of switching events is shown in Figure 4. Nevertheless, further studies as a function of the pulse voltage and the position of the STM tip are required for a more complete understanding of the multistable molecule operation. These

results reveal that a precise control of each atom position around the molecule needs to be achieved if a quantitative operation of a molecular device is required. This single atom sensitivity can give rise to very interesting perspectives for engineering the performance of a molecular device. One can expect being able to control, by single atom manipulation, not only the operation of a molecular device but moreover its intrinsic performance (e.g the switching frequency or the number of stable states).

Conclusion

We have shown two examples demonstrating that the picometer-scale precision is required to properly control the operation of a single molecule. The localization of charge injection inside the molecule with a picometer-scale precision offers an interesting method to control the charge transfer through the molecule. This has been evidenced here by studying inelastic charge transfert. However, one can anticipate that this will be valid also to control elastic charge transfert. The second example demonstrates that the intrinsic performances of a single molecule device can be

controlled by manipulating a single atom nearby. These examples reveal the complexity of molecular electronics. However, they offer interesting grounds to develop new concepts for single molecule electronics.

References

- [1] C. Durkan, M. A. Schneider and M. Weiland, *J. Appl. Phys.* 86, 1280 (1999).
- [2] M. Galperin, M. A. Ratner, A. Nitzan and A. Troisi, *Science* 319, 1056 (2008).
- [3] E. Lörtscher, J.W. Cizek, J. Tour and H. Riel, *Small* 2, 973 (2006).
- [4] M. Di Ventra, S.T. Pantelides and N. D. Lang, *Phys. Rev. Lett.* 84, 979 (2000).
- [5] M. Lastapis, M. Martin, D. Riedel, L. Hellner, G. Comtet and G. Dujardin, *Science* 308, 1000 (2005).
- [6] R. A. Wolkow, G. P. Lopinski, D. J. Moffart, *Surf. Sci.* 416, 1107 (1998).
- [7] H. Rabitz, R. de Vivie-Riedle, M. Motzkuz and K. Kompa, *Science* 288, 824 (2000).
- [8] M. Martin, M. Lastapis, D. Riedel, G. Dujardin, M. Mamatkulov, L. Stauffer and P. Sonnet, *Phys. Rev. Lett.* 97, 216103 (2006).

2b. Semi-classical

Semi-classical OR, AND, XOR molecule logic gate circuits

M. Hliwa^{1,2}, N. Jlidat² and C. Joachim¹

¹Centre d'Elaboration de Matériaux et d'Etudes Structurales (CEMES-CNRS)
29, rue Jeanne Marvig, BP 94347, 31055 Toulouse Cedex 4, France

²Faculté des Sciences Ben M'Sik, Université Hassan II- Mohammédia
BP 7955, Sidi Othman, Casablanca, Morocco

Introduction

To construct an electronic circuit, electronic devices are normally interconnected in series and parallel following the Kirchhoff electrical circuit laws. For mono-molecular electronics, one can follow the same: (1) to design specific chemical group able to perform like a wire, a rectifier, a switch and even like a transistor and (2) to create an intramolecular complex logic function by covalently bonding all those chemical groups together. For such an intramolecular architecture, there are 2 main options: to copy the standard electronic circuit architecture inside a molecule or to use quantum intramolecular circuit properties to design the circuit. For standard circuit architecture, new and more efficient intramolecular diode have been designed and molecule integrated to form a molecule-OR and a molecule-NAND. For the molecule-XOR, intramolecular inelastic effects are necessary to provide the carry instead of using a zener diode as usually proposed in the literature. Finally, we have shown that already for a simple molecule OR gate, it is better to abandon the usual diode logic approach and to play with intramolecular electron transfer property to design better molecule logic while keeping a circuit design.

An efficient intramolecular diode logic

Standard molecule OR and AND diode logic have already been proposed in the literature. But the rectifier chemical groups used in those design were the original Aviram-Ratner rectifier. The electron transfer rate through such long molecule is too small to permit the design of an intramolecular circuit larger than an AND

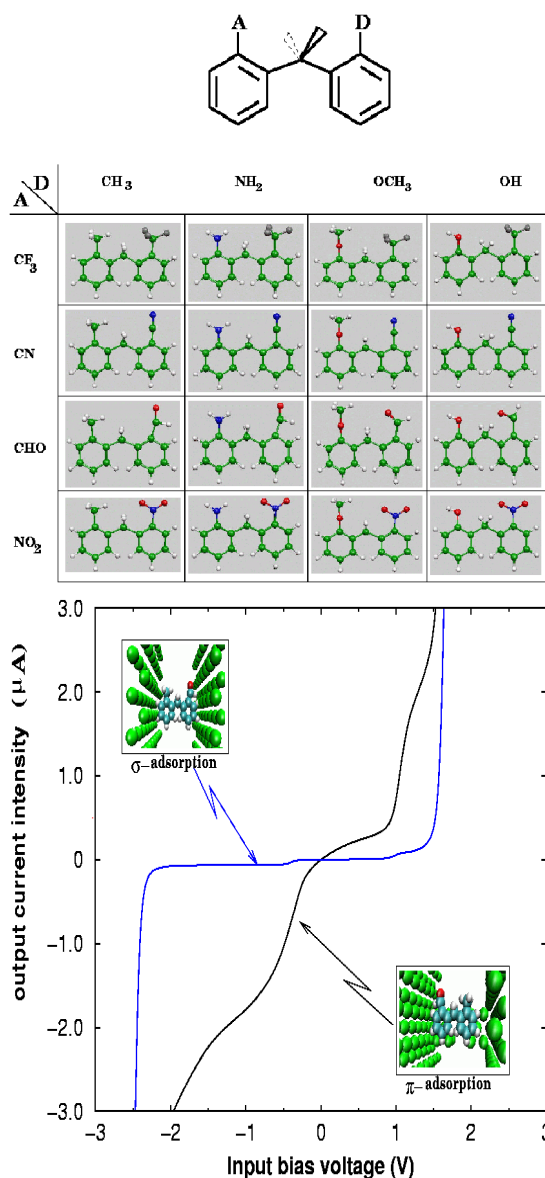


Figure 1: A systematic study of the D- σ -A molecular rectifiers using a simple CH_2 ligand between the D and A chemical group. (b) The I-V characteristics of our best molecular rectifier for a σ or a π adsorption. The tunnel current is now reaching $1 \mu\text{A}$ in the rectification Voltage range.

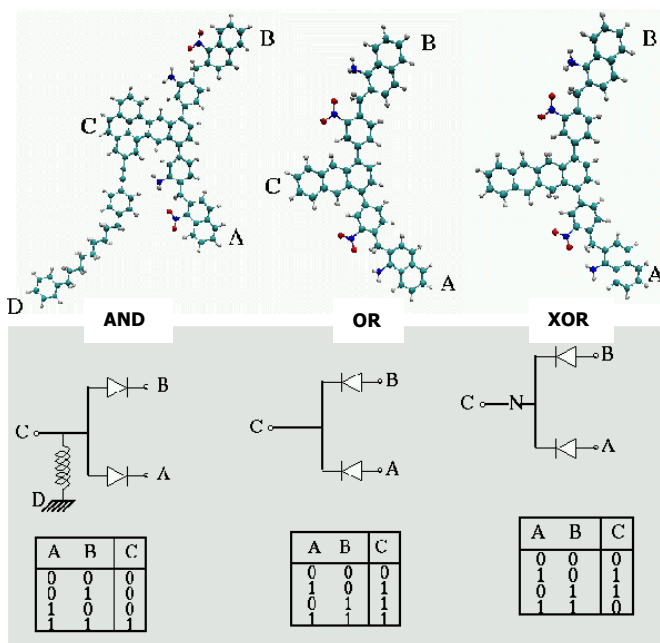


Figure 2: Intramolecular tunnel circuit implantation of an AND, OR and XOR logic gate using a full diode logic implantation. A, B, C and D are the part of the molecule chemisorbed on the atomic scale electrode (See one example below using our N-ESQC routine)

molecule. We have selected very short Donor-Acceptor (D-A) rectifiers where the electronic decoupling between D and A is obtained via a very short saturated bridge. Our best one is with A = NO₂ and D = NH₂ as presented in Figure 1.

Having a very efficient molecular rectifier, two of those were integrated in a single molecule to recover the OR and AND functions within one molecule and to attempt the design of an XOR gate as proposed by the Mitre corporation. All the calculation were performed using our N-ESQC calculation technique at the Extended Huckel molecular orbital level of approximation taking into account the full valence molecular orbital of the molecule positioned between N electrodes. For the OR and AND gates, new molecules were designed as compared with

our previous design using the Aviram-Ratner. For the XOR, we have followed the Mitre corporation design as presented in Figure 2.

To assess each design, we have calculated the logic surface of each molecular logic gate. The logic surface is just the output current as a function of the 2 input voltages on the molecule. As presented in Figure 2, only the OR molecular gate is working almost fine. There are 2 logic level "1". But a good external threshold device will clear this problem. Furthermore and as expected, the running current of this OR gate is around 100 nA instead of 10 fA in the previous design. This is not the case for the AND and XOR molecule logic gates. For the AND gate, the problem comes from a bad optimisation of the 4th D branch supposed to mimic the output resistance in a diode logic approach. For the XOR gate, the proposed Mitre molecule was tested and compared to our own design (Figure 3). The Mitre idea of mimicking a zener diode by an intramolecular asymmetric tunnel barrier is not working. This demonstrates the limit of implementing intramolecular diode logic in a single molecule.

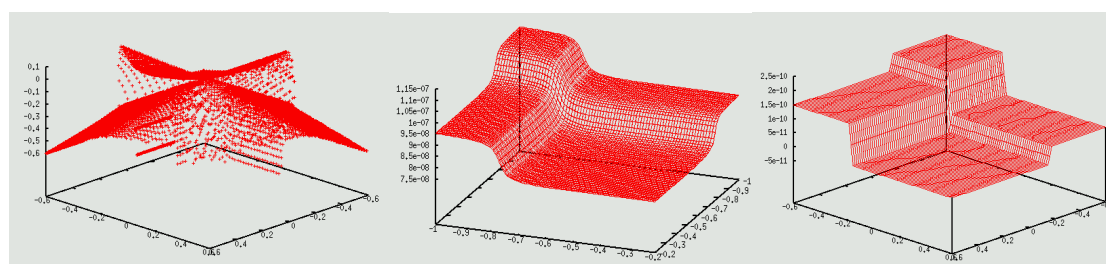


Figure 3: The surface logic of the AND, OR and XOR gate molecule given in Fig. 2. Only the OR surface (middle) is almost the answer of an OR gate.



A semi-classical XOR molecule

Since the standard diode logic approach is not working for logic gates more complex than an OR gate, we have explored inelastic effects to realise the threshold detection function required for an XOR gate. The intramolecular XOR design is based on diode logics, bonding together 2 molecular rectifiers to fulfil the $a+b$ operation followed in series by an intramolecular gating effect based on the rotation of a short molecular wire activated by the $a+b$ tunnelling current as formally illustrated in Figure 4. The main difference with an electrical circuit is that from the electrodes 2, 3 to the ground 1 on one side and to the XOR output 4 on the other side, there is no voltage drop inside the molecule at nodes 5 or 6. This peculiar property leads to molecule OR gates with 2 different current intensity outputs assigned to the same output logic status "1". In the following and as illustrated in Figure 4, this inconvenience was transformed in an advantage by using this large output current intensity to force the gate output current to zero when $(a,b)=(1,1)$. The inelastic tunnel effect has been studied in detail for the XOR gate to work realistically.

The number of electrons transferred per second through the central pyrene controls now its conformation relative to the planar axis of the 3 electrode tunnel junction. A small variation of the pyrene rotation angle Φ has a large effect on the tunnelling current circulating in the output 1-4 meshes. The voltage source V of this 1-4 mesh brings the energy required to set-up the current intensity I_{14} of the XOR output. This mesh is independent of the 3-1 and 2-1 input meshes driven by the voltage input V_2 and V_3 . For the $\Phi = 120^\circ$ pyrene equilibrium conformation, the N-ESQC $T_{12}(E)$ spectrum (respectively the $T_{13}(E)$ spectrum) from nano-electrode 1 to nano-electrode 2 (respectively from 1 to 3) accumulates all the MO resonances of the pyrene and of both molecular rectifiers. The LUMO is almost degenerated and corresponds to the π^* nitrophenyl MO of the 2 molecular rectifiers. On the HOMO side, the incursion of the π pyrene and hybrid pyrene-phenyl MO is an indication of the difficulty to pill up many classical functions (here 2 rectifiers and one rotor) in a single molecule and expecting at the same time to preserve intact their individuality in the overall electronic structure of the final molecule. The HOMO of the molecule-XOR is now a π pyrene MO and not a rectifier MO. As a consequence, an almost symmetric $T_{12}(E)$ spectrum arises around E_f from the HOMO to the LUMO resonances. At 120° , the mixing between all those states

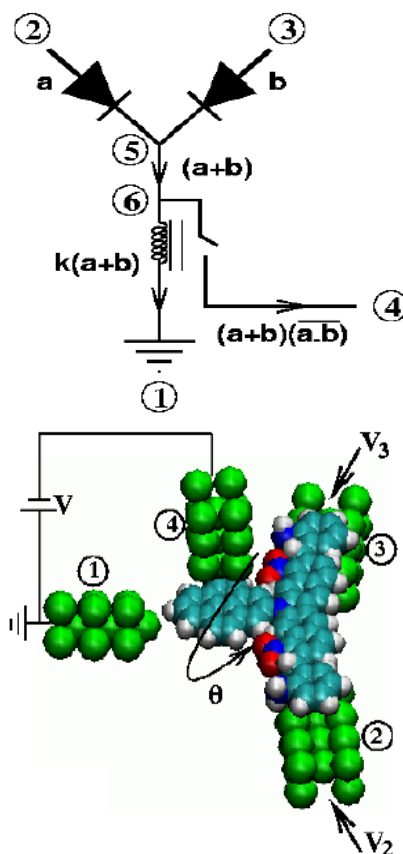


Figure 4: Design principle of the XOR molecular gate and its proposed implementation with a 4 terminal tunnel junction properly interconnecting a single molecule.

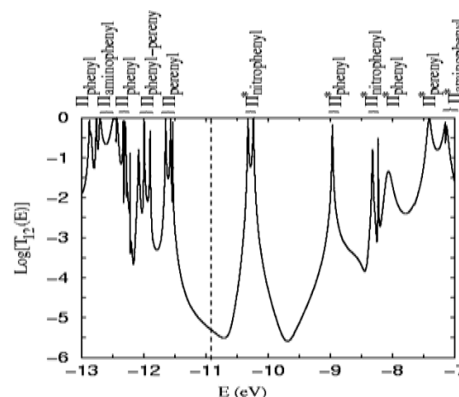


Figure 5: The $T(E)$ spectrum of the full gate from the nano-electrode 2 to the ground 1. Notice how the HOMO is no more a rectifier state and how $T(E)$ is almost symmetric around the Fermi level indicated by the dashed line.

is less pronounced than in a planar conformation which preserves a bit of the rectification effect.

Starting at the equilibrium $\Phi = 120^\circ$ conformation for $V_2 = V_3 = 0.0$ V where $I_{14}(120^\circ)$ encodes the "0" logic output depending on the V bias voltage, the dynamic equilibrium Φ is determined by I_c as a function of V_2 and V_3 . A semi-classical inelastic tunnelling approach was used to model how I_c controls this pyrene conformation change. In this approach, the tunnelling current intensity calculated using the N-ESQC technique provides the necessary energy to force the rotation of the pyrene fragment. $I_c(\Phi)$ is maximum for $\Phi = 165^\circ$. But this is not the pyrene equilibrium angle at $\Phi = 120^\circ$. Therefore, $I_c(\Phi)$ drives the dynamic equilibrium angle up to an angle where the inelastic force equilibrates with the gradient of the rotation potential energy curve of the molecule. The position of 4 was optimised in such a way that for the pyrene inelastic tunnel constants and for V_2 or (exclusive) V_3 larger than 400 mV, the Φ value where both forces equilibrate is around 135° . For the nano-electrodes optimised position presented in Figure 4, this leads to the $I_{14}(\Phi)$ local maximum encoding for a "1". When now both V_2 and V_3 are reaching 400 mV, I_c doubles just by superposing the 2 meshes 1-2 and 1-3 current via the common pyrene branch. The dynamic equilibrium conformation is shifted toward $\Phi = 157^\circ$ corresponding to the second $I_{14}(\Phi)$ minimum encoding for a "0".

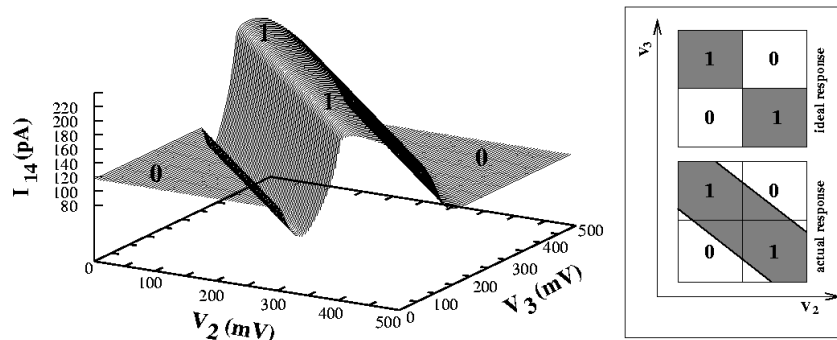


Figure 6: The surface logic of the Molecule XOR proposed in Fig. 2. The ideal XOR response and its actual one are presented from the top for comparison.

The full surface logic of the P1.1 molecule-XOR is presented in Figure 6. The "0" output is corresponding to an I_{14} current around 100 pA for $V = 100$ mV. The "1" plateau is large enough to stabilise a I_{14} current around 220 pA for $V = 100$ mV. The difference between "0" and "1" is large enough to be detectable even if as presented in the Figure 6 insert.

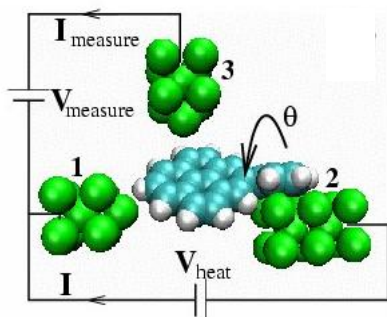


Figure 7: Atomic scale implantation of a 3 electrode detector based on the rotation of the pyrene angle as a function of incident tunnelling current intensity. Electrode 3 is here to detect the pyrene rotation.

Our design deforms the ideal XOR response logic and therefore reduces the immunity of the molecule-XOR gate to input voltage noise especially for the "0" inputs.

To support the design this XOR intramolecular logic gates where a non-linear effect is clearly required we have considered vibrational and rotational excitation effected by the tunnelling electrons. The calculation technique developed links the elementary electron transfer phenomenon through the molecule to its vibrational degrees of freedom. A time dependant generalisation of the Davydov vibronic Hamiltonian is first used.

The time dependence is compulsory to respect the detail quantum time dependent process of the super-exchange mechanism through the molecule. Then, two averaging procedures are done. One for the electron transfer process to get the tunnel current intensity using the Erhenfest theorem and one for the mechanical degree of freedom of the molecule. This is self-consistent process between the electronic and the mechanical degree of freedom. The outcome is the average geometrical change of the molecule as a function of the tunnelling current intensity. This is a generalisation of the procedure introduced for a single Xe atom tunnelling heating process. The complication with a large molecule is to determine what are the active and not active mechanical degrees of freedom during an electron transfer process since the selection rules are not the same as if the electrons were transported ballistically through the molecule.

Before applying our technique to the XOR molecule gate presented in Figure 4 and as a first application of our I-ESQC approach, a simple 3 terminal single electron detector molecule interacting with 3 electrodes was studied as presented in Figure 7. The multi-channel multi-electrode problem being calculated using our N-ESQC routine with a full valence molecular orbital description of the junction.

We have calculated 2 essential characteristics of the 3 terminal device presented in Figure 7: 1) The detail mechanics of the pyrene rotation with and without the third electrode using a fairly good precision MP2 (6-31G) quantum chemistry technique and 2) the electronic transparency of the molecule as a function of the pyrene torsion angle using the N-ESQC technique (See Figure 8). Those 2 characteristics are used to self consistently calculate the inelastic induced conformation

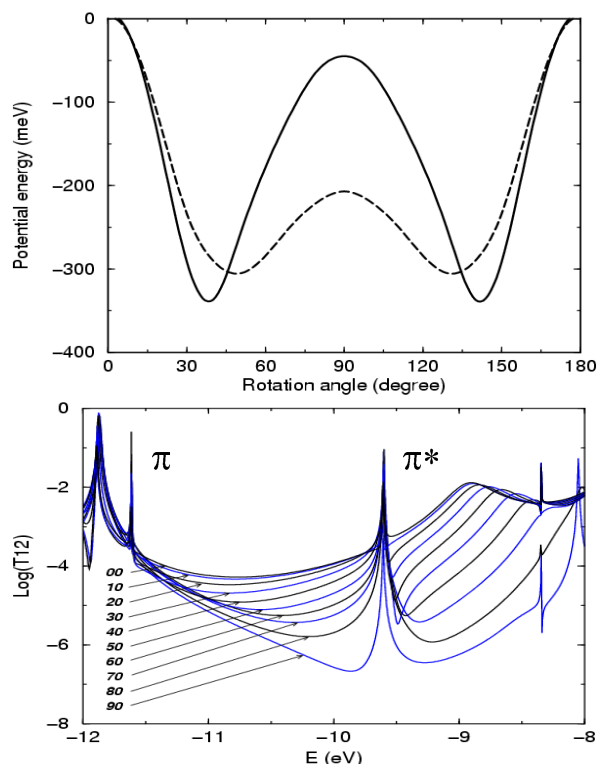


Figure 8: (a) Variation of the molecule potential energy as a function of the pyrene rotation angle with and without the detection tip on. (b) Electronic transparency variation through the full molecule as a function of the pyrene rotation angle.

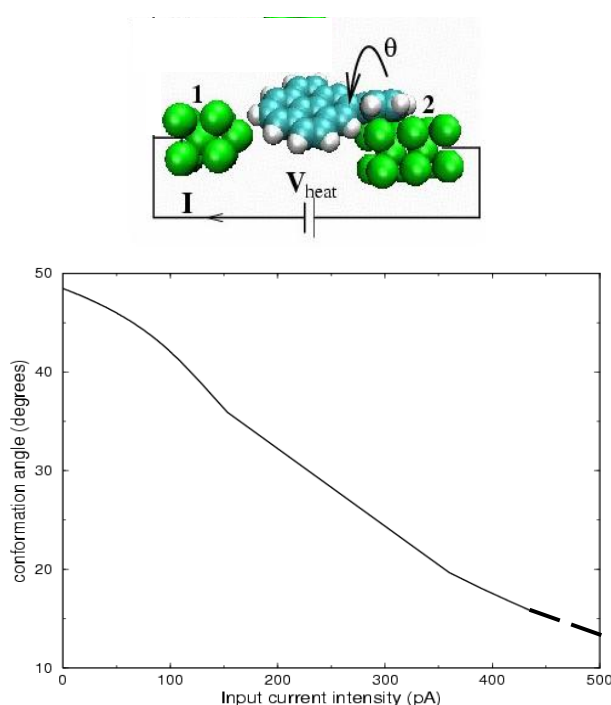


Figure 9: Variation of the pyrene rotation angle as a function of tunneling current intensity passing through the molecule. The 2 electrodes atomic scale implantation is also presented.

change of the molecule in a semi-classical approximation.

One curve of interest is the permanent rotation angle of the pyrene as a function of the current intensity (Figure 9). At very low tunnel current intensity and starting at the equilibrium 48° equilibrium conformation, this curve is almost linear until saturation occurs due to large spring constant of the pyrene rotation. This model was used to calculate the logic surface of the molecule logic gate presented in Figure 4.

Using intramolecular circuit rules to design a simple OR gate

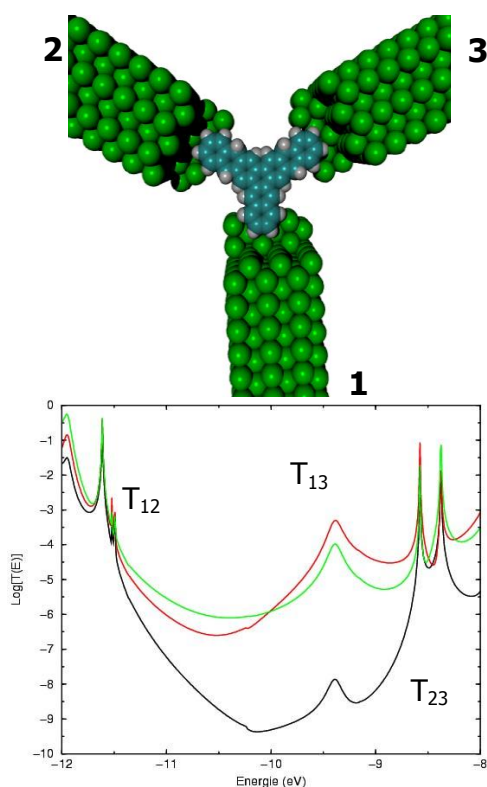


Figure 10: The $T(E)$ spectrum of a simple molecule-OR designed without any molecular rectifier chemical groups. There is a conjugation break along the branch 2 and 3 which is creating a faster tunnelling decay with length between 2 and 3 than between 2 and 1 (3 and 1).

A first consequence of the work on the XOR molecule above is that it is very difficult to pill up in a single molecule many classical logic function and to recover the detail spectrum of each classical part in the $T(E)$ spectrum of the final molecule. Pilling up MO resonances of different elementary logic functions like wire, rectifiers and switches produces a $T(E)$ spectrum formally equivalent to the one of the XOR where the rectifiers resonances are no more the one which play a role in the molecule XOR. For a complex logic function, it seems more "natural" to pill up those resonances playing with interference effects than to simply superpose those levels.

A second consequence comes also from the absence of the HOMO rectifier state in determining the overall logic performance of the semi-classical molecule XOR (Figure 5). Since a rectification effect is not required to get the XOR, we have decided to explore the design of an OR function without any rectifier. This is not possible with standard electrical classical circuit, but very easy to get inside a molecule and in the tunnel regime.

The explanation for an OR design without any molecular rectifiers is the following. In a standard electrical circuit, the two rectifiers of an OR gate are required to avoid any direct current from one input to the other in a 01 or

10 input configuration. But with molecular wires, the tunnelling current decay exponentially with an increase of the length of the wire. Therefore and relative to the output electrode, a simple way to isolate the 2 inputs whatever the input logic configuration is to play with this exponential decay which must be much faster between the 2 inputs than between one input and the output. The $T(E)$ spectrum of a simple molecule designed following this principle is presented in Figure 10. In Figure 11, a simple molecule without any break of its conjugation is presented. Here, all the 3 $T_{ij}(E)$ are equivalent. A series of those molecules are now under synthesis.

Conclusion

A molecule OR logic gate built by assembling two Ratner-Aviram diodes delivers a too small output current intensity (in order of fA, when the input branches are biased up to 100 mV) to be used as building block for a mono-molecular logic device like for

example to construct a half-adder or a full one-bit adder. This is the main limitation of a semi-classical approach of monomolecular electronics. By reducing the molecular diode length, we have designed a molecular logic gate where the output current intensity is of order of few ten nA (for input applied bias voltage of 100mV). However, this improvement is not sufficient for integrating these gate inside a large logic circuits and to obtain a measurable output current intensity.

Notice that the output current intensity does not depend only on the molecular length of the circuit but also on the intrinsic electronic structure of each of these components, on the degree of molecular orbital mixing and on the amplitude of the electronic clouds associated with these components. An electronic component chemical group (diode, or elementary logic gate) embedded inside a molecule can play the role assigned to it. But in this case, its structural and electronic identity must be protected inside the molecule chemical structure. It can be done only by inserting insulating aliphatic chains in between these chemical groups. But this separation goes against the necessity of a delocalization of the electronic cloud over the full molecule to achieve a measurable output current intensity.

The electronic interactions between the molecular orbitals of different chemical groups (diodes, branches...) of a molecule circuit induces (by superposition of the symmetry adapted levels) interference phenomena, resonances and $T(E)$ transmission peak overlapping in the valence region of the electronic spectrum. This modifies in a drastic way the electronic behaviour of the individual chemical group initially optimized to perform a given logic function inside a large molecule. These modifications have an incidence on the nature of the frontier orbitals, on the width of the homo-lumo energy gap and then on the shape of the logic responses.

These remarks bring us to the final conclusion that the assembling of a circuit chemical group by chemical group expecting the larger molecule to behave like a complex logic function is not working for molecular electronics. New strategies must be followed instead of forcing a molecule to mimic the shape of an electronic circuit.

References:

- [1] A. Aviram and M. A. Ratner; Chem. Phys. Lett. 29 (1974) 277.
- [2] M. Magoga and C. Joachim; Phys. Rev. B59 (1999) 16011.
- [3] J. C. Ellenbogen and J. C. Love; IEEE 88 (2000) 386.
- [4] M. Hliwa and C. Joachim, Physical Review B, 65, 085406 (2002).
- [5] S. Ami and C. Joachim, Physical Review B, 65, 155419 (2002).
- [6] S. Ami, M. Hliwa and C. Joachim; Chem. Phys. Lett. 367 (2003) 662.
- [7] M. Hliwa, S. Ami & C. Joachim, Chem. Phys. Lett., 425, 356 (2006).
- [8] N. Jlidat, M. Hliwa and C. Joachim, Chem. Phys. Lett., 451, 270 (2008).
- [9] N. Jlidat, M. Hliwa and C. Joachim, Chem. Phys. Lett., 470, 275 (2009).

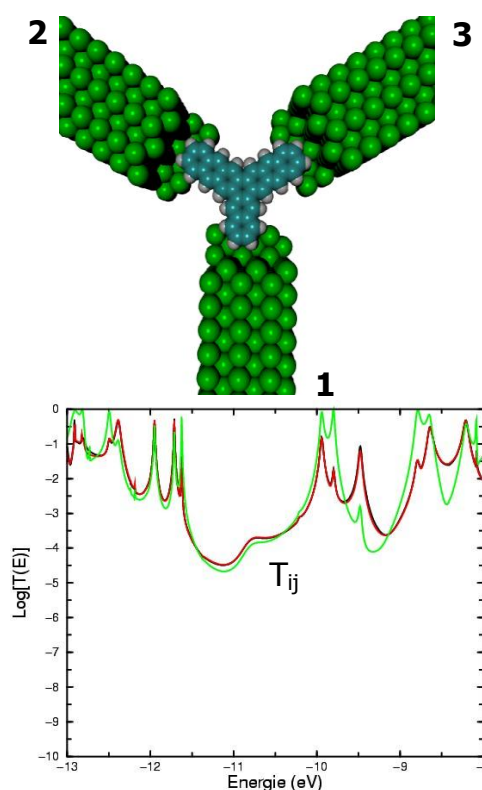


Figure 11: The $T(E)$ spectrum of a simple molecule designed without any molecular rectifier chemical groups nor any conjugation breaking. As a consequence there is no independence of the 2 inputs in comparison with the Figure 10 molecule.

2c. Quantum (qubits and QHC)

Geometrical Approach of Quantum Hamiltonian Computer

N. Renaud¹, P. Solinas², R. Mosseri² and C. Joachim¹

¹ CEMES, 29 rue Jeanne Marvig, 31055 Toulouse, France

² LPTMC, CNRS et UPMC, 4 Place Jussieu, 75252 Paris, France

1 Introduction

Recent progresses in atomic-scale technologies are opening the possibility to control the intrinsic time evolution of a unique quantum system like a single molecule. This evolution, described by the time dependant Schrödinger equation, can be used to realize a quantum logic gate. In one design studied by Pico-Inside, the energy necessary for the quantum system to compute is brought by the preparation of a non-stationary state, the data are encoded directly in the Hamiltonian and the results of the calculation are measured on the occupation probability of the system on the target states beforehand defined [1] [2] .

In this Quantum Hamiltonian Computer (QHC) approach, it can be easily shown that, in order to compute, the system requires at least three quantum states. A complete representation of the evolution of this system on its quantum state space is required to appreciate how the quantum trajectory is controlled by the input. Without losing information, the Bloch representation can only map the evolution of two states systems. In Pico-Inside we explored an other approach, adapted from a representation originally proposed by E. Majorana in 1932 [4] in the context of high spin systems, and which allows to completely describe the evolution of a N states system.

2 Design of a Quantum Hamiltonian Logic Gate

Like any quantum machine, a QHC needs energy to work [3]. An elegant solution to supply this energy is to initially prepare the system, described by a Hamiltonian H in a non stationary state $|\Psi_0\rangle$ increasing its energy with respect to its ground state energy. This state can be written on the eigenbasis of the system, $\{|\phi_1\rangle \dots |\phi_n\rangle \dots\}$, as:

$$|\psi_0\rangle = \sum_n a_n(0) |\phi_n\rangle$$

The system will then evolve spontaneously, following the time dependant Schrödinger equation:

$$i\hbar \frac{d|\psi(t)\rangle}{dt} = \mathcal{H}|\psi(t)\rangle$$

leading to the standard expression for $|\Psi(t)\rangle$:

$$|\psi(t)\rangle = e^{-i\mathcal{H}t/\hbar} |\psi_0\rangle = \mathcal{U}(t) |\psi_0\rangle$$

where $U(t)$ is the evolution operator which drives the evolution through the Hilbert space. For this evolution to allow for a computation process, the input data have to be encoded somewhere in the system. This can be done either in the Hamiltonian H or in the initial state $|\Psi_0\rangle$. In the QHC approach, the first strategy is followed: the initial state is fixed (among the local basis states) whereas the Hamiltonian $H(\theta_1, \theta_2, \dots, \theta_n)$ depends of the input data θ_i . Starting from this constant initial state, the system therefore experiences different time evolutions (distinct paths through the Hilbert space) depending on the Hamiltonian. This is in sharp contrast with the well known

quantum computer qubit approach where unitary transforms associated with the different logical gates are driven by constant Hamiltonians, while the input data are coded in the initial state $|\Psi_0(\theta_1, \theta_2, \dots, \theta_n)\rangle$ (in addition, handling linear combination of basis states is central in that approach).

The simplest way in which the result of the computation could be read from the system time evolution is to measure the population, $P(t)$, of a beforehand defined target state, at a specific measurement time (called here t_m). Besides, periodic evolutions should allow to perform the measurement not only at t_m but at each odd multiple of t_m .

$$P(t_m) = |\langle \psi_{target} | \mathcal{U}(\Theta_1, \Theta_2 \dots \Theta_n)((2k + 1)t_m) | \psi_0 \rangle|^2$$

One expects for instance that the population of the target state reaches exactly one, whenever the (logical) result of the computation is expected to be one, and be zero otherwise. Note once again that the above expression supposes that one has been able to define a system which behaves periodically with a quantum state oscillation between the initial and the target state.

The general scheme of a quantum Hamiltonian computer is illustrated in Figure 1.

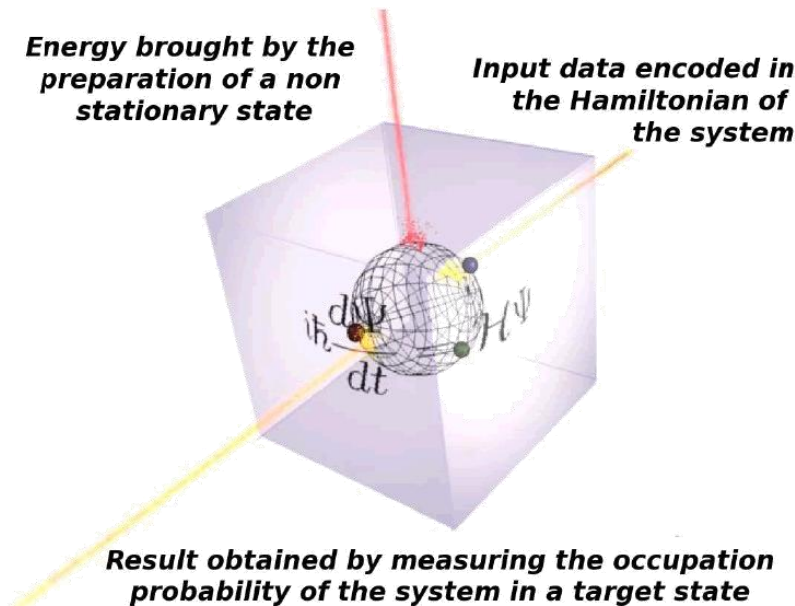


Figure 1: General scheme for a quantum Hamiltonian computer

3 Realisation of a quantum Hamiltonian XOR gate

input 1	input 2	output
0	0	0
0	1	1
1	0	1
1	1	0

Figure 2: Truth table of a XOR gate

To give a clear example of a QHC, we present here a simple analytical model of an XOR gate embodied in a four level system. The truth table of a such gate is recalled on Figure 2. We have studied the four level quantum system shown in Figure 3 represented by the Hamiltonian 5, where μ and e are fixed parameters, and α and β are the two parameters which will be used to encode the input data of the computation.

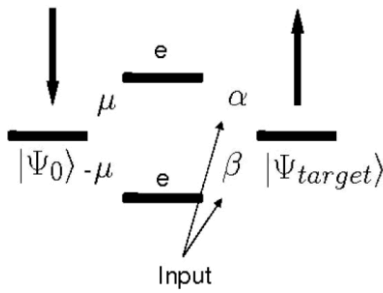


Figure 3: Four level system chosen to perform a XOR gate

The initial state is the first state of the basis and the target state is the last one. The input data can be either encoded in the phase of the two parameters α and β or in the strength of those couplings. In the following we present Hamiltonian \mathcal{H} generating periodic evolution leading to $P(t_m) = 1$. It can be proved that a periodic evolution is obtained for commensurate eigenvalues of the Hamiltonian.

$$\mathcal{H} = \hbar\omega \begin{pmatrix} 0 & \mu & -\mu & 0 \\ \mu & e & 0 & \alpha \\ -\mu & 0 & e & \beta \\ 0 & \alpha & \beta & 0 \end{pmatrix}$$

3.1 Encoding in the phase of the couplings

If one only allows for phase control in the Hamiltonian entries, the inputs parameters can be written as: $\alpha = e^{i\phi_1}$ and $\beta = e^{i\phi_2}$. In this case the Hamiltonian is:

$$\mathcal{H} = \hbar\omega \begin{pmatrix} 0 & \mu & -\mu & 0 \\ \mu & e & 0 & e^{i\phi_1} \\ -\mu & 0 & e & e^{i\phi_2} \\ 0 & e^{-i\phi_1} & e^{-i\phi_2} & 0 \end{pmatrix}$$

The eigenvalues of this system are given by:

$$\lambda = \hbar\omega \frac{e}{2} \pm \frac{1}{2} \hbar\omega \sqrt{e^2 + 4\{(1 + \mu^2) \pm \sqrt{1 + \mu^4 - 2\mu^2 \cos(\phi_1 - \phi_2)}\}}$$

To simplify the study of the eigenvalues commensurability, we can impose $e=0$. Note, nevertheless, that this is not a necessary condition and equivalent results could be reached with $e \neq 0$. In the 00 and 11 configurations, so when $\phi_1 = \phi_2 = \phi$, the result of the computation must be equal to zero. In this case the eigenvalues are given by the simple formula: $\lambda = \hbar\omega 2^{1/2} [-\mu, -1, 1, \mu]$. Computing the evolution of the system of the target state we find it is never populated along the evolution. To understand this interference phenomenon we can apply a $\pi/4$ rotation defined by:

$$\mathcal{R}(\theta) = \begin{pmatrix} 1 & 0 & 0 & 0 \\ 0 & \cos(\theta) & \sin(\theta) & 0 \\ 0 & -\sin(\theta) & \cos(\theta) & 0 \\ 0 & 0 & 0 & 1 \end{pmatrix}$$

on the two central state of the Hamiltonian. This rotation does not change the initial and the final state, applying the rotation we find:

$$\tilde{\mathcal{H}} = \mathcal{R}^\dagger\left(\frac{\pi}{4}\right)\mathcal{H}\mathcal{R}\left(\frac{\pi}{4}\right) = \sqrt{2}\hbar\omega \begin{pmatrix} 0 & \mu & 0 & 0 \\ \mu & 0 & 0 & 0 \\ 0 & 0 & 0 & e^{i\phi} \\ 0 & 0 & e^{-i\phi} & 0 \end{pmatrix}$$

So as the initial and the target state are still the first and the last on the basis we clearly see here that they are not connected by the Hamiltonian. This explains why the population of the target state remains zero during the evolution. In the two others configurations, i.e when $\phi_1 \neq \phi_2$, the eigenvalues are $\lambda = \hbar\omega 2^{1/2}[-(1+\mu^2)^{1/2}, 0, 0, (1+\mu^2)^{1/2}]$, and the population of the target state must reach one. Applying the same rotation on the Hamiltonian we find:

$$\tilde{\mathcal{H}} = \frac{\hbar\omega}{\sqrt{2}} \begin{pmatrix} 0 & 2\mu & 0 & 0 \\ 2\mu & 0 & 0 & e^{i\phi_1} - e^{i\phi_2} \\ 0 & 0 & 0 & e^{i\phi_1} + e^{i\phi_2} \\ 0 & e^{-i\phi_1} - e^{-i\phi_2} & e^{-i\phi_1} + e^{-i\phi_2} & 0 \end{pmatrix}$$

So if $\phi_1 = \phi_2 + \pi$ one coupling in the Hamiltonian is null since $e^{i\phi_1} + e^{i\phi_2} = 0$ and the system is like a three states system, where the initial and the target state are coupled through a third state, this situation is represented by the Hamiltonian:

$$\tilde{\mathcal{H}} = \sqrt{2}\hbar\omega \begin{pmatrix} 0 & \mu & 0 & 0 \\ \mu & 0 & 0 & e^{i\phi} \\ 0 & 0 & 0 & 0 \\ 0 & e^{-i\phi} & 0 & 0 \end{pmatrix}$$

In this configuration a necessary condition to have a resonant evolution is to have the two modules of the coupling equals, so we must have $|\mu| = 1$. In a three state system, we already know which values of the energy of the central state gives a resonant evolution [5]. Then, we can modify the energy of the central state in the Hamiltonian and compute the inverse rotation. Doing this we find more complex Hamiltonians with resonant evolution. To give a clear example, we show on Figure 4 the evolution of the population of the target state in the four different input configurations in the simplest case, i.e where $e=0$, $\mu=1$ and the two phases can take two values 0 or π .

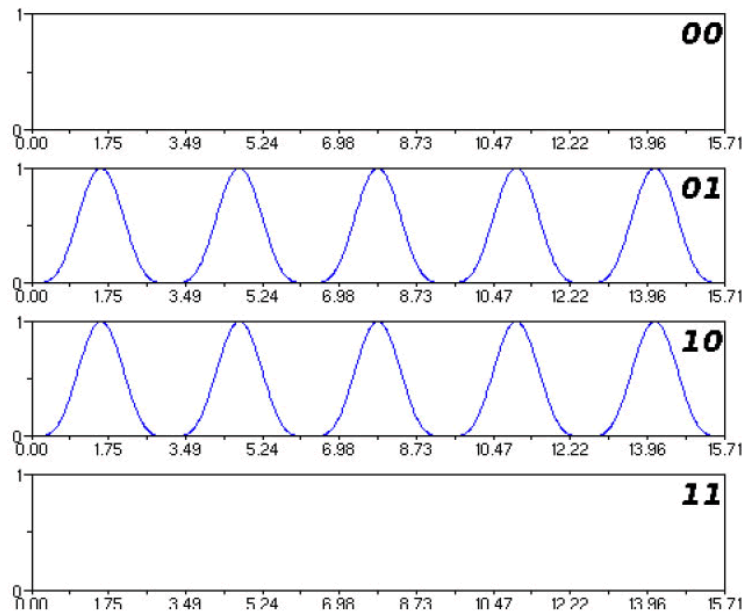


Figure 4: Evolution of the population of the target state for $\mu=1$, $e=0$, $a = e^{i\phi_1}$, $\beta = e^{i\phi_2}$ and $\phi_i = 0$ or π

The truth table of a *XOR* gate is satisfied since measuring at $t_m=(2k+1)\pi/(2\omega)$ the population of the target state will be one in the case of 01 and 10 input configurations and will be zero in the two other cases.

3.2 Encoding in the amplitude of the couplings

In the second solution, α and β take only two values 0 or 1, like their classical logic gate input counterparts. The optimisation in that case is trickier. In the 00 configuration, since the target state is not coupled with the rest of the system, its population will remain equal to zero. In the 11 configuration the system, like in the previous section, is again in a perfect interference case, so the population of the target state will remain equal to zero too. We now have to tune the 01 and the 10 configurations in such a way that the population of the target state reaches one at equal times. We first need to determine the value of μ . It can be shown that the only value of μ which allows the population of the target state to reach one is: $\mu = (1/2)^{1/2}$. We have then to find the values of e (a real quantity) which approach a periodic evolution.

$$\mathcal{H} = \hbar\omega \begin{pmatrix} 0 & \frac{1}{\sqrt{2}} & -\frac{1}{\sqrt{2}} & 0 \\ \frac{1}{\sqrt{2}} & e & 0 & \alpha \\ -\frac{1}{\sqrt{2}} & 0 & e & \beta \\ 0 & \alpha & \beta & 0 \end{pmatrix}$$

The eigenvalues of the Hamiltonian (12) are:

$$\lambda = \hbar\omega \frac{e}{2} \pm \hbar\omega \frac{\sqrt{e^2 + 2 \left[(\alpha^2 + \beta^2 + 1) \pm \sqrt{(\alpha^2 + \beta^2)^2 - 4\alpha\beta + 1} \right]}}{2}$$

In the 01 case, the eigenvalues become:

$$\lambda_{01} = \hbar\omega \frac{e}{2} \pm \hbar\omega \frac{\sqrt{e^2 + 2(2 \pm \sqrt{2})}}{2} = \begin{cases} \lambda_1 = \hbar\omega \frac{e}{2} - \hbar\omega \frac{\sqrt{e^2 + 2(2 + \sqrt{2})}}{2} \\ \lambda_2 = \hbar\omega \frac{e}{2} - \hbar\omega \frac{\sqrt{e^2 + 2(2 - \sqrt{2})}}{2} \\ \lambda_3 = \hbar\omega \frac{e}{2} + \hbar\omega \frac{\sqrt{e^2 + 2(2 - \sqrt{2})}}{2} \\ \lambda_4 = \hbar\omega \frac{e}{2} + \hbar\omega \frac{\sqrt{e^2 + 2(2 + \sqrt{2})}}{2} \end{cases}$$

For a periodic evolution, the Hamiltonian must have four commensurate eigenvalues. We can tune easily the system to present at least two commensurate eigenvalues by finding the e values which lead to:

$$p(e) = \frac{\lambda_3(e)}{\lambda_2(e)} \in \mathbb{Q}$$

Solving (15) we find:

$$e = \pm(p - 1) \sqrt{\frac{2 - \sqrt{2}}{2p}}$$

where $p \in \mathbb{Q}$. We can then optimize p such that the four eigenvalues are almost commensurate. One simple example is $p = 42/10$ leading to:

$$e = \pm 3.2 \sqrt{\frac{2 - \sqrt{2}}{8.4}}$$

which gives the eigenvalues: $\lambda \approx 1/\lambda_2 [-3.6, -1, 4.2, 6.8] \hbar\omega$, and the evolution presented in Figure 5. This evolution is quasi-periodic since λ_1 and λ_4 are not commensurate with λ_2 and λ_3 .

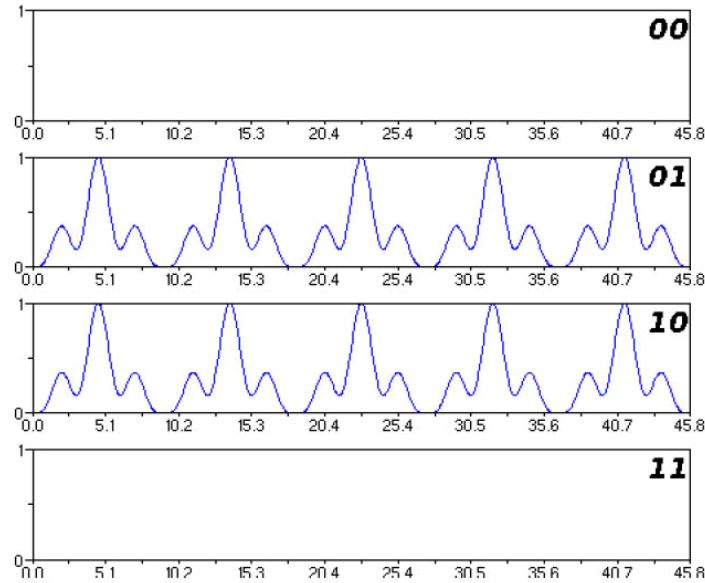


Figure 5: Evolution of the population of the target state for $\mu = 2^{-1/2}$, $e \sim 0.85$, $a = 0$ or 1 and $\beta=0$ or 1

Like in the previous case, the truth table of a *XOR* gate is satisfied, since the population of the target state reaches almost one. For instance $P(t_m) > 90\%$ in the 01 and 10 configurations for k values as big as 10^3 , with:

$$t_m = \frac{2k+1}{\omega} \frac{2\pi}{\sqrt{e^2 + 2(2+\sqrt{2})} - \sqrt{e^2 + 2(2-\sqrt{2})}} \approx \frac{2k+1}{\omega} 4.57$$

4 Study of the trajectory of a N state system by the Majorana representation

There are several ways to represent the evolution of a quantum system. For two-state systems, which are ubiquitous in physical systems, the most useful representation is the so-called *Bloch representation* where the quantum state is represented as a point on a sphere. In this case, the Hamiltonian is even displayed as a vector, threading the sphere around which the representative point precesses, in full analogy with a spin $1/2$ precessing around a magnetic field.

For N -level quantum systems, the situation is more complex. An unambiguous quantum state representation is still possible with $N-1$ points on a sphere, by considering the old, but poorly known, Majorana high spin representation. But in this case, as discussed below, the nature of the quantum state evolution can be rather complex on the sphere.

For a N -level quantum system, we associate to the state $|\Psi\rangle = \{a_1, a_2, \dots, a_N\}$ a polynomial of degree $N-1$ defined as:

$$P_\psi = \sum_{j=0}^{N-1} (-1)^j \binom{d}{j}^{\frac{1}{2}} a_{j+1} z^j = a_{N-1} \prod_{j=1}^{N-1} (z - z_j)$$

In this way the state $|\Psi\rangle$ can be associated to the $N-1$ roots of the equation $P_\psi=0$. These roots z_i ($i=1, \dots, N-1$) are complex numbers, which can be represented on a sphere by means of an inverse *stereographic projection*:

$$(x(z_i), y(z_i), z(z_i)) = \frac{1}{1 + |z_i|^2} \{\Re(z_i), \Im(z_i), 1 - |z_i|^2\}$$

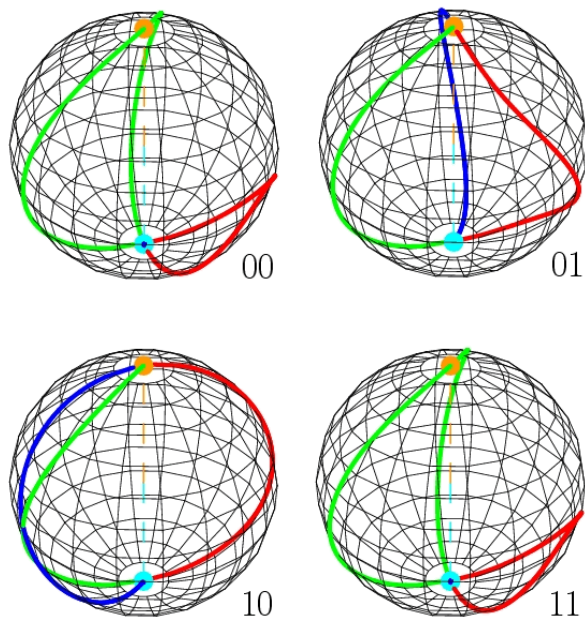


Figure 6: Evolution on the Majorana sphere for the XOR phase gate given by Hamiltonian (6). The evolution start with all the points at the south pole (cyan point) and the target state is reached when all the points are at the north pole (orange point). The curves represent the evolution of the points on the Majorana sphere.

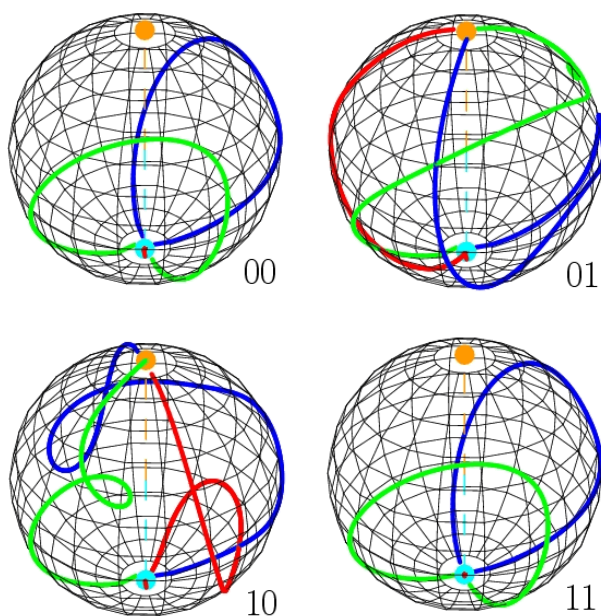


Figure 7: Evolution on the Majorana sphere for the XOR amplitude gate given by Hamiltonian (12). The evolution start with all the points at the south pole (cyan point) and the target state is reached when all the points are at the north pole (orange point). The curves represent the evolution of the points on the Majorana sphere.

Therefore, the Majorana representation allows to describe a quantum state (and its evolution) with $N-1$ points on the sphere. To show how the Majorana representation can be useful in describing the quantum evolution, we analyse in details the two logical gates constructed in section 3 in both phase and amplitude cases. Since we are dealing with a 4-level system, the quantum state is described by three points on the Majorana sphere. The initial state, with respect to the local basis used in (5), is $|\Psi_0\rangle = \{1,0,0,0\}$ while the target state is $|\Psi_{\text{target}}\rangle = \{0,0,0,1\}$. Then, starting from $|\Psi_0\rangle$, if after a defined time interval the system ends up in the target state $|\Psi_{\text{target}}\rangle$, the logical 1 value is assigned to the computation; if it does not end up in $|\Psi_{\text{target}}\rangle$ the logical 0 is assigned.

In the Majorana representation these states correspond to the (three) points gathered at the south pole ($|\Psi_0\rangle \rightarrow (0,0,-1)$) or at the north pole ($|\Psi_{\text{target}}\rangle \rightarrow (0,0,1)$). Then, for the studied gate, we expect the system to reach the final state $|\Psi_{\text{target}}\rangle$ if the logical input in the Hamiltonian (6) are (1,0) or (0,1). In terms of evolution on the Majorana sphere, we expect the three points to evolve from the south pole to the north pole, as can be seen in Figure 6.

For the logical 0 output (logical (0,0) and (1,1) inputs), the points never reach (simultaneously) the north pole, Figure 6. Note that, in these cases, only two curves are shown meaning that the third point remains at the south pole during all the evolution. We have further degree of freedom with the Majorana representation in order to simplify or to clarify some aspects of the evolution. Particularly useful is the possibility to describe the evolution in the basis which diagonalise the

Hamiltonian (5). In this case the initial and the final states no more sit at the poles, but the evolution on the Majorana sphere is simplified.

These simple examples show that the Majorana representation can be useful to describe the evolution of a quantum system. The possibility to visualise the quantum state on a sphere allows to clarify some features that in other cases should be more difficult to grasp. For example, in case of non-periodic evolution, the corresponding curves of the points on the Majorana sphere are not closed, as can be readily seen in this representation.

5 Performance of the XOR gate in phase and amplitude implantation

What is the most efficient implementation of an *XOR* gate in a QHC architecture? To answer this question we need to find a criterion which allows us to quantify the efficiency of those two approaches. One good solution is to compare the energy required for the computation. The initial non-stationary state presents an higher energy, $\langle \Psi_0 | H | \Psi_0 \rangle$ than the ground state energy E_0 of the system. Therefore the energy required for the computation is given by:

$$\Delta E = \langle \psi_0 | \mathcal{H} | \psi_0 \rangle - E_0$$

For the same computation time we can then estimate how much energy is required in the two versions in the different input configurations. The time-energy inequality $\Delta E \Delta t \geq \hbar$ can also be used as a criterion to compare the efficiency of the logic gates. We have seen that the computation time for the *XOR* phase gate is $t_m = 1/2\pi\hbar$. We have now to force the amplitude-*XOR* gate to have the same computation time. We just have to multiply its Hamiltonian by the ratio of the two computation times. Since the initial state is not the same on the eigenbasis for all the different configurations, the energy required is not the same. Following this approach we find the results shown in Figure 8.

Logical Input	E_{phase}	E_{Amp}
00	$\sqrt{2}\hbar\omega$	$1.92\hbar\omega$
01	$2\hbar\omega$	$2.75\hbar\omega$
10	$2\hbar\omega$	$2.75\hbar\omega$
11	$\sqrt{2}\hbar\omega$	$3.05\hbar\omega$

Figure 8: Energy required to perform the computation in the same time for both phase and amplitude implantation

The performance of the two implementations is quite the same even if the phase implementation is a little better in terms of energy, especially in the 00 and 01 configurations. Another interesting point is the encoding of the information in the system. In the classical case, the words used here are quite easy since they contain only two binary letters. As soon as we change the two parameters in the Hamiltonian we change its four eigenvalues, the four eigenvectors, and the development of the initial state in the eigenbasis. So eight real numbers are changed to encode the *XOR* four possible input configurations. Therefore this quantum input word contains in fact the four eigenvalues and the four coefficients of the initial state on the eigenvectors (eight in the generic case where eigenvectors may have complex coordinates). Following this procedure for the *XOR* amplitude gate we find the result shown in fig 9.

eWord	qWord							
00	-0.663	0.000	0.845	1.508	0.833	0.000	0.000	-0.552
01	-0.950	-0.264	1.109	1.795	0.571	-0.635	0.310	-0.416
10	-0.950	-0.264	1.109	1.795	-0.571	-0.635	0.310	-0.416
11	-1.053	-0.663	1.508	1.898	0.000	-0.833	0.552	0.000

Figure 9: Encoding of the input data to go from a classical word (cWord) to a quantum word (qWord)

In the tabular 9 the four first numbers of the quantum word are the eigenvalues of the system and the last four are the coefficients of the initial state on the eigenbasis. Even if we still need new tools to understand better this translation process from the classic to the quantum word, we clearly see here that the classical logic input word is turned into a complex quantum word.

6 Conclusions

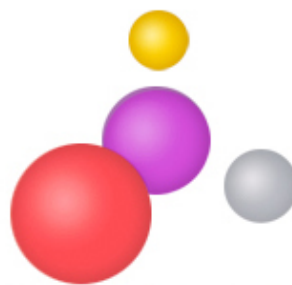
We have shown here how to design an *XOR* gate taking in account only the intrinsic quantum evolution of a three state system. The criteria of fidelity impose the system to present a periodical evolution and then commensurable eigenvalues in each input configurations. Even if finding a $M \times N$ Hamiltonian with commensurable eigenvalues is an easy task, finding an Hamiltonian $H(\theta_1, \theta_2, \dots, \theta_p)$, depending of p binary parameters with commensurable eigenvalues in each 2^p input configurations is much more complex problem. We can get around this difficulty finding quasi-periodic evolution of the population of the target state. Those kinds of evolutions are able to reach almost one and the measurement can be performed during many quasi-period of the evolution. However this periodicity problem plus the difficulty to access the exact wave function of the system at a very specific time leads, in the context of Pico-Inside, to design logic gates with others measurement process. One of those processes could be to encode the result of the computation in the frequency of the evolution of the population of the target state since we know that this frequency is related to the intensity of tunnelling current through the system.

The use of the Majorana representation provides a geometrical representation of the evolution of a general N -states system without any loss of information. Consequently it is a good tool to follow the evolution and understand the control of its trajectory by its own Hamiltonian.

References

- [1] J. Furjasek, N. Cerf, I. Duchemin, C. Joachim. Hamiltonian Logic Gates: computing inside a molecule. *International Journal of Nanoscience* 24, 161-172, 2005
- [2] I. Duchemin, C. Joachim. *A quantum digital half adder inside a single molecule*. Chem. Phys. Letter, 406, 167-172, 2005
- [3] C. Joachim. *The diving Power of the superposition principle for molecules-machines*. J. Phys. Condensed Matter, 18, S1935-S1942, 2006
- [4] E. Majorana. *Atomi orientati in campo magnetico variabile*. Il Nuovo Cimento, 9, 1932
- [5] P. Sautet, C. Joachim. *The switching ability of a three-level tight-binding system: the isolated and embedded case*. J. Phys. C: Solid State Physics, 21, 3939-3957, 1988.

3. Nano-hardware



3a. Introduction: constructing but preserving atom precision

Chemistry towards intramolecular computing

A. Gourdon

NanoSciences Group, CEMES-CNRS 29 rue J. Marvig, P.O. 94347,
F-31055 Toulouse Cedex 04, France

1 Introduction

The objective of the Pico-inside project was the exploration of the fundamental and technological aspects towards intramolecular computing. In its final design (Figure 1), the envisioned device, working at room-temperature, will comprise a large molecular circuit fixed on an insulator and connected to several nano-electrodes in ultra-clean environment, in a perfectly controlled geometry on a planar insulating substrate. Each term of this proposition is nowadays highly prospective and will obviously require extensive studies. By consequence carefully designed molecules perfectly adapted to the experiments towards these aims will have to be imagined and synthesized.

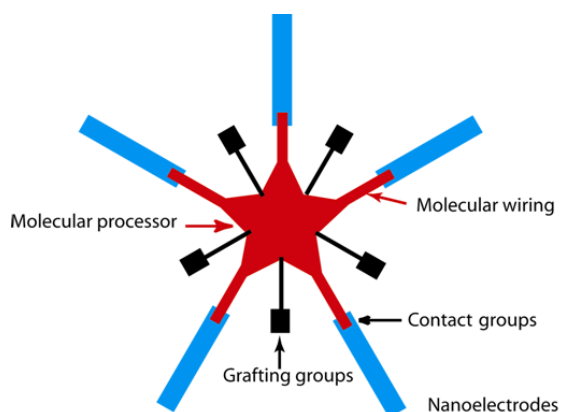


Figure 1: Schematic view of a monomolecular computing device.

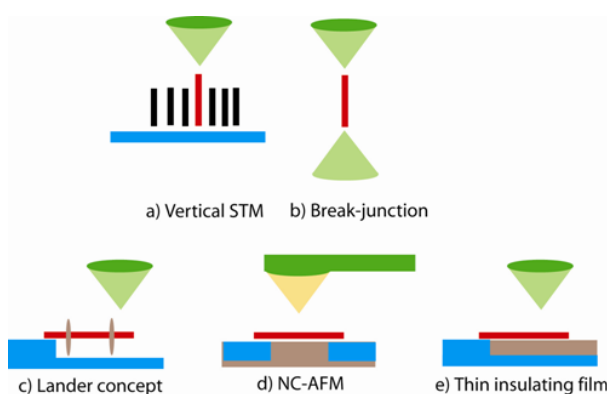


Figure 2: Experimental set-ups to measure molecular conductances and switching. The molecule is in red, the metallic substrates in blue, the tip in green and the insulators in brown. In a) and b) the molecule is parallel to the tunnel current which prevents any determination of the molecular conformation and electrode-contact geometry. The set-ups c) to d) are named planar in the text. They allow full submolecular imaging, atomic and molecular manipulation.

On the way to this complex design, the Pico-Inside consortium focus on simpler model systems, smaller molecules connected to two to three electrodes, with the objective to understand the fundamental laws at this scale and to propose theories and technological solutions. Let's now address some of the key problems to be solved:

a) Planar experiment

Clearly the design schematized in Figure 1 implies to work on planar insulating surfaces. But so far most conductance measurements and switching experiments on a single or a few molecules have been done in a "vertical" geometry with the molecule more or less perpendicular to the metallic surface (Figure 2a) and addressed by a STM tip or in a "suspended" geometry with the studied molecule between two meso-scale electrodes in break junctions (Figure 2b), holes, cross-bars...

The main draw-backs of these experimental set-ups (a and b) are first the impossibility to connect the molecule to more than 2 electrodes, but also their blind character: no control of the number of molecules, no access to the molecule conformation, to the precise molecule-electrode

contact geometries etc... But we now know that these parameters are crucial and that they rule all conductance and switching experiments. As a consequence, to tackle this problem one has to get a precise image of the molecule and its environment during or just before the measurement. Accordingly it is required to work in planar configuration, ie with set-ups in which the electrode-molecule direction is more or less parallel to the STM or AFM scanning plane so that it gives access to all physical and chemical parameters during the experiments. These constraints have led the Pico-Inside partners to focus on three experimental geometries (c to e) shown on Figure 2 for which different types of molecules have to be designed:

-STM on metallic or semi-conducting surfaces (Figure 2c) using specifically designed molecules in which the active part is lifted above the substrate by molecular spacers to reduce as much as possible the metal-molecular wire electronic coupling. This is the lander concept. It has been largely explored in the European project BUN and most parameters describing the properties of these molecules have been explored: adsorption, mobility, conductance, surface restructuring etc...[1]

But this concept is a sort of trick which allows the study of molecular devices by STM on metals but is limited to a reduced number of experiments and further advances in this domain require now to work on insulating substrates

-Non-contact AFM on bulk insulators (Figure 2d). This is the most exploratory system since even though the properties of large organic molecules on metallic surfaces have been extensively studied in the past decades [2], much less is known on molecules on insulators. This situation can be explained by several factors like (a) the less advanced development and the difficulty of NC-AFM techniques when compared with STM, but this situation is improving rapidly, (b) the lack of complete understanding of the image formation mechanism and of precise simulation tools, and (c) a more fundamental difficulty: the high mobility of organic molecules on some insulating surfaces, an even worth problem for isolated molecules. For points b and c, the solutions will arise from extensive collaborations between theoreticians, chemists and microscopists. Indeed, the complete understanding of the NC-AFM image contrast for isolated soft organic molecules, the manipulation control at sub-molecular level will necessitate series of experiments on well identified families of molecules on different substrates. The use of NC-AFM in this domain will only be effective once these parameters are fully mastered.

-STM on insulating layers/metal (Figure 2e). This intermediate solution permits to exploit all STM possibilities (imaging at atomic scale, manipulation, spectroscopy) but with reducing the molecule-surface electronic coupling by use of thin layers of insulators (salts or oxides) on metals. Several experiments in the frame of the European project CHIC (Consortium for Hamiltonian Intramolecular Computing) have shown that it was possible to image and manipulate planar polyaromatic compounds like pentacene [3] on two monolayers of sodium chloride on

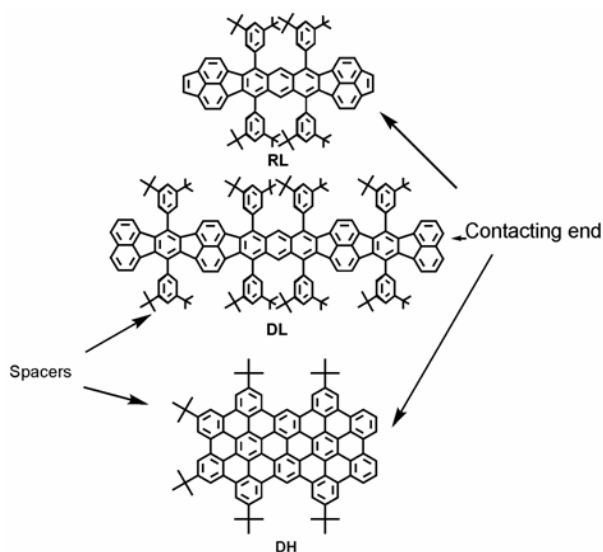


Figure 3: Examples of molecular landers. The molecules comprise an active part (the central polyaromatic hydrocarbon), 4 to 8 spacers, and one or two contacting ends.

copper. The electronic decoupling between the molecule and the copper surface is high enough to allow an imaging of the "free molecule frontier orbitals" without too much broadening. This breakthrough opens numerous possibilities like the study of molecular devices in action for instance. Several other experiments on phtalocyanine on ultrathin alumina film grown on NiAl(110) surface have also shown the potential of this geometry for the study of electronic properties of single molecules [4]. The major foreseen difficulty will be to fabricate planar, monolayer or buried, nanoelectrodes to address these molecules [5].

b) Processing unit.

Despite the theoretical design of a complete realistic molecular processor, many preliminary experiments have been carried out on smaller systems and simpler functions to test the validity of recently described new concepts such as Hamiltonian computing explored in the IST-FET programme (www.cemes.fr/chic/). For instance we will first focus on 3 terminal planar polyaromatic devices such as described by A. M. Echavarren: *Design of New Polyarene* (page 61).

c) Molecular wiring.

Although this molecular wiring is a part of the central unit, the conception of efficient high conductance branches will probably be necessary for practical reasons to maintain the nanoelectrodes at a large enough distance which will also avoid inter-electrode cross-talk. Electronic addressing of the core "molecular processor" will be done by molecular wiring which implies studies of high conductance molecular systems like the polyacenes or polyrylenes ribbons. One solution currently explored in the Pico-Inside project is the use of (hetero) helicenes. This point will be discussed by I. Stara: *Helicenes as Intriguing Objects for Chemical and Physical Studies* (page 63).

d) Contacting groups.

These molecular wires or ribbons will be addressed by nanoelectrodes and the quality of the contact was a problem tackled by the Pico-inside project since we know that reproducible addressing requires 0.05 nm precision. Two components of this problem will be studied: first, the type of molecule-electrode chemical bonding remains an open question. It is now known that the creation of a strong chemical bond between the molecule and the electrode can be detrimental to the contact conductance by localization of the involved orbitals. One solution could be the use of large physisorbed polyaromatic ribbons as suggested above. Second the precise positioning of the molecular wire with respect to the nanoelectrode atoms, possible by STM molecular manipulation for scientific exploration, will have to be replaced by self-position in large scale fabrications. One possible solution could be the development of molecular moulding which will be discussed in *Molecular moulding* (page 65). It could allow the fabrication in UHV of nanoscale electrodes directly contacting their molecular mould.

e) Immobilisation on the insulating surface.

The high mobility of organic molecules on perfect insulating surfaces at room temperature may require the addition of anchoring groups to maintain the molecular processor in a fixed place at room temperature and reduce intramolecular movements. One possible solution currently being explored is to change the surface geometry by creation of single defects or nanopits in which one or a few molecules can be trapped as described by Socoliuc et al. [6]. The main advantage of this approach is that it readily provides highly charged centres for the nucleation of a 2D ordered molecular

island. The disadvantage is that the molecules are then in a trench, surrounded by strong electric dipoles and that it will be difficult to contact them unless 2D metallic nanoelectrodes could also be formed inside the pitches. But the most general solution will be to use the molecule surface interactions by equipping the molecules with various grafting arms depending on the type of substrate (ionic, oxide, diamond). The main benefit here is that these equipments can be external branches with little electronic coupling with the active core of the molecule. Of course the central part will also be in interaction with the surface but it is foreseen that, in the case of polyaromatic hydrocarbons, this molecule-surface interaction will be significantly weaker than chemisorbed groups or highly polar arms. Therefore experiments on the mobility of series of molecules on various substrates can be decoupled from those on the "molecular processor" which simplifies the design of molecular benchmarks.

f) Ultra-clean environment.

Using a single molecule in a perfectly controlled way obviously necessitates working in ultra-clean environment. So far, a large majority of the conductance experiments described in the literature have been carried out between ductile gold electrodes (or tips) on self-assembled monolayers of organic thiols obtained by dipping electrodes in organic solutions. Most of the time, the molecule being studied is inserted in the self-assembled monolayer by chemical substitution of one or some alkyl thiols. Obviously these chains prone to substitution are the mobile ones, those bonded to defects, step-edges, grain boundaries for instance and not those nicely packing on the flat parts of the surface. And the inserted studied molecule is then loosely bonded to the substrate and it has been shown that this bond-formation/bond-breaking mechanism was the cause of most blinking or switching observations. Furthermore most measurements are done in air at room temperature or in low vacuum, environment for which even partially hydrophobic surfaces are covered with several nanometers of water. Many other potential problems have also been identified like the SAM reorganisation under applied potential, the formation of metallic filaments between electrodes etc, etc..In these conditions it is exceedingly difficult to extract significant, unquestionable laws from poorly reproducible experiments.

Therefore, one of the specifications of the Pico-Inside project was to carry out experiments in UHV on ultra-clean surfaces and of course this point transfers several constraints on the chemical design.

References

- [1] F. Moresco and A. Gourdon Proc. Natl. Acad. Sci. USA 2005, 102(25), 8809-8814 and references therein.
- [2] F. Rosei, M. Schunack, Y. Naitoh, Ping Jiang, A. Gourdon, E. Laegsgaard, I. Stensgaard, C. Joachim, F. Besenbacher ProG Surf. Sci., (2003), 71, 95-146.
- [3] J. Repp and G. Meyer, S. M. Stojkovic, A. Gourdon, and C. Joachim Phys. Rev. Letters 2005, 94, 026803 1-4.
- [4] G. Mikaelian, N. Ogawa, X. W. Tu and W. Ho, J. Chem. Phys. 2006, 124, 131101 and references therein.
- [5] D. Martrou, H. Guo, T. Zambelli, L. Guiraud, S. Gauthier and C. Joachim E-nano newsletter 2006, 3, 27-30.
- [6] A. Socoliuc, O. Pfeiffer, S. Maier, L. Zimmerli, E. Gnecco, E. Meyer, L. Nony, R. Bennewitz E-nano newsletter 2006, 3, 22-24.

3b. Chemistry

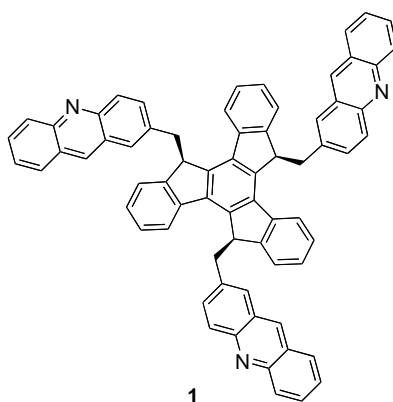
Design of New Polyarenes

P. Mendoza, C. H. M. Amijs and A. M. Echavarren

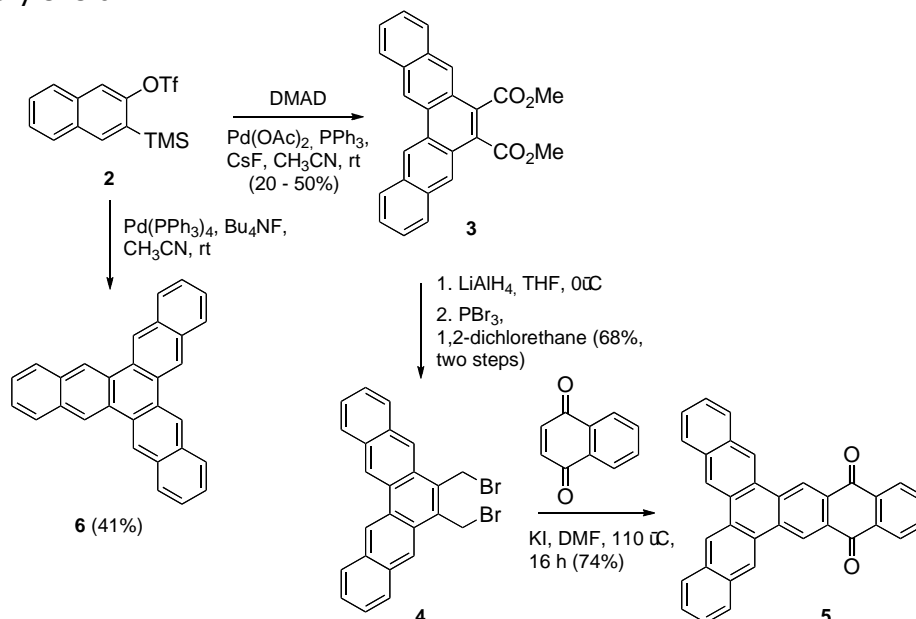
Institute of Chemical Research of Catalonia (ICIQ), Av. Països Catalans 16, 43007 Tarragona, Spain

Keywords: Polyarenes, Palladium, Truxenes

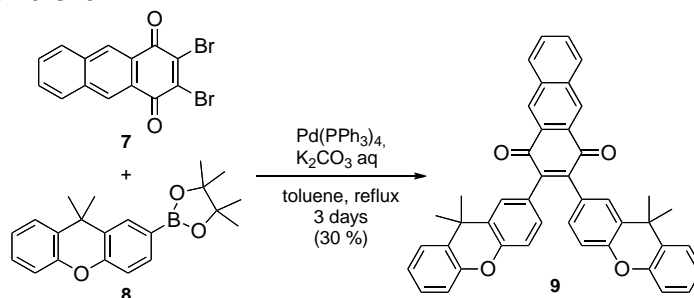
Our group developed a simple synthesis of truxene derivatives [1], [2] which has been recently applied for the synthesis of large C₆₀ polyarenes and related compounds [3]. Recently, two of these polyarenes have been converted into fullerenes by heating under ultra high vacuum conditions on a Pt surface [4]. As one of the first goals of the Pico-Inside project, we have prepared new truxene derivatives such as **1** bearing larger aromatic substituents.



For the synthesis of Y-shaped molecules that could act as molecular "OR" logic gates we have applied the palladium-catalyzed [2+2+2]-cyclootrimerization between arynes generated in situ from **2** with dimethyl acetylenedicarboxylate (DMAD) [5] to yield **3**. Reduction of the ester groups and reaction of the diol with PBr₃ afforded the benzylic bromide **4**. Treatment of **4** with KI gave the *o*-quinodimethane, which was trapped with 1,4-naphthoquinone to give the Y-shaped molecule **5** (benzo[*b*]trinaphthalene-13,18-dione). A palladium-catalyzed [2+2+2] trimerization [6] of 2-naphptyne provided trinaphthylene **6**.



Other routes based on palladium-catalyzed cross-coupling reactions (for example: 7 + 8 to give 9) and photochemical or oxidative cyclizations are also being pursued for the synthesis of related Y-shaped molecules in which two of the three branches are topologically equivalent.



References

- [1] (a) Ó. de Frutos, B. Gómez-Lor, T. Granier, M. A. Monge, E. Gutiérrez-Puebla, A. M. Echavarren, *Angew. Chem. Int. Ed.* 1999, *38*, 204-207. (b) Ó. de Frutos, T. Granier, B. Gómez-Lor, J. Jiménez-Barbero, A. Monge, E. Gutiérrez-Puebla, A. M. Echavarren, *Chem. Eur. J.* 2002, *8*, 2879-2890.
- [2] (a) B. Gómez-Lor, Ó. de Frutos, P. A. Ceballos, T. Granier, A. M. Echavarren, *Eur. J. Org. Chem.* 2001, 2107-2114. (b) Ruiz, M.; Gómez-Lor, B.; Santos, A.; Echavarren, A. M. *Eur. J. Org. Chem.* 2004, 858-866. (c) Gómez-Lor, B.; Echavarren, A. M. *Org. Lett.* 2004, *6*, 2993-2996.
- [3] (a) B. Gómez-Lor, Ó. de Frutos, A. M. Echavarren, *Chem. Commun.* 1999, 2431-2432. (b) B. Gómez-Lor, C. Koper, R. H. Fokkens, E. J. Vlietstra, T. J. Cleij, L. W. Jenneskens, N. M. M. Nibbering, A. M. Echavarren, *Chem. Commun.* 2002, 370-371. (e) A. M. Echavarren, B. Gómez-Lor, J. J.; González, Ó. de Frutos, *Synlett* 2003, 585-597. (f) Gómez-Lor, B.; González-Cantalapiedra, E.; Ruiz, M.; de Frutos, Ó.; Cárdenas, D. J.; Santos, A.; Echavarren, A. M. *Chem. Eur. J.* 2004, *10*, 2601-2608. (g) B. Gómez-Lor, E. González-Cantalapiedra, M. Ruiz, Ó. de Frutos, D. J. Cárdenas, A. Santos, A. M. Echavarren, *Chem. Eur. J.* 2004, *10*, 2601-2608.
- [4] G. Otero, G. Biddau, C. Sánchez-Sánchez, R. Caillard, M. F. López, C. Rogero, F. J. Palomares, N. Cabello, M. A. Basanta, J. Ortega, J. Méndez, A. M. Echavarren, R. Pérez, B. Gómez-Lor, J. A. Martín-Gago, *Nature* 2008, *454*, 865-868.
- [5] D. Peña, A. Cobas, D. Pérez, E. Guitián, *Synthesis* 2002, 1454-1458.
- [6] (a) D. Peña, S. Escudero, D. Pérez, E. Guitián, L. Castedo, *Angew. Chem. Int. Ed.* 1998, *37*, 2659-2661. (b) C. Romero, D. Peña, D. Pérez, E. Guitián, *Chem. Eur. J.* 2006, *12*, 5677-5684.

Helicenes as Intriguing Objects for Chemical and Physical Studies

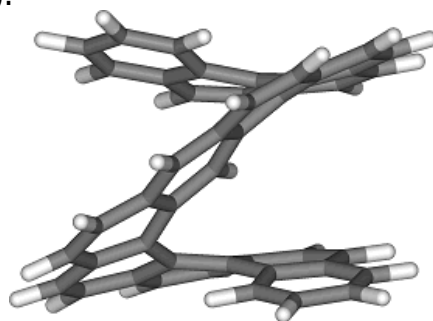
I. Stara

Institute of Organic Chemistry and Biochemistry, Czech Republic

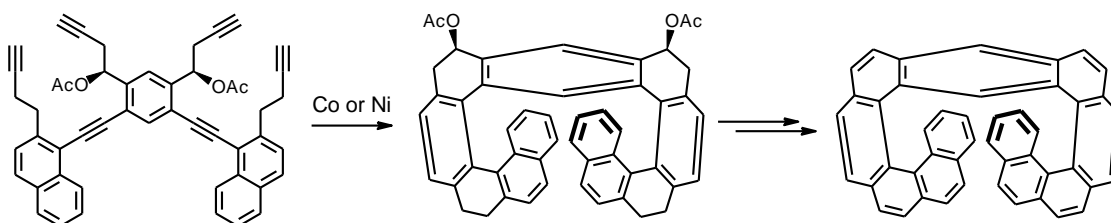
Aromatic compounds are frequently used in the multidisciplinary research directed to molecular electronics. There are a vast number of aromatic compounds ranging from archetypal benzene to graphene being studied in this regard theoretically and/or experimentally. In addition to the unique electronic structure of aromatics, practical aspects of their synthesis, handling and stability play also an important role.

Following the idea of single-molecule electronics, an aromatic compound should integrate manifold elemental functions to behave, for instance, as a logic circuit. Regardless of the necessity of multiple electric contacts with the outer world, we focus on a node structure represented by non-trivial, large aromatic molecules that depart from planarity. We have decided to evaluate pros and cons of such promising systems so far unexplored within single-molecule electronics.

The model compounds chosen belong to the family of helicenes, which contain several ortho-fused benzene rings and, therefore, exhibit a screw-like molecular shape. Non-planarity raises the question of chirality (helicity) but, at the same time, it leads to generally good solubility in various organic solvents as spontaneous aggregation (due to the intermolecular π - π stacking) is minimised. The larger molecule, the lower susceptibility to current leakage between interconnects may be expected. Accordingly, we designed extended helical aromatics as exemplified by [11] helicene (provisionally without this interconnects):



The key synthetic operation is multiple [2 + 2 + 2] cycloisomerisation of aromatic hexayne under transition metal catalysis (Co, Ni) to form the helical backbone in the late stage of the synthesis:

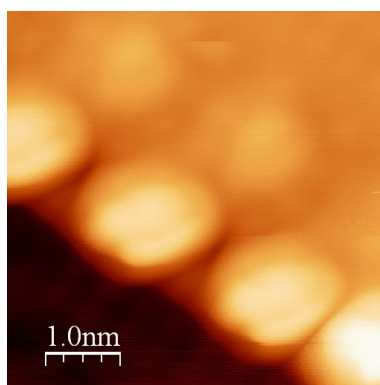


We have shown this synthetic approach to racemic or nonracemic helicenes is robust and general allowing for an effective construction of other extended aromatic systems. Such helical compounds have been found to be stable and, moreover, soluble in contrast to their planar counterparts. Thus, from practical point of view, helical aromatics represent a good basis for designing complex aromatic molecules applicable in single-molecular electronics.

Helical molecules exist as mixtures of enantiomers. Such racemates can be resolved into individual enantiomers preferably by liquid chromatography on a chiral column or their helicity can be already controlled through the asymmetric synthesis. Although challenging enantio- or diastereoselective synthesis requires further effort to develop general methods for the practical preparation of nonracemic helical aromatics, we have successfully demonstrated feasibility of such approaches.

To date, there is little known about the synthetic limits as far as the length of helical aromatics (number of benzene rings) is concerned. These compounds can be, at least in principle, decorated by various carbon and/or heteroatom substituents at different positions. However, the initial studies have revealed that modern synthetic tools (e.g., C-C bond forming coupling reactions) can fail when moving on from simple benzene derivatives to extended helical aromatics. Thus, further attention to the development of general synthetic methods is required to be suitable for more complex aromatic systems.

In order to address single molecules and to study their physical properties attractive for molecular electronics, it is advantageous to deposit them on a proper solid support in a controlled way. We have succeeded (at NANOSAM Centre of the Jagiellonian University) in evaporating [11] helicene onto InSb (001) wafers as well as in imaging them with the sub-molecular resolution using UHV LT STM:



In summary, we have demonstrated that extended helical aromatic systems (higher helicenes and their congeners) are suitable and promising candidates for further studies towards single-molecule electronics. In comparison with other extended aromatic molecules they possess significant structural diversity without losing practical attributes as stability and solubility. In addition, they represent unique 3D aromatic systems combining a π -conjugated path with intramolecular π - π stacking both of them being suitable for charge transport. Further effort should be focused on exploring their conductance because individual helicene molecules are envisaged to serve as lateral junction (a wire) between two insulated conductive layers or molecular structures. Creating ordered molecular arrays, where individual molecules communicate with neighbours in a controlled way, remains a challenging task. As the preparation of complex aromatic systems is all but trivial, an extensive use of molecular modelling and theoretical approaches to predict properties are required.

Molecular Moulding

A. Gourdon

NanoSciences Group, CEMES-CNRS 29 rue J. Marvig, P.O. 94347, F-31055 Toulouse Cedex 04, France

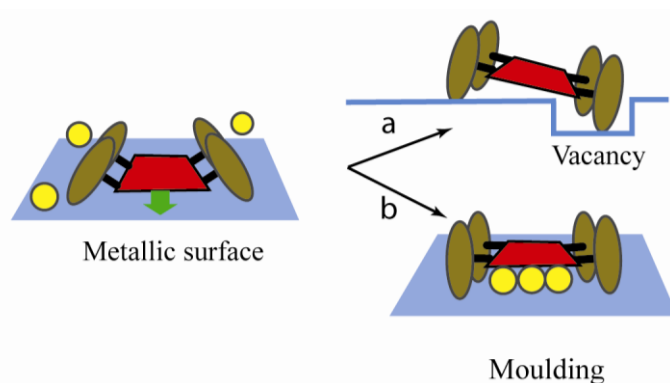


Figure 1: Mechanism of surface restructuring by lander molecules. The lander polyaromatic plateau is in Van der Waals interaction with the surface which induces severe strain energy. This strain can be released by (a) creating or stabilizing a trench or (b) by trapping mobile metal atoms (static moulding). In both cases the polyaromatic plateau complexes the zero-valent metal atoms underneath.

As recently described by Linderoth and Besenbacher [1], the idea of molecular moulding has recently opened a new possibility for the fabrication of atomically defined nano-electrodes in UHV-environment. This concept is indeed a part of molecule induced surface restructuring, [2] in which the presence of molecules on bare metallic surfaces (Figure 1) can also induce interfacial roughening, stabilization of diffusing vacancies, creation of trenches [3, 4].

The background idea is that suitable molecules able to create a niche between their polyaromatic

part and the metal surface can trap and stabilize metal adatoms (Figure 2). The stabilization mechanism comprises: a) a distortion of molecule from its adsorption conformation to allow the entrance of the atoms b) which eventually reduces the molecule distortion induced by Van der Waals forces c) chemical complexation of isolated zero-valent metal atoms with the molecule aromatic pi-electrons. Of course the geometry of these metallic nano-islands is function of the molecular mould geometry as shown for different types of landers [5, 6] which opens the way to complex designs using suitable polyaromatic boards. This moulding can be considered as a static moulding since the molecule is fixed and the adatoms are mobile; but we also have recently described a dynamic moulding when, at low temperature, the metal adatoms are not mobile and the mould is displaced by STM manipulation to gather the atoms (molecular Hoover) [7].

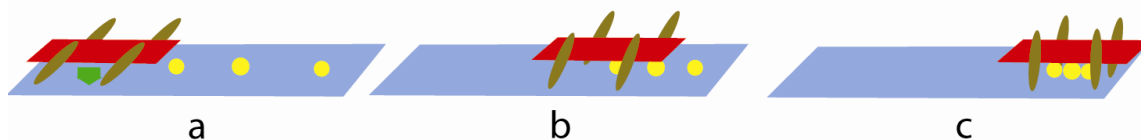


Figure 2: Dynamic moulding. In this case, a STM tip is used to move the lander above metal adatoms which are then trapped under the polyaromatic plateau and glide with the molecule toward the next adatom.

The beauty of this technique is the foreseen possibility to fully exploit the chemistry potential: versatility of chemical designs, softness-rigidity, self-assembly to create ab-initio metallic nanostructures.

We have recently shown that this concept could be used to fabricate a nanoelectrode using a molecular wire as a static mould and then use this nanoelectrode as a rail to manipulate the molecule up to a position where the polyaromatic wire extremity is in

contact allowing the measurement of the electronic coupling between the molecular wire and its own electrode [8]. The main advantage here is that the atomically precise nanoelectrode is made in ultra-clean conditions and that this electrode exactly fits its "mother molecule". The Figure 3 shows schematically this experiment:

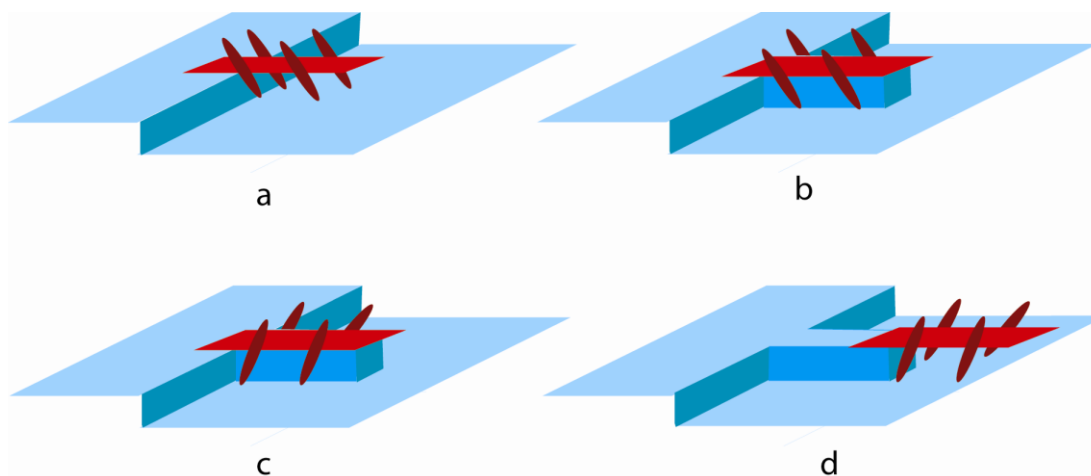


Figure 3: Contacting a single molecular wire by molecular moulding and STM manipulation. a) The lander (for instance RL; see Figure 1 in the introduction) is transferred on a metallic surface and the molecule decorates monoatomic step-edges by adsorption through its contacting end. b) Then diffusion of mobile atoms underneath the plateau creates a nanoelectrode. c) The temperature is then decreased to stabilize the nanopad and allow STM manipulation using it as a rail to push the molecule to the situation: d) where the molecular is in contact position, ready for measurement.

This clean contacting experiment will be used to probe different types of molecule-electrode chemisorption and physisorption using landers with a variety of contacting ends.

So far we have only described static and dynamic molecular moulding on metal surfaces but it would be of course much more useful to realize moulding of nano-scale electrodes or clusters on *insulating surfaces*. In a first step, the self-assembling properties of well-designed molecules could give a 2D molecular network (Figure 4a) with a design depending mainly on the molecules chemical structures. Then, diffusion of metal atoms (Figure 4b) at high enough temperature would give metallic nano-wires or nano-islands.



Figure 4: Concept of extended molecular moulding using molecular self-assembly.

This concept could also be extended to "molecular masking". In this case the molecular assembly on the substrate leaves well defined bare spaces that can then be filled with metal atoms or molecules. This idea has already been described by Beton et al. [9] who prepared 2D open honeycomb networks by assembly of PTCDI and melamine. The templated network then acted as an array of 2D large pores which could accommodate in a second step small islands of fullerene molecules.

Obviously these very attractive and promising new ways of fabricating metallic networks in UHV by a bottom-up approach require extensive studies of fundamental processes: thermodynamics of self-assembly on insulators, mobility of metal atoms on these substrates, mechanism of trapping.

References

- [1] T.R. Linderoth and F. Besenbacher, E-Nano Newsletters 2006, 3, 25.
- [2] F. Rosei, M. Schunack, Y. Naitoh, Ping Jiang, A. Gourdon, E. Laegsgaard, I. Stensgaard, C. Joachim and F. Besenbacher, Prog. Surf. Sci. 2003, 71, 95-146.
- [3] L. Gross, F. Moresco, M. Alemani, H. Tang, A.Gourdon, C. Joachim and K.-H. Rieder, Chem. Phys. Lett. 2003, 371, 750-756.
- [4] a) M. Schunack, L. Petersen, A. Kuhnle, E. Laegsgaard, I. Stensgaard, I. Johannsen and F. Besenbacher, Phys. Rev. Lett. 2001, 86, 456-459. b) M. Schunack, E. Laegsgaard, I. Stensgaard, I. Johannsen and F. Besenbacher, Angew. Chem., Int. Ed. Engl. 2001, 40, 2623-2626.
- [5] F. Rosei, M. Schunack, P. Jiang, A. Gourdon, E. Laegsgaard, I. Stensgaard, C. Joachim and F. Besenbacher, Science 2002, 296, 328-331.
- [6] R. Otero, F. Rosei, Y. Naitoh, P. Jiang, P. Thostrup, A. Gourdon, E. Laegsgaard, I. Stensgaard, C. Joachim and F. Besenbacher, Nanoletters 2004, 4, 75-78.
- [7] L. Gross, K.-H. Rieder, F. Moresco, S. Stojkovic, A. Gourdon and C. Joachim, Nature Materials 2005, 4, 892-895.
- [8] L. Grill, F. Moresco, K.-H. Rieder, S. Stojkovic, A. Gourdon and C. Joachim, Nanoletters 2005, 5, 859-863.
- [9] J. A. Theobald, N. S. Oxtoby, M. A. Phillips, N. R. Champness and P. H. Beton, Nature 2003, 424, 1029-1031.

3c. Surface selection and preparation, launching, imaging and assembling on a surface and manipulation

- Metal

STM Investigations of Molecular Moulds on Metal Surfaces

Miao Yu¹, Wei Xu¹, Youness Benjalal^{2,3}, Regis Barattin², Erik Lægsgaard¹, Ivan Stensgaard¹, Mohamed Hliwa^{2,3}, Xavier Bouju², André Gourdon², Christian Joachim², Trolle R. Linderoth^{1*} and Flemming Besenbacher^{1*}

¹ Interdisciplinary Nanoscience Center (iNANO) and Department of Physics and Astronomy, University of Aarhus, Ny Munkegade, 8000 Aarhus C, Denmark

² Nanoscience group, CEMES-CNRS, 29 rue Jeanne Marvig, 31055 Toulouse, France

³ Faculté des Sciences Ben M'Sik, Université Hassan II-Mohammédia, BP 7955, Sidi Othman, Casablanca, Morocco

*fbe@inano.dk, trolle@inano.dk

Keywords: Scanning tunneling microscopy, molecular moulding, hydrogen bonding, manipulation, nanotechnology

Introduction

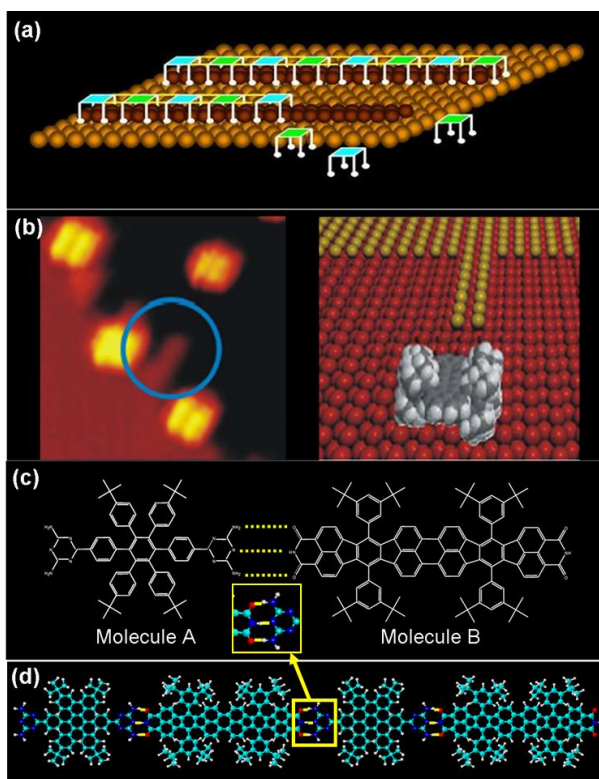


Figure 1: Concept of self-assembly of molecular mould. (a): Schematic drawing of the growth of one-dimensional metallic wires (red) by the alternating A-B-A-B molecule chains (pale blue and green) with elevating legs; (b): Molecular moulding of atomic wires, adapted from [3]; (c): the interaction of two molecule, i.e. Lander A and B by triple complementary hydrogen bond between the diamino-triazine and imide functional groups; (d): A-B-A-B... molecular chain formed by the triple hydrogen bond. (red: O, blue: N, pale blue: C, white: H)

Functionalized organic molecules organised at surfaces play a vital role in the rapidly growing area of nanotechnology, especially within areas such as molecular electronics, nanodevices, and molecular recognition [1, 2]. A central goal within the Pico-Inside integrated project was to form metallic nanostructures that may act as nanoscale “connectors” to molecular devices. An interesting bottom-up approach towards this goal is to use organised molecular structures that may act as moulds for subsequent formation of metallic nanostructures, as shown schematically in Figure 1(a). The essential idea in molecular moulding is to use the interaction between an organic molecule and metal atoms to form well-defined metallic nanostructures on surfaces. Molecular Landers are a class of compounds consisting of an aromatic backboard (the π system) equipped with bulky moieties (such as *tert*-butyl groups, $-C_4H_9$) that act as legs, lifting the board away from the surface. Molecular moulding was first demonstrated by Rosei et al [3] who used a simple Lander molecule ($C_{90}H_{98}$) to assemble Cu adatoms into metallic nanostructures on a Cu(110) surface as shown in Figure 1(b). Thermal activation creates free adatoms at the Cu surface by ejection

from steps and kinks, and it was demonstrated that deposited Lander molecules can trap and stabilize these atoms to form a well-defined metallic nanostructure at the step edge with a shape determined by the Lander molecule. In this case, the space underneath the molecular board favourably matches the dimension of a double-row of Cu adatoms and the low-coordinated atoms of these metallic protrusions are patterned by the attraction to the π -system of the aromatic board. The shape of the organic molecule is thus effectively used as a mould that is replicated in the resulting metallic nanostructure which was revealed by scanning tunnelling microscope (STM) manipulation at low temperature. Molecular moulding has also been demonstrated for isolated metal structures underneath molecules adsorbed at terraces [4, 5] and different Lander-type molecules have performed as molecular moulds for metallic nanostructures of various shapes [3-7].

To form an extended one-dimensional (1D) metallic wire by molecular moulding, prearrangement of the individual molecular moulds into a 1D molecular chain is required. Growth of 1D molecular structures from Lander-type compounds was previously realized by adsorption onto nano-templates formed by exposure of a Cu(110) surface to oxygen [8], where the bare Cu and CuO 1D rows confine the Lander molecules to form a well-defined adsorption pattern. However, this approach relies on a very special choice of substrate, and it is therefore desirable to explore a more versatile approach where the molecules are organised through specific intermolecular interactions.

Supramolecular chemistry based on noncovalent interactions is a powerful synthetic tool for the self-assembly of complex molecular architectures [9, 10]. Especially, hydrogen (H)-bonding is an important driving force for molecular hierarchical nanostructures due to the reversibility, specificity, directionality, and cooperative strength of this class of interactions [11, 12]. In recent years, a vast number of studies have reported on H-bonded structures formed by molecules adsorbed on solid surfaces under vacuum conditions [13–15]. Most studies so far have involved only homomolecular interactions, and relatively few structures based on heteromolecular interactions have been investigated [16–18]. To enable the synthesis of self-assembled multicomponent nanostructures on surfaces, suitable protocols of stoichiometry, deposition order, and thermal treatment have to be established and systems with sufficiently high intermolecular binding strengths have to be identified [19, 20].

A typical heteromolecular H-bonding motif results from the interaction between diamino-pyridine and imide moieties, exhibiting triple complementary N-H•••O and N-H•••N H-bonds [11, 21–23]. This classic H-bonding interaction has been exploited in the solution phase [22, 23], in the solid state [11], and more recently at interfaces [16, 17]. With the aim to form 1D self-assembled structures of molecular moulds, two Lander-type molecules exhibiting this type of complementary interaction have therefore been designed as shown in Figure 1 (c) and (d). Lander A, bis(diaminotriazine) ($C_{64}H_{68}N_{10}$), consists of a hexaphenyl benzene core with four *tert*-butyl groups as spacer legs and a diamino-triazine functional group at each end. Lander B ($C_{112}H_{102}N_2O_4$) is a functionalized violet-Lander molecule with imide endgroups at both ends and di-*tert*-butyl groups as the 'spacer legs'. These two molecules may be anticipated to create a one-dimensional chain with alternating A-B-A-B molecules via triple complementary H-bonding between the diamino-triazine and imide functional groups as shown in Figure 1 (d). Subsequently, the 1D Lander molecular chains are envisioned to act as moulds for formation of metallic nanowires by capturing diffusing metal atoms, in initial experiments at metal surfaces, but eventually at insulating substrates.

In the present contribution we describe progress towards the goal of depositing and organising functionalised molecular Landers at metal surfaces under Ultra High Vacuum conditions.

First, we review results obtained [24] for the adsorption and organisation of two simpler molecules, cyanuric acid (CA, $C_3H_3N_3O_3$) and melamine (M, $C_3H_6N_6$) at the Au(111) surface. Cyanuric acid and melamine is a prototypical example of a molecular co-deposition system exhibiting the same complementary groups for molecular interaction as those chosen for the Lander A and B system (see Figure 2). Detailed understanding of the interactions and organisational principles for both homo- and hetero-molecular structures formed in this system are therefore of paramount importance for for guiding our efforts towards formation of self-assembled structures from the more complex Lander-type compounds.

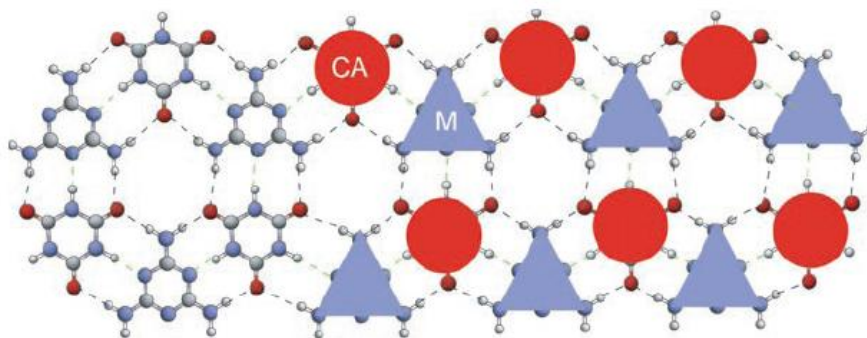


Figure 2: Schematic representation of the cyanuric acid-melamine- (CA1M1) lattice stabilized by $O\cdots H$ and $N\cdots H$ hydrogen bonds. (red: O, blue: N, white: H)

We secondly describe STM imaging and organisation of Lander A on the Au(111) surface. The transfer to the surface of molecular compounds for self-assembly studies under UHV conditions is typically performed by in-situ sublimation. For large and complex compounds as those used in the envisioned bi-molecular wires, this process involves a risk of thermal decomposition of the molecular building blocks if the intermolecular cohesive strength in the molecular source material exceeds the intramolecular binding energy. Careful optimisation of the deposition conditions is therefore required. In the present case, the STM results for the deposited Lander A compounds suggested the possibility that thermally induced fragmentation had occurred, since no STM signature of the peripheral diamino-triazine groups was observed. This possibility was investigated, both by theoretical modelling and by synthesis and deposition of a Lander A derivative, Lander C, in which the diamino-triazine (melamine-like) groups were removed on purpose and which could therefore serve as a control. From the results obtained, we conclude that intact deposition of Lander A is indeed achieved since the self-assembled structures found for Lander A and C are quite different from each other, and the STM image simulations furthermore show that an STM contrast for the diamino-triazine groups is not anticipated at the experimentally applied bias voltages.

Finally, we describe experiments where individual Lander A compounds adsorbed at terraces and at atomic steps are manipulated by the STM tip, including both lateral translation and rotation. Experiments such as these provide important information on the nature of the molecule-substrate interaction, including the possibility of molecule-induced deformations of step-edges that may be of relevance for the question of molecule-electrode contacting. To guide the choice of an appropriate substrate for the growth of molecular wires, we compare the cases of the close-packed, quasi-isotropic herringbone reconstructed Au(111) surface to the case of the more open and anisotropic Cu(110) substrate. The latter surface may be favourable in terms of aligning the molecular moulds due to its reduced symmetry, and most experiments on molecular moulding so far have been performed on this

substrate [3-5, 25-29]. However, a strong molecule-substrate interaction may also be detrimental to realising organisation dominated by intermolecular forces. The manipulation experiments confirm qualitatively that the diffusion barrier for Lander A on the Au(111) surface is less than for Cu(110), signalling a flatter molecule-substrate potential energy landscape for the Au(111) surface. This suggests that substrate alignment effects may be less pronounced on the Au(111) surface and suggest that this substrate may be optimum for future experiments where Lander A and Lander B are codeposited.

Experimental Details

The experiments were performed in a UHV chamber (typical base pressure $\sim 10^{-10}$ Torr) equipped with standard facilities for sample preparation and a variable-temperature Aarhus STM [30] for characterization. Electrochemically etched polycrystalline W tips were used. The Au(111) and Cu(110) single-crystal samples were cleaned by repeated cycles of 1.5 keV Ar^+ ion bombardment and annealing to 800 K for 15 min. The Lander A molecules were synthesized by Rosenmund-von Braun cyanation of 1,4-bis(4-bromophenyl)-2,3,5,6-tetrakis (4-*tert*-butylphenyl) benzene, followed by reaction with dicyandiamide under microwave irradiation. Powders of M and CA (99% and 98% purity, respectively; Acros) as well as Lander A and Lander C molecules were thoroughly degassed prior to deposition. All molecules were deposited by thermal sublimation from molecular evaporators held at ~ 356 K for CA and M, at ~ 510 K for Lander A and at ~ 465 K for Lander C, respectively. Simultaneous deposition of CA and M was achieved by heating both evaporators and overlapping their output beam on the surface. Molecules were deposited onto a sample held at room temperature (≈ 300 K). All images presented here were recorded in the constant current mode and STM measurements were performed in a temperature range of 100–160 K to stabilize the molecules on the surfaces. The lateral manipulation was performed by reducing the tunnel resistance during scanning via increasing the tunneling (up to ~ 1.5 nA) current while reducing the tunneling voltage (down to ~ 200 mV) [3]. The molecular interaction energies underlying the formation of CA and M structures are calculated by the self-consistent charge density functional tight-binding method (SCC-DFTB) as described in reference [24]. Theoretical simulations of Lander A and Lander C have been performed using the Elastic Scattering Quantum Chemistry (ESQC) method [31] after having relaxed the molecule on the surface using the Molecular Mechanics MM4 (2003) code [32].

Results and Discussion

Adsorption structures formed upon deposition of CA or M individually on Au (111) are shown in Figure 3 and Figure 4 respectively along with optimized models for the resulting H-bonded molecular networks. In both cases, large well-ordered islands are observed. The herringbone reconstruction does not appear to change upon molecular adsorption or affect the self-assembly patterns

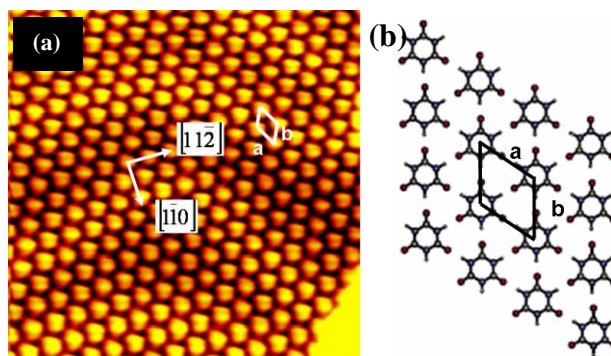


Figure 3: (a): A STM image ($102 \text{ \AA} \times 102 \text{ \AA}$) of CA ($I_t=0.72\text{ nA}$, $V_t = 1250 \text{ mV}$) on Au(111); (b): Optimized models for the hydrogen-bonded network of CA.

observed in this study, implying a weak molecule-substrate interaction. STM images of CA and M, as shown in Figure 3(a) and Figure 4(a), respectively, depict CA as compact entities with near-circular symmetry, whereas M molecules are resolved with a characteristic three-spoke shape, attributed to the position of the amino groups.

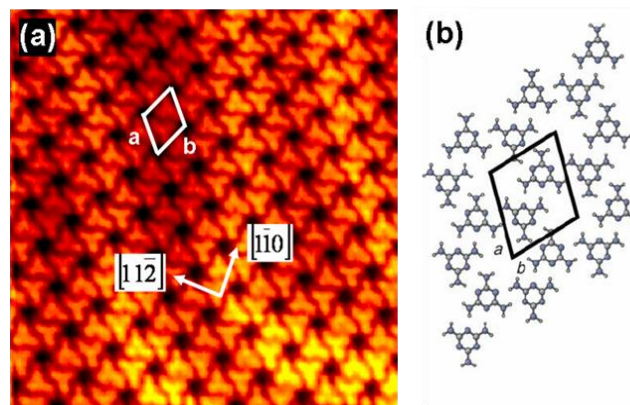


Figure 4: (a): A STM image ($102 \text{ \AA} \times 102 \text{ \AA}$) of Melamine ($I_t = 0.57 \text{ nA}$, $V_t = 1486 \text{ mV}$) on Au(111); (b): Optimized models for the hydrogen-bonded network of Melamine.

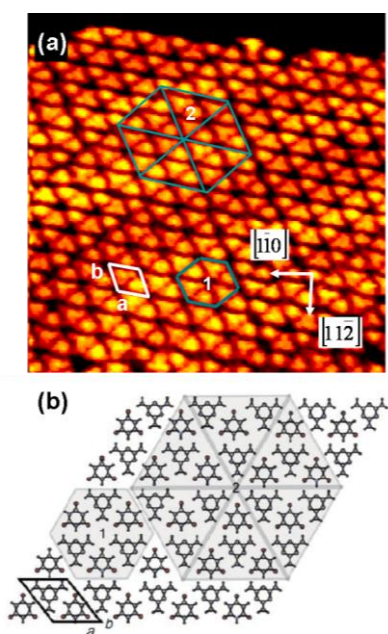


Figure 5: (a): STM image ($102 \text{ \AA} \times 104 \text{ \AA}$) of a self-assembled network resulting from simultaneous deposition of M and CA on Au (111). The characteristic ball- and three-spoke shapes for CA and M are clearly resolved. The structure is a mixed phase corresponding to the network presented in Figure 2 ($I_t=0.56 \text{ nA}$, $V_t=1250 \text{ mV}$); (b): Optimized model for CA_1M_1 network. The hexagon marked "2" in (b) shows corresponding areas as a guide to the eye.

The overlayer formed from pure CA (Figure 3(a)) is hexagonally close-packed and can be modelled by the structure shown in Figure 3(b), in which each molecule associates through six H bonds to symmetrically distributed neighbours. In contrast, M forms a more complicated structure in which the spokes of neighbouring molecules interdigitate, leading to the formation of six-membered rings surrounding open pores in the network. From the corresponding optimized model for M (Figure 4(b)) the structure is seen to involve double H-bonding interactions to three neighbours surrounding each molecule.

Simultaneous deposition of CA and M leads to a self-assembled network as shown in Figure 5(a). The characteristic circular and three-spoke shape for CA and M is resolved (most clearly seen at the top-left side of the image), showing that the structure is a binary mixed phase involving heteromolecular H-bonding. Comparison of the area indicated with the hexagon marked "1" in Figure 5(a) to the model for the CA_1M_1 structure shown in Figure 2 reveals that the observed structure corresponds to a motif based on the complementary $CA \cdots M$ coupling (see Figure 5(b)). Figure 6(a) shows a space-filling model of the Lander A molecule and (b) presents a high-resolution STM image of a Lander A molecule on Cu(110), showing four bright lobes in a rectangular shape ($11.0 \text{ \AA} \times 6.5 \text{ \AA}$), and some sub-protrusions in the centre. A similar morphology of the Lander A molecule is observed on the Au(111) surface. A simulated STM image obtained using the ESQC

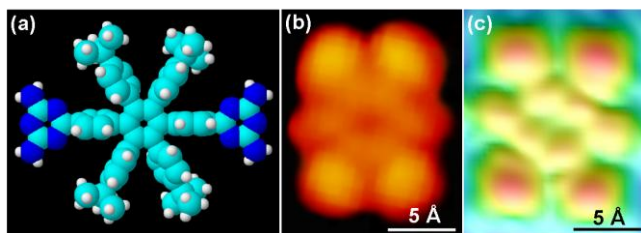


Figure 6: (a): Space-filling model of bis(diaminotriazine) molecule ($C_{64}H_{68}N_{10}$). It consists of a benzene ring connected with four *tert*-butyl groups and two diamino-pyridine groups by σ bonds, where the carbon, hydrogen and nitrogen atoms are represented in pale blue, white and blue, respectively; (b): A typical high-resolution STM image of a Lander A molecule on Cu(110), which reveals four bright lobes in a rectangular shape and some delicate sub-protrusions in the middle. ($I_t = -0.66$ nA, $V_t = -1730$ mV); (c): ESQC-simulated STM image of the Lander A on Cu(110) as the same tunneling conditions as the experimental result in (b).

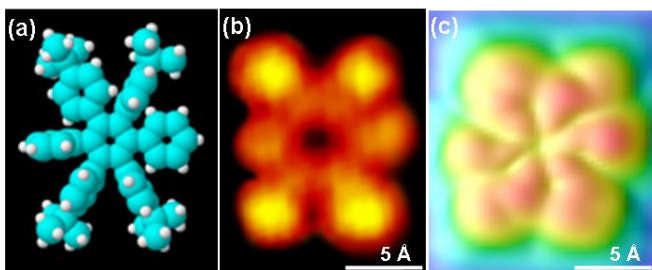


Figure 7: (a): Space-filling model of Lander C ($C_{58}H_{62}$); (b): A typical high-resolution STM image of a Lander C molecule on Au(111) revealing four bright lobes in a rectangular shape and some delicate sub-protrusions in the middle. ($I_t = -0.31$ nA, $V_t = -1250$ mV); (c): ESQC-simulated STM image of the Lander C on Au(111) as the same tunneling conditions as the experimental result in (b).

the melamine-type end groups have been deliberately removed. A high-resolution STM image of a Lander C molecule on Au(111) is displayed in Figure 7(b), showing a similar morphology to that for Lander A molecule in Figure 6. The theoretically calculated STM images using the ESQC approach is shown in Figure 7(c), and is consistent with the experimental results. Similarly to the case for Lander A, we attribute the four bright lobes in a rectangular shape ($11.0 \text{ \AA} \times 6.5 \text{ \AA}$) to the four *tert*-butyl groups, and the sub-protrusions in the centre to the hexa-phenyl rings.

The self-assembled nanostructures formed by Lander A and Lander C, respectively, were subsequently investigated. Based on the adsorption structure for pure melamine described above, Lander A may be anticipated to form structures guided by double hydrogen bonding between neighbouring diamino-triazine moieties. In the experiments, a number of different phases have been observed for Lander A, which are either co-existing or result from slight variations in the deposition conditions. Some of the arrangements involve the anticipated H-bonding motifs, while others are close-packed and appear to be driven predominantly by Van der Waals (VdW) forces. A

approach is shown for comparison in Figure 6(c). The theoretical result is consistent with the experimental findings. In both cases, there are four bright lobes in a rectangular arrangement, corresponding to tunneling through the four *tert*-butyl groups [33], and some sub-protrusions in the centre attributed to the hexa-phenyl rings which are connected with the central benzene by σ bonds. An important feature of the observed STM signature is that there are no features in the recorded STM images that can be attributed to the diamino-triazine groups. This may in principle cause concern that the functional groups have been lost during the thermal sublimation of the compound onto the surface. However, the endgroups do not provide contrast in the simulated STM image either, showing that the contribution of the diamino-triazine groups to the tunneling current is minor at the investigated bias voltages.

To experimentally address the possibility that the melamine-like end groups have been lost during sublimation, we synthesized and investigated as a control the compound Lander C shown in Figure 7(a) which has the same structure as Lander A except that

systematic description of these structures is beyond the scope of the present contribution, but an example of a self-assembled structure formed from Lander A on the Au(111) surface is shown in the high-resolution STM image of Figure 8(a). The structure displays a crisscross arrangement, where each molecule has its axis orthogonal to the axis of the four nearest neighbours in the structure. There are 2 molecules in each unit cell which has dimensions $23.5 \text{ \AA} \times 23.5 \text{ \AA}$ and an included angle of about 90° . A tentative molecular model is presented in Figure 8(b). The diamino-triazine endgroups appear to embed between two *tert*-butyl groups on a neighbouring molecule. The proposed model involves some steric crowding but this may be alleviated by possible tilting/rotation of the melamine endgroups.

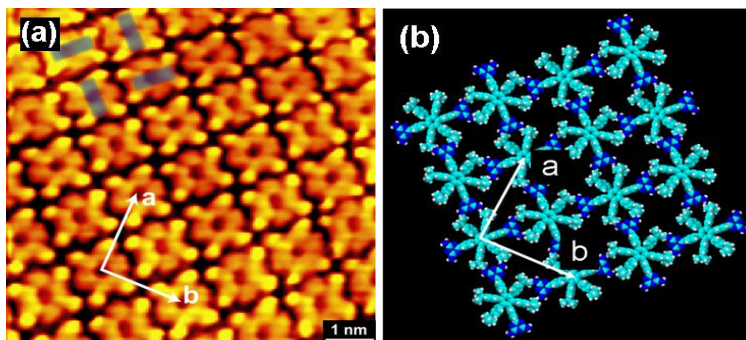


Figure 8: (a): A high-resolution STM image ($100 \text{ \AA} \times 100 \text{ \AA}$) of a close-packed structure formed by Lander A on the Au(111) surface. Unit cell vectors are indicated. ($I_t = -0.80 \text{ nA}$, $V_t = -625 \text{ mV}$); (b): A tentative model for the observed structure.

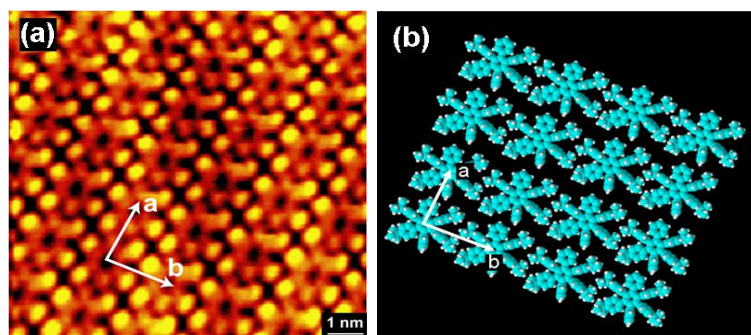


Figure 9: (a): A high-resolution STM image ($100 \text{ \AA} \times 100 \text{ \AA}$) of close-packed structure of Lander C on Au(111) ($I_t = -0.31 \text{ nA}$, $V_t = -1250 \text{ mV}$); (b): A tentative model of the observed structure.

For comparison, the observed arrangement of Lander C on Au(111) is shown in Figure 9(a). The compound adopts a close-packed row-like structure with one molecule in each unit cell which has a size of $12.5 \text{ \AA} \times 15.4 \text{ \AA}$ and with an included angle is 85° . A tentative model is given in Figure 9(b). We suggest that within the Lander C rows, the molecules are stabilized by π - π interaction between the phenyl rings of neighboring molecules and that the molecular rows are close-packed sideways by VdW interaction. Because the side phenyl groups are connected with the central benzene ring by σ bond and the molecular board is lifted, the peripheral phenyl groups on both sides have flexibility to rotate and tilt to optimize the intermolecular π - π interaction. That different packing arrangements are observed for Lander A and

Lander C molecules provide further evidence that the Lander A molecules are deposited intact on the surface such that the melamine-type endgroups may guide or influence the molecular self-assembly.

We finally describe results obtained by STM-tip induced manipulation of individual Lander A molecules on Cu(110) and Au(111) substrates. Some of the discussed processes are illustrated in the high resolution STM images in Figure 10 where white dashed arrows show the direction of applied operations. Figure 10(a) shows an atomically resolved STM image of clean Cu(110) surface with indication of the two high

symmetry directions. From a thorough statistical analysis of STM results on consecutive manipulations of both individual Lander A molecules and Lander A dimers on terraces, three adsorption orientations of the Lander A molecule on Cu(110) are found with the long axis of the molecule oriented at -30° , 0° and 30° relative to the $[1\bar{1}0]$ direction of the substrate. At low temperature (~ 110 K), the orientation of single molecule on a Cu(110) terrace can be changed from -30° to 30° with respect to the $[1\bar{1}0]$ direction of the substrate, as shown by the molecule marked 'A' in Figure 10(b-c). By means of STM manipulations, the molecular orientation with respect to the substrate lattice on terraces can in this way be varied. The mobility of organic molecules has been found to be closely related with its adsorption configurations, in particular the molecule-substrate complementarity, an effect referred as the lock-and-key effect [34].

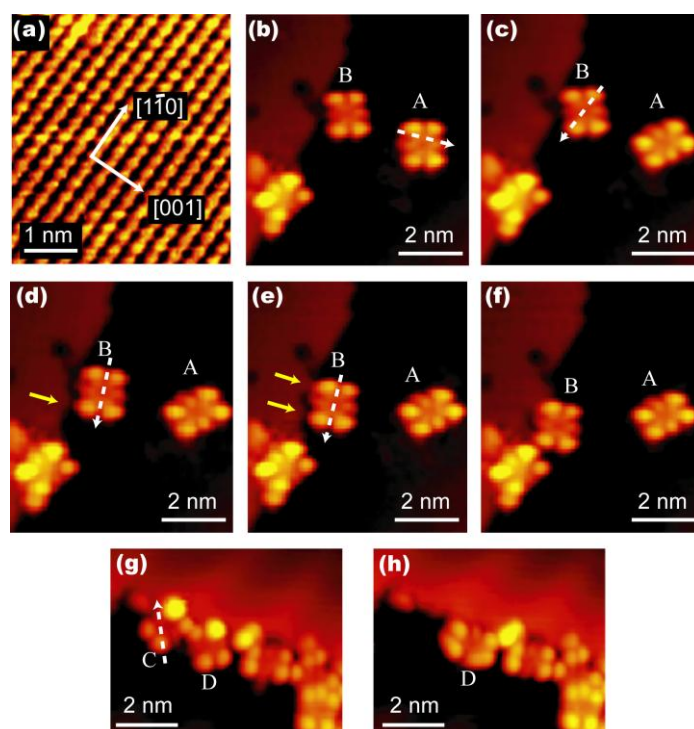


Figure 10: High-resolution STM images showing the atomically resolved Cu(110) surface in (a) and the manipulation sequences of individual Lander A molecules on Cu(110) in (b-f) and on Au(111) in (g, h). On Cu(110), three different manipulation processes can be performed on the molecule: on the terrace, the molecule marked 'A' can be rotated as shown in (b,c); the molecule marked 'B' can be moved along the step edge while changing its orientation as shown in (c-f). On Au(111), as shown in (g,h), the Lander A molecule is relative mobile. As the molecule marked 'C', it is easily removed from the step edge to the terrace and diffuses away while the neighboring molecule 'D' was rotated simultaneously.

In general, when a large complex molecule is adsorbed on metal surfaces, an energetically-preferred geometry is adopted rather than the desired one for an electronic contact. To achieve an efficient charge transfer between the molecule and the connected electrode, it is required that the elevated molecular board of Lander molecular wire is attached to the electrode, for example a protrusion of the step edges. In this case, it is necessary to modify the contact configuration by changing the adsorption site or/and orientation of Lander molecules relative to the step edges. As shown in the sequence of STM images depicted in Figure 10(c-f), the molecule marked 'B' is steered by the STM tip and displaced gradually along the step edge of Cu(110) from the top toward another Lander A molecule adsorbed on the step edge near the bottom of the images. During this lateral translation, the orientation of the molecule marked 'B' is simultaneously changed. An appropriate electronic contact may be assembled by such STM manipulation.

It should be noticed that compared to the smooth and flat step edge along $[1\bar{1}0]$ direction in Figure 10(c), protrusions at the step edge exist which are induced by the movement of molecule 'B', as pointed out in Figure 10(d) and 10(e) by the yellow arrows. The ability of Lander molecules to mould nanostructures at the step edge of Cu(110) has been reported previously [3-5]. In these cases the reshaping occurred at room temperature where the diffusivity of Cu adatoms is relative high such that diffusing Cu adatoms can be trapped under the molecular π board to form specific metallic nanostructures. Subsequent STM manipulation of the molecular moulds was performed at low temperature to thermally stabilize the underlying metallic nanostructures. The case presented here is different, revealing that even at low temperature (~ 110 K), the attractive interaction between the Lander A molecule and the Cu(110) step edge is sufficient to induce a rearrangement of the step edges. However, in this case the reconstruction is temporary and reversible since once the molecule is moved away, the atoms of the protrusions re-accommodate into the step edges.

For a comparison, similar STM manipulation sequences are also performed on Au(111) at the same low temperature (~ 110 K). In Figure 10(g), where two legs of the molecule 'C' are in contact with the step edge, an STM manipulation operation as shown is applied to the Lander A molecule to rotate and push the molecule towards the upper terrace like in the case on Cu(110). Surprisingly, molecule 'C' is removed completely from the step edge and even diffuses out of scanning region as a result of the manipulation process. Furthermore, seen from Figure 10(h), the manipulation of molecule 'C' also induces the rotation of the neighbouring molecule 'D' from an approximately perpendicular to parallel to the step edge. These findings indicate that the Lander A molecule is more weakly bound to the Au(111) substrate than to Cu(110).

These experimental findings are consistent with previous theoretical and experimental results for the adsorption of organic molecules on metal substrates [e.g. 35, 36]. Au is a noble inert metal and it is to be expected that the molecule-substrate interaction on Au(111) surface is weaker than that on Cu(110). Furthermore the corrugation of the potential energy of Au(111) surface is smaller than that of Cu(110), which implies that the diffusion barrier for molecules is lower on Au(111) as compared to the anisotropic Cu(110) which affects the dynamic behavior. These findings are relevant for selecting suitable substrates to assemble 1D conducting molecular chains. The specific closed-packed orientation of the anisotropic Cu(110) substrate might guide the build-up of the 1D molecular chains, but the fairly strong local molecule-substrate interaction may hinder the formation of hydrogen bonded patterns which are determined mainly by molecule-molecule interactions. In this respect the weak molecule-substrate interaction may make the close packed Au(111) surface a preferred template for the formation of self-assembled molecular structures.

Summary and Outlook

In summary, we have described efforts towards the goal of forming molecular assemblies suitable for molecular moulding based on complementary H-bonding recognition between specially designed Lander compounds. We systematically investigated the selected intermolecular recognition motif between complementary diamino- triazine and imide moieties in the simpler model system of cyanuric acid and melamine and concluded that it indeed directs the self-assembly of molecular structures. Subsequently, the deposition of Lander A compounds on both Cu(110) and Au(111) substrates were investigated and compared to theoretical modelling. We conclude that it is possible to transfer the complex Lander A compound to the surface

by thermal sublimation without fragmenting the delicate molecular structure. Using STM lateral manipulation, we have furthermore studied the anchoring of Lander A molecule on both Cu(110) and Au(111) substrates. On Cu(110), various contact configurations were formed at step edges. The manipulation experiments show that the diffusion barrier for Lander A is higher on Cu(110) than on Au(111). Based on these experimental results, we conclude that Au(111) may be the more suitable substrate for the molecular self-assembly of the Lander molecules since the weaker molecule-substrate interaction will be beneficial for formation of ordered molecular architecture mainly driven by intermolecular interaction.

Further experiments are in progress to co-adsorb Lander A and Lander B molecules in order to utilize the complementary triple H-bonding interaction to self-assemble unidirectional molecular arrangements relevant for experiments into molecular moulding of metallic wires.

Acknowledgement

The authors acknowledge the financial support of IST Pico-Inside and NMP Frontiers European projects as well as grants from the Danish Ministry for Science, Technology and Innovation and from the Danish Research Councils. MH and YBJ thank the CMIFM via the Volubilis France-Morocco exchange program.

References

- [1] C. Joachim, J. K. Gimzewski and A. Aviram, *Nature* 2000, 408, 541-548.
- [2] W. R. Browne and B. L. Feringa, *Nature Nanotechnology* 2006, 1, 25-35.
- [3] F. Rosei, M. Schunack, P. Jiang, A. Gourdon, E. Lægsgaard, I. Stensgaard, C. Joachim and F. Besenbacher, *Science* 2002, 296, 328-331.
- [4] M. Schunack, F. Rosei, Y. Naitoh, P. Jiang, A. Gourdon, E. Lægsgaard, I. Stensgaard, C. Joachim and F. Besenbacher, *Journal of Chemical Physics* 2002, 117, 6259-6265.
- [5] L. Gross, K.-H. Rieder, F. Moresco, S. M. Stojkovic, A. Gourdon and C. Joachim, *Nature Materials* 2005, 4, 892-895.
- [6] R. Otero, F. Rosei, Y. Naitoh, P. Jiang, P. Thostrup, A. Gourdon, E. Lægsgaard, I. Stensgaard, C. Joachim and F. Besenbacher, *Nano Letters* 2004, 4, 75-78.
- [7] F. Rosei, M. Schunack, Y. Naitoh, P. Jiang, A. Gourdon, E. Lægsgaard, I. Stensgaard, C. Joachim and F. Besenbacher, *Prog. Surf. Sci.* 2003, 71, 95-146.
- [8] R. Otero, Y. Naitoh, F. Rosei, P. Jiang, P. Thostrup, A. Gourdon, E. Lægsgaard, I. Stensgaard, C. Joachim and F. Besenbacher, *Angew. Chem.Int. Ed.* 2004, 43, 2092-2095.
- [9] J.-M. Lehn, *Science* 2002, 295, 2401-2403.
- [10] D. N. Reinhoudt and M. Crego-Calama, *Science* 2002, 295, 2403-2407.
- [11] D. C. Sherrington and K. A. Taskinen, *Chem. Soc. Rev.* 2001, 30, 83-93.
- [12] T. Steiner, *Angew. Chem.* 2002, 114, 50-80; *Angew. Chem. Int. Ed.* 2002, 41, 48-76.
- [13] J. V. Barth, J. Weckesser, C. Cai, P. Günter, L. Bürgi, O. Jeandupeux, K. Kern, *Angew. Chem.* 2000, 112, 1285-1288; *Angew. Chem. Int. Ed.* 2000, 39, 1230-1234.
- [14] Q. Chen and N. V. Richardson, *Nat. Mater.* 2003, 2, 324-328.
- [15] R. Otero, M. Schöck, L. M. Molina, E. Lægsgaard, I. Stensgaard, B. Hammer and F. Besenbacher, *Angew. Chem.* 2005, 117, 2310-2315; *Angew. Chem. Int. Ed.* 2005, 44, 2270-2275.
- [16] J. A. Theobald, N. S. Oxtoby, M. A. Phillips, N. R. Champness and P. H.

- Beton, *Nature* 2003, 424, 1029–1031.
- [17] J. A. Theobald, N. S. Oxtoby, N. R. Champness, P. H. Beton and T. J. S. Dennis, *Langmuir* 2005, 21, 2038–2041.
- [18] J. C. Swarbrick, B. L. Rogers, N. R. Champness and P. H. Beton, *J. Phys. Chem. B* 2006, 110, 6113–6114.
- [19] J. V. Barth, G. Costantini and K. Kern, *Nature* 2005, 437, 671–679.
- [20] M. Stöhr, M. Wahl, C. H. Galka, T. Riehm, T. A. Jung and L. H. Gade, *Angew. Chem.* 2005, 117, 7560–7564; *Angew. Chem. Int. Ed.* 2005, 44, 7394–7398.
- [21] C. T. Seto and G. M. Whitesides, *J. Am. Chem. Soc.* 1990, 112, 6409–6411.
- [22] J. A. Zerkowski, C. T. Seto and G. M. Whitesides, *J. Am. Chem. Soc.* 1992, 114, 5473–5475.
- [23] G. M. Whitesides, E. E. Simanek, J. P. Mathias, C. T. Seto, D. N. Chin, M. Mammen and D. M. Gordon, *Acc. Chem. Res.* 1995, 28, 37–44.
- [24] W. Xu, M.-D. Dong, H. Gersen, E. Rauls, S. Vázquez-Campos, M. Crego-Calama, D. N. Reinhoudt, I. Stensgaard, E. Laegsgaard, T. R. Linderorth and F. Besenbacher, *Small* 2007, 3, 854–858.
- [25] L. Grill and F. Moresco, *J. Phys.: Condens. Matter* 2006, 18, S1887–1908.
- [26] L. Grill, F. Moresco, P. Jiang, C. Joachim, A. Gourdon and K.-H. Rieder, *Phys. Rev. B* 2004, 69, 035416.
- [27] F. Moresco, G. Meyer, K.-H. Rieder, H. Tang, A. Gourdon and C. Joachim, *Phys. Rev. Lett.* 2001, 86, 672–675.
- [28] L. Grill, K.-H. Rieder, F. Moresco, S. Stojkovic, A. Gourdon and C. Joachim, *Nano Lett.* 2005, 5, 859–863.
- [29] M. Alemani, L. Gross, F. Moresco, K.-H. Rieder, C. Wang, X. Bouju, A. Gourdon and C. Joachim, *Chem. Phys. Lett.* 2005, 402, 180–185.
- [30] E. Lægsgaard, L. Osterlund, P. Thostrup, P. B. Rosmussen, I. Stensgaard and F. Besenbacher, *Rev. Sci. Instrum.* 2001, 72, 3537–3542.
- [31] P. Sautet and C. Joachim, *Chem. Phys. Lett.* 1991, 185, 23–30.
- [32] N. L. Allinger, K. Chen, J.-H. Lii, *J. Comput. Chem.* 1996, 17, 642–668.
- [33] T. Zambelli, S. Goudeau, J. Lagoute, A. Gourdon, X. Bouju and S. Gauthier, *Chem. Phys. Chem.* 2006, 7, 1917–1920.
- [34] R. Otero, F. Hümmelink, F. Sato, S. B. Legoas, P. Thostrup, E. Lægsgaard, I. Stensgaard, D. S. Galvão and F. Besenbacher, *Nature Materials* 2004, 3, 779–782.
- [35] W. Lange, M. Jirikowsky and A. Benninghoven, *Surf. Sci.* 1984, 136, 419–436.
- [36] C.-T. Tzeng, W.-S. Lo., J.-Y. Yuh, R.-Y. Chu and K.-D. Tsuei, *Phys. Rev. B* 2000, 61, 2263–2272.

3c. Surface selection and preparation, launching, imaging and assembling on a surface and manipulation

- Insulator on metal

Nanostructuring of an ultrathin insulating film of NaCl on Cu(111)

Ch. Bombis¹, F. Ample², J. Mielke¹, M. Mannsberger¹, Ch. Joachim²
and L. Grill¹

¹Institut für Experimentalphysik, FU Berlin, Arnimallee 14, D-14195 Berlin, Germany

²CEMES-CNRS, 29 rue J. Marvig, PO Box 4347, F-31055 Toulouse Cedex, France

Keywords: growth, NaCl, LT-STM, Cu(111), alkali halide, manipulation, nanostructuring, nanomechanics, cracking

Introduction

Regardless of the insulating character of bulk alkali halides, ultrathin films of those materials grown on an electrically conducting substrate still enable electron tunnelling through the film offering the possibility of investigation with scanning tunnelling microscopy (STM) and scanning tunnelling spectroscopy (STS) [1] [2]. In the emerging field of molecular electronics [3] [4], mandatory electronic decoupling of organic molecules from an underlying metallic substrate was successfully demonstrated by the deposition of single molecules on top of ultrathin films of NaCl [5] [6] [7]. Apart for applications in molecular electronics, the understanding of the alkali halides ultrathin films (nano)mechanical behaviour was up to now mainly limited to film thickness of several tens monoatomic layers and more [8] [9] [10]. The tip of a STM is known as a structuring tool for surfaces in UHV environment [11] [12]. In this article, the nano-mechanical properties of NaCl crystalline nanoplates adsorbed on a metal substrate are presented together with their nano-structuring using the atomic scale STM manipulation ability.

Experimental

The experiments were performed in an ultra high vacuum (UHV) chamber operating at a base pressure in the low 10^{-10} mbar region, equipped with standard facilities for sample preparation, and a LT-STM from Createc [13]. Deposition of approx. 0.4 ML of NaCl occurred in 5 min. onto a clean Cu(111) sample held at a temperature between

270 K and 280 K. After deposition, the sample was directly cooled down and transferred into the cold STM working at approx. 12 K. STM imaging was performed in the constant-current mode, bias voltages are given with respect to the sample.

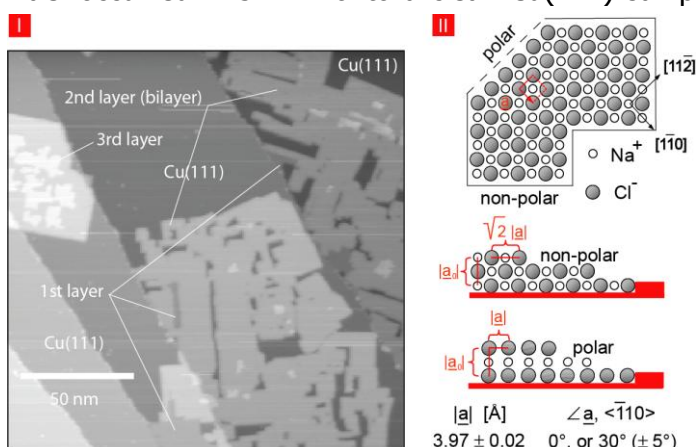


Figure 1: Growth of NaCl on Cu(111): (I) Overview image presenting clean copper terraces partially covered with 1, 2 or 3 layers of NaCl ($I_T = 0.31$ nA, $U_T = -1$ V). (II) Ball models of the NaCl lattice in top-(IIa) and side view (IIb) illustrating surface unit cell as well as polar and non-polar step edges of NaCl in comparison to a step edge of Cu(111).

Growth of NaCl on Cu(111):

The growth of NaCl on different vicinals of a copper single crystal is already described in many details in the literature (e.g. Cu(100) and Cu(111) [4] [14]). However, in most cases reported earlier, NaCl was grown on a sample held at

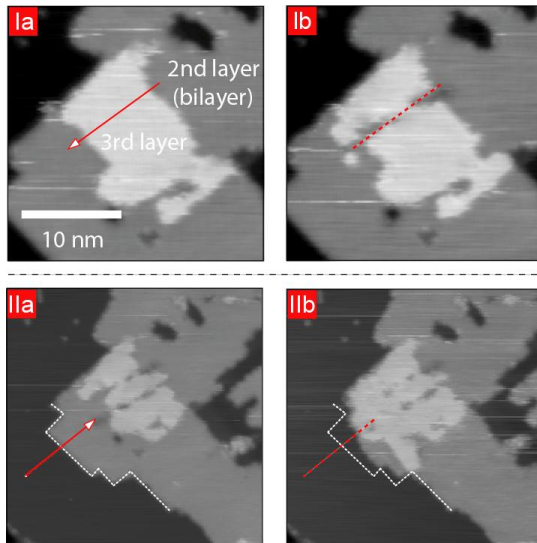


Figure 2: Image sequences visualizing the influence of lateral manipulation (LM) with the tip of the STM on different layers of NaCl on Cu(111): (I) $IT = 0.31$ nA, $UT = -1$ V; LM in const. height mode: $U = -0.05$ V, $z\text{-offset} = +4\text{\AA}$, 10 \AA/s . (II) $IT = 0.31$ nA, $UT = -1$ V; LM in const. height mode: $U = -0.05$ V, $z\text{-offset} = +7\text{\AA}$, 10 \AA/s .

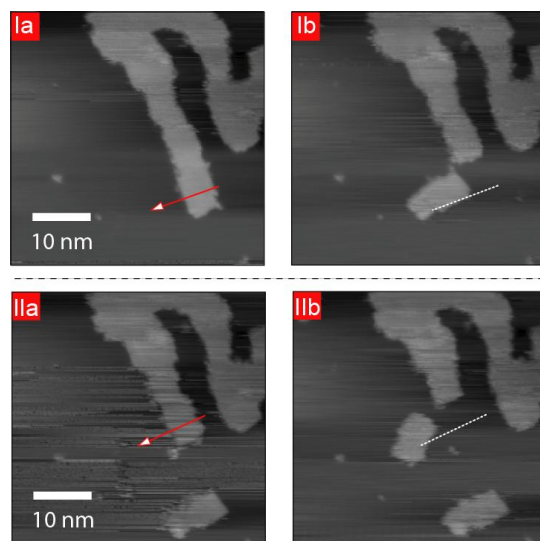


Figure 3: Cracking of bilayer islands of NaCl by lateral manipulation: $IT=0.31$ nA, $UT=-1$ V; LM in const. height mode: $U=-0.05$ V, $z\text{-offset}+7\text{ \AA}$, 10 \AA/s .

room temperature or even slightly above during deposition, while we deposited NaCl on a slightly cooled substrate [4].

Figure 1 (I) illustrates an overview image of the resulting preparation, different atomic layers of NaCl are indicated, respectively. The bilayer islands contain openings and have almost a dendrite-like shape consisting of large branches. NaCl often grows in a carpet-like mode over step edges of the underlying substrate [15]. Nevertheless, we additionally observed NaCl island edges located directly at descending and in particular also at ascending step edges of Cu(111), which is highly interesting for the formation of molecular interconnects from a conducting to a non-conducting substrate. Figure 1 (II) summarizes the crystallographic assembly of the NaCl film in particular of NaCl step edges in comparison to a step edge of the homogeneously sketched Cu(111) substrate.

Nanostructuring:

By performing lateral manipulation of the 3rd layer of NaCl, the ultrathin insulating film can be cut, as illustrated exemplarily in Figure 2 (I). The manipulation path along a non-polar direction and across an island in the 3rd layer of NaCl on Cu(111) is indicated by the red arrow in Figure 2 (Ia). The STM image after manipulation (Figure 2 (b)) reveals that NaCl is removed presumably only in the 3rd layer along the manipulation path indicated here as a dashed line. For comparable experiments at a bilayer and monolayer (not shown) of NaCl we observe a rather crude reorganization of material revealed by a comparison of NaCl step edges before (Figure 2 (IIa)) and after (Figure 2 (IIb)) manipulation. The original step edge before manipulation is in each case indicated by white dashed lines. Based on a visual inspection we assume that most of the

missing material at the island edge is deposited in the grown 3rd layer. Thus, cutting of monatomic NaCl films is possible in the 3rd layer, but not in the first and second layer, where the manipulation process causes uncontrolled reorganization of NaCl atoms.

In contrast to this cutting behaviour of NaCl, we discovered in several cases crack formation within the film as illustrated e.g. in the image sequences presented in Figure 3. Lateral manipulation indicated by the red arrows in Figure 3 (Ia/IIa) is performed in each case across a long and narrow bilayer island of NaCl. After manipulation a piece of the island cracked along a non-polar direction. Further on, the

cracked piece rotated and moved on the surface from the original connection point, i.e. it is also possible to manipulate a (small) NaCl island entirely on the metallic substrate. The dashed lines in Figure 3 (Ib/IIb) indicate for comparison the preceding manipulation revealing that the cracking edge is not just formed along but shifted parallel from the manipulation path. The cracked pieces have approximately the same size.

Island manipulation:

Island manipulation was successfully performed by lateral manipulation in constant height mode [16]. We assume in each case a contact between the tip of the STM and the nanoisland, confirmed by the fringed appearance of an island (Figure. 4) at the edges or in the interior after manipulation.

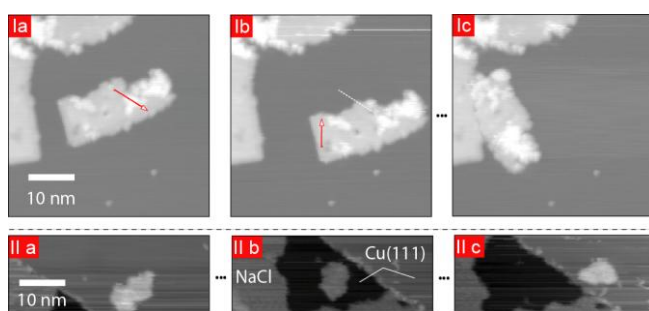


Figure 4: Lateral manipulation in constant height mode of bilayer NaCl mesa-islands on Cu(111): $IT = 0.31$ nA, $UT = -1$ V; LM in const. height mode: $U = -0.05$ V, z -offset = $+7$ Å, 10 Å/s.

Figure 4(I) presents an image sequence, which demonstrates, how a NaCl bilayer island is in summary rotated by 90° , and manipulated on top of the Cu(111) substrate towards a step edge of NaCl. The largest bilayer island, which we manipulated successfully, covers an area of 250 nm². Aiming to explore whether a bilayer of NaCl is stable but also flexible, thus behaving also like a carpet during lateral motion as in the case of growth [15], we performed an island manipulation across a step

edge of Cu(111) as presented in the image sequence in Figure 4 (II). We were able to move the bilayer island from an upper terrace (Figure 4 (IIa)) across a descending step edge of Cu(111) to the next lower terrace (Figure 4 (IIb)) and back across the ascending step edge again onto the upper terrace (Figure 4 (IIc)). Even though the island size shrunk after many manipulation steps leading also to a change in the island shape, we still observe an intact bilayer island, which is still crystalline as conformed by atomic resolution.

Theory:

In order to understand the process of island cutting, cracking, and manipulation, molecular mechanics simulations were performed using the ASED+ program [17]. All NaCl atomic interactions were treated pair wise considering the atoms as rigid ions with the interaction potential as described in reference [18]. The interactions of the Na and Cl atoms with the Cu surface were also modeled using a Van der Waals pair wise potential as in [17]. The interactions of the tip composed with 10 rigid atoms with the Na and Cl atoms were described just with a repulsive potential. To simulate the cracking of the NaCl clusters, the tip was positioned 7 Å away from the surface and moved laterally toward the island in steps of 1 Å. The main findings can be summarized as follows. The simulations show in accordance with the experiment that small islands can freely be manipulated across the copper terrace independent of the registry to the substrate. To reproduce the cracking behaviour of a bilayer NaCl island two columns of NaCl pairs of the island are held fixed during the simulated manipulation. This corresponds to an experiment where a long and narrow island is directly connected to a larger island like a branch of a center island. For long islands the cracking distance between the point of contact and the cracking edge remains nearly constant and independent of the island length. A direct consequence of this

result is that cracked pieces of a long island have approximately the same size, which is in agreement with the experimental observation discussed before (see Figure 3).

Summary

We have successfully grown an ultrathin film of NaCl on a cold Cu(111) substrate and performed cutting, cracking and island manipulation with the tip of a LT-STM. We were thereby able and have conceptually shown how to realize a configuration, where a bilayer NaCl island is connected to an ascending copper step edge. Such a configuration is highly interesting for the formation of molecular interconnects from a conducting to a non-conducting (NaCl island) substrate, as it reduces the geometrical height differences from 5.64 Å (bilayer island of NaCl on copper terrace) to 3.55 Å (bilayer island of NaCl at ascending step edge of (111) surface of copper) between the different substrates.

References

- [1] S. Schintke and W. D. Schneider, *J. Phys.: Condens. Matter* 2004, 16, R49.
- [2] R. J. Bennewitz, *Phys.: Condens. Matter* 2006, 18, 417.
- [3] P. Liljeroth, J. Repp and G. Meyer, *Science* 2007, 317, 1203.
- [4] J. Repp and G. Meyer, *Applied Physics A* 2006, 85, 399.
- [5] J. Repp, et al. *Phys. Rev. Lett.* 2005, 94, 026803.
- [6] E. Cavar, et al. *Phys. Rev. Lett.* 2005, 95, 196102.
- [7] C. J. Villagomez et al. *Chem. Phys. Lett.* 2007, 450, 107.
- [8] M. D. Kriese, et al. *Engineering Fracture Mechanics* 1998, 61, 1.
- [9] Z. C. Xia and J.W. Hutchinson, *Journal of the Mechanics and Physics of Solids* 2000, 48, 1107.
- [10] J. Malzbender, et al. *Materials Science & Engineering R* 2002, 36, 47.
- [11] L. C. Venema, et al. *Appl. Phys. Lett.* 1997, 71, 2629.
- [12] M. Riehl-Chudoba, W. Richter and V. A. Gasparov, *J. Appl. Phys.* 1998, 83, 2500.
- [13] G. Meyer, *Review of Scientific Instruments* 1996, 67, 2960.
- [14] F. E. Olsson and M. Persson, *Surf. Sci.* 2003, 540, 172.
- [15] C. Schwennicke, J. Schimmelpfenning and H. Pfnür, *Surf. Sci.* 1993, 293, 57.
- [16] F. Moresco, et al. *Appl. Phys. Lett.* 2001, 78, 306.
- [17] F. Ample and C. Joachim, *Surf. Sci.* 2008, 602, 1563.
- [18] H. Tang, et al. *J. Chem. Phys.* 1998, 108, 359.

STM imaging of molecules on a thin insulating film

Carlos Javier Villagomez Ojeda¹, Sébastien Gauthier¹, André Gourdon¹,
Sladjana Stojkovic¹, Christian Joachim¹ and Tomaso Zambelli²

¹CEMES-CNRS, 29 rue J. Marvig, P.O. Box 94347 31055 Toulouse (France)

Fax: (+33) 5 62 25 79 99 E-mail: gauthier@cemes.fr

²Laboratory of Biosensors and Bioelectronics, ETH Zurich

Gloriastrasse 35, CH-8092 Zurich (Switzerland)

Keywords: Scanning Tunneling Microscopy and Spectroscopy, Molecular orbitals, single adsorbed molecules

Introduction

Until recently, STM was the only technique allowing to image individual molecules adsorbed on surfaces. For this reason, single molecule studies were restricted to conducting substrates. Some strategies were developed to allow well defined electrical connections to single molecules on metals, based on the synthesis of specially designed molecules [1], but these approaches are not suited for further developments, such as planar electrical connections to a single molecule. The emergence and progress of AFM in the non-contact mode make now possible to image a single molecule on an insulating substrate [2], but this technique is rather difficult and molecular manipulations are not yet well mastered, as it is the case for STM. It was realized recently [3-6] that it is possible to use STM to study molecules adsorbed on ultrathin insulating films on conducting substrates. In this situation the insulating film electronically decouples the molecule from the substrate, while still allowing the transport of a weak tunneling current through the structure.

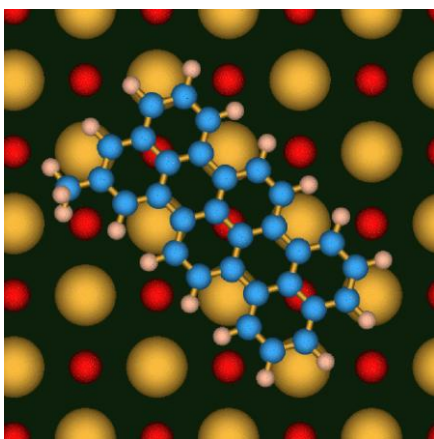


Figure 1: Position of methylterrylene (MeT) on the NaCl top layer for the EH-ESQC calculation. Red dots correspond to Na⁺ ions, yellow dots to Cl⁻ ions.

A recent achievement in this research area was the imaging of the frontier molecular orbitals of a single adsorbed molecule by STM [5]. When a molecule is directly adsorbed on a conductive surface, the discrete molecular levels are broadened, shifted and mixed by interaction with the electronic continuum of the substrate. As a consequence, many MOs contribute to the tunneling current through the molecule, even when their energies are far away from the Fermi level of the substrate [7]. This phenomenon makes the observation of a well-defined MO by STM exceptional [8]. The key point in ref. 5 is the use of a NaCl bilayer as an ultrathin insulating layer interposed between the molecule and the substrate. Its role is to electronically decouple the molecule from the supporting metallic substrate. In this way, images that are strikingly similar to the frontier orbitals of the isolated free molecule were obtained for pentacene adsorbed on

a NaCl bilayer on Cu(111) [5]. This method provides a systematic and efficient way to visualise MOs. It opens the fascinating possibility to investigate at the submolecular level many of the concepts developed to understand organic chemistry basic rules.

In this paper, we report the first step in a program aimed at exploring substituent effects on a π -electron system at the single molecule level using STM. We chose

terrylene, a medium size conjugated molecule and a methyl group as substituent (Figure 1). The methyl group is considered as a weak donor, which should perturb only slightly the frontier orbitals via its hyperconjugative interaction with the terrylene core. The molecules were adsorbed on a NaCl bilayer on Cu(111) and studied by low temperature (5K) STM [9]. Some of the results presented in this report have been already published elsewhere [10].

Results

STM images of the MeT molecule adsorbed directly on Cu (111) are shown for different bias voltages in Figure 2a, b and c. At low voltage (Figure 2a), the molecules, which interact with the surface state of Cu(111), appear as elongated protrusions, with a size which is of the order of the size of the molecule and only weak internal structure. No significant differences are observed when the bias voltage is changed in the [-3 V, 3 V] range, as shown in Figures 2 b and c.

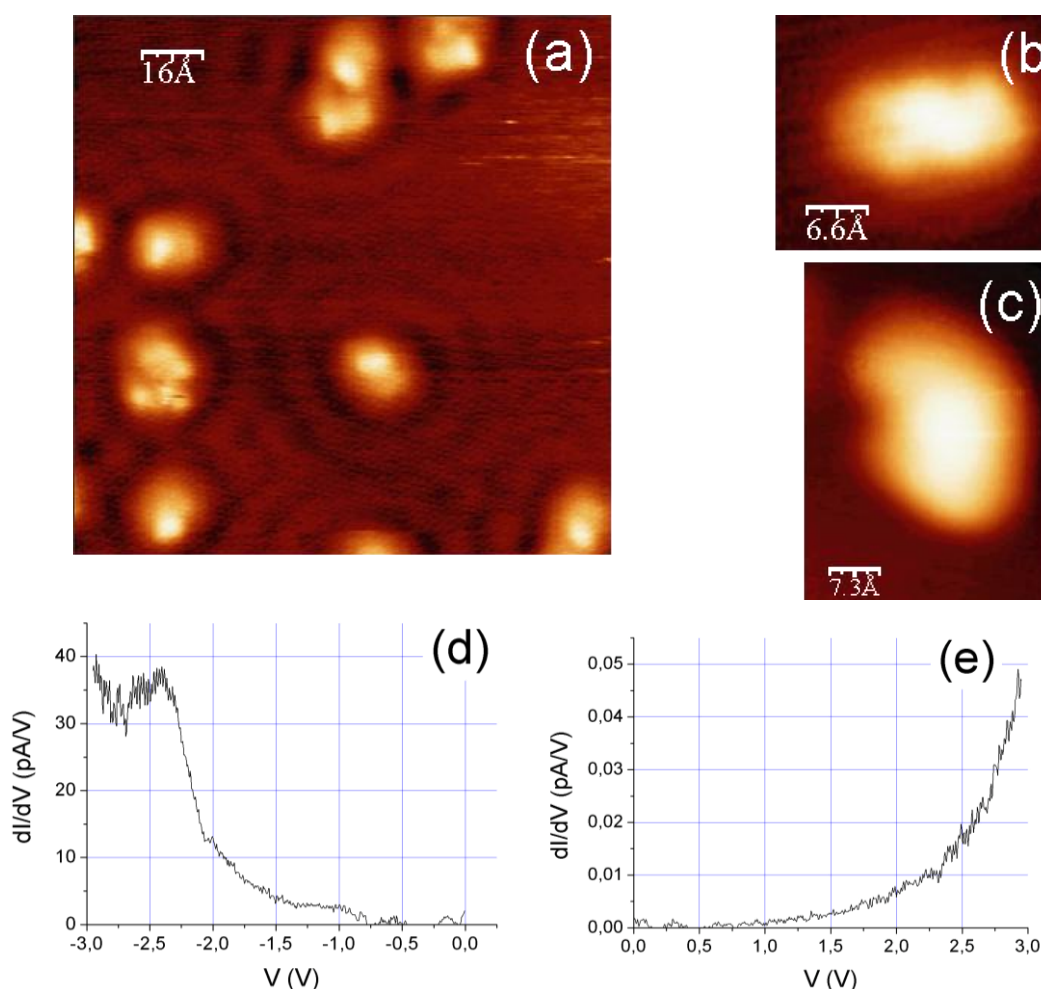


Figure 2: Constant-current STM images of MeT adsorbed on Cu(111) at 5K. (a) $V_t=0.2$ V, $I_t=10$ pA, (b) $V_t=-2.5$ V, $I_t=1$ pA (c) $V_t=2.5$ V, $I_t=1$ pA and dI/dV spectra for (d) occupied and (e) unoccupied states.

Differential conductance $dI/dV(V)$ spectra for occupied (Figure 2d) and unoccupied (Figure 2e) states have the characteristic shape usually observed on metallic substrates, except for a peak near -2.5 V, which is not systematically observed. These observations are typical for molecules adsorbed on metallic substrates, where due to the mixing of the molecular orbitals mentioned previously, the images are not clearly related to specific, single molecular orbitals.

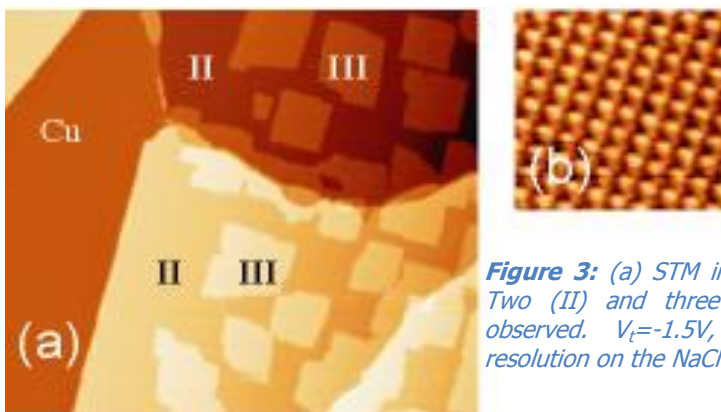


Figure 3: (a) STM images of a NaCl deposit on Cu(111). Two (II) and three (III) NaCl layers thick areas are observed. $V_t = -1.5V$, $I_t = 1pA$, $40 \times 40 \text{ nm}^2$ (b) Atomic resolution on the NaCl bilayer. $V_t = 1.5V$, $I_t = 50 \text{ pA}$, $4 \times 4 \text{ nm}^2$

NaCl was grown on Cu(111) at room temperature from a copper crucible heated to approximately 300 °C (Figure 3). The sample was then transferred to the STM and the MeT molecules were deposited by thermal sublimation from a tungsten filament on the sample surface held at low temperature ($T < 10 \text{ K}$).

Two conductance spectra, acquired above the centre of a MeT molecule are shown in Figure 4a (resp. 4b) for negative (resp. positive) bias voltage. They exhibit two broad peaks, near -2.5 V and +1.4 V, separated by a flat region. The position and the width of these features vary slightly from one molecule to the other. A constant-current STM image obtained at low bias, in the flat spectral region separating the two peaks reflects the overall shape of the molecule (Figure 4d). The methyl group is revealed by a protrusion that extends outside the rectangular board of the molecule. The image size is of the order of the geometrical structure of the molecule. The height is around 0.1 nm. No internal structure is discernible.

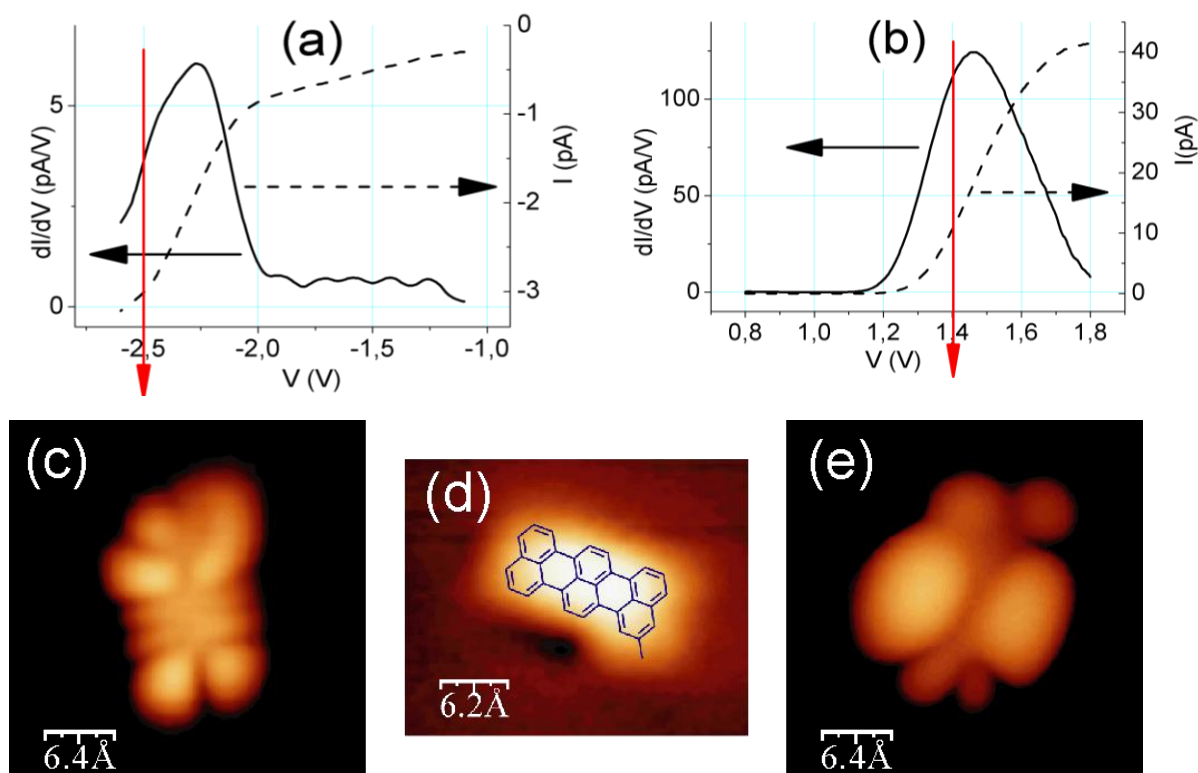


Figure 4: dI/dV spectra for (a) occupied and (b) unoccupied states for MeT on a NaCl bilayer on Cu(111). Constant-current STM images at $I_t = 1 \text{ pA}$ and (c) $V_t = -2.5 \text{ V}$, (d) $V_t = -1.5 \text{ V}$ and (e) $V_t = 1.4 \text{ V}$.

Much more extended and structured images are obtained when the bias voltage is within or beyond the spectroscopic peaks of Figure 4a and b. An experimental STM image obtained at negative sample bias is displayed in Figure 4c. The image is much larger than in the spectral gap and exhibits well defined lobes separated by dark lines. The height of the image of the molecule can reach 0.2 nm, depending on the value of the bias voltage. The image obtained at positive bias voltage displays similar features (Figure 4e). It shows 6 lobes and its height can reach 0.5 nm.

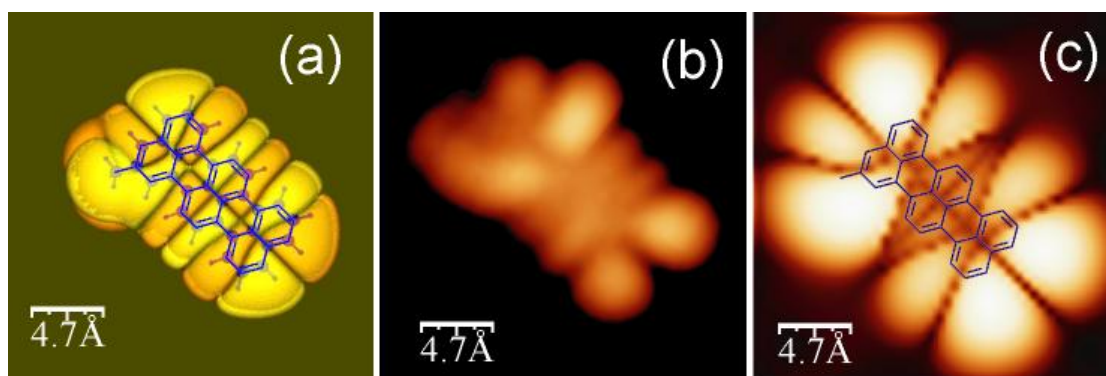


Figure 5: (a) Electronic probability density of the HOMO of the free MeT molecule for $\rho = 10^{-7} \text{ \AA}^{-3}$, (b) experimental image ($I_t = 1\text{pA}$, $V_t = -2.5\text{ V}$), (c) calculated image.

The HOMO of the free molecule, calculated using the semi-empirical Extended Hückel approximation [11], is shown in Figure 5a for a value of the orbital electronic probability density $\rho=10^{-7} \text{ \AA}^{-3}$. The similarities between the STM image (Figure 5b) and the calculated HOMO (Figure 5a) are striking. Not only the topology of the orbital's lobes is reproduced but also their size and their shape. One difference is that the central transversal nodal plane is not visible in the experimental image. This is probably related to a limited resolution of the tip used for this experiment.

These similarities suggest that in the experimental conditions corresponding to Figure 5b, the STM probes the HOMO of the adsorbed molecule at a very low density. As seen from the scale in Figure 5, this density corresponds to a distance from the board of the molecule of the order of 0.5 nm, unusually large for a MO in the context of chemistry.

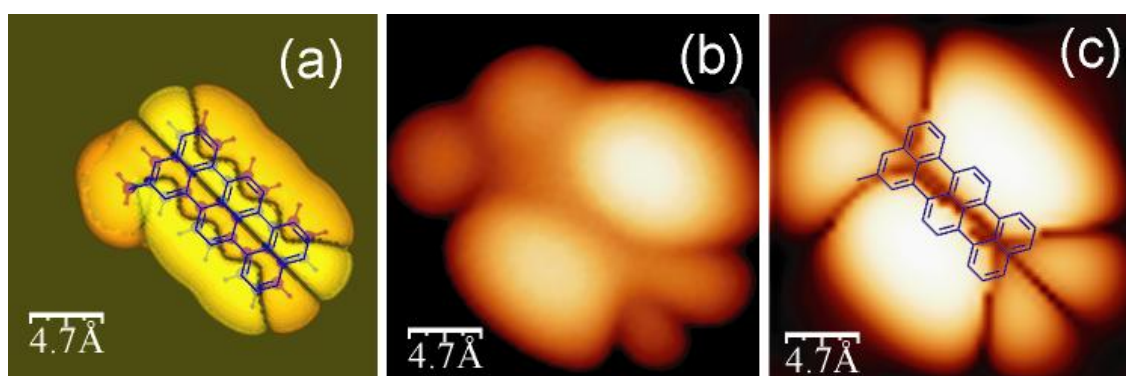


Figure 6: (a) Electronic probability density of the LUMO of the free MeT molecule for $\rho = 10^{-7} \text{ \AA}^{-3}$, (b) experimental image ($I_t = 1\text{pA}$, $V_t = 1.4\text{ V}$), (c) calculated image.

Images calculated by Elastic Scattering Quantum Chemistry (ESQC) calculations [12] are displayed in Figure 5c and 6c. The structure of the system used for the calculation is shown in Figure 1. The molecule was positioned at 0.3 nm above the bulk-like and rigid NaCl bilayer. The molecular conformation was deduced from a molecular mechanics optimization on Cu(111) [13]. This results in a nearly flat molecular board with one of the C-H bonds of the methyl group oriented near a vertical plane. Different tests showed that the calculated images are not very dependent on the precise orientation of the methyl group. The agreement between experimental and calculated images is satisfactory: the size and shape of the orbital lobes are well reproduced, except for the central part of the molecule of Figure 5b, as already mentioned. In particular, the two wavy longitudinal nodal surfaces that are observable on the calculated LUMO electronic density do not appear in the calculated STM image.

The LUMO of the free molecule calculated at the same electronic density $\rho = 10^{-7} \text{ \AA}^{-3}$ is shown in Figure 6a. Here again, strong similarities with the experimental image of Figure 6b appear, except for the middle portion of the two wavy longitudinal nodal surfaces that appear in the calculated LUMO but not in the experimental image.

Discussion

These results confirm the conclusions already reached for the simpler case of pentacene [5]: the peaks observed in the spectra of fig 4 are closely related to the HOMO and the LUMO of the molecule. The energy gap separating these resonances is approximately 3.8 eV, quite different from the 2.35 eV observed for the optical HOMO-LUMO gap of terrylene [14]. The reason for this discrepancy is that, as a consequence of the increased lifetime of an electron on the molecule due to the decoupling effect of the insulating layer, these peaks should be considered as characterizing a transient negative ion for the LUMO and a transient positive ion for the HOMO [5]. The ionization potential and the electron affinity of terrylene are 6.42 eV [15] and 1.66 eV [16]. When referred to the work function of NaCl/Cu(111) which is about 4 eV, the corresponding energy levels are at -2.42 eV and + 2.34 eV, but their interaction with the substrate is expected to shift them toward the Fermi level. The observed peak widths (0.3 to 0.4 eV) is not related to the lifetime of the electron but to the coupling of the molecular states with the phonons of the NaCl film [17].

Previous studies showed that even orbitals (atomic or molecular) located very far (a few eV) from the Fermi level of the substrate can contribute to the STM image [7, 18] at least when the molecule is adsorbed on a metallic surface. The comparison of the experimental and calculated images demonstrates that this is not the case here, due to the decoupling effect of the insulating layer. It was checked that the MO that have a strong contribution on the methyl group do not contribute to the calculated images of the frontier orbitals of MeT. There is no "direct" contribution of the methyl group, but an "indirect" one, which is the consequence of a hyperconjugative interaction between the methyl group and the terrylene core. As shown for example in ref. 19, methyl group orbitals of π symmetry can significantly interact with a neighboring π system.

This work confirms that there are strong similarities between the STM images of a molecule adsorbed on an ultrathin insulating film and its frontier orbitals at very low electronic density. There are nevertheless some differences that are not fully understood. For instance, as mentioned previously, two nodal surfaces that appear on the LUMOs of the free molecule are not observed on the experimental and on the calculated STM images. A truly quantitative understanding of these observations is not yet achieved. Further studies on different and more complex molecules will certainly help in reaching this goal.

Acknowledgements

Partial support by the European Commission within the projects CHIC (Contract n° IST-2001-33578) and PicoInside (Contract n° IST-015847) is gratefully acknowledged. CVO thanks CONACYT/Mexico for support.

References

- [1] V. J. Langlais, R. R. Schlittler, H. Tang, A. Gourdon, C. Joachim and J. K. Gimzewski; *Phys. Rev. Lett.* 83, 2809-2812 (1999).
- [2] S. Hirth, F. Ostendorf, J. Schütte, R. Bechstein, A. Kühnle and M. Reichling; *E-Nano Newsletter* 6, 22 (2006).
- [3] X. H. Qiu, G. V. Nazin and W. H. Ho; *Science* 299 542 (2003).
- [4] E. Cavar, M. C. Blüm, M. Pivetta, F. Patthey, M. Chergui and W. D. Schneider; *Phys. Rev. Lett.* 95, 196102 (2004).
- [5] J. Repp, G. Meyer, S. M. Stojkovic, A. Gourdon and C. Joachim; *Phys. Rev. Lett.* 94, 026083 (2005).
- [6] J. Repp, G. Meyer, F. Olsson and M. Persson; *Science* 305, 493 (2004).
- [7] C. Chavy, C. Joachim and A. Altibelli; *Chem. Phys. Lett.* 214, 569 (1993).
- [8] J. I. Pascual, J. Gomez-Herrero, C. Rogero, A. M. Baro, D. Sanchez-Portal, E. Artacho, P. Ordejon and J. M. Soler; *Chem. Phys. Lett.* 321, 78 (2000).
- [9] OmicronNanoTechnology GmbH Limburger Str. 75 65232 Taunusstein (Germany).
- [10] C. Villagomez, T. Zambelli, S. Gauthier, A. Gourdon, C. Barthes, S. Stojkovic and C. Joachim; *Chemical Physics Letters* 450 (2007) 107
- [11] <http://yaehmop.sourceforge.net/>
- [12] P. Sautet and C. Joachim; *Chem. Phys. Lett.* 185, 23 (1991).
- [13] N.L. Allinger, K.-H. Chen, J.-H. Lii and K.A. Durbin; *J. Comput. Chem.* 24, 1447 (2003).
- [14] T. M. Halasinski, J. L. Wiesman, R. Ruitkamp, T. J. Lee, F. Salama and M. Head-Gordon; *J. Phys. Chem. A* 107, 3660 (2003).
- [15] E. Clar and W. Schmidt; *Tetrahedron* 34, 3219 (1978).
- [16] G. Malloci, G. Mulas, G. Cappellini, V. Fiorentini and I. Porceddu; *A&A* 432, 585 (2005).
- [17] J. Repp, G. Meyer, S. Paavilainen, F. E. Olsson and M. Persson; *Phys. Rev. Lett.* 95, 225503 (2005).
- [18] D. M. Eigler, P. S. Weiss, E. K. Schweizer and N. D. Lang; *Phys. Rev. Lett.* 66, 1189 (1991).
- [19] L. Libit and R. Hoffmann; *J. Amer. Chem. Soc.* 96, 1370 (1974).

Scanning Probe Microscopy of Adsorbates on Insulating Films

Gerhard Meyer¹, Peter Liljeroth¹ and Jascha Repp^{1,2}

¹IBM Zurich Research Laboratory 8803 Rüschlikon, Switzerland

²Institute of Experimental and Applied Physics University of Regensburg,
93040 Regensburg, Germany
gme@zurich.ibm.com

Ultrathin insulating films on metal substrates are unique systems to use the scanning tunnelling microscope to study the electronic properties of single atoms and molecules, which are electronically decoupled from the metallic substrate.

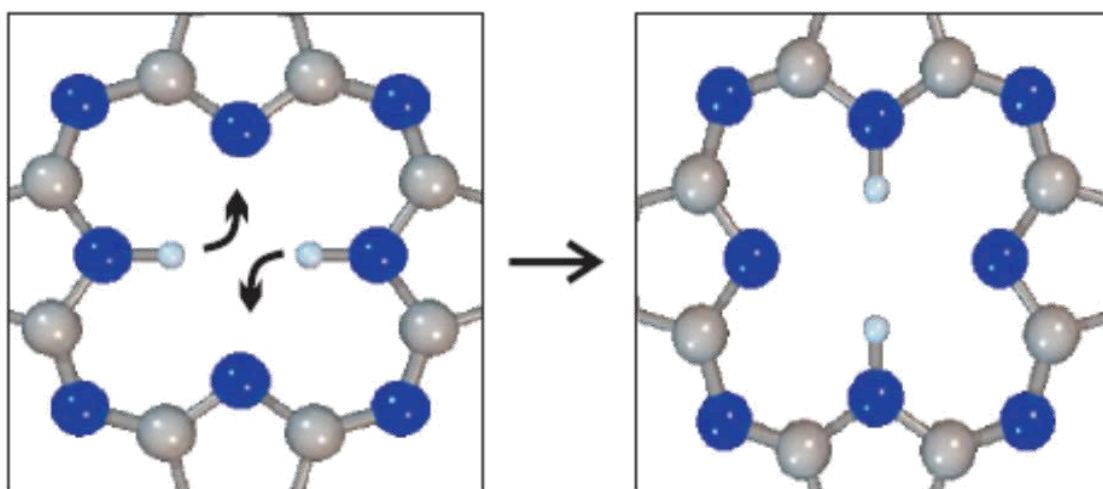


Figure 1: Model of hydrogen tautomerization in the inner cavity of a naphthalocyanine molecule

Individual gold atoms on an ultrathin insulating sodium chloride film supported by a copper surface exhibit two different charge states, which are stabilized by the large ionic polarizability of the film [1]. The charge state and associated physical and chemical properties such as diffusion can be controlled by adding or removing a single electron to or from the adatom with a scanning tunneling microscope tip. The simple physical mechanism behind the charge bistability in this case suggests that this is a common phenomenon for adsorbates on polar insulating films. For example in the particular case of Ag adatoms even three different charge states could be observed [2]. In the case of molecules on ultrathin NaCl films the electronic decoupling allows the direct imaging of the unperturbed molecular orbitals. This has been shown for individual pentacene molecules [3]. Scanning tunneling spectroscopy of these double-barrier tunneling-junctions reveals strong electron-phonon coupling to NaCl phonons. Using atomic/molecular manipulation a covalent bond between an individual pentacene molecule and a gold atom can be formed. This bond formation is reversible and different structural isomers can be produced. Direct imaging of the orbital hybridization upon bond formation provides insight into the energetic shifts and occupation of the molecular resonances.

Molecular switches will be an essential part of possible future molecular devices. The bistability in the position of the two hydrogens in the inner cavity of single free-base naphthalocyanine molecules (Figure 1) constitutes a two level system that can be manipulated and probed by low temperature scanning tunnelling microscopy. When

adsorbed on an ultrathin insulating film, the molecules can be switched in a controlled fashion between the two states by excitation induced by the inelastic tunnelling current. The tautomerization reaction can be probed by resonant tunnelling through the molecular orbitals (Figure 2). Coupling of the switching process such as charge injection in one molecule induced tautomerization in an adjacent molecule was demonstrated [4].

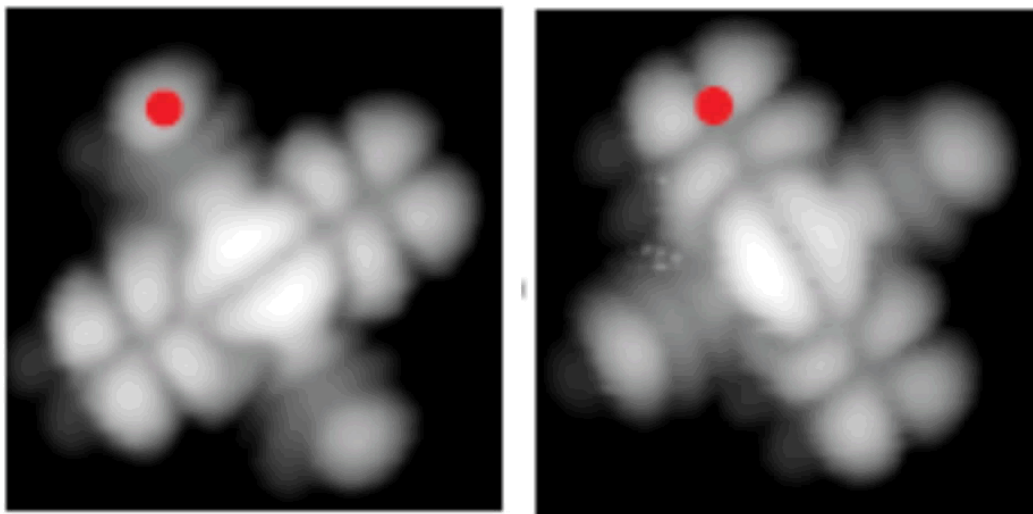


Figure 2: Switching between the two configurations as imaged directly by the orientation of the LUMO of the naphthalocyanine molecule.

References:

- [1] J. Repp, G. Meyer, F. E. Olsson and M. Persson, 'Controlling the Charge State of Individual Gold Adatoms', *Science* 305, 493 (2004)
- [2] F. E. Olsson, S. Paavilainen, M. Persson, J. Repp and G. Meyer, 'Multiple Charge States of Ag Atoms on Ultrathin NaCl Films', *Phys. Rev. Lett.* 98, 176803 (2007)
- [3] J. Repp, G. Meyer, S. M. Stojkovic, A. Gourdon and C. Joachim, 'Molecules on Insulating Films: Scanning-Tunneling Microscopy Imaging of Individual Molecular Orbitals', *Phys. Rev. Lett.* 94, 026803 (2005)
- [4] P. Liljeroth, J. Repp and G. Meyer, 'Current-Induced Hydrogen Tautomerization and Conductance Switching of Naphthalocyanine Molecules', *Science* 317, 1203 (2007)

3c. Surface selection and preparation, launching, imaging and assembling on a surface and manipulation

- Semiconductor

STM study of organic molecules adsorbed on semiconductor surfaces

Antoni Tekiel, Grzegorz Goryl, Szymon Godlewski, Jakub S. Prauzner-Bechcicki, Jacek J. Kolodziej, Janusz Budzioch and Marek Szymonski

*Research Centre for Nanometer-scale Science and Advanced Materials (NANOSAM),
Faculty of Physics, Astronomy and Applied Computer Science, Jagiellonian University,
Reymonta 4, 30-059 Krakow, Poland*

Keywords: semiconductors, organic molecules, InSb, TiO₂, PTCDA, Violet Landers, [11]helicene, nano-electronics, high resolution STM imaging, molecular wires, single molecule manipulation

The very heart of future nano-electronics will be a single organic molecule designed to perform specific operations within an electronic circuit. Therefore, manipulation and imaging of single organic molecules deposited onto semiconductor surfaces are among the main challenges to be faced. Various molecular species are used in such a type of research, for example: 3,4,9,10-perylene-tetracarboxylic-dianhydride (PTCDA), Violet Landers (C₁₀₈H₁₀₄, VL) or [11]helicene to name only few. Some of those molecules are interesting as being representative for molecular electronics and the others are especially designed in a way to possess some unique properties. For instance, PTCDA may be regarded as a prototypical, planar stacking, organic semiconductor and Violet Lander molecules possess especially designed lateral groups acting like legs and, therefore, separating a molecular board from the substrate. Here we would like to report on measurements of several types of the molecule-semiconductor system. Three substrates were used, namely: InSb(001), TiO₂(110) and TiO₂(011), as well as, three different molecular species: PTCDA, Violet Landers and [11]helicene. Results concerning PTCDA molecules deposited on InSb(001) surface has been already reported in E-nano-newsletter [1], therefore here only PTCDA/TiO₂ system will be considered. Violet Lander molecules were deposited on both InSb and TiO₂ substrates, respectively. Finally, [11]helicene molecules were measured on InSb only.

In case when a sub-molecular resolution is of interest, very often scanning tunnelling microscopy at low temperatures, down to liquid nitrogen or even helium temperatures has to be applied. Due to lowering of the temperature thermal excitations of the system are reduced to a minimum and the ultrahigh resolution imaging is possible. Therefore, in order to achieve such a sub-molecular resolution experiments were performed in two distinct ultra-high vacuum systems both allowing measurements at low temperatures. First system was equipped with low temperature scanning tunnelling microscope device (LT-STM) and the second was provided with varied temperature scanning probe apparatus (VT-AFM/STM), both commercially designed by Omicron.

Molecules deposited on InSb(001) surface were generally imaged using LT-STM system with sample holder mounted directly on the cryostat filled-up with liquid nitrogen. Measurement were carried on with use of etched tungsten tips as probes in constant current mode with a tunnelling currents varying from 50 pA to 150 pA. InSb wafers (Kelpin Crystals) were pre-annealed at 700K for several hours and then cleaned by ion sputtering with a 700eV Ar⁺ beam. The quality of the InSb(001)-c(8×2) surface was controlled with low energy electron diffraction (LEED) and STM techniques. [11]helicene and Violet Lander molecules were evaporated on InSb surface kept at room temperature from the Knudsen cell heated up to 490K and 635K, respectively. Scanning probe imaging of clean and covered with molecules TiO₂ samples was carried out with use of VT-AFM/STM microscope. STM images of empty-states were acquired

in the constant current mode (very low tunnelling currents, of the order of a few pA, were used) at positive sample bias voltages with electrochemically etched tungsten tips. Polished $\text{TiO}_2(110)$ and $\text{TiO}_2(011)$ wafers (MaTeck GmbH) were mounted on the sample holder with a Si wafer as a resistive heater. The $\text{TiO}_2(110)-(1 \times 1)$ and $\text{TiO}_2(011)-(2 \times 1)$ surfaces were initially pre-annealed at 800K and thereafter prepared by cycles of 1keV Ar^+ sputtering and subsequent annealing at 920-960K. The quality of surface was controlled via STM measurements. PTCDA molecules were deposited on $\text{TiO}_2(011)-(2 \times 1)$ surface kept at elevated temperature, stabilized in the range of 300-370K (more details on evaporation procedure may be found in [2]). VL molecules were evaporated on $\text{TiO}_2(110)-(1 \times 1)$ and $\text{TiO}_2(011)-(2 \times 1)$ surfaces kept at room temperature. In each case, molecular flux was checked with quartz micro-balance and for image processing and analysis WSxM software was used [3].

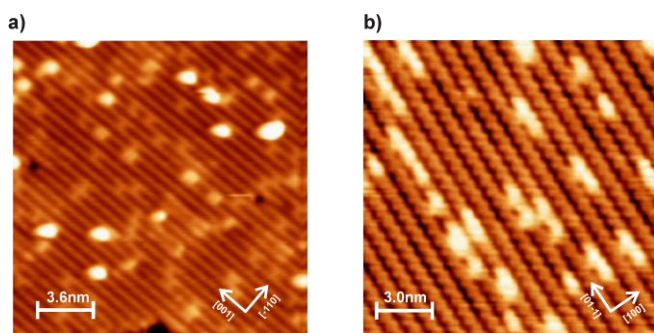


Figure 1: STM image of clean surfaces of rutile $\text{TiO}_2(110)-(1 \times 1)$ (a) and $\text{TiO}_2(011)-(2 \times 1)$ (b). (a) bias voltage: 1.6V, tunnelling current: 100pA; (b) bias voltage: 2V, tunnelling current: 2pA.

Firstly, clean substrate surfaces were scanned with atomic resolution. A high resolution STM images of $\text{InSb}(001)-c(8 \times 2)$ surface and appearance of, so called, charge density waves at temperatures below 180K were discussed in March 2007 issue of E-Nano-newsletter [1] and therefore are not reproduced here. In Figure 1a high resolution STM images of clean $\text{TiO}_2(110)-(1 \times 1)$ and $\text{TiO}_2(011)-(2 \times 1)$ surfaces are shown. In the case of the (110) face of rutile (see Figure 1a) oxygen rows are seen as dark lines along the [001] direction with bright spots indicating oxygen vacancies (big, bright spots are probably due to bridging hydroxyl and pairs of bridging hydroxyl groups adsorbed on the surface [4]), whereas for the (011) face a bright zigzag pattern parallel to the [01-1] direction is clearly visible (see Figure 1b). It is worth nothing that theoretical model of the (011) face is still under debate and several proposition has been made to date (see for example [5;6]). Here the model proposed by Beck *et al.* [5] is adopted, in which the zigzag pattern corresponds to under-coordinated oxygen atoms. However, one exception is made, coordination of oxygen atoms within the zigzag pattern is left undetermined in contrast to single coordination suggested in original model [5].

Secondly, adsorption of [11]helicene molecules on $\text{InSb}(001)-c(8 \times 2)$ surface was examined. [11]helicene molecule is an organic molecule consisting of eleven benzene rings angularly annulated so as to give a helically shaped molecule. There are two possible chiralities of the molecule due to clockwise and counter-clockwise arrangement of benzene rings. Measurements of [11]helicene molecules adsorbed on $\text{InSb}(001)-c(8 \times 2)$ showed that molecules adsorb on step-edges rather than on terraces (see

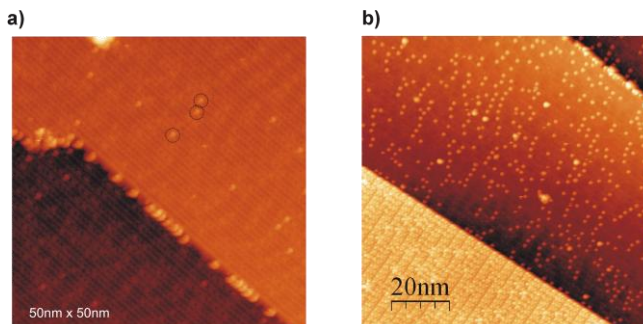


Figure 2: STM image of [11]helicene adsorbed on $\text{InSb}(001)-c(8 \times 2)$ surface at different coverage: (a) 0.1ML coverage, bright protrusions characteristic for low temperature phase of $\text{InSb}(001)$ are marked with circles, bias voltage: -3V, tunnelling current: 10pA; (b) 0.2-0.4ML coverage, bias voltage: -3V, tunnelling current: 10pA.

Figure 2a) [7]. Molecules were deposited on substrate kept at room temperature, therefore their absence on terraces and appearance on edges suggest that diffusion length of the molecules at room temperature is fairly large. For higher coverage, molecules tend to form islands (see Figure 2b). In Figure 3 high resolution images of [11]helicene molecules near a step-edge are presented as a topographic scan and a current map taken at sample bias of -3V. Presence of [11]helicene molecules at step-edges opens possibility to use the molecule as an interconnection between two parts of future nano-electronic circuit placed on two terraces of InSb. Moreover, the height of the [11]helicene molecule adsorbed on InSb(001) is similar to the height of the InSb terrace covered with one monolayer of KBr. That in turn allows to use KBr as an insulator layer on a semiconductor InSb substrate and still [11]helicene as an interconnection between two levels in the future electronic circuit design [7].

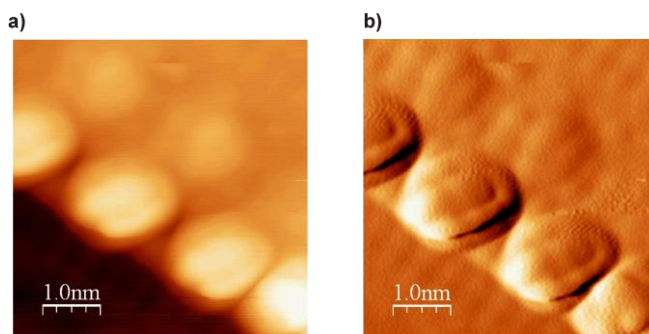


Figure 3: High resolution images of [11] helicene adsorbed near a step-edge on InSb(001)-c(8x2) surface. Bias voltage: -3V, tunnelling current: 10pA. (a) topographic image; (b) current map.

Thirdly, another, rather complex, molecule was examined during the experiment, namely, Violet Lander molecule. Violet Lander molecule belongs to Lander series of molecules that consist of planar polyaromatic board with four 3,5-di-tert-butyl-phenyl (TBP) side groups. TBP groups attached to the molecular board act as legs separating the board from the substrate. VL molecules have longer board and the legs that could rotate independently as

compared to other Lander type molecules. In STM images VL molecules are seen as four bright lobes in a rectangular configuration. The lobes correspond to four spacer groups. In the following, as a substrate for VL molecules both InSb and TiO₂ (both faces) surfaces were used [8,9].

Measurements of adsorption of VL molecules on InSb(001)-c(8x2) surface showed, that at room temperatures the mobility of molecules is high enough to allow their diffusion towards step-edges. However, approx. 23% of molecular population still stayed on the terraces, probably immobilized by surface defects (see Figure 4). Molecules that have adsorbed on InSb terraces were observed in at least six different conformations. Those conformation could be grouped into three sets: the first would consist of molecules adsorbed perpendicularly to the InSb reconstruction rows (the [110] direction) of the surface - approx. 35% of molecules fell into this group; the second would include molecules rotated with respect to the reconstruction troughs - approx. 25% of molecules and the third group involve molecules with their longer axis parallel to the [110] direction - approx. 40%. More detailed discussion on the observed conformation may be found in [8]. Nonetheless,

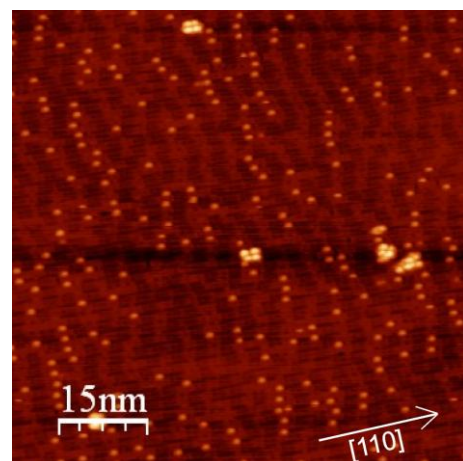


Figure 4: STM image of VL molecules on InSb(001)-c(8x2) terrace. Molecules are seen as four bright lobes in a rectangular configuration. Bias voltage -2.5V, tunnelling current: 10pA.

most of the VL molecules were adsorbed on the step-edges of InSb(001)-c(8×2) surface. Their appearance in STM scans depended on the orientation of the step-edge on which the molecule adsorbed with respect to the reconstruction rows. On edges running along the [110] direction molecules were placed with two legs on the upper terrace and remaining pair was placed on the lower one as it is envisaged in Figure 5a. Molecules seemed to form chains due to diffusion along the step-edge. In case of steps oriented along the [1-10] direction (across the reconstruction troughs) the VL molecules were always placed on the lower terrace, however, oriented either perpendicularly (see Figure 5b, circle A) or parallelly (see 5b, circle B) with respect to the [110] direction [8].

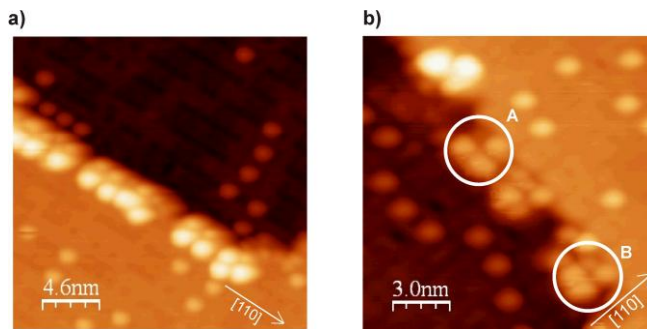


Figure 5: STM image of VL molecules adsorbed on InSb step-edges. (a) Adsorption on the edge running along the [110] direction; bias voltage: -3V, tunnelling current: 10pA. (b) Adsorption on the edge perpendicular to the direction of reconstruction troughs; circles mark molecules with board perpendicular (A) and parallel (B) to the [110] direction, respectively; bias: -3V, tunnelling current: 5pA.

During the experiments with the VL molecules on InSb(001) the feasibility of a single molecule manipulation was also tested. Ability to move the molecule both parallel and perpendicular to the reconstruction rows was achieved, as well as, the possibility to rotate the molecule [8]. The manipulation was performed by increase in tunnelling current by an order of magnitude while scanning over the molecule. Results of the VL molecules manipulation on InSb(001) substrate are promising for future formation of electronic circuits, however, they cannot be simply related to other types of molecules, especially planar ones.

Subsequently, some preliminary experiments on the adsorption of VL molecules on the TiO₂(110)-(1×1) and the TiO₂(011)-(2×1) surfaces were made. As the surface reconstructions of both faces of rutile differ significantly, one may expect a quite diverse behaviour of Lander molecules on the (110) and the (011) surfaces. If the TiO₂(011)-(2×1) surface was the substrate in question, molecules tended to adsorb on the step-edges, however, some molecules were still present on the terraces (see Figure 6) [9]. Presumably, similarly to the appearance of VL molecules on the InSb(001) surface, such a distribution of molecules on the TiO₂(011)-(2×1) surface was a result of high enough mobility of molecules at room temperatures that allowed their diffusion towards step-edges. The remaining fraction of molecular population, that stayed on the terraces, was probably immobilized by surface defects such as domain boundaries often

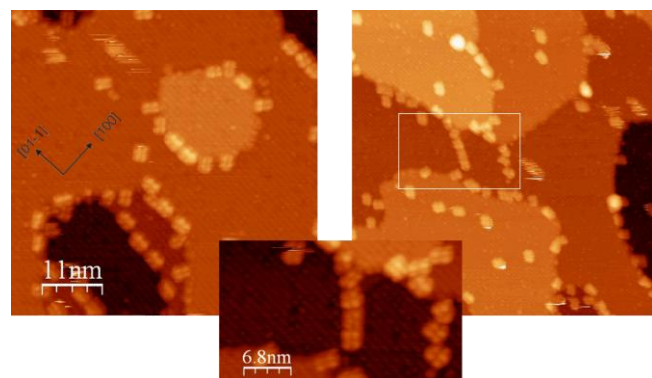


Figure 6: STM image of VL molecules adsorbed on the TiO₂(011)-(2×1) surface. Left panel: molecules adsorbed on step-edges. Right panel and inset (enlargement of scan area marked by a white rectangle) show adsorption of molecules on the terrace on the surface defect (a domain boundary often present on the (011) face of rutile TiO₂ (8)) in a form of chain. Bias voltage: 2.8V, tunnelling current 1pA.

present on the (011)-(2×1) surface of rutile TiO₂ [10]. Moreover, another analogy to the VL/InSb(001) system could be drawn. Molecules on the step-edges quite often adsorbed with one pair of legs on the upper terrace and the other pair on the lower terrace, although, other orientations on the edges were also found. The former orientation seemed to be preferred for the step-edges running along the [01-1] direction, which is the direction of the zigzag pattern [9]. This observation is similar to the one made in case of VL molecules adsorbed on the InSb(001) surface, where for the step-edges running along the reconstruction rows molecules were adsorbed with one pair of legs on the upper terrace and the other one on the lower terrace [8]. Finally, if the molecule was found on the terrace it showed up in either of two possible positions: along or at angle of 41° with respect to the zigzag pattern [9]. For the (110) face of rutile molecules were mostly observed on the terraces, where approx. 90% of population was found to be oriented along the reconstruction rows (see Figure 7). Remaining 10% of molecules were located at angle of 30° with respect to the [001] direction [9]. Moreover, a single molecule manipulation was observed – the VL molecule was moved along the [001] direction during scanning procedure (see Figure 7).

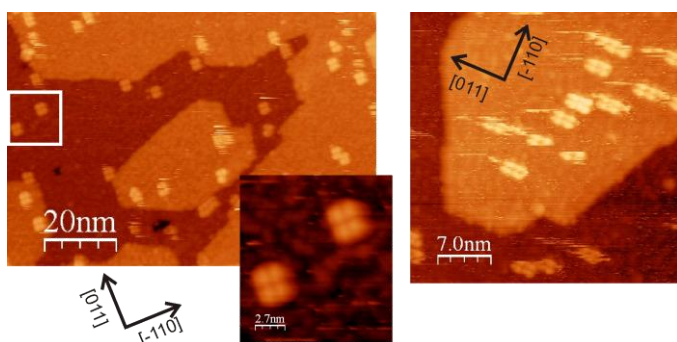


Figure 7: STM image of VL molecules on the TiO₂(110)-(1×1) surface. An inset shows an enlarged fragment of scan (marked with a white square) with molecules that have a molecular board parallel to the [001] direction. Right panel display a single molecule manipulation along the reconstruction troughs.

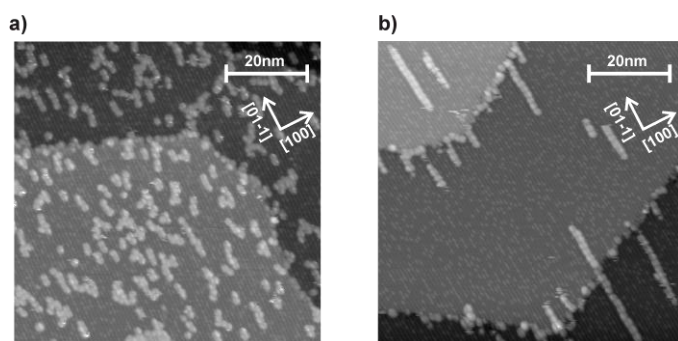


Figure 8: STM images of PTCDA adsorbed on rutile TiO₂(011). (a) PTCDA sub-monolayer deposited at RT on TiO₂(011)-(2×1). (b) PTCDA sub-monolayer deposited at 373 K. Image parameters for both scans: area 80nm×80nm; sample bias 3.8 V, tunnelling current 1pA.

In the end, adsorption of PTCDA molecules on the (011) face of rutile was investigated. It appeared, that PTCDA molecules deposited on rutile TiO₂(011)-(2×1) surface at room temperature (RT) formed aggregates of an elongated shape along the [01-1] direction (see Figure 8a). At elevated temperatures of the substrate during the deposition different growth modes appeared, and especially for a narrow temperature window creation of molecular chains was favoured (see Figure 8b) [2]. Each molecule was seen as two bright protrusions in a form of lobe. However, molecules assembled in chains were recorded in two distinct contrast: either two lobes were equally bright or one was brighter. The modulated appearance of the molecular chain is a manifestation of the fine interplay between adsorbate-adsorbate and adsorbate-substrate interactions, which determines

the final structure of a molecular wire. Though, precise analysis and interpretation of the adsorption configuration is limited due to the lack of reliable theoretical knowledge about the TiO₂(011)-(2×1) surface [2]. Multiple scanning of the same surface area showed tip-induced surface modifications, such as molecule removing from and attaching to the chain or enlargement and straightening of the aggregates created at RT. This observation opens a possibility for a single molecule manipulation. More

detailed discussion on adsorption of PTCDA molecules on $\text{TiO}_2(011)-(2\times 1)$ surface may be found in [2].

Summarizing, a high resolution imaging of clean semiconductor surfaces and of molecule-semiconductor systems was carried out for several subjects. Three different surfaces, namely $\text{InSb}(001)-c(8\times 2)$ and two faces of rutile: $\text{TiO}_2(110)-(1\times 1)$ and $\text{TiO}_2(011)-(2\times 1)$ were used as substrates. Moreover, three different molecular species: PTCDA, VL and [11]helicene, were examined. For the [11]helicene/ $\text{InSb}(001)$ system it was observed that molecules adsorb on the edges. In case of the VL/ $\text{InSb}(001)$ system, majority of molecules was found also on step-edges. The orientation of molecule with respect to the edge depended on the orientation of the edge with respect to the reconstruction rows. For edges running along the [110] direction molecules were adsorbed with one pair of legs on the upper terrace and the other pair on the lower terrace. Similar adsorption geometry was often found for the VL/ $\text{TiO}_2(011)-(2\times 1)$ system for molecules adsorbed on edges running along the [01-1] direction, being the direction of the zigzag pattern, however, other orientations were also possible. For molecules on terraces, both for the VL/ $\text{InSb}(001)$ and the VL/ $\text{TiO}_2(011)-(2\times 1)$ systems, few possible orientations of molecules were found. Moreover, a feasibility of a single molecule manipulation was demonstrated for VL molecules on the $\text{InSb}(001)$ and on the $\text{TiO}_2(110)-(1\times 1)$ surfaces. Finally, PTCDA molecules adsorbed on the $\text{TiO}_2(011)-(2\times 1)$ surface, for a narrow window of substrate's temperatures during deposition, tended to form one-dimensional molecular chains.

References

- [1] G. Goryl, et al. E-Nano-newsletter. 2007, 7, 28.
- [2] A. Tekiel, et al. Submitted to Nanotechnology.
- [3] I. Horcas, et al. Rev. Sci. Instrum. 2007, 78, 013705.
- [4] S. Wendt, et al. Surf. Sci. 2005, 598, 226; S. Wendt, et al. Phys. Rev. Lett. 2006, 96, 066107.
- [5] T. J. Beck, et al. Phys. Rev. Lett. 2004, 93, 036104.
- [6] T. Kubo, H. Orita and H. J. Nozoye, Am. Chem. Soc. 2007, 129, 10474.
- [7] G. Goryl, et al. in preparation.
- [8] S. Godlewski, et al. in preparation.
- [9] S. Godlewski, et al. in preparation.
- [10] O. Dulub, et al. Surf. Sci. 2006, 600, 4407.

3c. Surface selection and preparation, launching, imaging and assembling on a surface and manipulation

- Insulator on semiconductor

Insulators on semiconductor

A. Bellec, F. Chiaravalloti, D. Riedel and G. Dujardin

*Laboratoire de Photophysique Moléculaire
Bâtiment 210, Université Paris-Sud
91405, Orsay, France*

Introduction

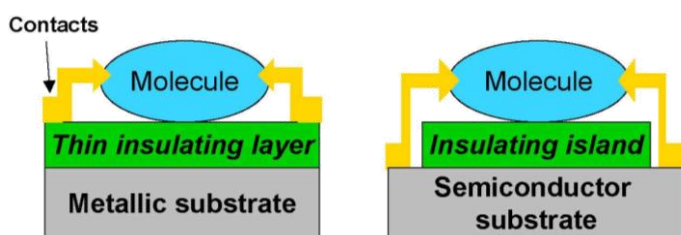


Figure 1: Schematics of a single molecule adsorbed on an insulating layer with a metallic (left) and semiconductor (right) substrate.

The multiple electrical contact of a single molecule is actually one of the main problems to be solved in particular, in the Pico-Inside project to demonstrate the computing inside a molecule. For that purpose, two principal problems are to be addressed. Firstly, the molecule needs to be electronically isolated from the substrate.

This can be best achieved by using insulating layers (see Figure 1) thin enough (thickness of the order of 1 nm) to allow STM imaging by tunneling through the molecule and the insulating layer. The advantage of an insulating layer grown on a semiconductor substrate compared to a metallic substrate is that the insulating layer is expected to suppress all the surface conductive channels having energies within the bulk band gap. By this way, the electronic isolation of the molecule is complete for all energies lying within the bulk band gap whereas some weak electronic coupling is always present in the case of the metallic substrate. Another advantage of semiconductor substrates is that the electrodes contacting the molecule can be built directly on the semiconductor substrate. Indeed, growing conducting electrodes is a priori much easier on semiconductors than on insulators due to the stronger interactions between adsorbates and semiconductor surfaces as compared to insulator surfaces. The second problem to be solved for electrically contacting a single molecule is to control, with atomic-scale precision, the contact between the molecule and the electrodes. Building conducting atomic lines by atom manipulation with the STM is probably the most controlled way to contact a single molecule. We will illustrate this method in the case of the hydrogenated silicon surface.

Thin insulating layer on a semiconductor substrate; the case of CaF₂ on Si(100)

In recent years, there have been a number of studies for investigating the growth of insulating layers on metallic surfaces with the aim to deposit molecules on top of them for molecular self-assembling or molecular electronics purposes [1,2]. Similar studies on semiconductor surfaces are very scarce in the literature. Limitations are related to the necessary matching between the crystalline structure of the layer and that of the semiconductor substrate. So far, two main systems have emerged: (i) Oxide layers on silicon. Initially motivated by the fabrication of high K gate oxides for CMOS devices, oxide layers have been recently assigned much more functionalities (sensor, actuator). As a result, an integrated multi-function oxide electronics is now emerging. Although,

crystalline structures of such oxide layers on silicon have been demonstrated [3], the quality of their surface at the atomic-scale has not yet been tested, (ii) CaF_2 layers on silicon. Calcium fluoride layers have been successfully grown on both $\text{Si}(111)$ and $\text{Si}(100)$ and their structure analysed by synchrotron radiation based techniques and atomic force microscopy (AFM) [4,5]. However, the atomic-scale structure and electronic properties of these calcium fluoride layer surfaces have not yet been studied. We have investigated the growth, the atomic-scale structure and the electronic properties of thin calcium fluoride layers on $\text{Si}(100)$ surfaces by using the low temperature (5K) STM. CaF_2 molecules sublimated from CaF_2 crystals have been

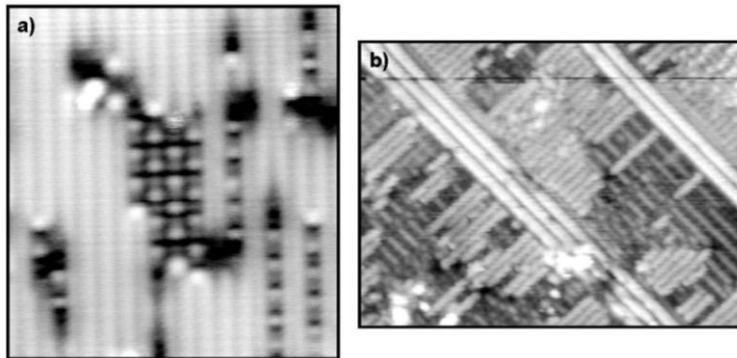


Figure 2: Low temperature STM topographies of CaF_2 adsorbed on $\text{Si}(100)$. a) $29 \times 29 \text{ nm}^2$, $V_s = 1.8\text{V}$, $I = 61 \text{ pA}$, coverage ($< 0.3 \text{ ML}$). b) $23 \times 31 \text{ nm}^2$, $V_s = -2\text{V}$, $I = 160 \text{ pA}$, coverage 1.2 ML .

deposited under UHV on highly n doped $\text{Si}(100)$ substrates maintained at 650°C . After cooling down to 5K, the resulting layers have been imaged with the STM as shown in Figure 2 for low coverage ($< 0.3 \text{ ML}$) and higher coverage (1.2 ML). At low coverage (Figure 2a), one dimension (1D) and two dimension (2D) islands with

regular structure are observed. The 1D structures enable to distinguish the unit cell. At higher coverage (Figure 2b), islands with the same structure as at low coverage cover most of the sample surface (darkest areas in Figure 2b). In addition, very long stripes (hundreds of nm) having very few defects are observed. It is believed that the stripes are grown on top of the first layer seen as islands in Figure 2a. STM $I(V)$ spectroscopy of the stripes (not shown here) has yielded a surface gap of about 4 eV. These preliminary results open interesting perspectives. Within the energy range from -1.5 eV to $+2.5 \text{ eV}$, molecules adsorbed on top of (or between) the stripes should be electronically decoupled from the silicon substrate. Furthermore, the 1D structure of the stripes might allow the self-organisation of molecular lines or alternatively of atomic lines along the calcium fluoride stripes.

Thin insulating layer on a semiconductor substrate; the case of hydrogenated $\text{Si}(100)$

The simplest method to insulate the surface of silicon is to passivate its surface by adsorbing hydrogen atoms on the silicon dangling bonds. By this way, surface state conductivity within the bulk band gap is expected to be suppressed. This has been quantitatively demonstrated by Doumergue et al. [6] who calculated the electron transmission through various types of atomic lines on the hydrogenated $\text{Si}(100)$ surface (see Figure 3). In the case of the perfect $\text{Si}(100)$ - (2×1) : H surface, the

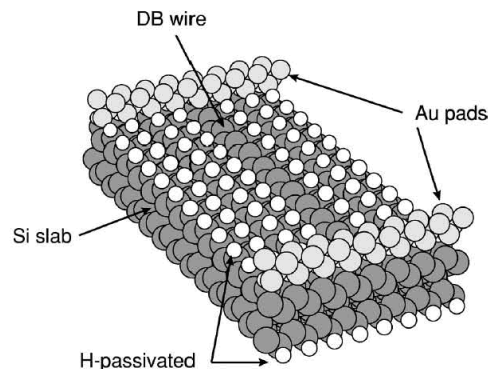


Figure 3: Schematics of a Si dangling bond (DB) wire connected to two Au pads on a $\text{Si}(100)$ surface, taken from ref. 13.

transmission has been found to strongly exponentially decrease as a function of the inter-pads distance. The calculated inverse decay length was $\gamma = 0.41 \text{ \AA}^{-1}$, i.e. smaller than for tunneling through vacuum ($\gamma = 2.21 \text{ \AA}^{-1}$). When a silicon line is de-passivated (hydrogen desorbed), the resulting silicon dangling bonds form a metallic wire whose electron transmission is constant as a function of the inter-pads distance (see Figure 3). However, it has been demonstrated that the silicon dangling bond line is not stable and undergoes a Peierls-like distortion [7]. This removes the metallic character of the atomic line and results in opening a small gap of 0.2 eV. The electron transmission through this distorted atomic line has been found to slightly decrease as a function of the inter-pads distance with an inverse decay length of $\gamma = 0.09 \text{ \AA}^{-1}$ [6]. Experimentally measuring these electron transmissions as described in Figure 3 is still difficult due to the need of two pads with the appropriate atomic-scale precision. We have recently initiated a different method to measure these electron transmissions.

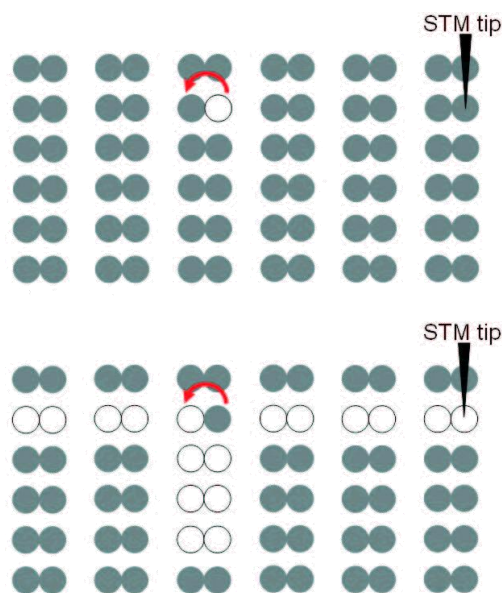


Figure 4: Schematics of atomic lines on a Si(100) surface. The grey circles are the hydrogenated silicon atoms. The white circles are the silicon dangling bonds. The red arrow indicates the atom switch. The STM tip position for injection of charges is also indicated. The surface is fully hydrogenated (top) or partially dehydrogenated (bottom).

This is illustrated in Figure 4. Atomic lines of hydrogenated silicon atoms can be easily selected either parallel or perpendicular to the silicon dimer rows. Atomic lines of dehydrogenated silicon dangling bonds can be precisely produced by selectively desorbing hydrogen atoms one by one through electron excitation with the STM tip [8]. The method for measuring the electron transmission (see Figure 4) consists in using the STM tip as one of the two pads at one end of the atomic line. At the other end, a silicon dangling bond atom switch is placed to detect the transmitted charges. Indeed, it is known that a silicon dangling bond, produced by desorbing one hydrogen atom from an hydrogenated silicon dimer, behaves as an atom switch which can be activated by charging [9]. The atom switch is then working as a charge detector at the second end of the atomic line (see Figure 4). Charges injected at one end of the atomic line with the STM tip are transmitted through the atomic line and then activate the atom switch at the other end. The yield for activating the atom switch (probability of switching per injected charge) can be measured for various types (hydrogenated or dangling bonds), lengths and orientations (relative to the dimer row direction) of the atomic line.

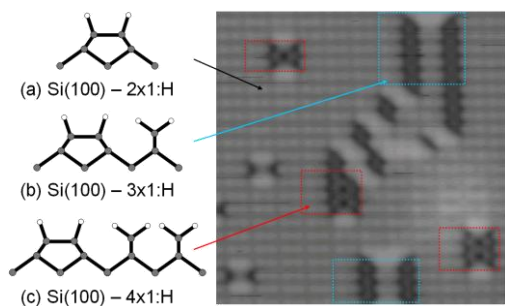


Figure 5: Low temperature (5K) STM topography of the hydrogenated Si(100) surface ($8.5 \times 8.5 \text{ nm}^2$, $V_s = 1.7\text{V}$, $I = 110 \text{ pA}$) showing the various surface reconstructions

The STM topography of the hydrogenated Si(100) surface recorded at 5K is shown in Figure 5. Several surface reconstructions are seen. The 2x1 and 3x1 reconstructions have been previously observed at room temperature. However, a new 4x1 reconstruction which has never been

observed at room temperature is seen at 5 K. A tentative structure for this new reconstruction is given in Figure 5. For the fabrication of the silicon dangling bond lines, we have been working on the 2x1 reconstructed areas. The desorption of individual hydrogen atoms with the STM tip has been performed as previously described [8] by locating the STM tip on top of the chosen hydrogen atom, opening the feedback loop and applying a surface pulse voltage of +2.5 V. The result is shown in Figure 6 where the silicon dangling bond is seen as a bright protusion in the STM topography. We have first tested the activation of the atomic switch made of the single dangling bond by locating the STM tip directly on top of the neighbouring hydrogen atom and applying a negative surface voltage pulse. The atom switch probability has been measured as a function of the pulse surface voltage for both n and p type doped

silicon samples (see Figure 7). For n type doped silicon, the switching probability has a maximum for surface voltages around -3.0 V as observed at room temperature [9]. Very surprisingly, we have found that the switching process is very unefficient for p type doped silicon. This is most probably related to the charging effects of surface states of silicon samples which are known to depend on the type of dopant in silicon [10]. We emphasize that such charging effects may have important implications in the charge transport along atomic lines although they have been neglected in the calculations by Doumergue et al. [6]. Preliminary experiments of charge transport along silicon dangling bond lines have been performed as illustrated in Figure 8. After fabricating a 3 dangling bond line, the switching of a dangling bond at one end has been activated by injecting positive charges (-2.5 V surface voltage pulse) at the other end with the STM tip. Although much further measurements as a function of the atomic line length and for different types of atomic lines are needed, these preliminary results demonstrate the feasibility of measuring the charge transport efficiency along well defined atomic lines on the hydrogenated silicon surface.

Finally, we have tested the passivation of the hydrogenated Si(100) surface by studying the STM imaging of a pentacene molecule adsorbed at low temperature (5 K) on this surface [11]. Pentacene molecules have been observed to be very mobile on the surface and thus very difficult to be imaged. However, as shown in Figure 9, it has been possible to

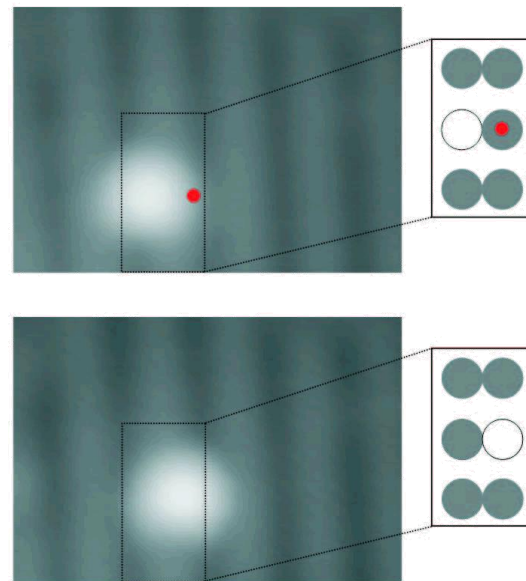


Figure 6: Low temperature STM topographies ($4 \times 2.75 \text{ nm}^2$, $V_s = -1.7 \text{ V}$, $I = 69 \text{ pA}$) showing the atom switch. Initially the silicon dangling bond (white circle) is on the left side of the silicon dimer row (top STM topography). Then the STM tip is positioned on top of the hydrogen atom (red circle) and a negative surface voltage pulse is applied (- 2.5 V). As a result, the silicon dangling bond has been switched to the right side of the silicon row (bottom STM topography).

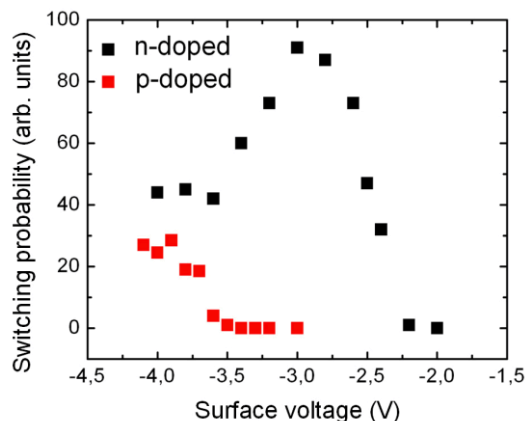


Figure 7: Switching probability (arbitrary units) of the atom switch as a function of the pulse surface voltage for n and p type doped Si(100).

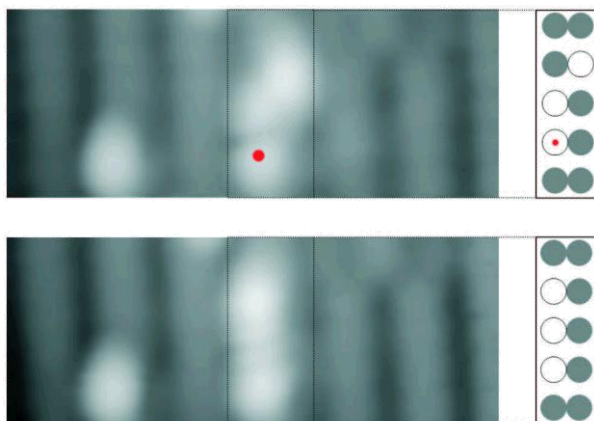


Figure 8: Low temperature STM topographies ($5 \times 1.9 \text{ nm}^2$, $V_S = -1.7\text{V}$, $I = 69 \text{ pA}$) showing the activation of the atom switch through charge transport along the dangling bond line. The top STM topography shows the initial system. Then, a pulse voltage (-2.5V) is applied with the STM tip at the red dot position. The bottom STM topography shows that the atom at the other end of the dangling bond line has been switched.

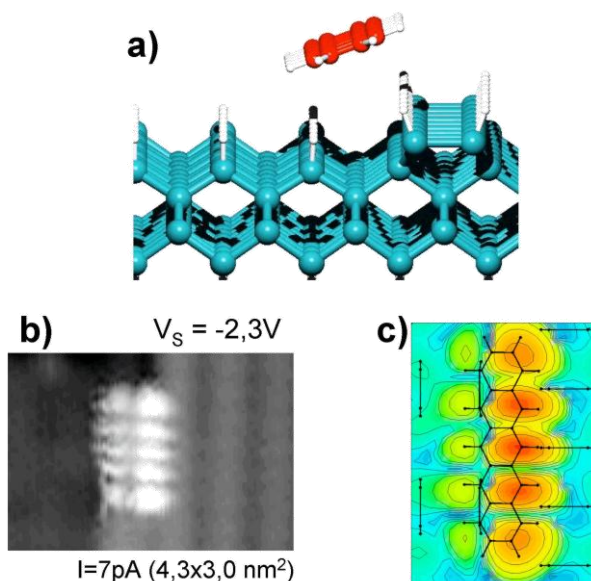


Figure 9: a) calculated adsorption structure of a pentacene molecule over a step edge of a passivated $\text{Si}(100) :\text{H}$ surface. b) STM topography ($V_S = -3\text{V}$, $I_t = 27 \text{ pA}$, $6.5 \times 6.5 \text{ nm}^2$) of a pentacene molecule sitting astride the step edge. c) ESQC calculated constant current STM topography of pentacene at the step edge at the -1.7 eV HOMO tunnel resonance.

layers of calcium fluoride offers interesting properties, i.e. a surface band gap of about 4 eV and 1D structuration, which can be exploited for positioning and electrically connecting molecules. The hydrogenated $\text{Si}(100)$ surface offers a surface band gap of only 2 eV. However, hydrogen atoms can be manipulated one by one with the STM tip. By this way, charge transport along atomic lines on the surface can be tested.

observe some isolated molecules when they are near a step edge. In Figure 9, the molecule is observed to sit astride the step edge. Even so, the molecule can easily move along the step during the imaging. This indicates that the molecules are physisorbed and that the surface diffusion barrier is very low. Indeed, the adsorption energy of a pentacene molecule on $\text{Si}(100) : \text{H}$ and the barrier energy for diffusion computed with ASED+ [12] have been found to be 0.11 eV and 0.01 eV respectively. Figure 9 shows the experimental STM topography recorded at the energy of the highest occupied molecular orbital (HOMO) ($V_S = -3\text{V}$) compared to the corresponding calculated topography using the electron scattering quantum chemistry (ESQC) method [13]. Both the experimental and calculated STM topographies clearly resemble the topography of the HOMO orbital of the free molecule, thus indicating that the native electronic properties of the free molecule are preserved upon adsorption on the $\text{Si}(100) : \text{H}$ surface. The lowest unoccupied molecular orbital (LUMO) of the pentacene molecule cannot be imaged with the STM because its energy is located within the hydrogenated silicon surface energy band gap. These results demonstrate that the physisorbed pentacene molecule is electronically decoupled from the passivated hydrogenated $\text{Si}(100)$ surface.

4 Conclusions

With the aim to electronically isolate the molecule from the substrate, we have investigated the fabrication and the properties of two kinds of insulating layers on $\text{Si}(100)$, namely calcium fluoride and hydrogen. Thin

Furthermore, the passivation of the silicon surface by hydrogen atoms enables an efficient electronic decoupling of pentacene molecules physisorbed at low temperature (5 K) on this surface.

So far, low temperature molecular electronics experiments have been limited to relatively narrow band gap semiconductors such as silicon (band gap 1.1 eV). In the future, it might be possible to extend such studies to wide band gap semiconductors such as silicon carbide (band gap 3.0 eV) or diamond (band gap 5.5 eV). This would open exciting perspectives to electrically contact single molecules and to further address them optically through these transparent substrates.

References

- [1] X. H. Qiu, G. V. Nazin and W. Ho, *Science* 299, 542 (2003).
- [2] J. Repp, G. Meyer, S. M. Stojkovic, A. Gourdon and C. Joachim, *Phys. Rev. Lett.* 94, 026803 (2005).
- [3] R. A. McKee, F. J. Walker and M. F. Chisholm, *Phys. Rev. Lett.* 81, 14 (1998).
- [4] H. Rauscher et al. *Chem. Phys. Lett.* (2004).
- [5] H. L. Pasquali et al. *Phys. Rev.* B72, 045448 (2005).
- [6] P. Doumergue, L. Pizzagalli, C. Joachim, A. Altibelli and A. Baratoff, *Phys. Rev.* B 59, 15910 (1999).
- [7] T. Hitosugi et al. *Phys. Rev. Lett.* 82, 4034 (1999).
- [8] L. Soukiassian, A. J. Mayne, M. Carbone and G. Dujardin, *Phys. Rev. B* 68, 035303 (2003).
- [9] U. J. Quaade, K. Stokbro, C. Thirstrup and F. Grey, *Surf. Sci.* 415, L1037 (1998).
- [10] L. Liu, J. Yu and J. W. Lyding, *Mat. Res. Soc. Symp. Proc.* 705, Y6.6.1 (2002).
- [11] A. Bellec, F. Ample, D. Riedel, G. Dujardin and C. Joachim, *Nano-Letters* (2009)
- [12] F. Ample and C. Joachim, *Surf. Sci.* 600, 3243 (2006).
- [13] P. Sautet and C. Joachim, *Chem. Phys. Lett.* 185, 23 (1991).

Thin insulating KBr layers deposited on InSb as a tool to study properties of organic molecules

Szymon Godlewski, Grzegorz Goryl, Bartosz Such, Jacek J. Kolodziej, Jakub S. Prauzner-Bechcicki and Marek Szymoński

Research Centre for Nanometer-scale Science and Advanced Materials (NANOSAM), Faculty of Physics, Astronomy and Applied Computer Science, Jagiellonian University, Reymonta 4, 30-059 Krakow, Poland

Keywords: InSb, PTCDA, KBr

The core of the molecular electronics is an idea to design a single molecule performing specific logical operations [1]. Such a molecular processor would be incorporated into the future nanoelectronic device, interconnected with its other elements and especially with an output interface. Apart from the synthesis of the molecule with desired properties, several technical obstacles arise, for example positioning of the molecule in required place within the electronic circuit or interconnecting it with metal electrodes. However, these technical aspects are not the only difficulties. Properties of the molecular processor would rely on its internal structure. Nevertheless, the shape of the molecular orbital and the electronic structure are prone to the chemical surrounding of the molecule and may be changed by interaction with it [2;3]. Thus, *modus operandi* of the molecular processor may be altered as well. Therefore, before very sophisticated molecular electronics systems will be designed and fabricated, the role of the interaction between the molecule and its environment must be comprehended. In this context, schemes for avoiding a strong coupling of molecules with substrate on which they are deposited seem to be of a great importance. At least partial decoupling of the molecule from the conducting or semi-conducting substrate surface may be achieved via an ultrathin insulating layer between the substrate and the molecule [4]. And such an approach will be followed in the present study.

Experiment was carried out in multi-chamber ultra-high vacuum (UHV) system with a base pressure less than 10^{-10} mbar. Apparatus was equipped with a low temperature scanning tunnelling microscope (LT-STM) commercially designed by Omicron, a low energy electron diffraction system (LEED), an ion gun, a 4-cell Knudsen evaporation cell, resistive and electron heaters, an infrared pyrometer and thermocouples for temperature monitoring and a quartz microbalance for molecular flux control. Epi-ready InSb(001) wafers (Kelpin crystals) were pre-annealed at 700K for several hours without prior chemical treatment and then cleaned by several cycles of 0.7keV Ar⁺ ion sputtering and subsequent annealing at 700K. The cleaning cycles were repeated until clear c(8×2) LEED pattern was registered. In order to outgas evaporation cells they were kept at the stand-by temperature just below the operation temperature (720K for KBr and 585 for PTCDA molecules) for several hours. KBr was evaporated on a substrate kept at 425K and PTCDA was deposited on a substrate kept at room temperature. Constant current STM measurements were carried out with use of electrochemically etched tungsten tips as probes. Typically, tunnelling current was in the range of 10 to several hundreds of pA. Reduction of noise, an increased measurement stability and imaging with atomic resolution were achieved partially due to low temperature (down to 77K) measurements. WSxM software was employed for image processing and data analysis [5].

Growth of thin KBr films on the InSb(001)-c(8×2) surface and the substrate surface structure itself have been studied quite intensively [4,6-9]. Reconstructed surface of the semiconductor exhibits atomic rows running along the [110] direction separated by four basic surface lattice constants ($4 \times 4.58 \text{ \AA}$). However, at temperatures below 180K

surface appearance is changed noticeably by presence of additional protrusions. Those protrusions have both electronic and structural origin and may be expounded in terms of the surface phase transition and the charge density waves creation [8;10]. Nevertheless, due to a small lattice mismatch between InSb and KBr lattices (InSb: 0.6479nm, KBr: 0.6586nm) high quality epitaxial films of KBr on InSb may be created. Thus, KBr/InSb with molecules adsorbed on top of it, seems to be an excellent candidate for studying properties of a semiconductor-insulator-molecule system.

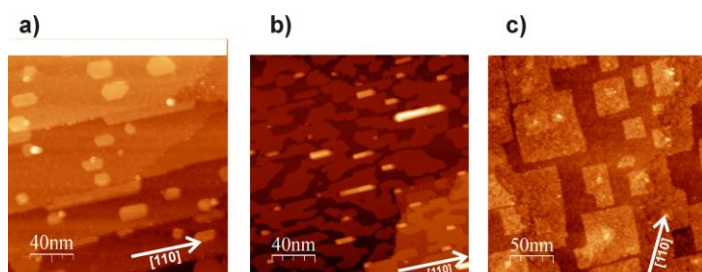


Figure 1: LT-STM images of KBr deposited on InSb(001)-c(8×2). (a) a submonolayer coverage; (b) wetting layer of KBr; (c) 1.5 ML coverage (2nd and 3rd layer island are visible).

Figure 1 shows InSb covered by three different amounts of KBr, i.e. a submonolayer, a wetting layer and 1.5 monolayer coverage. At the submonolayer coverage islands of monoatomic height and characteristic size of 10-20nm are formed (see Figure 1(a)). Those islands are often joined with substrate step-edges and since the topographic height of

a KBr step is nearly the same as the one for the InSb [11] the boundary between the KBr island and the InSb step-edge is atomically flat. Increase of the coverage up to a monolayer leads to merging of islands and in a consequence to creation of the wetting layer of monoatomic height (see Figure (b)). Further growth of KBr proceeds in a layer by layer mode (see Figure 1(c)). However, the 3rd and higher layers start to grow even before previous layers were completed. This type of behaviour is a consequence of rather slow diffusion of KBr molecules down across steps [9]. The 2nd and higher order layers start to grow in a form of islands with edges oriented at the angle of 45° with respect to the [110] direction of the InSb substrate.

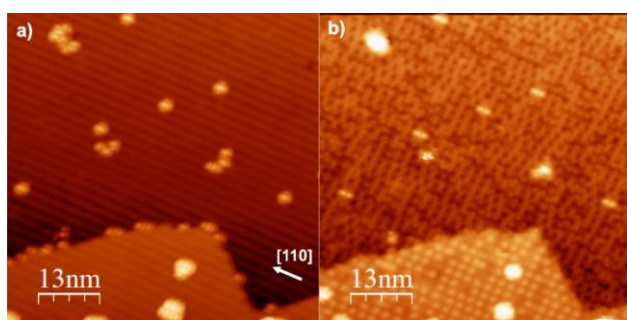


Figure 2: KBr deposited onto InSb; both images mostly show 1st monolayer of KBr, however, in the lower part a small fragment of 2nd layer is visible with an edge. (a) $U=-2.3V$, $I=6pA$ - the filled states STM image; (b) $U=2.3V$, $I=6pA$ - the empty states STM image. Both scans have an area of $63 \times 63 nm^2$. Both panels exhibit also PTCDA molecules ($\sim 0.02ML$ coverage), especially on panel a) they are seen as bright protrusions.

Images of thin films of KBr, up to 2 ML, in a filled state STM present only attenuated striped pattern, being characteristic for InSb surface (see Figure 2(a)). Thus, the 1st and the 2nd KBr monolayer both similarly appear as virtually transparent [4]. However, in an empty state STM surfaces covered by mono and bilayer present themselves quite distinctively (see Figure 2(b)). For the 1st KBr layer, bright stripes meandering, without strict order, close to the [1-10] direction and the periodicity ($\times 4$) along the [110] direction are observed. In result a virtually square mesh is observed locally on the surface [4;9]. The 2nd

KBr layer exhibits rows of unordered protrusions along the [110] direction that are separated by exactly four InSb surface lattice constants. The lack of ordering within rows results in a rather poor correlation between the position of protrusions in adjacent rows and therefore only sporadically a rectangular (4×4) lattice is seen [4;9].

Further, more elucidated analysis and especially, high resolution images of KBr deposited onto InSb (up to the 4th layer) may be found in [9].

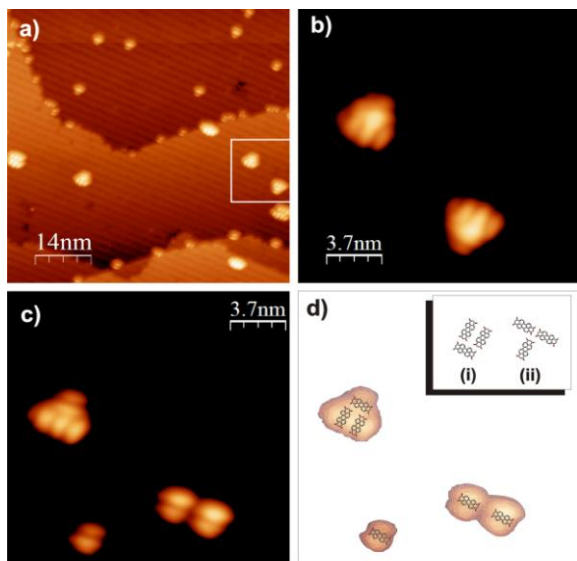


Figure 3: High-resolution STM images of PTCDA molecules adsorbed on KBr/InSb ($U=-2.3V$; $I=6pA$): (a) $70 \times 70 \text{ nm}^2$ scan area; (b) zoom into $19 \times 19 \text{ nm}^2$ area marked by a white square in Figure 3(a), exposing molecules adsorbed on the 2nd KBr layer in groups of three molecules; (c) tip-induced modification of one of groups seen in Figure 3(b); (d) proposed model for position and orientation of molecules within a groups seen in Figure 3(c).

the molecule-molecule interaction is responsible for the aggregates formation. On the other hand, for molecules adsorbed on the 1st layer stronger molecule-substrate interaction may dominate mutual molecular interaction and thus prevent from the formation of larger groups [4]. For the case of molecules adsorbed on the 1st KBr layer the preference for molecular orientation with long molecular axis parallel to the [110] direction was noticed. Moreover, it was found that reversing the sign of the bias voltage from negative (the filled state imaging) to positive (the empty state imaging) quite often led to manipulation of the molecules by the scanning tip (see Figure 3, panels (b) and (c)). More thorough study on the PTCDA molecules adsorbed onto KBr thin layers on the InSb substrate, including detailed analysis of observed molecular configurations and contrasts, may be found in forthcoming publication [4].

Thin insulating KBr layer deposited on InSb substrate was also used to study the adsorption of Violet Lander molecules [12]. In such a case it appeared that molecules were mainly adsorbed on the terraces of KBr layer, contrary to clean InSb surface, where molecules were mostly found on the step-edges. Supposedly, VL molecules are immobilized by some impurities or trapped by KBr layer itself [12]. Figure 4 shows a high-resolution image of VL molecule adsorbed on the 1st KBr layer deposited on InSb(001) in one of two possible orientations, i.e. parallel with

In the next step PTCDA molecules were evaporated onto the KBr layer deposited on the InSb substrate. PTCDA molecules (3,4,9,10-perylene-tetracarboxylic-dianhydride) are representative organic molecules for the molecular-electronics-oriented studies as being a prototypical, planar stacking, organic semiconductor. In Figure 2, especially in panel (a) – the filled state STM image - PTCDA molecules are seen as bright protrusions. Here the coverage was approximately 0.02 ML. During the measurement no preference for the adsorption on the 1st or the 2nd KBr layer was observed. What is more, molecules tend to adsorb equally frequently on step edges and on flat terraces. On the 1st KBr layer molecules are mostly found as single or in pairs, and rarely in larger groups. In contrast to such an observation, on the 2nd monolayer, they are always seen in aggregates of at least three molecules (see Figure 3). It is plausible to assume, that molecules on the 2nd KBr layer rather weakly interact with the InSb substrate and therefore

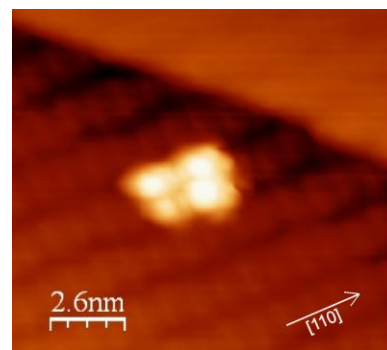


Figure 4: High-resolution STM image of Violet Lander molecule adsorbed on the 1st KBr layer on InSb. $U=-2.0V$; $I=20pA$. Molecule is adsorbed parallel to the reconstruction rows of InSb substrate.

respect to the reconstruction rows of InSb. Molecule perpendicular to the [110] direction, was the other orientation found on the KBr layer [12]. More detailed discussion on the influence of the structure of KBr layer on the conformation and orientation of adsorbed Violet Lander molecules may be found in upcoming article [12]. In summary, several properties of the KBr/InSb system, described in brief above, are of great importance for future molecular electronics applications. Especially in respect of creating a high quality, well ordered insulating layers following characteristics are significant: (i) the epitaxial growth due to small lattice mismatch, (ii) identical height of InSb and KBr monolayers and (iii) the existence of covalent bonds between In and Br. The influence of such an insulating layer on organic molecules was presented in a case of PTCDA/KBr/InSb system, where presence of the 2nd KBr layer allowed creation of larger molecular groups due to strong enough mutual molecular interaction. Reported results and measurements for other organic molecules, such as Violet Landers [12] or [11]helicene [13], show that indium antimonide covered with potassium bromide seems to be very efficient, insulator-semiconductor type of system for studying properties of adsorbed organic molecules in great detail.

References

- [1] C. Joachim, J. K. Gimzewski and A. Aviram; Nature. 2000, 408, 541.
- [2] B. Such, et al. Appl. Phys. Lett. 2006, 89, 093104.
- [3] J. Kroeger, et al. Chem. Rev. Lett. 2007, 438, 249.
- [4] B. Such, et al. Accepted to Nanotechnology. 2008.
- [5] I. Horcas, et al. Rev. Sci. Instrum. (2007), 78, 013705.
- [6] J. J. Kolodziej, et al. Phys. Rev. Lett. 2003, 90, 226101.
- [7] J. J. Kolodziej, et al. Surf. Sci. 2002, 506, 12.
- [8] G. Goryl, et al. Surf. Sci. 2007, 601, 3605.
- [9] S. Godlewski, et al. in preparation.
- [10] G. Goryl, et al. E-nano-newsletter. (2007), 7, 28.
- [11] F. Krok, et al. Surf. Sci. 2004, 566-568, 63.
- [12] S. Godlewski, et al. in preparation.
- [13] G. Goryl, et al. in preparation.

3c. Surface selection and preparation, launching, imaging and assembling on a surface and manipulation

- Insulator / NC-AFM Instruments

Atomic resolution AFM on NaCl at 5 K using the QPlus sensor

M. Maier, A. Bettac, J. Köble and A. Feltz

Omicron NanoTechnology GmbH, Limburger Str. 75, D-65232 Taunusstein, Germany
m.maier@omicron.de

Over many years, low temperature STM has been established as an advanced imaging and spectroscopy tool in various scientific fields. A large number of self-built as well as commercial instruments are working on a high performance level with a z-stability in the picometer range and allow for applications such as molecule spectroscopy (including inelastic tunnelling spectroscopy, IETS), atom and molecule manipulation, spin-polarised STM/STS and many others. One reason for the widely spread use of this technique is the relative technical simplicity of a scanning tunnelling microscope, even under the stringent experimental conditions when working at liquid Helium temperatures.



Figure 1: Image of a QPlus sensor mounted to the LT STM sensor carrier. Tungsten tips are glued onto the oscillating prong of the tuning fork. The use of W enables the QPlus sensor to be used simultaneously or alternatively in STM mode.

However, in the field of atomic force microscopy the situation is different. A comparatively limited number of self-built or commercial low temperature instruments are successfully working on a high performance level, which is basically resulting from the technical complexity of an optical beam deflection or interferometric AFM detection.

Nevertheless, applications drive the development of an easy to handle, reliable and high performance AFM technique. A prominent example can be found within the PicoInside project: A molecule based computing circuit requires a single molecule to be locally manipulated and electronically de-coupled from the underlying substrate. Current approaches use wide band gap semiconductors for decoupling or thin insulation layers which would still allow for an STM based manipulation process. On the other hand, the use of an insulating substrate or thicker insulating layers would ensure perfect electronic de-coupling of

the molecule but require AFM based manipulation. The realisation of a reproducible experimental route for this process represents a major milestone of the PicoInside project.

Aiming at a low level of technical complexity, purely electrical AFM sensors are favourable. Among a small number of approaches, the piezo-resistive (PR) detection scheme is one of the few that has proven atomic resolution but never been established as a reliable and routine AFM technology at a high performance level. One reason is that the first stage PR signal detection is highly integrated into the cantilever itself, thus requires a high level of cantilever process technology and basically depends on the sensor availability from commercial suppliers. In addition, the simultaneous use in high performance STM and STS mode is limited since cantilever probes need metal coating for conductivity reasons. Also electric power dissipation of the sensor has considerable impact when working at low temperatures.

An alternative (and also purely electrical) approach for Non-Contact AFM is based on a quartz tuning fork and uses of the piezo-electric effect of quartz. In general, tuning forks are mass products (e.g. used in wristwatches) and comparably cheap. Although

the commercial availability for a complete sensor is still very limited, it is accessible for the scientific community since probe tips can easily be mounted (glued) onto a tuning fork. In the late 90`s Franz Giessibl presented a new approach that makes use of a quartz tuning fork, commonly called the "QPlus sensor", which showed excellent atomic resolution in NC-AFM images on Si(111) [1,2]. One prong of the tuning fork is fixed while the SPM probe tip is mounted to the (free oscillating) second prong. It thus acts as a quartz lever transforming it's oscillation (f_{res} typ. 20-30 kHz, depending on tip mass) into an electrical signal as a result of the piezo-electric effect. The sensor can either be excited electrically by an AC voltage or mechanically by employing the scan piezo. The employed feedback signal is based on the frequency shift originating from tip-sample force interaction. However, for true force detection in non-contact AFM operation mode on conducting samples, the role of the tunnelling current cross-talk needs careful consideration.

The basic motivation of the QPlus sensor is to improve AFM resolution for short range forces by the high spring constant of the sensor (approx. 1800 N/m, cantilever typ. a few ten N/m) and small oscillation amplitudes in the range of 1nm or below (cantilever typ. 10 nm), which more precisely matches the range of the involved (chemical) forces. In addition, the high spring constant also helps to avoid jump-to-contact problems.

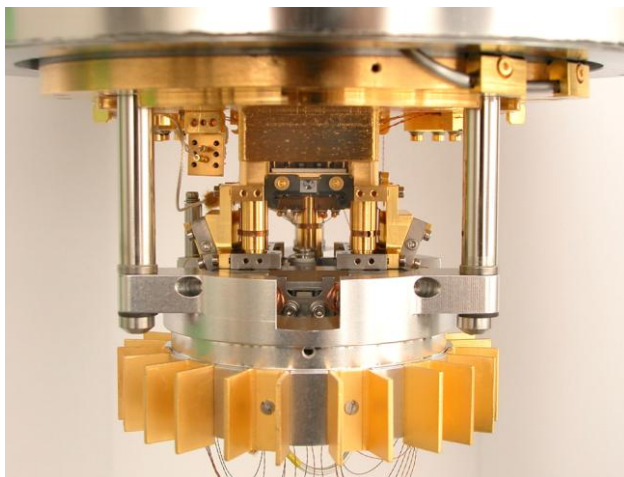


Figure 2: The "Omicron LT STM" microscope stage (version with in-UHV lens arrangement for optical detection and evaporation from below)

From a technical point of view, the integration of such a sensor is straight forward in terms of instrument design. Due to the high sensor spring constant and close distance between tip and sample, smallest external (mechanical) perturbations may have strong impact since involved forces are nearly three orders of magnitude larger and may easily induce image contrast changes by changing the tip's atomic formation and instable imaging. This requires an extremely stable SPM platform with a z-stability in the range of a few picometers and is the reason why the well established "Omicron Low Temperature STM" (Figure 2) (LT STM, up to date

built more than 100 times), has been chosen for integration. A relevant design change is the implementation of three electrical contacts at the sensor carrier in conjunction with a fully UHV compatible transfer concept. Also here, well proven and existing technology from the "Omicron VT SPM" has been employed and two sensor carriers can alternatively be used (STM only, QPlus). The QPlus sensor can be operated in AFM feedback mode with simultaneous detection of a (dynamic) tunnelling current or even in STM feedback mode. As an important requirement, the technical realisation ensures the known STM/STM performance level of the instrument.

The major technical challenge in QPlus AFM is the pre-amplification technique. The detection circuit scheme guarantees distance control based on the pure vibrational (piezo-electric) AFM signal with clear separation from the tunnelling current, as proven by measurements on Si(111) 7x7 and Au(111). This separation is especially important for quantitative AFM on conducting samples, since cross-talk by tunnelling current can easily dominate the force feedback signal. Using electrically connected tunnelling tips

has two advantages: (i) the amount of glue can be minimised for maximum sensor resonance frequency since the glue does not serve as electrical insulation and (ii) the tunnelling tip floating on U_{gap} potential allows for easy compensation of electrostatic forces originating e.g. from strong local charging on insulating single crystals such as MgO. Using insulating glue for tip mounting and separate wiring is an alternative approach for signal separation (also possible within our LT STM set-up) but not required for the employed detection technique.

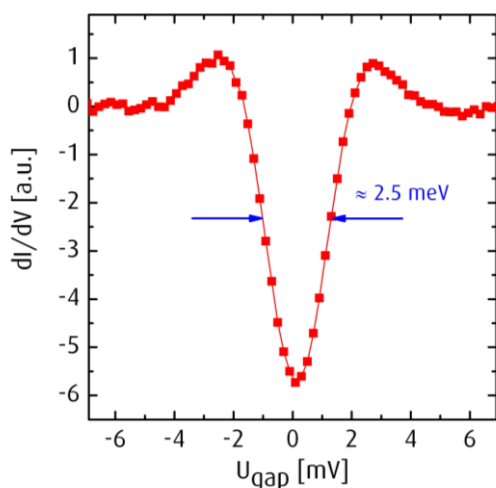


Figure 3: STS reveals the superconducting gap of a Niobium STM tip, sample: (Au(111)).

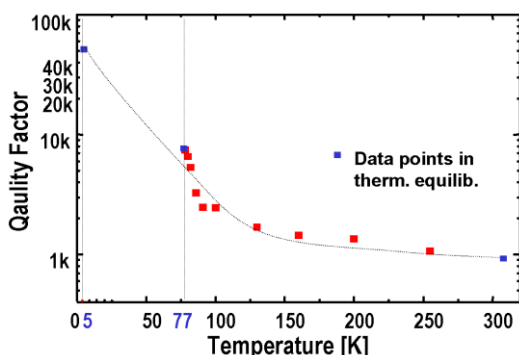


Figure 4: Temperature dependency of the Q-factor, increasing from approx. 1000 at 300K to up to 50,000 at $T=5\text{K}$. Blue data points are taken in thermal equilibrium.

Piezo-electrically generated signals are very small and therefore the first stage detection circuit needs to be close to the sensor in order to ensure sufficient S/N ratio. In fact, this required the development of a low temperature ($T < 5\text{K}$) pre-amplifier, fully UHV compatible and bakeable. In addition, the design ensures continuous operation over the full temperature range up to room temperature without re-calibration of the pre-amplifier.

However, the use of a low temperature pre-amplification circuit requires careful consideration of the absolute temperature of the sample-tip system since the circuit generates heat and is thermally connected to the sensor by the signal lines. The sample temperature can be precisely measured by a thermally well coupled Si diode. In contrast, the temperature of the sensor tip is not directly accessible, since the wiring of a temperature sensor would change the thermal situation completely. Therefore, we utilised a superconducting Niobium ($T_C \approx 9.3\text{K}$, $2\Delta_{T=5\text{K}} = 2.53\text{meV}$) STM tip for modulation spectroscopy on an Au(111) surface. The width of the superconducting gap is directly determined by the absolute temperature of the tunnelling gap and thus represents a direct access to the sensor temperature. With active AFM pre-amplifier, the measured width of $2\Delta \approx 2.5\text{meV}$ ($f_{\text{Mod}} = 1967\text{Hz}$, $V_{\text{Mod}} = 150\mu\text{V}_{\text{pp}}$) corresponds well to what has been measured by S. H. Pan et al. in 1998 [3]. With active QPlus

preamplifier, a slight temperature increase of the whole STM stage of about 0.5 K is observed and the results prove that the pre-amplifier is thermally well coupled to the STM stage and heat flow to the tip is minimal. Moreover, this measurement proves that the STM/STS performance of the system is not altered and the energy broadening in STS is exclusively determined by temperature and modulation amplitude.

In addition, the detection concept avoids electronic damping of the sensor (as known for IV-converter based concepts) to allow for Q factors up to 100,000 at a temperature of 5 K, which results in increased force sensitivity. A large bandwidth of more than 100kHz has key advantages enabling approaches such as: (i) the use of sensors with higher resonance frequencies, potentially increasing force sensitivity; (ii) higher harmonics AFM; or (iii) using a higher flexural mode of the QPlus sensor for frequency

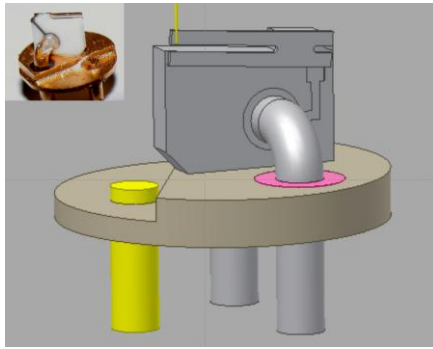


Figure 5: Optimized sensor carrier for the QPlus sensor

shift (Δf) feedback which basically leads to smaller effective oscillation amplitudes and allows to even come closer to the surface. First measurements (Figure 7a) prove that working at those high frequencies is possible with high resolution but images reveal an unexpected topography with structure dimensions below the atomic lattice constant. The image contrast however is not yet understood and tip artefacts cannot be excluded.

So far, QPlus sensors are not commercially available from sensor suppliers. We thus established a reliable manufacturing process for assembling sensors on dedicated LT STM carriers. After evaluation of Si cantilever tips from six different suppliers, the best image performance was achieved using conventionally wet-chemically etched tungsten tips, glued onto the tuning fork. This approach is very simple, does not involve a sophisticated process technology, and basically gives access to employ virtually any tip material. In addition, the use of solid metal tips allows for highest performance in simultaneous or alternative STM/STS operation. In addition to that, the high sensor stiffness and related small oscillatory noise are key reasons that make the QPlus sensor probably the most suitable AFM probe for STM/STS operation, superior to conventional metal coated cantilevers.

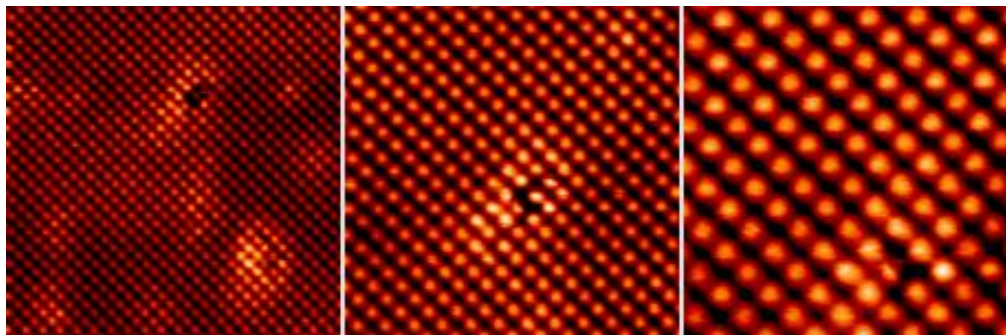


Figure 6: Atomic resolution on single crystal NaCl(100) using QPlus force detection at $T=5K$. No FFT filtering applied. Measurement in df feedback (not constant height). $df = -2Hz$, $A_{osc} \approx 1.5nmpp$, $f_{res} \approx 25kHz$, $Q = 36671$. Image size from left to right: $10 \times 10 nm^2$, $6 \times 6 nm^2$, $3.5 \times 3.5 nm^2$.

NaCl single crystals have been selected to fundamentally prove AFM performance due to the fact, that preparation is very simple by just cleaving in UHV and that possible impact on the feedback loop from I_T cross talk is excluded fundamentally. Benchmark measurements on NaCl(100) with a typical corrugation of approx. 10pm prove that resolution on insulating samples is competitive to best cantilever based AFM results (Figure 6). Measurements with comparable quality have been performed at LN2- and room temperature to prove the performance of the detection circuit at elevated temperatures. The stability of the Δf feedback and amplitude regulation has been proven by measurements with small oscillation amplitudes below 100pm peak-to-peak (Figure 7a).

A further example is shown in Figure 7c MgO(001) single crystals are extremely difficult to image with atomic resolution. The cleaving process leads to a high defect density and strong surface charges, which results in strong long range electrostatic forces. Usually vacuum annealing is required to reduce this strong charging and achieve atomic resolution with conventional cantilevers. Nevertheless, the shown performance has been achieved with the QPlus sensor without any annealing and can

be explained by the fact that the QPlus sensor's small amplitudes predominantly sense chemical short range forces for atomic contrast in comparison to comparatively soft cantilevers with higher oscillation amplitudes.

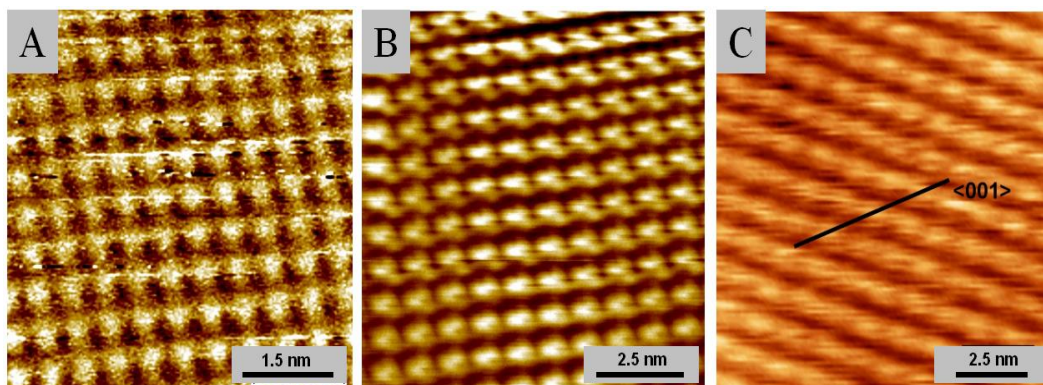


Figure 7: (a) Stable imaging of NaCl(100) in Δf feedback mode at small oscillation amplitudes of $A \approx 100$ pmpp. No filtering applied. $T = 77$ K, $df = -37$ Hz, $Q = 1200$, $f \approx 25$ kHz. (b) NaCl(100) with higher flexural mode as feedback. Base frequency $f_0 = 23.866$ Hz, $Q_0 = 13000$, $f_1 = 178.982$ kHz (used for Δf distance regulation), $Q_1 = 10\,000$, scan speed 4 nm/s. (c) QPlus AFM on MgO(001), small corrugation ≈ 15 pm. Raw data & plane correction. $T \approx 5.5$ K, $f = 25$ kHz, $AO_{SC} = 4$ nmpp, $U_{bias} = -10$ V. Sample by courtesy of C. Barth (Marseille).

In summary, a low temperature QPlus AFM detection has successfully been developed on a well proven experimental platform without compromising on the original STM/STS performance. Especially the combination of both QPlus AFM and STM modes on an extremely high performance level has a great potential for various applications, including AFM based molecule manipulation on insulating surfaces representing a key application of the PicoInside project.

References

- [1] F. J. Giessibl, Appl. Phys. Lett. 73, 3956 (1998)
- [2] F. J. Giessibl, Appl. Phys. Lett. 76, 1470 (2000)
- [3] S. H. Pan, E. W. Hudson, J. C. Davis, APL. 73, 20 (1998)

Dielectric substrates for anchoring organic molecules

**S. Hirth, F. Ostendorf, R. Bechstein, J. Schütte, P. Rahe, M. Nimmrich,
A. Kühnle and M. Reichling**

*Fachbereich Physik, Universität Osnabrück, Barbarastraße 7, 49076 Osnabrück,
Germany*

Keywords: dielectric surface, insulator, organic molecule, immobilisation, anchoring, NC-AFM

Electrical insulation is a key issue in the design of any electronic circuit. While there are plenty of trivial solutions available for insulation with synthetic materials for wiring in conventional circuits, insulation, or more precisely leakage currents, may become a technical challenge or an effective limitation in present and future integrated circuit design. It has been shown, for instance, that the thickness of the gate oxide that is a vital part of any field effect transistor in an integrated circuit based on Si-SiO₂ technology cannot be made thinner than 1.3 nm since otherwise the leakage current will prohibit proper operation [1]. According to the roadmap of the Semiconductor Industry Association [2], this would imply reaching the end of the silicon road in the year 2012 [1].

The problem of leakage current may impose also severe limitations when introducing single molecule electronics for computing. As molecules that are likely candidates for molecular electronics applications have a rather low conductance compared to that of doped silicon, an effective insulation against a (semi)conducting substrate is of utmost importance. One concept that has been developed to facilitate the controlled contact of a molecule to a metallic structure while avoiding unwanted channels of current flow is to decouple the conducting molecule from the substrate by weakly conducting spacer legs [3]. While this approach has successfully been demonstrated in a proof-of-concept experiment [4], it is of limited value for practical applications as for molecular device operation, not only the molecule but also the conducting pad contacting the molecule has to be isolated from any conducting substrate. Therefore, a design integrating molecules and electrodes on a non-conducting substrate would be more desirable for molecular electronics devices.

The quest for suitable combinations of functional conducting molecules and electrically insulating substrates that will eventually allow molecular device fabrication is one of the central issues in the development of atomic scale technologies for the PicoInside project [5]. While techniques for the preparation and characterisation of suitable insulating substrates and the deposition of organic molecules are well developed, the big challenge is the fabrication of stable structures by their combination. In this contribution, we introduce three candidates for dielectric substrates that are investigated in the framework of the PicoInside project, namely calciumdifluoride, titania and muscovite mica and discuss their suitability as substrate materials for molecular electronics. The main point here is a detailed analysis of the substrate surface structure and the mechanisms of interaction of molecules with the surface including physi- and chemisorption as well as anchoring by firm chemical bonds. The method of choice for such studies that is also utilised here is dynamic scanning force microscopy (SFM) operated in the so-called non-contact mode of operation (NC-AFM). This technique has been shown to be capable of revealing the details of surface structures on fluorides, oxides and other dielectric surfaces with a resolution ranging from the micrometer scale to atomic resolution [6-8].

Prototype materials that are principally suitable for our purpose are alkali halides and alkaline earth halides where surfaces can be prepared by cleaving bulk crystals [9, 10]

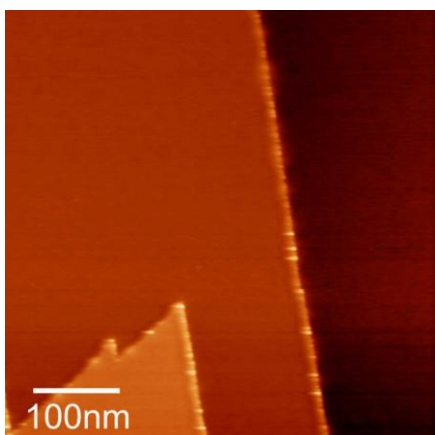


Figure 1: Face of a CaF_2 crystal cleaved along the (111) direction. The bright spots located at step edge and kink sites are due to charges.

or by growing them on metallic substrates [11, 12]. We have extensively investigated the $\text{CaF}_2(111)$ surface that allows the preparation of large, atomically flat terraces by a simple cleavage technique typically yielding results as shown in Figure 1. The step edges have a height of 0.31 nm corresponding to a F-Ca-F triple layer in the fluorite structure. They frequently appear to be slightly charged what is apparent in Figure 1 by the small bright spots that are not found on flat terraces but localise at edge or kink positions. The precise origin of the charging features is not yet clear, however, we speculate that they are due to charges trapped by sub-surface structural defects. Dislocation defects may, for instance, easily be created in the vicinity of step edges by the cleavage process imposing considerable stress on the crystal. While it is possible to reduce the overall charge present on

the crystal by heat treatment, it is most difficult to remove the charged spots like the ones shown in Figure 1 as they are apparently tightly bound to the crystal. Charges may, of course, be detrimental for the controlled adsorption of molecules as the local electric field may strongly polarise, attract or repel a molecule and fundamentally change its adsorption properties.

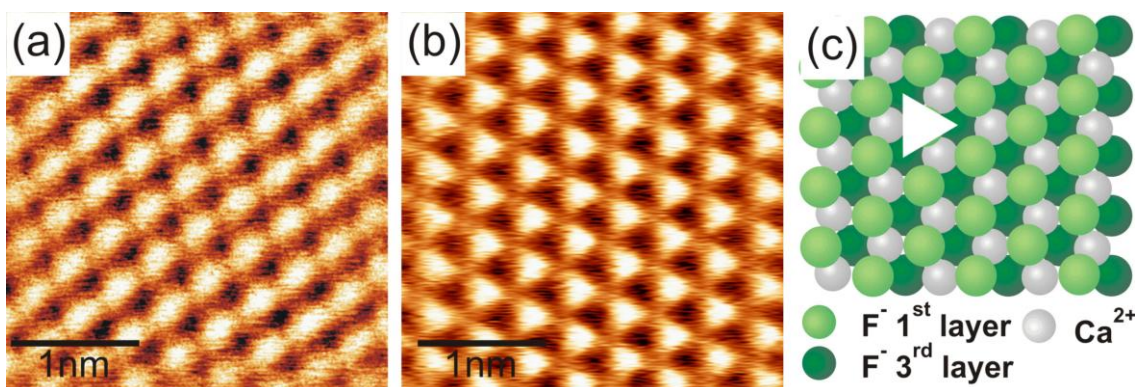


Figure 2: Imaging the cationic (a) and anionic (b) sub-lattices of the $\text{CaF}_2(111)$ surface on a flat terrace with atomic resolution dynamic scanning force microscopy. Frame (c) is a schematic representation of the topmost surface layers illustrating the formation of triangular contrast features that are characteristic for the anionic sub-lattice.

The surface areas between step edges of a cleaved $\text{CaF}_2(111)$ surface are atomically flat and perfectly well ordered. The two fundamental contrast patterns obtained in atomic resolution imaging of the surface with a dynamic force microscope are reproduced in Figure 2 and are well understood [13]. Frames (a) and (b) represent the cationic and anionic sub-lattices, respectively. The apparent triangular contrast feature dominating frame (b) is the result of a weighted superposition of contributions from first and third layer fluorine ions as depicted schematically (white triangle) in frame (c). When imaging a large number of flat terraces, one can hardly find any atomic scale defect, although, one would expect intuitively that the process of cleavage should produce at least a primary population of surface vacancies or F-centres. Vacancy related defects are not apparent in our measurements, however, there is indirect evidence that they exist due to their interaction with water [9, 14].

In a preliminary deposition experiment, we evaporated perylene-3,4,9,10-tetracarboxylic-3,4,9,10-diimide derivative molecules (PTCDI-S13, see Figure 3(a)) further on referred to as S13 onto the surface to obtain a sub-monolayer coverage on $\text{CaF}_2(111)$. The S13 molecule is based on the aromatic board of the perylene molecule that is functionalised by carboxylic and aliphatic groups. The original intention of these measurements was to study SFM contrast formation of individual deposited molecules and explore properties of binding the molecule to a flat terrace. It turned out, however, that S13 cannot easily be attached to the $\text{CaF}_2(111)$ surface as molecules readily diffuse towards step edges where molecules cluster in packages with several nanometres side length. This phenomenon is illustrated in Figure 4 showing a string of molecular clusters positioned at the lower side of a step edge. The molecular clusters are apparently not well ordered and it is not possible to highly resolve these structures. At present stage it is not clear how the clusters are formed, however, we speculate that local charges may provide initial nucleation centres.

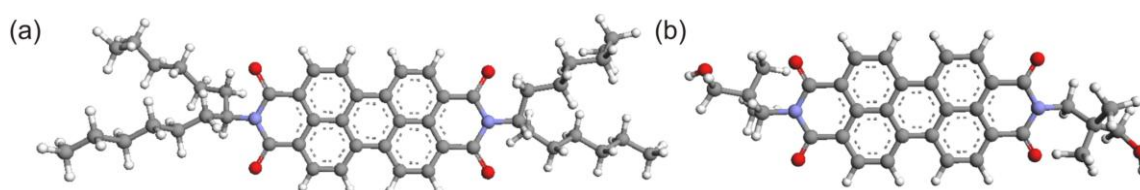


Figure 3: Structure of the two PTCDI compounds. (a) is termed S13 because of the side chain that contains 13 carbon atoms. The molecule in pane (b) is termed DMHP-PTCDI. It is smaller and lighter than S13 but has hydroxyl groups at the end of each side chain that may form additional bonds to a substrate.

These measurements reveal a common problem faced when depositing organic molecules on well prepared alkali halide and alkaline-earth halide surfaces. The interaction between molecules and surface is rather weak and diffusion barriers so low that molecules readily diffuse across the surface to surface irregularities acting as trapping centres [15]. This process often effectively suppresses the controlled adsorption of single molecules as well as the formation of well ordered structures by molecular self-organisation. While nucleation at step edges is detrimental for the controlled deposition on dielectric surfaces with large terraces, it can be utilised for creating molecular arrangements on nanostructured dielectric surfaces. Recently, nanometre sized shallow pits created by electron irradiation of $\text{KBr}(001)$ have successfully been used to trap SubPc molecules and to create regular molecular arrangements within the pits [16].

Muscovite mica is a universal dielectric substrate that has extensively been used for the deposition of metallic clusters [17], organic [18] and especially bio-molecules [19]. Its most appealing feature as a substrate is the possibility to create extremely large atomically flat terraces by a very simple procedure of peeling off layers. There is much expert knowledge available about this mineral material and its applications; however, the vast amount of knowledge on surface and adsorption is based on studies performed in a liquid environment. This also applies to atomic scale studies of the surface that have recently been introduced by advanced SFM techniques facilitating atomic scale imaging in a liquid environment. In these studies it was possible to

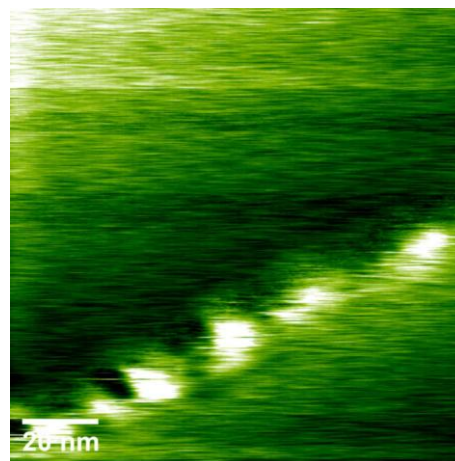


Figure 4: Step edge on a $\text{CaF}_2(111)$ surface decorated a string of clusters composed of S13 molecules.

identify the hexagonal structure of surface SiO_2 units on mica (see Figure 5) and to demonstrate the order and cleanliness of the surface present in aqueous solution [20].

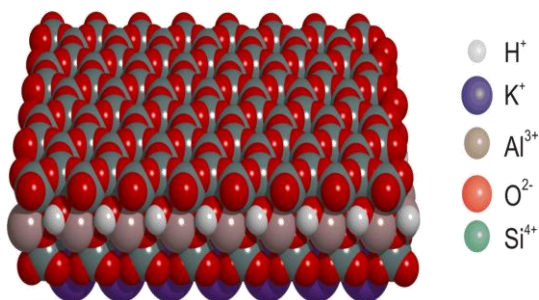


Figure 5: Structure model of a Muscovite mica surface layer.

Imaging the mica surface in an ultra-high vacuum environment with high resolution is a much more challenging task. As the material contains layers of K^+ ions that are exposed upon cleaving the material, the cleavage process normally produces a large amount of surface charge as the interface K^+ ions will never stick in equal parts to separated cleavage

faces. As mica is a very good bulk electrical insulator, these charges will prevail in an ultra-high environment and result in a very high and in homogeneously distributed surface potential that strongly hampers and mostly prohibits high resolution force microscopy imaging. The charge can be removed by cleaving mica in air what results in a significant coverage of the surface with molecular adsorbates and surface reaction products [21].

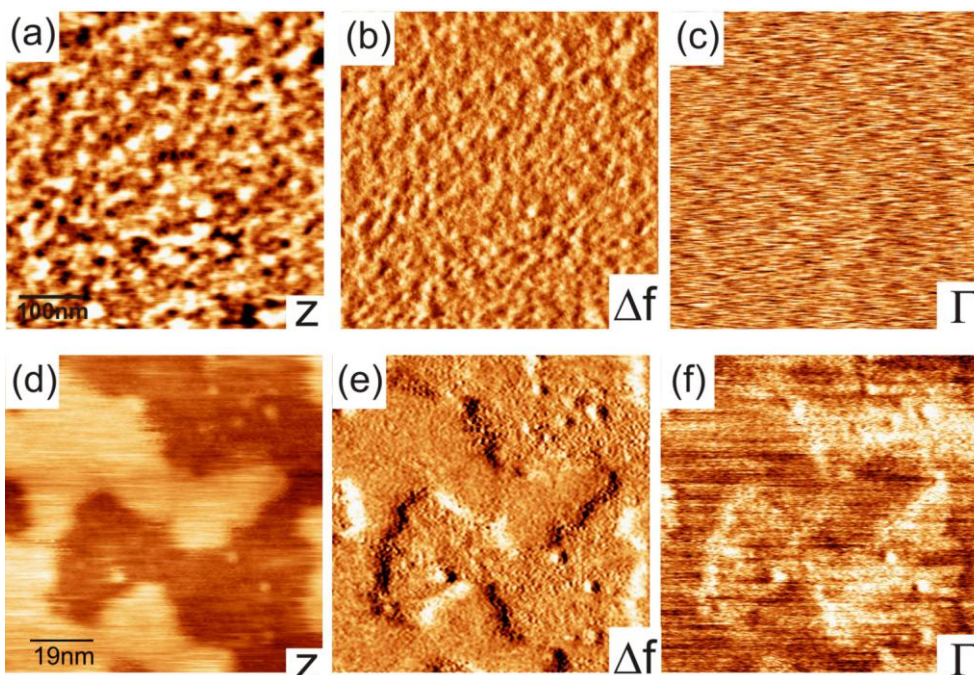


Figure 6: (a) to (c) surface structure of muscovite mica cleaved in air as revealed by dynamic scanning force microscopy. (d) to (f) deposited molecules of DMHP-PTCDI, condense into irregularly shaped flat island the images display the (a, d) topography, (b, e) detuning and (c, f) dissipation signals, respectively.

A typical result for such a surface investigated with dynamic force microscope is shown in Figure 6 (a) to (c). It is evident from the images that the surface coverage introduces a sub-nanometre roughness and the overall result is a much less well defined surface than one would expect from an atomically flat substrate. When depositing DMHP-PTCDI onto the surface it is found that this molecule indeed sticks to the surface and condenses into irregularly shaped islands as shown in Figure 6 (d) to (f). These islands appear to be rather flat on the surface, however, it has not yet been possible to image the molecular layer with high resolution and to test its structural order.

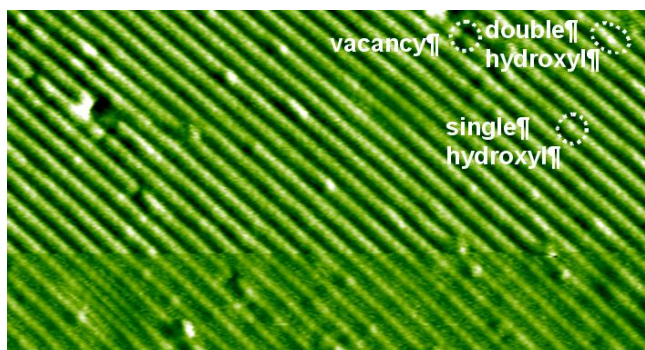


Figure 7: The $\text{TiO}_2(110)$ surface imaged with dynamic SFM. Bright features are oxygen rows along $[001]$. The horizontal line marks a tip change resulting in a change of the imaging mode. In the upper part, pits on the oxygen rows represent oxygen vacancies while small and extended protrusions are single and double hydroxyls, respectively.

The (110) surface of rutile TiO_2 is a dielectric substrate that is apparently well suited as a substrate for molecular structure formation in the context of molecular electronics. Fixing small organic molecules on this surface by a carboxylic anchor has been demonstrated for molecules deposited under conditions of an ultra-high vacuum [22, 23] as well as adsorption of larger molecules from solution [24, 25]. The surface is prepared by mechanical polishing followed sputtering/annealing cycles in the ultra-high vacuum and reveals an atomic row structure as shown in Figure 7. Rows are

protruding oxygen ions and under fortunate conditions they exhibit atomic resolution in SFM imaging. The apparent pits and protrusions on the rows are oxygen vacancies, substitutional hydroxyls and double hydroxyls, respectively. The identification of these species on the oxygen rows with SFM has recently been established and explained in great detail [26-28] and scanning tunnelling microscopy (STM) studies reveal the complex mechanisms of their formation [29, 30]. Vacancies that are the result of surface preparation under slightly reducing conditions determine the anchoring of molecules on this surface. STM and SFM investigations clearly show that vacancies are rapidly (within minutes) converted into hydroxyl species in the presence of a water partial pressure in the 10^{-9} Pa region what is typical for ultra-high vacuum conditions. Therefore, processing under very clean conditions will be a central issue for molecular deposition on $\text{TiO}_2(110)$. In the imaging mode present in the upper part of Figure 8, the bright features are rows of oxygen and vacancies appear as pits while single and double hydroxyls are small and extended protrusions.

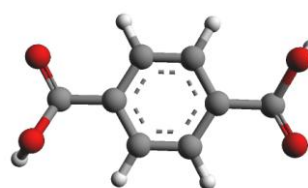
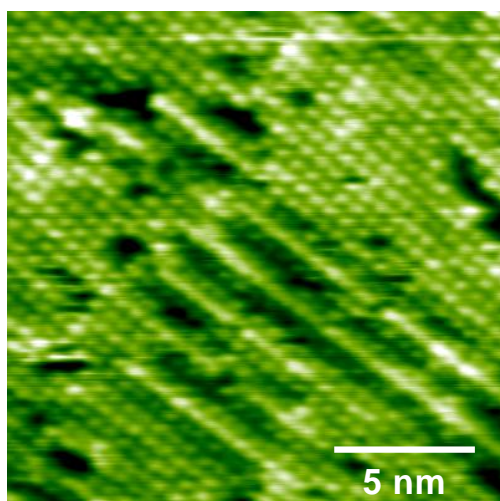


Figure 8: Upper image: Structure model of terephthalic acid (TPA). Left image: The $\text{TiO}_2(110)$ covered with TPA molecules. The predominant structure is a (2×1) array of molecules that is interrupted by linear arrangements at coverages close to a monolayer.

Simple aromatic molecules with a carboxylic functionality have been found to be well suited for adsorption on a $\text{TiO}_2(110)$ surface. Such molecules can often be sublimated from a powder of microcrystals in the ultra-high vacuum facilitating the deposition of layers with any desired thickness under very clean conditions. Single molecules observed at low coverage readily adsorb on the Ti rows and appear to be firmly

anchored as one does not observe diffusion or tip induced manipulation during scanning. Molecules are found to be statistically distributed on flat terraces and do not exhibit an affinity towards adsorption at step edges. A molecule that has been found to be specifically well suited for the formation of ordered layers observed at higher coverage is terephthalic acid (TPA). Figure 8 demonstrates the formation of a regular (2 x 1) array of such molecules that is interrupted by linear arrangements at coverages close to a monolayer.

In summary, we introduced three dielectric materials as potential substrates in the context of molecular computing applications. CaF_2 and muscovite mica allow the preparation of large atomically flat terraces by simple cleavage procedures. However, terraces on $\text{CaF}_2(111)$ do not naturally provide anchoring sites and it has to be explored how they can be prepared on the fluorite surface in a controlled way. Air cleaved mica readily facilitates molecular adsorption, however, the molecule-substrate interaction is mediated in this case by surface contaminants and the details of the resulting surface structure has to be characterised in detail. The $\text{TiO}_2(110)$ surface requires elaborate preparation in the ultra-high vacuum but facilitates anchoring of molecules with carboxylic functionality. The substrate provides a base for both, the adsorption of single molecules as well as the formation of a well ordered molecular layer. Apparently, the well known hydroxyl defects present on the $\text{TiO}_2(110)$ surface after a standard preparation procedure do not hamper the formation of a well ordered molecular carpet. Hence, this substrate is a very promising candidate for the development of molecular systems with computing functionality.

References

- [1] M. Schulz; Nature 1999, 399, 729-730.
- [2] www.itrs.net
- [3] A. Gourdon; Eur. J. Org. Chem. 1998, 2797 (1998).
- [4] L. Grill, F. Moresco, P. Jiang, C. Joachim, A. Gourdon and K. H. Rieder; Phys. Rev. B 2004, 69, 035416.
- [5] www.picoinside.org
- [6] C. Barth, A. S. Foster, M. Reichling and A. L. Shluger J.; Phys.: Condens. Matter 2001, 13, 2061-2079.
- [7] C. Barth and M. Reichling; Nature, 2001, 414, 54-57.
- [8] S. Gritschneider, Y. Namai, Y. Iwasawa and M. Reichling; Nanotechnology, 2005, 16, S41.
- [9] M. Reichling and C. Barth; Phys. Rev. Lett. 1999, 83, 768-771.
- [10] M. Schmid, A. Renner and F. J. Giessibl; Rev. Sci. Instrum. 2006, 77, 036101.
- [11] R. Bennowitz, A. S. Foster, L. N. Kantorovich, M. Bammerlin, C. Loppacher, S. Schar, M. Guggisberg, E. Meyer and A. L. Shluger; Phys. Rev. B 2000, 62, 2074-2084.
- [12] J. Repp, S. Fölsch, G. Meyer and K. H. Rieder; Phys. Rev. Lett. 2001, 86, 252-255.
- [13] A. S. Foster, C. Barth, A. L. Shluger and M. Reichling; Phys. Rev. Lett. 2001, 86, 2373-2376.
- [14] S. Hirth, F. Ostendorf and M. Reichling; Nanotechnology 2006, 17, S148.
- [15] L. Nony, R. Bennowitz, O. Pfeiffer, E. Gnecco, A. Baratoff, E. Meyer, T. Eguchi, A. Gourdon and C. Joachim; Nanotechnology 2004, 15, S91.
- [16] L. Nony, E. Gnecco, A. Baratoff, A. Alkauskas, R. Bennowitz, O. Pfeiffer, S. Maier, A. Wetzel, E. Meyer and C. Gerber; Nano Letters 2004, 4, 2185-2189.

- [17] S. Ferrero, A. Piednoir and C. R. Henry; *Nano Letters* 2001, 1, 227-230.
- [18] B. R. A. Neves, M. E. Salmon, P. E. Russell and E. B. Troughton; *Langmuir* 2001, 17, 8193-8198.
- [19] T. Kanno, H. Tanaka, N. Miyoshi and T. Kawai; *Jpn. J. Appl. Phys.* 2000, 39, L269-L270.
- [20] T. Fukuma, K. Kobayashi, K. Matsushige and H. Yamada; *Appl. Phys. Lett.* 2005, 87, 034101.
- [21] F. Ostendorf, C. Schmitz, S. Hirth, A. Kühnle, J. J. Kolodziej and M. Reichling; *Nanotechnology* 2008, 19, 305705.
- [22] A. Sasahara, H. Uetsuka and H. Onishi; *J. Phys. Chem. B* 2001, 105, 1-4.
- [23] T. Ishibashi, H. Uetsuka and H. Onishi; *J. Phys. Chem. B* 2004, 108, 17166-17170.
- [24] C. L. Pang, T.-a. Ishibashi and H. Onishi; *Jpn. J. Appl. Phys.* 2005, 44, 5438-5442.
- [25] A. Sasahara, C. L. Pang and H. Onishi; *J. Phys. Chem. B* 2006, 110, 4751-4755.
- [26] J. V. Lauritsen, A. S. Foster, G. H. Olesen, M. C. Christensen, A. Kühnle, S. Helveg, J. R. Rostrup-Nielsen, B. S. Clausen, M. Reichling and F. Besenbacher; *Nanotechnology* 2006, 17, 3436-3441.
- [27] G. H. Enevoldsen, A. S. Foster, M. C. Christensen, J. V. Lauritsen and F. Besenbacher; *Phys. Rev. B* 2007, 76, 205415-205414.
- [28] G. H. Enevoldsen, H. P. Pinto, A. S. Foster, M. C. R. Jensen, A. Kühnle, M. Reichling, W. A. Hofer, J. V. Lauritsen and F. Besenbacher; *Phys. Rev. B* 2008, 78, 045416.
- [29] S. Wendt et al.; *Surf. Sci.* 2005, 598, 226-245.
- [30] S. Wendt, J. Matthiesen, R. Schaub, E. K. Vestergaard, E. Laegsgaard, F. Besenbacher and B. Hammer; *Phys. Rev. Lett.* 2006, 96, 066107.

Immobilization of organic molecules on insulators

**A. Socoliuc¹, O. Pfeiffer¹, S. Maier¹, L. Zimmerli¹, E. Gnecco¹, B. Such¹,
Th. Glatzel¹, S. Kawai¹, E. Meyer¹, L. Nony² and R. Bennewitz³**

¹*Institute of Physics and National Center of Competence in Research "Nanoscale Science", University of Basel, Klingelbergstr. 82, CH-4056 Basel, Switzerland*

²*Université d'Aix Marseille III, L2MP, Campus de Saint Jérôme, Service 151, 13397 Marseille Cedex 20, France*

³*McGill University, Physics Department, 3600 rue University, Montréal, Canada*

Silicon microelectronics has undergone continuous miniaturization during the last three decades leading to dramatic improvements in computational capacity and speed. As fundamental limit of electronic devices, individual molecules have been foreseen as functional electronic structures. The wide variety of organic molecules would seem to make viable the hope that single molecules will be able to perform for instance the logic functions [1]. With this goal in mind, adsorption of organic molecules on flat and patterned surfaces has become a subject of intensive studies [2]. Such studies have been performed mainly using metallic substrates, although the coupling between the electrons of the molecules and the surface could prevent their use. In order to separate the functional electronic systems from the substrate, molecules with spacer legs have been designed [3], adsorption on thin insulating spacer films [4] and in pits produced on an alkali halide sample by electron irradiation have been explored [5].

Since its invention, the non-contact atomic force microscope (nc-AFM) has proven its capability of yielding images with atomic resolution on a wide variety of surfaces [6], ranging from metals to semiconductors to polymers to biological materials [7]. The nc-AFM offers unique advantages compared to other scanning probe techniques, such as contact atomic force microscopy (c-AFM) and scanning tunneling microscopy (STM). The absence of repulsive forces in nc-AFM permits its use in the imaging of "delicate" samples [5] and, the nc-AFM does not require conducting samples. This technique relies on a microfabricated tip at the end of a cantilever excited at its fundamental bending eigenfrequency. After approaching the surface, the tip first senses an attractive force that decreases the resonance frequency. The negative frequency shift, Δf , varies rapidly with the minimum tip distance, especially a few angstroms away from the surface. When Δf is used for distance control, contrasts down to the atomic scale can be achieved in ultrahigh vacuum.

This non-destructive imaging technique, led to several studies where atomic rows [8], steps, or vacancies on flat surfaces [9] could be obtained via the tip-sample interaction as distance control. Apart from the imaging capabilities, force microscopy experiments can also quantify forces involved in the manipulation of molecules [10]. Some successful attempts to utilize nc-AFM for these purposes have been made; well-controlled lateral manipulations of single atoms even at room temperature become possible [11].

For the first time Nony et al. were able to resolve single organic molecules on an insulating sample by nc-AFM [5]. The high mobility of the organic molecules on insulating surfaces at room temperature makes their imaging very difficult [12]. Therefore, an essential condition to obtain molecular arrangements on such surfaces is to lower the mobility of the molecules. One solution was to change the morphology of the ionic crystals by electron irradiation. Square and rectangular pits of nanometer size and of monolayer depth were formed [13].

Irradiation of alkali halide crystals leads to the production of defects in a subsurface region of the crystal. Subsequent diffusion and interaction of these defects with the

surface results in desorption processes at the surface [13]. In the literature formation of nanopits is reported on different ionic crystals (KBr, NaCl...). The desorption process takes place layer-by-layer and the efficiency of the process is influenced by the surface topography.

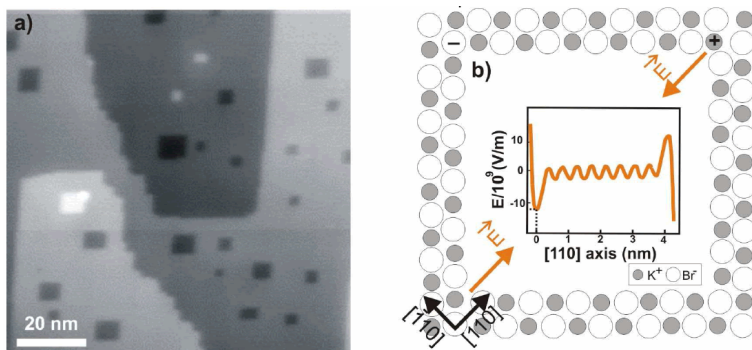


Figure 1: a) Pits produced by electron bombardment on KBr. b) Electrostatic field inside the pit along the [110] direction. The field was calculated by summing up the Coulomb contributions of 100x100x100 alternating electrical charges and subtracting the contribution of a 10 x10x 10 squared monolayer of ions.

On KBr (001), straight-edged pits can be created by exposing the surface to an electron beam of 1keV for a short time. The pits are square or rectangular and one monolayer (i.e., 0.33 nm) deep (Figure 1a). The keV energy of the electrons arriving on the surface is transferred to valence-holeconduction-electron pair and lattice vibration. This leads to the formation of defects like F centers when an electron

is trapped in a halogen vacancy and, H center resulted from an interstitial halogen atom. Thermally activated motions of the defects carries energy to the surface of the crystal and provoke the emission of halogen atoms and the neutralization of the surface alkali atoms [14]. One mono-atomic pit created by electron bombardment and the electrostatic field inside the pit are depicted in Figure 1b. The electrostatic field presents rapid variation at the corner sides and weaker modulations in the middle of the pit.

The first attempt to exploit the increased interaction of molecules with the topographically modified KBr was the evaporation of 3,4,9,10-perylene tetracarboxylic dianhydride (PTCDA) molecules [15] without spacer legs. Figure 2 shows a KBr surface with pits after evaporating a submonolayer of PTCDA. Some pits were partially or totally filled with molecules, but the resolution of single molecules could not be achieved [12].

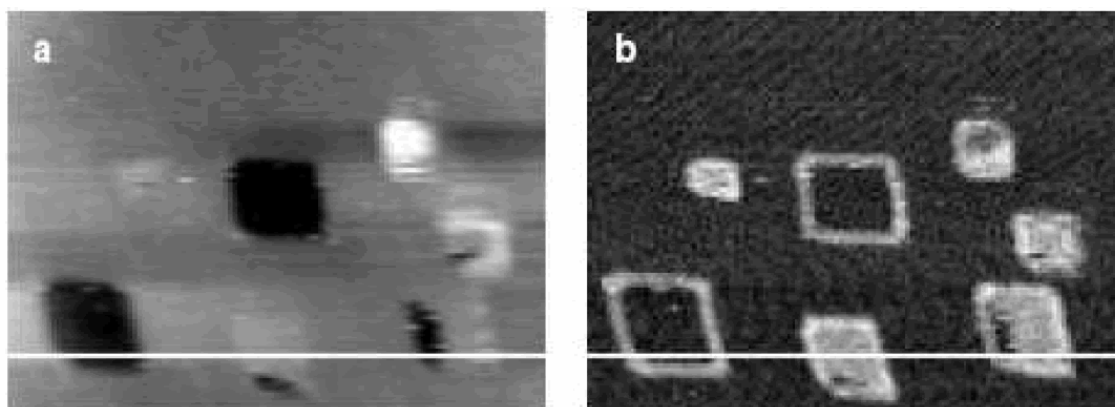


Figure 2: KBr(001) surface with electron irradiation-induced rectangular pits, covered with one-tenth of a monolayer of PTCDA molecules. a) Topography signal recorded by nc-AFM (frame edge 132 nm x 98 nm). b) Damping signal

The turning point in achieving molecular resolution for molecules evaporated on insulating materials was the evaporation of the sub-phthalocyanine (SubPc), into the pits produced in a KBr sample. The three fold symmetry SubPc molecule has a strong dipole moment of 4.8 Debye pointing away from the protruding electronegative Cl atom and the electrostatically fitted effective charge on Cl was estimated to be $-0.4 e$.

Figure 3 summarizes the results of this experiment. Frame (a) shows the surface after the pit formation and the evaporation of the molecules. Only smaller pits (below 15 nm) are filled with molecules. Single molecules are clearly visible in frame (b). They are organized in rows tilted $\pm 45^\circ$ with respect to crystallographic axes. The distance between adjacent rows is 1.4 nm, and the distance between two consecutive molecules in a row is 1.0 nm. The apparent height of the rows is about 0.6 nm with respect to the surrounding KBr(001) terrace or equivalently 0.9 nm with respect to the bottom of the pit. The molecules are well ordered in the center of each pit, but rather mismatched structures occur along their edges. A blurred bright area in Figure 3b can be attributed to mobile molecules and a few protruding molecules on top of the organized layer

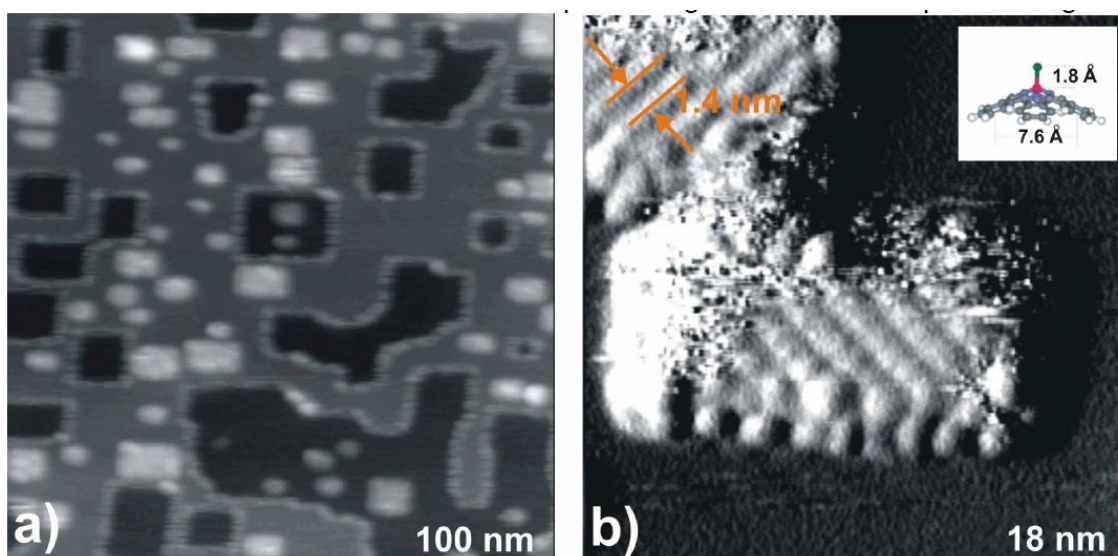


Figure 3: a) The molecules decorate steps and fill pits of width smaller than 15 nm. No molecules are observed on the KBr terraces. Molecular self-assembled structures are revealed within two pits. b) Frame size 18 nm. Molecular resolution reveals that the structures are tilted $\pm 45^\circ$ with respect to the pit edges. The inset image is a sketch of the SubPc molecule.

The attraction of the considerable charge of the Cl atom to the negatively charged corner of the pit, where the Cl atom gets surrounded by three K^+ ions is very strong. Consequently, those corners can act as efficient nucleation centers for molecules such as SubPc. Van der Waals attraction favors also the adsorption of the SubPc molecules to the bottom of the pit via two of the "feet" and their trapping at the right corner. Intermolecular forces based on dipole-dipole interaction are much weaker but nevertheless, they count for the relative orientation of molecules in adjacent rows. The total trapping interaction leads to an energetic barrier of about 0.15 eV ($\sim 6k_B T$), preventing thus, the diffusion of a single molecule at room temperature.

Following the idea of using strong dipole as anchors for molecules of ionic surface a new molecules were synthesized by one of Pico-Inside partners (ICIQ, A Echavarren). The functionalized truxene molecules [15] have three cyanobenzyl groups (with dipole moment of 4.5D) on bonded flexibly to the aromatic core. The molecules fill the pits created if KBr surface, similarly to SubPc, forming a bilayer which occasionally is

ordered. In contrast to SubPc, however, three anchoring groups provide enough binding interaction to immobilize a single molecule on a kink of a monolayer step of KBr at room temperature (RT). Moreover, the interaction between the molecules and substrate is strong enough to restructure the steps of the KBr crystal in order to form additional kinks able to accommodate the molecules in regular fashion [16].

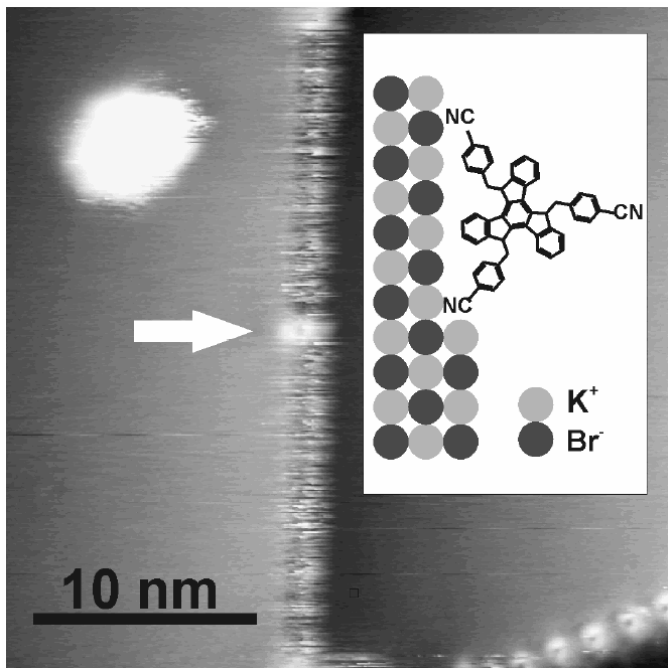


Figure 4: Functionalized truxene molecules adsorbed on a cleaved KBr crystal. An arrow points at a single molecule adsorbed at a kink. The inset shows the size of the truxene molecule in comparison to KBr lattice.

Described results allow for formulation basic rules for design of molecules intended to be adsorbed at ionic substrates: (i) strong dipoles (three dipoles of 4.5D are enough to immobilize a molecule on a kink on a KBr surface) within the molecule are needed in order to provide enough electrostatic interaction to bind a molecule; (ii) either the dipoles have to be placed in the distance exactly matching the substrate lattice or they have to be placed on flexible joints in order to allow them to adapt to the substrate electrostatic landscape; (iii) thanks to flexibility of anchoring groups there is possibility that the aromatic boards of such a molecule remains intact and can perform intended logical function.

Keeping in mind the main goals of this research, namely integrating a calculation unit in a molecule, the next main challenge would be to study the connections of anchored molecules to the outer world allowing to exchange the information of the molecular processor with the environment.

References

- [1] C. Joachim, J. Gimzewski and A. Aviram; Nature 408, 541, 2000.
- [2] M. de Wild, S. Berner, H. Suzuki, H. Yanagi, D. Schlettwein, S. Ivan, A. Baratoff, H.-J. Güntherodt and T. Jung; ChemPhysChem 3, 881, 2002.
- [3] V. Langlais, R. Schlittler, H. Tang, A. Gourdon, C. Joachim and J. Gimzewski, Phys. Rev. Lett. 83, 2809, 1999.
- [4] H. Rauscher, T. Jung, J-L Lin, A. Kirakosian, F. Himpsel, U. Rohr and K. Müllen; Chem. Phys. Lett. 303, 363, 1999.
- [5] L. Nony , E. Gnecco, A. Baratoff, A. Alkauskas, R. Bennewitz, O. Pfeiffer, S. Maier, A. Wetzels, E. Meyer and Ch. Gerber; NanoLett. 4, 2185-2189, 2004.
- [6] F.J. Giessibl; Science 267, 68, 1995.
- [7] R. Wiesendanger; Scanning Probe Microscopy and Spectroscopy (Great Britain: Cambridge University Press), 1994.
- [8] Y. Sugawara, H. Ueyama, T. Uchihashi, M. Ohta, S. Morita, M. Suzuki and S. Mishima, Appl. Surf. Sci. 113/114, 364, 1997.

- [9] R. Lüthi, E. Meyer, M. Bammerlin, A. Baratoff, T. Lehmann, L. Howald, Ch. Gerber and H.-J. Güntherodt; *Z. Phys. B* 100, 165, 1996.
- [10] F. Rosei, M. Schunack, Y. Naitoh, P. Jiang, A. Gourdon, E. Laegsgaard, I. Stensgaard, C. Joachim and F. Besenbacher; *Prog. Surf. Sci.* 71, 95-146, 2003.
- [11] Y. Sugimoto, M. Abe, S. Hirayama, N. Oyabu, O. Custance and S. Morita; *Nature Materials* 4, 156–159, 2005.
- [12] L. Nony, R. Bennewitz, O. Pfeiffer, E. Gnecco, A. Baratoff, E. Meyer, T. Eguchi, A. Gourdon and C. Joachim; *Nanotechnology*, 15, S91-S96, 2004.
- [13] J.J. Kolodziej, B. Such, P. Czuba, F. Krok, P. Piatkowski, P. Strutski, M. Szymonski, R. Bennewitz, S. Schär and E. Meyer; *Surf. Sci.* 482-485, 903-909, 2001.
- [14] B. Such, P. Czuba, P. Piatkowski and M. Szymonski; *Surf. Sci.* 451, 203, 2000.
- [15] O. de Frutos, T. Granier, B. Gomez-Lor, J. Jimenez-Barbero, A. Monge, E. Gutierrez- Puebla and A. M. Echavarren; *Chem. Eur. J.*, 8, 2879, 2002.
- [16] B. Such, Th. Glatzel, S. Kawai, L. Zimmerli, E. Meyer, C. H. M. Amijs, P. de Mendoza and A. M. Echavarren in preparation.

Non-contact AFM as Indispensable Tool for Investigation of Patterned Insulators

**A. Socoliuc, Th. Glatzel, O. Pfeiffer, E. Gnecco, A. Baratoff, L. Nony^(*),
B. Such, S. Kawai and E. Meyer**

Institute of Physics, Klingelbergstr. 82, CH-4056 Basel, Switzerland

() UMR CNRS 6137, Université Paul Cézanne Aix-Marseille III, Case 151, 13397
Marseille, Cedex 20, France*

Surface modifications induced by electronic transitions are quite important for nanofabrication [1,2]. For instance, modified insulating surfaces can be used as templates for adsorbing medium-sized (<100 atoms) functional organic molecules, which is extremely interesting in the development of hybrid molecular electronic devices [3, 4]. The mobility and aggregation of molecules as well as their eventual ordering on an insulating surface is determined by the weak balance between intermolecular and molecule- substrate interactions. The final arrangement of the molecules can be observed by non-contact force microscopy (NC-AFM) [5, 6] even with sub-molecular resolution.

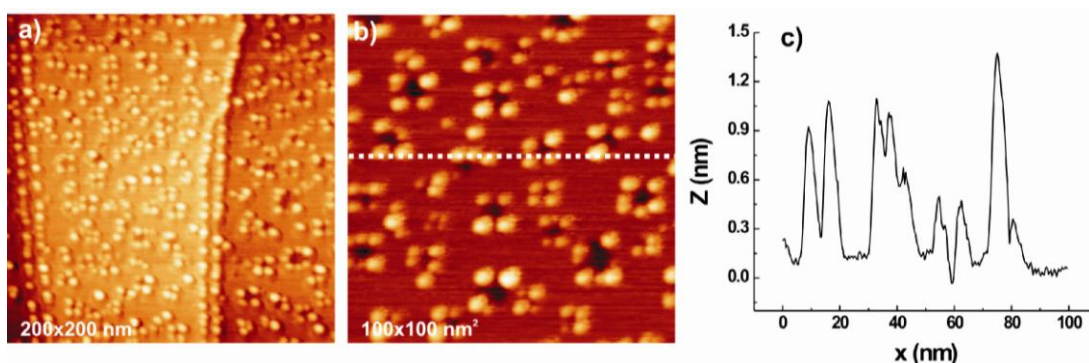


Figure 1: a) NC-AFM topographical image of 200x200 nm² on KBr(100) with pits created by electron evaporation and 0.3ML gold. b) Zoom on 100x100nm² for a better view of how the gold clusters decorate the pit corners. c) Cross section of the topography over 100 nm proving that the gold formed indeed clusters (due to the large dimensions).

When an ionic crystal is excited by electrons [1], the desorption of surface atoms is induced by the formation of Frenkel defects in the bulk (F and H centers), which diffuse and recombine with the surface. At the first stages of the typically layer-by-layer surface removal monatomic depth rectangular pits are formed, which are several nanometers in size. These pits can be successfully used as molecular traps. For instance, our group has succeeded in confining chloro-[subphthalocyaninato] boron-(III) (SubPc) and functionalized truxene molecules on a modified KBr(001) surface in ultrahigh vacuum (UHV) at room temperature [3, Such]. In order to realize a viable device based on an ordered array of few molecules, such arrangement has to be connected to metallic electrodes. Fortunately, nanopatterns can also serve to control the nucleation of metal nanostructures at surfaces [7]. Figure 1 shows almost 0.3 ML of gold evaporated on a KBr surface with pits at room temperature. The gold decorates the step edges and the pit edges from outside being located on the upper terrace edge. No gold atoms or clusters were observed at the bottom of the pits. In a recent study Matievsky et al. observed that metal nanoparticles on KBr can even be used to nucleate the growth of pits, resulting in pits with metal nanoparticles inside [8]. The same group was also able to finely tune the size of the pits by using an electron-beam evaporator with extremely small current densities. A minimum pit size of approx. 3 nm²

was observed. This size corresponds to the removal of 28 atoms and was attributed to the impingement of single charged particles on the surface of the crystal. These pits should be small enough to immobilize and isolate individual large molecules, such as SubPc, which otherwise have long diffusion lengths on insulating surfaces [9].

Electron-induced modification of alkali halide surfaces can also result in creation of straight edges running in the main crystallographic directions with isolated kinks. Such kinks, due to large modulation of electrostatic potential in their vicinity, have been shown to be able to immobilize a single functionalized truxene molecule at room temperature [10]. The challenge still remains how to produce in controlled way single isolated defects in alkali halide surface. However, since such defects should give similar variation of electrostatic potential as kinks, that would give a way of control of adsorption of single molecules on the flat terraces, as well.

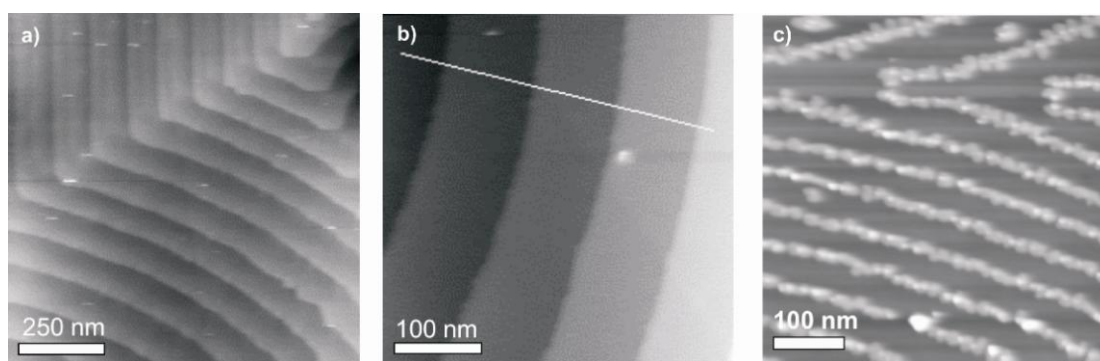


Figure 2: a) Topographical image of the spirals consisting of parallel monoatomic steps separated by atomically flat terraces on KBr, b) a closer look at the created structure, c) sublimation of 0.5 ML of Cu-TBPP at room temperature on the spirals. The structure was obtained by heating the crystal at 380°C in ultra high vacuum for 20 minutes.

An alternative method for getting patterned insulating surfaces is simply given by annealing [11]. Heating of ionic crystals in vacuum results in atomic diffusion from corner sites of steps. This process smoothes cleavage steps and evolves spirals of steps around the intersection of dislocations with the surface. These spirals provide a regular array of monoatomic or diatomic steps, separating atomically flat terraces (Figure 2a,b). The typical terrace width is between 50 and 150 nm [12]. The enhanced interaction at the steps of evaporation spirals makes them a candidate for guided growth of molecular adsorbates (Figure 2c).

References

- [1] M. Szymonski, J. Kolodziej, B. Such, P. Piatkowski, P. Struski, P. Czuba and F. Krok, *Prog. Surf. Sci.* 67, 123_2001
- [2] *Desorption Induced by Electronic Transitions I*, edited by N. H. Tolk, M. M. Traum, J. C. Tully and T. E. Madey, Springer, Berlin, 1983
- [3] L. Nony, E. Gnecco, A. Baratoff, A. Alkauskas, R. Bennewitz, O. Pfeiffer, S. Maier, A. Wetzler, E. Meyer and Ch. Gerber, *Nano Lett.* 4, 2185 2004 [Such]
- [4] C. Joachim, J. Gimzewski and A. Aviram, *Nature* 408, 541 2000
- [5] *Noncontact Atomic Force Microscopy*, edited by S. Morita, R. Wiesendanger and E. Meyer, Springer, Berlin, 2002
- [6] R. Bennewitz, S. Schär, V. Barwich, O. Pfeiffer, E. Meyer, F. Krok, B. Such, J. Kolodziej and M. Szymonski, *Surf. Sci.* 474, L197 2001
- [7] H. Höche, J. P. Toennies and R. Vollmer, *Phys. Rev. B* 50, 679 1994
- [8] J.M. Mativetsky, Y. Miyahara, S. Fostner, S. A. Burke and P. Grütter, *App. Phys. Lett.* 88 233121 2006



- [9] O. Pfeiffer, E. Gnecco, L. Zimmerli, S. Maier, E. Meyer, L. Nony, R. Bennewitz, F. Diederich, H. Fang and D. Bonifazi, *J. Phys.: Conf. Ser.* 19, 166 2005
- [10] B. Such, Th. Glatzel, S. Kawai, L. Zimmerli, E. Meyer, C. H. M. Amijs, P. de Mendoza and A. M. Echavarren in preparation.
- [11] K. Yamamoto, T. Iijima, T. Kunishi, K. Fuwa and T. Osaka, *J. Cryst. Growth* 94 629 1998
- [12] L. Nony L, R. Bennewitz, O. Pfeiffer, E. Gnecco, A. Baratoff, E. Meyer, T. Eguchi, A Gourdon and Joachim C, *Nanotechnology* 15 91 2004

PTCDA molecules adsorbed on rutile $\text{TiO}_2(011)-(2\times 1)$: STM and nc-AFM studies

Antoni Tekiel, Janusz Budzioch, Szymon Godlewski, Jakub S. Prauzner-Bechcicki and Marek Szymonski

*Research Centre for Nanometer-scale Science and Advanced Materials (NANOSAM),
Faculty of Physics, Astronomy and Applied Computer Science, Jagiellonian University
Reymonta 4, 30-059 Krakow, Poland*

Keywords: PTCDA, nc-AFM, $\text{TiO}_2(011)-(2\times 1)$, molecular chains, contrast inversion

Pico-Inside consortium had focused its efforts on integrating a complex logic gate inside a single molecule, therefore there is a necessity for development of manipulation strategies for single molecules. Such a single molecule manipulation for molecules assembled on wide band gap or insulating materials may be achieved by means of non-contact atomic force microscopy (nc-AFM). However, efficient manipulation strategy must always be preceded by well established imaging technique for a system in question. Therefore here we would like to report on combined STM and nc-AFM studies of 3,4,9,10-perylene-tetracarboxylic-dianhydride (PTCDA) adsorbed on the $\text{TiO}_2(011)-(2\times 1)$ surface. Recently, a role of rutile TiO_2 in a wide range of technical applications have become increasingly significant and therefore titanium dioxide is one of the most investigated oxides in surface science [1-3]. The TiO_2 crystal belongs to a group of materials with relatively wide band gap - 3.2eV [4]. On the other hand, PTCDA may be regarded as a prototypical, planar stacking, organic semiconductor for future nano-electronic devices. Thus a PTCDA/ $\text{TiO}_2(011)-(2\times 1)$ system appears to be an ideal subject for research carried within Pico-Inside consortium.

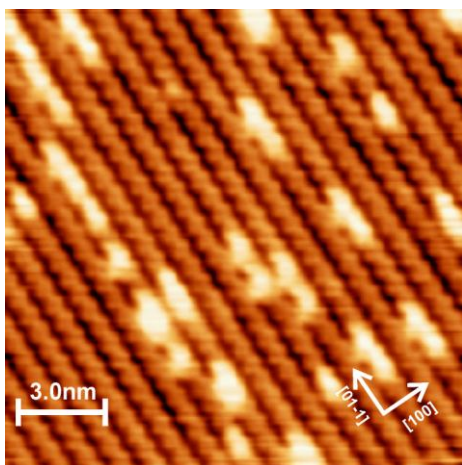


Figure 1: STM image of clean surface of rutile $\text{TiO}_2(011)-(2\times 1)$. Bright zigzag pattern along the $[0-11]$ crystallographic direction is ascribed to under-coordinated oxygen atoms, bias voltage: 2V, tunnelling current: 2pA.

Experiment was carried out in a multi-chamber ultra-high vacuum (UHV) system equipped with a commercial Omicron varied temperature scanning probe microscope (VT STM/AFM). In the microscope chamber base pressure was lower than 2×10^{-11} mbar. A preparation chamber was equipped with a noble gas ion gun, effusion cells, pyrometer and a MAXTEK thickness monitor. A polished $\text{TiO}_2(011)$ wafers (MaTeck GmbH) were mounted on the sample holder with a Si wafer as a resistive heater. The $\text{TiO}_2(011)$ surfaces were initially pre-annealed at 800K and thereafter prepared by repetitive cycles of Ar^+ sputtering and subsequent annealing at 920-960 K. The quality of the (2×1) surface reconstruction was controlled via STM measurements. The temperature of the TiO_2 sample was monitored by an infrared pyrometer. PTCDA molecules were deposited on the $\text{TiO}_2(011)-(2\times 1)$ surface kept at temperature stabilized in the range of 300-370 K (more

details on evaporation procedure may be found in [5]). Atomic-force images were obtained in the non-contact mode with frequency modulation. Commercially available silicon cantilevers with resonant frequencies in the range of 205-310 kHz were used as probes. In order to achieve better resolution tips were cleaned by 1keV argon ion

bombardment prior to measurements. STM images of empty-states were acquired in the constant current mode at positive sample bias voltages with electrochemically etched tungsten tips. Image processing and analysis was carried with use of WSxM software [6].

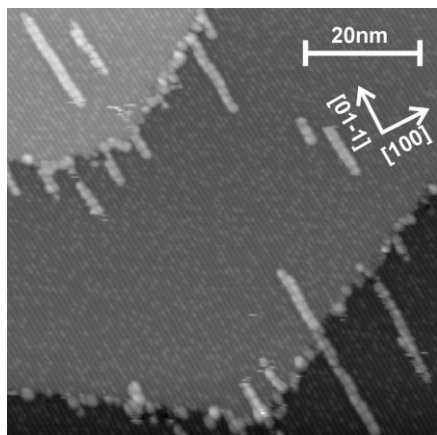


Figure 2: STM images of PTCDA adsorbed on rutile $\text{TiO}_2(011)$ at 373K when molecular chains formation is preferred. Image parameters: area $80\text{nm} \times 80\text{nm}$; sample bias 3.8 V, tunnelling current 1pA.

Firstly, clean substrate surfaces were STM scanned with the atomic resolution. In Figure 1 a high resolution STM image of a clean $\text{TiO}_2(011)-(2 \times 1)$ surface is shown. A bright zigzag pattern parallel to the $[01-1]$ crystallographic direction is clearly visible. Following the model proposed by Beck *et al.* [2] the zigzag pattern is ascribed to under-coordinated oxygen atoms with an exception, however, that the coordination of oxygen atoms within the zigzag pattern is left undetermined in contrast to the single coordination suggested in original model [2]. It is worth noticing, that theoretical model of the (011) face is still far from being well established and other proposition has been made to date (see for example [3]).

Secondly, adsorption of PTCDA molecules on the (011) face of rutile was extensively investigated with use of the STM technique. It was found that there exists a narrow window of substrate temperatures that favoured creation of molecular

chains (see Figure 2) [5]. Typically, molecules appeared as two bright lobes. However, it was observed that within a chain the brightness of the lobes altered. As a consequence of the interplay between the adsorbate-adsorbate and the adsorbate-substrate interactions, molecules assembled in chains were recorded in two contrasts: either two lobes were equally bright or one was brighter than the other. Albeit, lack of reliable theoretical model of the $\text{TiO}_2(011)-(2 \times 1)$ surface limits detailed analysis and interpretation of experimental results [5]. Moreover, during STM measurements a tip induced surface structure modification were commonly observed. I.e. molecules were removed from one chain and attached to the other [5]. This observation opens the possibility for a single molecule manipulation. An extended discussion on STM measurements of PTCDA molecules adsorbed on the (011) face of rutile may be found in [5].

Finally, PTCDA molecules adsorbed on the $\text{TiO}_2(011)-(2 \times 1)$ surface were imaged with use of the nc-AFM technique. For nc-AFM measurements only those samples for which STM scanning showed molecular chains on the surface were chosen. In Figure 3 molecules assembled in a form of wires along the $[01-1]$ crystallographic direction are clearly seen.

Images obtained during nc-AFM measurements appeared difficult not only in the acquisition but also in the interpretation. In proper analysis of acquired images a source of the observed contrast must be known. Molecules adsorbed on the surface appeared differently due to accidental tip termination changes during imaging in constant detuning mode. The tip apex alters even though the scanning parameters were kept constant. Therefore molecular chains may

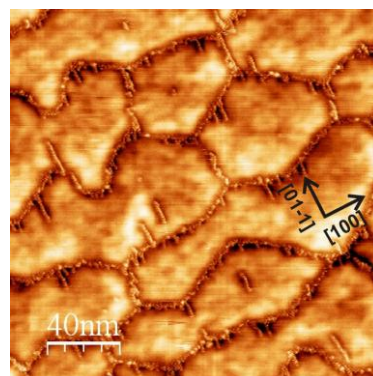


Figure 3: nc-AFM images of PTCDA adsorbed on rutile $\text{TiO}_2(011)$ at 373K when molecular chains formation is preferred.

be interpreted as protrusions or depressions in the very same image (see Figure 4). Possibly, the use of less reactive cantilevers, for example W_2C coated silicon cantilevers, could provide much stable nc-AFM imaging [3].

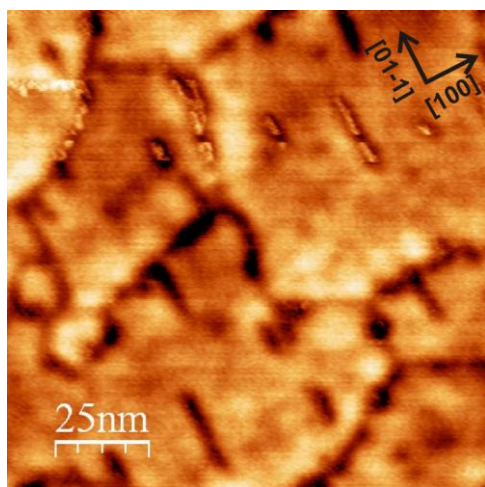


Figure 4: nc-AFM image: Tip termination influence on appearance of PTCDA adsorbed on rutile $TiO_2(011)$. Constant detuning mode; the scanning parameters are fixed for whole scanned area.

The resolution that could be achieved in the nc-AFM topography measurements depends not only on the tip termination. It relies also on the vibration amplitude and detuning value, Δf , that is set during the scanning. Figure 5 presents the same area that was scanned with different detuning applied. For both sets of parameters a molecular chain is clearly visible, however, its appearance is utterly different. For low detuning value, i.e. $\Delta f = 20\text{Hz}$, structure of the substrate surface cannot be resolved and the molecular chain emerges as a bright line without any sub-structure (see Figure 5a). Whereas, for larger detuning value, i.e. $\Delta f = 80\text{Hz}$, reconstruction rows of the substrate became visible, and what is more interesting, the sub-structure of the molecular chain may now be resolved to some extent. Molecules are seen as having a bright rim and a dark middle. Such a contrast inversion may suggest that oscillating tip at its

lower turning point was so close to the molecule that it entered into repulsive regime of tip-molecule interaction [7;8]. However, to further elucidate the source of observed contrast inversions additional experiments must be conducted.

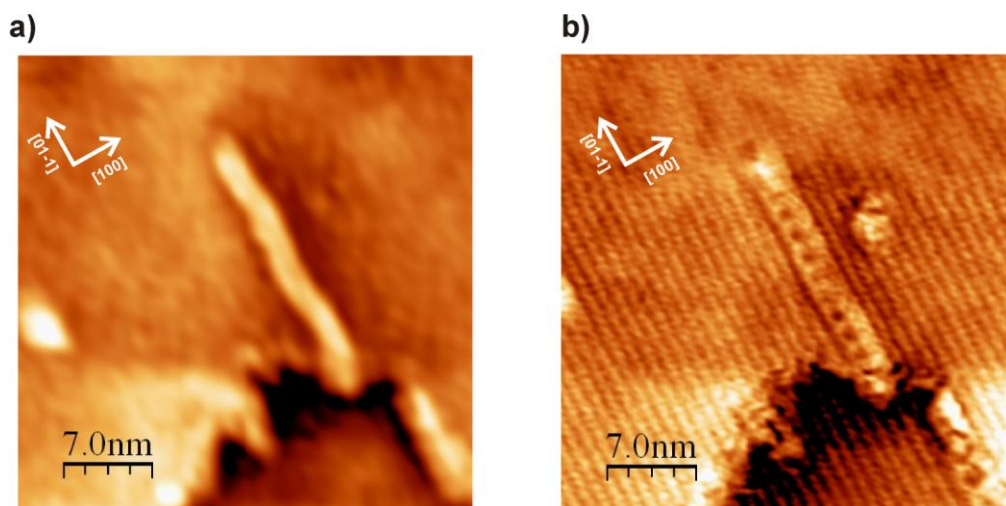


Figure 5: nc-AFM image of PTCDA adsorbed on rutile $TiO_2(011)$: Influence of detuning on the scan resolution. Vibration amplitude: 1.2nm. Detuning: a) $\Delta f=20\text{Hz}$, b) $\Delta f=80\text{Hz}$.

In both presented STM and nc-AFM measurements molecular chains of different length, from approx. 3.5 nm (two molecules) up to 40 nm (more than 20 molecules in a single chain) were seen. It is worth noticing, that a single molecule that has the length of 1.42 nm occupies a line segment of approx. 1.66 nm in length along the molecular chain. This value is close to the triple of the surface unit cell dimension of the $TiO_2(011)$ face along the oxygen rows, i.e. $3 \times 0.545\text{ nm} = 1.635\text{ nm}$. Such a coincidence suggests that the adsorbate-substrate registry can be commensurate. More extensive, however limited due to a lack of well established theoretical model of

the (011) surface of TiO_2 , discussion on the arrangement of molecules on the surface, not only within a chain, may be found in the forthcoming article [5].

Summarizing, the STM and the nc-AFM measurements of PTCDA molecules adsorbed on the $\text{TiO}_2(011)-(2 \times 1)$ surface were conducted. For a narrow substrate's temperature window molecular chains of length up to 40nm were created. During the STM imaging, tip induced surface structure modifications, including single molecule displacements, were observed. Measurements with the nc-AFM apparatus appeared far much difficult than the STM imaging. In nc-AFM scans a contrast inversion was frequently noted. The contrast that was detected depended not only on the uncontrolled tip termination changes, but also on the scanning parameters that has been chosen. Such observation suggests that the contrast inversion was partially an effect of tip reactivity and partially an effect of entering into repulsive regime of tip-molecule interaction. At the present stage no tip induced surface structure modifications during the nc-AFM scanning were observed. Thus the question on a single molecule manipulation with nc-AFM remains still open.

References

- [1] Dulub, O., et al. *Surf. Sci.* 2006, 600, 4407.
- [2] Beck, T. J., et al. *Phys. Rev. Lett.* 2004, 93, 036104.
- [3] Kubo, T., Orita, H. and Nozoye, H. *J. Am. Chem. Soc.* 2007, 129, 10474.
- [4] Diebold, U. *Surf. Sci. Rep.* (2003), 48, 53.
- [5] Tekiel, A., et al. *Submitted to Nanotechnology.*
- [6] Horcas, I., et al. *Rev. Sci. Instrum.* 2007, 78, 013705.
- [7] Kolodziej, J. J., et al. *Nanotechnology.* 2007, 18, 135302.
- [8] Rahe, P., et al. *Phys. Rev. B.* 2008, 77, 195410.

3d. Understanding the construction process (Image interpretation & adsorption theory)

- STM image cal.

Theory and numerical simulations for the Pico-Inside project

Xavier Bouju and Christian Joachim

*NanoSciences Group, CEMES-CNRS
29 rue Jeanne Marvig, B.P. 94347, F-31055 Toulouse Cedex 04, France*

The Pico-Inside project aims to develop the architecture, the atomic scale technology and the chemistry to explore and quantify intramolecular resources for integrating much more than a single logic gate inside a single molecule. To reach this goal, five units structure the network [1]. As molecules are the corner-stones, one unit is essentially dedicated to the design and the synthesis of large multi-functional molecules [2]. These molecules have to exhibit particular functionalisations not only to be able to produce a logic gate but also to be anchored on a surface. Another unit is thus focussing on theoretical aspects by looking for chemical groups able to transform an input information to an output signal. In other words, the involved partners want to theoretically demonstrate that intramolecular quantum evolution based on the non-stationary mixing of large molecule quantum states can perform digital operations. Two other units are dedicated to the interconnection technology at the atomic scale. In fact, a single molecule has to be deposited on a surface and connected to nano-electrodes in order to exchange information. The geometry adopted is planar and five degrees of interconnection are necessary to reach the macroscopic world starting from the single molecule level [3-6]. Experimental tools are low temperature UHV STM and UHV NC-AFM, providing information about elastic and inelastic intramolecular effects and about the adsorption of large organic molecules [7,8] on a surface together with the stability of metallic wires [3-5]. Specific moulding molecules will help in stabilising atomic metallic wire [4,9] in complement with atomic manipulation for creating those wires. A special attention will be focused on the metallurgy of nanoscopic mesa pads and on the mesoscale interconnect with the nano-stencil technique. All these experimental efforts are sustained by the Omicron compagny.

Finally, one unit explores the theoretical problem related to the adsorption of large molecules on perfect and hybrid (metal-insulator and metal-semiconductor) crystal surfaces such as their energetic on the surface including diffusion, stable adsorption sites, electronic and vibrational structures. Currently, this atomic scale technology requires a lot of modelisation. At the root of the Pico-Inside modelisation activity is the fact that we are going to deal with large molecules adsorbed on an insulating surface or at least on a large gap semi-conducting surface, where metallic electrodes will be in electronic interaction with a few chemical groups of those molecules. This requires a large effort in term of the understanding of the adsorption site and geometry of large conjugated molecules on semiconductors and insulators. A second topic concerns STM and NC-AFM image calculation, associated to simulations of molecular manipulations.

Theory of adsorption of large molecules on surfaces

Since the molecules targeted in Pico-Inside are quite large, mainly different molecular mechanics (MM) methods will be tested. The development of hybrid (embedding) electronic structure methods is undertaken, combining high quality quantum mechanical calculation of a finite part of the system (the cluster) with molecular mechanics calculations for the rest of the surface system. A. Shluger (UCL) and L. Kantorovich (KCL) follow other strategies as shown in [10] and [11]. In Toulouse, we are developing an embedding method based on a semi-empirical electronic structure technique and using the atom superposition and electron delocalization

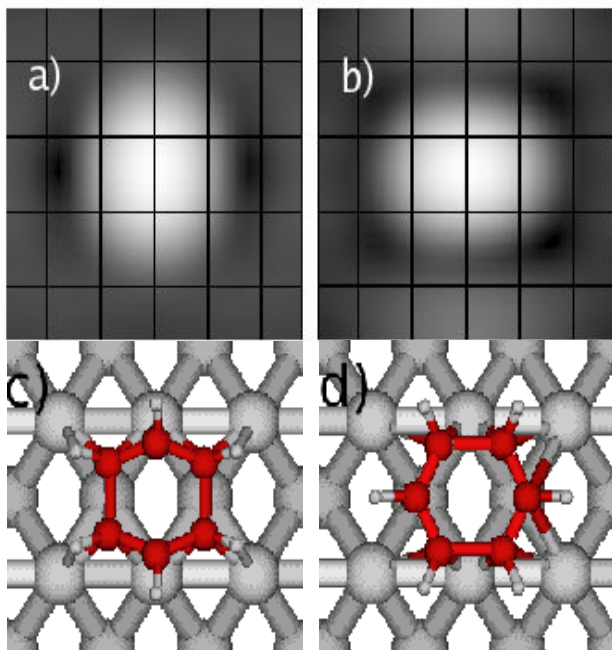


Figure 1: a) and b) STM images of a single benzene molecule adsorbed on Cu(110) calculated with the ESQC code. c) and d) Two different conformations obtained with ASED+ code and used for the simulated images. From [12].

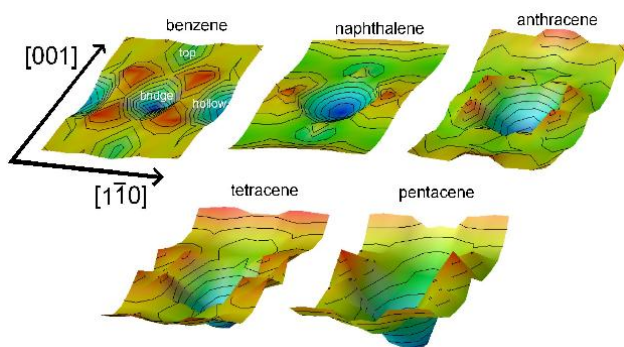


Figure 2: Minimal potential energy surface maps of five polyacene molecules adsorbed on Cu(110) calculated with the ASED+ code. The diffusion of polyacene molecule is more favorable in the [1-10] direction. From [12].

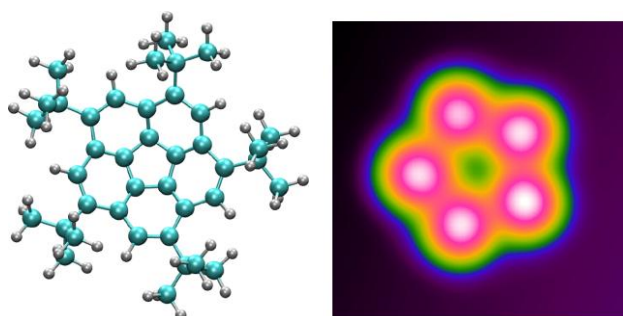


Figure 3: Ball-and-stick model of the a penta-tert-butyl corannulene molecule and the calculated ESQC-STM image of the molecule adsorbed on Cu(111) surface. From [14].

(ASED) scheme. At the initial code, a supplementary term has been added in order to take into account three-body interactions (ASED+) [12]. This new code can be seen as compromise between standard MM codes and DFT methods. In fact, MM codes using standard force-fields (MM4, UFF...) are fast and very well adapted for physisorbed systems and, of course, for intramolecular deformations. DFT calculations give a good description of the chemisorption but need huge computational costs for large molecules on a surface. On the other hand, ASED+ is faster than DFT and only few parameters (Slater exponents and ionization potentials) are necessary. As a benchmark, the case of a benzene molecule chemisorbed on Cu(110) has been studied (Figure 1). Very good agreements have been found with experimental and DFT results [12]. As an important concern in Pico-Inside is the structure and mobility of large molecules on crystal surface, it is important to use an efficient and reliable technique. Figure 2 shows a series of calculations with ASED+ of polyacenes on Cu(110) starting from benzene to pentacene. The key point is that these molecules can diffuse more easily along the [1-10], as experimentally observed [13]. Due to a large size of the molecules involved, there will be a number of stable adsorption sites and orientations of the molecules. We shall study their diffusion between these conformations, that is important for understanding molecules stability and mobility at various temperatures. These calculations are not trivial since translational and rotational degrees of freedom of any molecules during their diffusion are combined and will often be accompanied by bond breaking and bond forming events.

STM and AFM image calculations

Once the adsorption site and molecular conformation of the adsorbate is found, theoretical interpretation of experimentally acquired STM and NC-AFM images of adsorbed molecules has to be tackled. For ten years, the EHMO-ESQC method (extended Hückel molecular orbital – elastic scattering quantum chemistry) has demonstrated its efficiency to interpret experimental STM images with a very good degree of confidence. At least, some fifty papers have already been published where ESQC was used with various adsorbates (atoms, small and large molecules) on metallic (Figure 3) [14] and semiconducting (Figure 4) [15] substrates, and on thin insulating films as well (Figure 5) [16]. Actually, there are different ways to simulate a STM image, ranging from the simple Tersoff-Hamann model (especially for bare surface) to non-equilibrium Green's functions density functional theory for modeling the electrical properties of molecular systems. According to the size of the simulated systems that most people are dealing with (typically several hundreds of atoms), the ESQC method seems to be reliable with a reasonable computer time consuming. Now, efforts have to be focused to an improvement of ESQC code to speed up more the computation time. By reducing the image computation time, it may become possible to perform the optimisation between experimental and numerical results leaving the computer to follow the convergence automatically. A parallel version of ESQC is already running and is the main tool for simulated image production right now.

NC-AFM is not only able to obtain accurate images of various substrates, it is also efficient to get dissipation information of adsorbates. This dissipation signal indicates what are the efficient channels of a molecule. Such an identification of molecular soft phonons could be used to induce mechanical functions. With the help of a virtual NC-AFM, imaging and dissipation signals can be calculated once a specific force-field mesh is introduced as a data set.

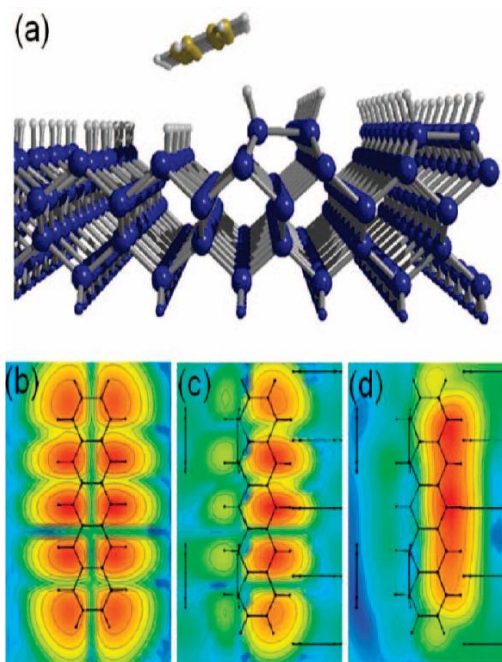


Figure 4: a) Calculated adsorption structure of pentacene molecule over a step edge of a passivated Si(100):H surface. (b-d) ESQC calculated constant current STM image of pentacene at the -1.7 eV HOMO tunnel resonance on (b) terrace, (c) at step, and (d) 1 eV up from the bottom of the Si conduction band on a step relative to the Fermi level. The structure in black lines corresponds to a pentacene skeleton and the hydrogenated Si dimers. From [15].

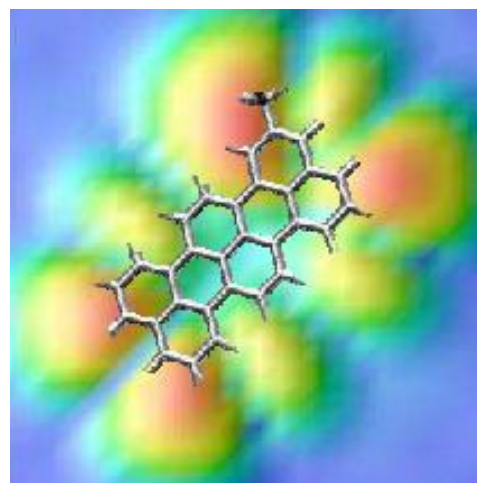


Figure 5: ESQC-STM image calculation of a single methylterrylene molecule adsorbed on two monolayers of NaCl(100) deposited on Cu(111) surface. The thin insulating film allows the decoupling of the electronic structure of the molecule from the metallic substrate. The structure of molecular orbitals can then be well resolved. From [16].

The improvement of our numerical code will consist in the introduction of the different noises of the experimental setup.

STM or NC-AFM manipulations of single adsorbates is an important topic in Pico-Inside. A virtual STM already exists [17] allowing the direct comparison between experimental manipulation signatures and theoretical ones. The precise mechanical behaviour can then be identified. The use of this numerical code will be applied for the manipulation of large molecules.

Acknowledgements

We would like to thank our collaborators (Stéphane Ami, Francesco Ample, Ivan Duchemin, Mohamed Hliwa, Sladjana Stojković, Carlos Villagómez Ojeda) of the NanoSciences group in Toulouse with whom we are sharing the work to address these theoretical and simulations topics. We also want to acknowledge our partners of Fujitsu compagnie (Pierre Lagier, Jean Latour) for the active collaboration in Pico-Inside.

References

- [1] C. Joachim, E-nano newsletter 2, 12-20 (2005).
- [2] A. Gourdon, E-nano newsletter 4, 22-24 (2006).
- [3] A. Socoliuc, O. Pfeiffer, S. Maier, L. Zimmerli, E. Gnecco, E. Meyer, L. Nony and R. Bennewitz, E-nano newsletter 3, 22-24 (2006).
- [4] T. R. Linderoth and F. Besenbacher, E-nano newsletter 3, 25-26 (2006).
- [5] M. Goryl, F. Krok, J. J. Kolodziej, P. Piatkowski and M. Szymonski, E-nano newsletter 3, 26 (2006).
- [6] D. Martrou, H. Guo, T. Zambelli, L. Guiraud, S. Gauthier and C. Joachim, E-nano newsletter 3, 27-30 (2006).
- [7] A. M. Echavarren, E-nano newsletter 4, 25-26 (2006).
- [8] I. G. Stará and I. Starý, E-nano newsletter 4, 27-29 (2006).
- [9] A. Gourdon, E-nano newsletter 4, 29-30 (2006).
- [10] T. Trevethan, M. Watkins, M.L. Sushko and A.L. Shluger, E-nano newsletter 5, 29-30 (2006).
- [11] L. Kantorovich, E-nano newsletter 5, 27-28 (2006).
- [12] F. Ample and C. Joachim, Surface Science. 600, 3243-3251 (2006); F. Ample, C. Joachim, Surface Science. 602, 1563-1571 (2008).
- [13] S. Lukas, G. Witte and Ch. Wöll, Phys. Rev. Lett. 88, 028301 (2002).
- [14] O. Guillermet, E. Niemi, S. Nagarajan, X. Bouju, D. Martrou, A. Gourdon and S. Gauthier, Angewandte Chemie, in press (2009).
- [15] A. Bellec, F. Ample, D. Riedel, G. Dujardin and C. Joachim, Nano Letters 9, 144-147 (2009).
- [16] C. J. Villagomez, T. Zambelli, S. Gauthier, A. Gourdon, C. Barthes, S. Stojkovic and C. Joachim, Chemical Physics Letters 450, 107-111 (2007).
- [17] X. Bouju, C. Joachim, Ch. Girard and H. Tang, Phys. Rev. B 63, 085415 (2001).

3d. Understanding the construction process (Image interpretation & adsorption theory)

- STM image + adsorption

Imaging and manipulation of molecules on reactive surfaces

L. Kantorovich

King's College London, Physics, The Strand, WC2R 2LS, London, UK.

STM imaging and manipulation of molecules adsorbed on crystal surfaces is an essential part of the Pico-Inside project. However, before the molecule is adsorbed or deposited on the surface, it is essential to make sure that the surface is "ready" for it, i.e. it is clean from defects, is of expected structure and possesses the necessary insulating properties. STM and AFM methods may be extremely useful in "looking" at surfaces prepared using a given method to assess their quality prior to deposition.

This point is illustrated here on an example of the hydrogenated Si(001) surface, studied using STM and *ab initio* DFT calculations by Orsay and KCL partners [1]. Depending on the supply of hydrogen atoms and temperature this surface may undergo a number of reconstructions; in addition, one may also see a co-existence of several domains and clusters of different reconstructions on the same terrace; see Figure 1.

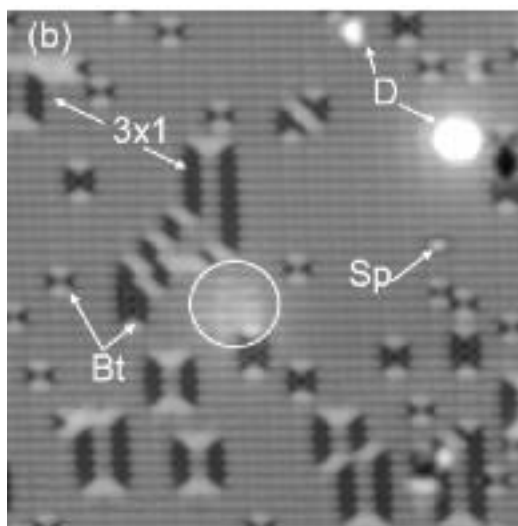


Figure 1: Positive bias (unoccupied states) STM image of a *p*-doped Si(001)-2x1:H surface. One can see different structures (marked) corresponding to various "defects" Bt, Sp and D, as well as domains of 3x1 reconstruction.

In this study we concentrated on "bow-tie" structures, denoted Bt, which extend over up to six Si dimers and are distinguished by a characteristic "signature" in the image: they appear as black features with dark dots inside. Note that in the negative bias STM image it is impossible to distinguish between different features on the surface, however, these show up in unoccupied states images. Since it was seen on images (the structure above the circle) that Bt feature can be connected with 3x1 reconstruction (two parallel black lines), it was suggested that Bt defects correspond to dihydride dimers, i.e. structures in which two hydrogen atoms are attached to each Si atom along a single dimer row. This hypothesis has been confirmed by the DFT calculations. Firstly, it was found that dihydride dimers are stable. Moreover, it was found that they can indeed extend over several Si dimers along the same row: the relative free energy goes

down if an extra hydrogen molecule (needed to create a single dihydride from a monohydride already existing on the Si(001)-2x1:H surface) is attached next to the existing dihydride along the same row. Secondly, STM images were simulated using the surface local DOS, which demonstrated most of the features observed in experimental images: (i) in the negative (occupied states) bias the defect appears simply as a 'blurred' feature; (ii) in the positive (unoccupied states) bias we have some brightening at the edges of the feature along the row and a dark spot in the middle which is positioned between Si dimers. This study provided an alternative characterisation of the Bt feature on this surface; the one existed before in literature attributed it to dopants.

Another important (and relevant for Pico-Inside) application of the AFM and STM methods is concerned with manipulation of molecules on surfaces. The problem here

is that it is not easy to manipulate large molecules with the tip without destroying them, especially, if molecules are strongly bound to crystal surfaces, so that special techniques are to be applied to do that.

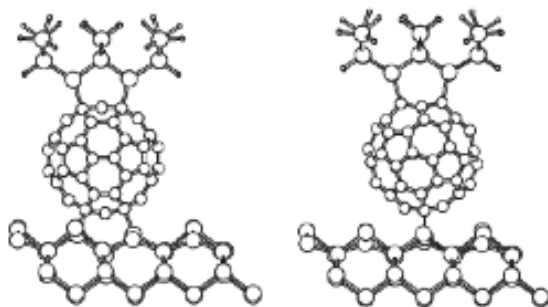


Figure 2: STM tip attached to the C_{60} molecule either at a stable site (left panel) or in the pivoting state (right panel).

We illustrate this point on our recent theoretical simulations of the manipulation of a C_{60} molecule on the Si(001) surface. In a stable adsorption configuration the molecule is strongly bound to the surface forming four C-Si chemical bonds. Our *ab initio* calculations based on the density functional theory show that the vertical manipulation of this molecule with STM tip is only possible if the C_{60} is first manipulated laterally towards the pivoting point when the interaction

with the surface is minimised, see Figure 2, i.e. the molecule forms only two C-Si bonds. Then, provided the STM tip can establish chemical interaction with the molecule, it can be lifted as a whole. The deposition can be done in the reverse order. Manipulation with AFM tip is ought to be based on a different mechanism since the AFM tip oscillates above the surface and hence cannot maintain a continuous contact with the molecule [3]. The molecule is also manipulated via the same pivoting state; however, in this case the role of the AFM tip is in reducing the barrier for the molecule to roll over the pivoting state thermally: when the tip is far away from the molecule, the energy barrier connecting two stable adsorption sites is too large for the molecule to roll by itself from one to another. However, when an oscillating tip comes close enough to the molecule, the barrier is reduced sufficiently to allow for the molecule to overcome it and roll to the other stable configuration, corresponding to its translation by a single lattice constant. The molecule remains the whole during this process since its manipulation basically corresponds to self-diffusion helped by the oscillating tip. In summary, we have shown the importance of using scanning probe techniques in assessing quality of semiconducting surfaces prior to molecules deposition and then for their manipulation. We find that manipulation based on reducing the molecule-surface interaction may provide a safe route for translating large molecule on surfaces to which they are strongly bound. This finding may assist us in finding ways of placing large molecules on crystal surfaces to which they will eventually get stuck.

References

- [1] A. Bellec, D. Riedel, G. Dujardin, N. Rompotis and L. Kantorovich, "Dihydride dimer structures on the Si(100):H surface studied by low-temperature scanning tunnelling microscopy. – Phys. Rev. B (2008), accepted.
- [2] N. Martsinovich and L. Kantorovich, "Vertical manipulation of a molecule with chemical forces". – Phys. Rev. B77, #205412 (2008).
- [3] N. Martsinovich and L. Kantorovich, "Manipulation of C_{60} with NC-AFM". – Phys. Rev. B (2008), submitted.

3d. Understanding the construction process (Image interpretation & adsorption theory)

- AFM image cal.

Virtual Atomic Force Microscopy for modelling NC-AFM imaging on insulators

T. Trevethan, L. N. Kantorovich and A. L. Shluger

*London Centre for Nanotechnology, University College London, Gower Street,
London WC1E 6BT, UK*

King's College London, Physics, The Strand, WC2R 2LS, London, UK

The interpretation of atomic resolution non-contact atomic force microscopy experiments is a difficult and challenging task, due to both the complexity of the imaging mechanism and the unknown nature of the tip-apex structure. Therefore it is often necessary to employ modelling in order to better understand the results produced by experiments [1]. The modelling of a NC-AFM experiment typically involves calculating a force-field, for a particular tip and a particular surface/adsorbate structure, from atomistic simulations. The force-field, which gives the vertical force on the tip as a function of tip position in three-dimensions above the surface, can then be used to calculate the frequency-shift (also as a function of tip position) from the cantilever parameters and the amplitude, by integrating over the tip trajectory [2]. This in turn can then be used to create either a constant height image of frequency, or a topography image at a given frequency shift set-point. This procedure however involves several important simplifying assumptions: that the NC-AFM instrumentation controlling the cantilever oscillations and the surface position act ideally, i.e. that the tip follows a sinusoidal trajectory, and that the lateral scanning speed is slow enough that any finite response of the amplitude or frequency feed-back loops can be neglected; in other words, it is assumed that the instrumentation reacts instantaneously during the scan on the constantly undulating surface. In addition, it is assumed that the tip-experiences a conservative force-field due to its interaction with the surface, and that no atomic scale structural changes occur during the entire imaging process. In many cases these assumptions are well accepted, however often they do not hold, for example when scanning is fast, when diffusion occurs on the surface or when a manipulation procedure is performed.

The NC-AFM experimental instrumentation controls the amplitude of the cantilever oscillations and the position of the surface with two feed-back loops: the Automatic Gain Control (AGC) and the Automatic Distance Control (ADC) respectively. These loops are implemented using a complex set-up of electronics, incorporating a digital Phase Locked Loop as a frequency demodulator, and a laser diode detection system to measure the deflection of the cantilever. The instrument outputs three signals which can be used for generating images: the sample height (topography), the frequency shift (detuning) and the excitation signal (dissipation).

To model the complex behaviour of the instrument and the imaging process, a Virtual Atomic Force Microscope (VAFM) can be employed, which consists of an explicit numerical simulation of the entire experiment in real time. A VAFM performs a numerical integration of the trajectory of the cantilever, the control electronics and the driving signal with a fixed time-step, which is small compared with the motion of the tip. The tip moves in the force-field above the surface as the tip is oscillated and the surface is scanned. The scanning of the surface takes place continuously and the oscillating tip follows a lateral path collecting line scans in order to produce an image, in real time. Several implementations of fast VAFMs have been realised, one written in Fortran [3] and one in C [4].

Virtual experiments have been performed to test their reliability and to compare it with the real setup. In these tests the interaction between tip and surface is modelled as the sum of Van der Waals long-range contribution and a short-range Morse potential.

Simulated scan lines along a sinusoidally corrugated surface and across a monatomic step have been compared with the assumed profile (see Figure 1). The computed “damping” and topography variations systematically change with the time constants of the controllers and the scan speed. The influence of various adjustments was studied: Working off phase, working with small and large oscillation amplitudes and in the presence of noise. The detailed analysis of these experiments allows one to determine optimum adjustments of the individual electronic blocks and their joint performance in real experiments.

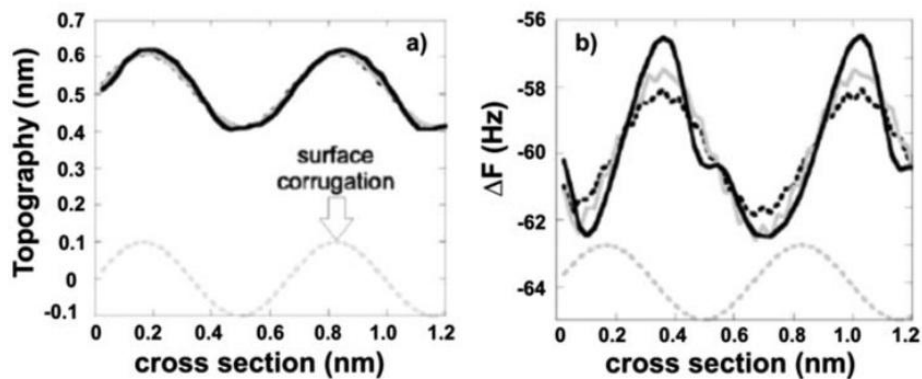


Figure 1: Calculated cross section of a sinusoidally corrugated surface for various PLL gains a) Topography, b) Frequency shift.

By performing a complete real-time simulation of the instrument, the force-field experienced by the tip can be altered to reflect a structural change in the surface during the imaging process. The simulation including the trajectory of the tip, all the control mechanisms and the output signals, will react in a completely realistic way as the experiment progresses.

To simulate the dynamical evolution of a surface process that results in a structural change during imaging, a kinetic Monte Carlo simulation is run simultaneously with the VAFM calculation [5], with the potential energy barriers for the process changing in real time as the tip moves and the surface is imaged. This means the position and motion of the tip alters the dynamics of the surface processes. When a microscopic transition occurs the force-field will switch instantaneously to the corresponding new microscopic structure. In this way both the microscopic and macroscopic parts of the system evolve in-step and self-consistently.

This method has been applied to model two realistic but qualitatively different systems: the manipulation and diffusion of a Pd adatom on the MgO (001) surface [6] and the thermally induced structural change of an H₂O molecule on the CeO₂ (111) surface [7]. In the first system, which consists of a metal adatom weakly bound to an ionic surface, we model how the atom can be manipulated at close approach and also the image contrast when the atom is freely diffusing across the surface. In the second system, we image the fast structural changes of a small molecule that is strongly bound and immobile on the surface but free to move between three equivalent states. Figure 2 shows a topography image of a Pd atom adsorbed on the MgO (001) surface, both with the Pd atom in a fixed position and with the Pd atom being manipulated upwards as the scan progresses (at a larger frequency shift). The instantaneous sample height and frequency shift (detuning) are also shown: the VAFM can predict the signals that are associated with manipulation events and other dynamical processes.

This approach can also be used to predict optimum protocols for manipulating adsorbed species on surfaces using only the force exerted by an AFM tip apex on the adsorbate. These may guide experimental efforts in achieving control over and adsorbed species: for example, calculations indicate that manipulation protocols based

on scanning provide only limited degree of control that strongly depends on the scanning direction. Choosing the manipulation trajectory and 'hitting' the right spot allows a much higher degree of control over the manipulated atom.

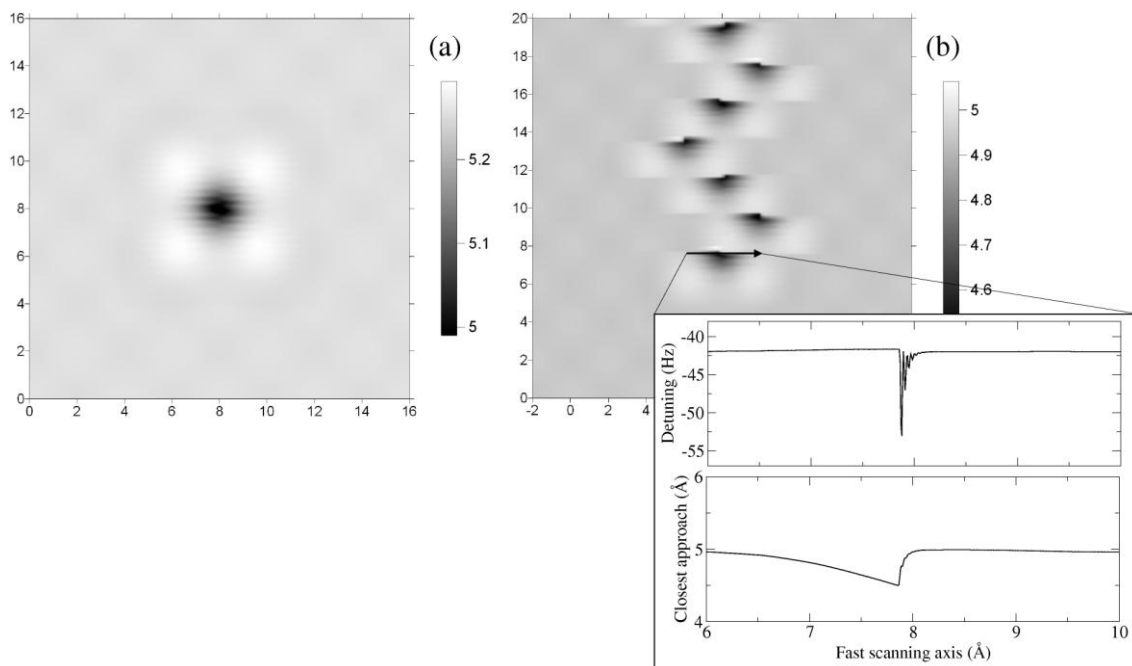


Figure 2: (a) Constant frequency shift ($\Delta f_0 = -38$ Hz) topography image of the Pd atom at the centre of a 16×16 Å area of the MgO (001) surface at 10 K. (b) Constant frequency shift ($\Delta f_0 = -42$ Hz) topography image of the Pd atom on a 20×20 Å area of the MgO (001) at 10 K. The frequency detuning along the fast scan line indicated and the corresponding distance of closest approach (topography) are shown as an insert.

The model that has been developed captures both the dynamical evolution of processes occurring in the tip-surface junction as well as the real-time response of the NC-AFM instrument, which represents an extension to the traditional method of modelling NC-AFM images in the conservative regime. This approach provides a reliable 'window' into atomic scale processes during imaging and manipulation, and combined with experimental data may give an important insight into atomic scale surface processes. Experiments exploiting this will significantly broaden the scope of application of the NC-AFM from analysing static structures to retrieving information about dynamical processes.

References

- [1] W. A. Hofer, A. S. Foster and A. L. Shluger, *Rev. Mod. Phys.* 75, 1287 (2003).
- [2] F. J. Giessibl, *Rev. Mod. Phys.* 75, 957 (2003).
- [3] J. Polesel-Maris and S. Gauthier, *J. Appl. Phys.* 97, 1 (2005).
- [4] G. Couturier, R. Boisgard, L. Nony and J. P. Aime, *Rev. Sci. Instruments* 74, 2726 (2003).
- [5] L. Kantorovich, *Phys. Rev. B* 75, 064305 (2007).
- [6] T. Trevethan, L. N. Kantorovich, J. Polesel-Maris, S. Gauthier and A. L. Shluger, *Phys. Rev. B* 76, 085414 (2007).
- [7] M. Watkins, T. Trevethan, A. L. Shluger and L. N. Kantorovich, *Phys. Rev. B* 76, 245421 (2007).

3d. Understanding the construction process (Image interpretation & adsorption theory)

- Adsorption on insulators

Theory of the adsorption of organic molecules on insulating surfaces

T. Trevethan, M. Watkins, M. L. Sushko and A. L. Shluger

*London Centre for Nanotechnology
University College London, Gower Street, London WC1E 6BT, UK*

There has been significant progress in recent years in the deposition, and then the subsequent imaging with non-contact Atomic Force Microscopy (NC-AFM), of a variety of organic molecules on insulating substrates. The control and utilisation of individual adsorbed molecules could have profound technological implications, specifically in the area of molecular electronics - which promises to dramatically increase the power and decrease the size of information technology.

One of the architectures proposed is that of an isolated molecule adsorbed on an insulating surface and connected to atomic scale electrodes, which can then exchange information with the molecule. In order to achieve this it is essential to understand in detail the interaction of the molecule with the surface. Specifically it is important to know how the molecule will bind and diffuse on the surface and how the interaction with the surface will modify its electronic structure. It will also be important to understand mechanisms of controlled manipulation with a scanning probe microscope tip, since it may be required to move the molecule into a specific position in order to connect it to the electrodes.

To help achieve this goal, the adsorption, diffusion and manipulation of organic molecules on the MgO (001), TiO₂(011) and KBr (001) are being investigated. These surfaces are extremely good candidates for a potential substrate, since they are well characterised and studied and are good insulators.

1. Ab-initio calculations

To accurately model both the molecule, the surface and their interaction it is essential to perform high quality electronic structure calculations. To study the adsorption of an isolated molecule, which is a non-periodic system, we employ an embedded cluster code called Gaussian Used for Embedded System Studies (GUESS) [1]. In this method the molecule and a small region of the surface directly below it (the quantum region) are treated from first principles using all-electron localised basis sets and the B3LYP hybrid functional, and are free to move. This cluster is then surrounded by a region of classical polarisable ions treated using the shell model [2], that are also free to move. Finally, this system is embedded in a large array of fixed point charges (see Figure 1).

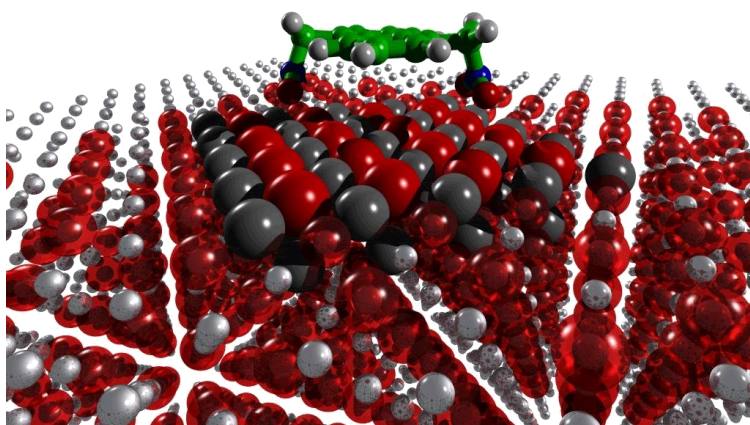


Figure 1: Illustration of the system configuration in an embedded cluster calculation.

This set-up allows us to treat the molecule and its interaction with the surface to a high level of accuracy and detail, while also having a realistic representation of the electrostatic field generated by the surface over a large area. In a typical calculation, a single organic molecule (such as that shown in Figure 1) is positioned on the surface and then the total energy of the system is minimised with respect to the coordinates of all free atoms. Quantities such as adsorption energies and equilibrium configurations as well as important information about the electronic structure, such as molecular orbital levels, electronic polarisation and charge transfer, can then be determined.

Extensive calculations have been performed using this method, studying the adsorption of various organic molecules (which consist of aromatic systems with various chemical groups) on the MgO (001), TiO₂(110) and KBr (001) surfaces. It has been found that there is virtually no transfer of charge between the molecule and the surface in each case and that the electronic structure of the adsorbed molecule is relatively unperturbed from that in isolation. The interaction is therefore purely electrostatic and non-polar molecular groups such as benzene and methyl groups have very little binding to the surface [3]. As a result of this, part of our efforts have been to investigate chemical groups and their configurations, that will bind strongly to the surface and prevent diffusion of the molecule.

2. Generating inter-atomic force-fields

The embedded cluster method makes it possible to accurately model the electronic structure of the molecule and the surface; however these calculations are very computationally expensive and are therefore limited to geometry optimisations on small molecules. To study in detail the dynamics, diffusion and manipulation of larger molecules a classical force-field must be used to describe the inter-atomic interactions. Reliable force-fields exist for the isolated surface and the isolated molecule; however there are no reliable force-fields to describe the interaction of the molecule with the surface.

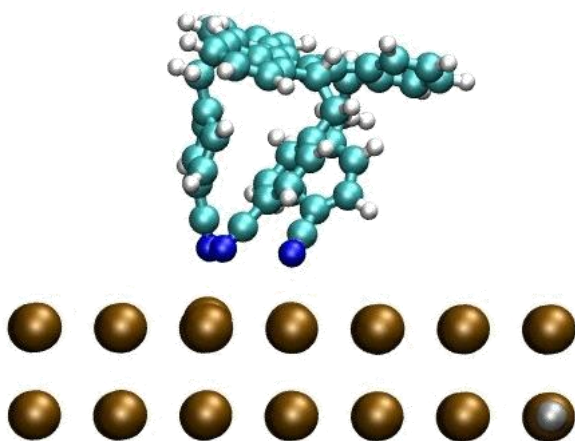


Figure 2: Functionalised truxene molecule adsorbed on the KBr (001) surface.

is treated as a collection of 'fragments' which consist of benzene groups, methyl groups and other chemical groups such as carboxylic acid and cyano groups. The pair potentials for the atoms in each 'fragment' will have been derived from separate extensive ab-initio modelling.

This approach has been used to develop potentials for organic molecules interacting with the TiO₂(110) and KBr (001) surfaces, where it has been demonstrated that they

To address this problem a systematic approach has been developed to deriving force-fields for the surface-molecule interaction from realistic ab-initio calculations that can be potentially used to model any organic molecule on a given surface [4]. The molecule is described with an intramolecular force-field (e.g. AMBER) and the surface with a separate appropriate force-field. Each atom in the molecule then interacts with each atom in the surface via pair-potentials which have been parameterised depending on which type of chemical group the atom in the molecule belongs to. Here, the organic molecule

reproduce adsorption energies and configurations to a high degree of accuracy. Figure 2 shows a minimum energy configuration of a truxene molecule, functionalised with benzonitrile groups, adsorbed on the KBr (001) surface.

3. Modeling Diffusion

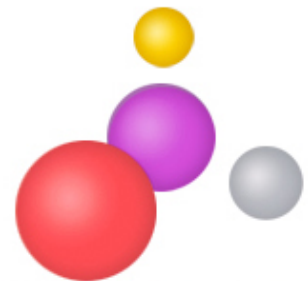
With a reliable force-field for the interaction of the molecule with the surface, it is possible to study a wide range of processes, such as the diffusion of large molecules, in detail with relatively low computational expense. The diffusive motion of a class of large organic molecules on the $\text{TiO}_2(110)$ surface was simulated using a combination of atomistic modelling and kinetic Monte Carlo calculations [5]. These molecules consist of polycyclic aromatic 'backbones' with four attached carboxylic acid based groups. The $\text{TiO}_2(110)$ surface structure is highly anisotropic: there are rows of Ti atoms and bridging O atoms along the $\langle 001 \rangle$ direction. Carboxylic acid groups bind to the surface in a bidentate configuration, with the two O atoms of the acid group bonding to two adjacent surface Ti atoms along the Ti rows. At room temperature, diffusion of this group along the rows can occur, but the barrier for diffusion across the bridging oxygen rows is insurmountable, leading to 1-D diffusive motion. As is the case with most oxide surfaces, the interaction of non-polar hydrocarbon molecules is very weak, and therefore polar molecular groups are often necessary to bind a molecule to the surface.

The diffusive motion of a molecule on a surface consists of transitions between many different minima on the complex potential energy surface of the surface-molecule system. For each of the molecules investigated, these accessible states and the energy barriers that separate them are determined, and then the resultant finite temperature dynamical behaviour of the molecule is evaluated with the kinetic Monte Carlo method [6]. With these simulations it is shown how the structure of the molecule is critical to its diffusive motion, and how making small adjustments to the molecular structure can have a dramatic effect on the overall behaviour of the system. Based on the results of these calculations it is possible to suggest general ways in which molecular structures can be designed to either maximise or minimise the mobility of the molecule on a surface. For the type of molecules considered in this study this can be achieved by changing the freedom of the binding groups and also the commensurability with the surface: increasing the flexibility of the binding groups increases the rate of diffusion, increasing the commensurability decreases the rate of diffusion.

References

- [1] P.V. Sushko, A.L. Shluger and C.R. Catlow *Surface Science* 450 (2000) 153-170
- [2] B. G. Dick and A. W. Overhauser *Phys. Rev.* 112 (1958) 90–103
- [3] T. Trevethan and A. L. Shluger *J. Phys. Chem. C* 111 (2007) 15375-15381
- [4] M.L. Sushko, A.Y. Gal and A.L. Shluger *J. Phys. Chem. B* 110 (2006) 4853-4862
- [5] L. N. Kantorovich *Phys. Rev. B* 75(2007) 064305
- [6] T. Trevethan and A. L. Shluger *J. Phys. Chem. C* (2008) (accepted)

4. Planar multiple interconnect Atom Technology



4a. Introduction

Introduction

Christian Joachim

*NanoSciences Group, CEMES-CNRS
29 rue Jeanne Marvig, B.P. 94347, F-31055 Toulouse Cedex 04, France*

Single molecule mechanics [1], mono-molecular electronics [2] and in general multi-probes experiments on atomic scale constructed devices [3] or machineries [4] are requiring a specific planar interconnection technology with a surface atomic precision and ultra cleanness [5]. This surface technology must be able to provide information and energy access channels to the atomic (or molecular) scale machinery constructed or fabricated on the surface (see Figure 1). At the end of the 80's, e-beam lithography was expected to provide such a technology [6]. But with its resist based approach (grown, deposited or contamination), e-beam lithography will not be able to make it [7]. It cannot respect at the same time the atomic scale precision, the cleanness and the expected large number N of access channels to the atomic scale or molecule machinery [8]. Alternative new surface lithography techniques such as nano-imprint [9] or nano-stencil [10] are neither adapted to encompass all the interconnection stages from the macroscopic to the atomic scale nor clean enough down to the atomic scale. At the turn of the century, this problem associated with new targets in atomic scale machineries like molecule logic gate [11], molecule-motor [1] and surface atomic scale electronic circuits [12] triggers a new approach starting at the bottom.

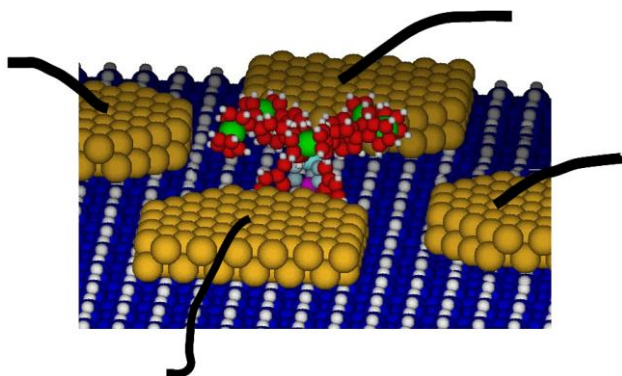


Figure 1: *A single molecule-motor [1] positioned between 4 Au nano pads constructed on the Si(100)-H surface. The motor is driven by the tunnelling electrons sequentially transferred through the motor wings. The 4 black wires getting out of the surface are indicative of the interconnections strategy to be developed.*

An atomic scale precision multiple access interconnection machine must provide N conducting wires converging toward a very small surface area where an active machinery has been constructed or assembled with an atomic scale precision. Those N interconnects are positioned somewhere on a large handle able wafer surface. As a consequence, a very efficient navigation system must be designed to locate this very small active area from a macroscopic starting point while keeping the local atomic precision of the interconnection construction. In this case, one needs to combine two type of microscope: a far field one (optical, scanning electron

microscope (SEM)) for large scale navigation and a near field one (Scanning Tunneling Microscope (STM), Atomic Force Microscope (AFM)) for the atomic scale part with a compulsory overlay between those 2 types of microscopy.

In air, the combination of an optical microscope with a standard AFM to interconnect a single wall carbon nanotube on e-beam lithography metallic nano-electrodes has already shown the power of this two-microscopes combination associated with a dedicated way to electrically contact the nano-pads [14]. Those contacts were taken by introducing under the AFM head a comb of metallic micro cantilever electrodes to minimize the overall length of the electrical circuit fabricated on the wafer surface [14]. While not atomic scale, this proof of concept demonstrates all the ingredients that are at the basis of the next generation UHV and atomic scale interconnection machine as schematically presented in Figure 2.

An UHV atomic scale interconnection machine is designed to follow a dedicated interconnection sequence. On an atomically clean well-prepared surface, an atomic scale circuitry is fabricated (A). To reach a large number N of interconnects and to be able to interconnect each atomic wire to the external world, there is a necessary lateral extension of this circuit to reach N contacting metallic nanopads (B) that are positioned around the atomic scale circuit. In the example of Figure 2, a molecule is connected to these nanopads by atomic metallic wires. Depending on the electronic surface gap of the supporting material, the nanopads (B) have to be contacted from the top by a series of N atomically sharp metallic tips (C1) or by a series of N nano-scale wires (C2) up to the point where mesoscopic metallic wiring or microelectrodes (D) can be surface fabricated and contacted by a series of N micro-scale metallic cantilever (E) also from the top of the wafer. During the process, the sequence of those different steps depends on the machine and on the supporting material. What is triggering the choice of the interconnection technology between C1 and C2 (and after the need for the D and E interconnection steps in Figure 2a) is the electronic gap of the surface that in turn will determine the kind of far field microscopy to be used for navigation over the wafer surface.

For a large valence-conduction band electronic surface gap (more than a few eV up to 12 eV for standard insulators), SEM is difficult to use because the electron beam will charge the surface. In this case, an optical microscope must be used. This microscope determines the minimum length of metallic surface wiring which must be fabricated starting from the nano-pads (B) in Figure 2a toward the next contact stage based on metallic micro-cantilever (Figure 2a). Fortunately enough, with a large surface gap, the surface area of those interconnects can be expanded laterally without too much lateral leakage current between the different electrodes. This is the basic of the UHV interconnection machine described in section 3 where a low temperature approach is not compulsory but preferable.

For a moderated valence band-conduction band electronic surface gap (around a few eV), it is not possible to use very long surface metallic circuitry due to the possible lateral surface leakage current between the surface electrodes. In this case, one solution is to use ultra sharp STM like tips positioned from the top on the surface (Figure 2b). In this case, the core of the tips will not be in contact with the supporting surface and one can go continuously from a tip apex radius of curvature of a few nanometer up to a 100 microns or more section for the tip body. In this case, navigation on the surface can be performed using an UHV-SEM (Figure 2b) by grounding the sample during the SEM imaging to avoid the surface charging effect. This is the basic of the UHV interconnection machine described in section 4. Here, a low temperature approach is compulsory because of the low electronic gap at the surface of the supporting material.

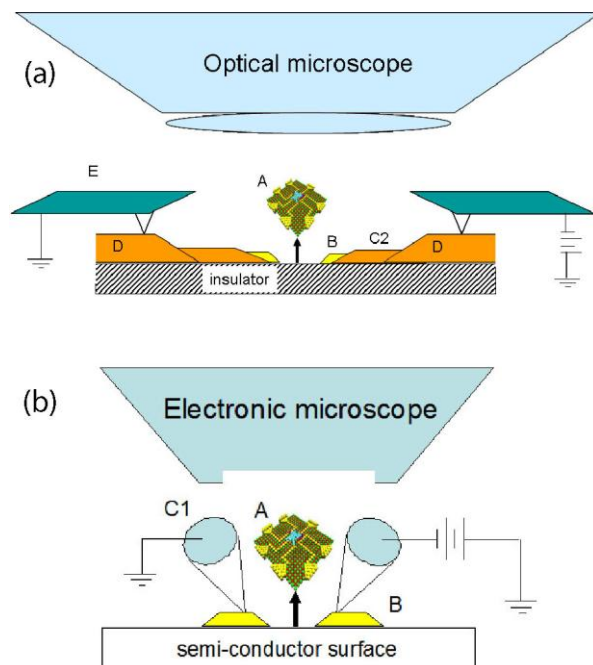


Figure 2: Scheme of the atomic scale interconnection machines for (a) wide and (b) moderate surface band gap substrates. A: Atomic scale circuitry, B: Contacting metallic nanopads, C1: Ultrasharp metallic tips, C2: Nanowires, D: Microelectrodes, E: Metallic microcantilevers

References

- [1] Rapenne G., Launay J.-P. and Joachim C. 2006 *J. Phys.: Condens. Matter* 18 S1797
- [2] Joachim C., Gimzewski J. K. and Aviram A. 2000 *Nature* 408 541
- [3] Wada Y. 1996 *Microelectronic Engineering* 30 375
- [4] Ample F., Ami S., Joachim C., Thieman F. and Rapenne G. 2007 *Chem. Phys. Lett.* 434, 280
- [5] Joachim C. 2002 *Nanotechnology* 13 R1
- [6] Itoua S., Joachim C., Rousset B. and Fabre N. 1992 *Nanotechnology* 3 10
- [7] Saifullah M. S. M., Ondarcuhu T., Koltsov D. F., Joachim C. and Welland M. 2002 *Nanotechnology* 13, 659
- [8] Cacciollati O., Joachim C., Martinez J.-P. and Carsenac F. 2004 *Int. Journ. Nanosci.* 3 233
- [9] Chou S. Y., Krauss P. R., Renstrom P. J. 1996 *Science* 272 85
- [10] Thet N. T., Lwin M. H., Kim H. H., Chandrasekhar N. and Joachim C. 2007 *Nanotechnology* 18, 335301
- [11] Duchemin I., Renaud N. and Joachim C. 2008 *Chem. Phys. Lett.* 452 269
- [12] Soukiassian L., Mayne A. J., Carbone M. and Dujardin G. 2003 *Surf. Sci.* 528 121
- [13] Lin S., Li M., Dujardin E., Girard C. and Mann S. 2005 *Adv. Mater.* 17 2553
- [14] Ondarcuhu T., Nicu L., Cholet S., Bergaud C., Gerdes S. and Joachim C. 2000 *Rev. Sci. Instrum.* 71, 2987

4b. Number of interconnection steps & interconnection strategies

How to exchange information with a single molecule

C. Joachim and D. Martrou

GNS, CEMES-CNRS, 29, rue Jeanne Marvig, BP 94347, 31055 Toulouse Cedex 4, France

At the laboratory scale, there is an urgent technological problem to be solved: how to interconnect a molecule with the prospect to exchange information in a multi-channel configuration with this molecule? Starting from a surface science point of view, one of the Research Unit aims of the Pico-Inside project was to explore the solutions of this problem. Whatever the type of information to be exchanged, connecting a molecule to electrodes or dielectric waveguides means creating an interaction between a few parts of this molecule and the surface-end of each interconnect. From the surface science point of view adopted in Pico-Inside, any change of the detail atomic ordering at the “molecule-surface-end” junction or any change in the adsorption site of the molecule in interaction with the interconnects will modify the orbital mixing between the surface and the molecule. Then, the quality of the information exchange will be degraded.

In the following, research work of Pico-Inside partners is presented in a way to indicate the starting point of the Pico-Inside exploration of this interconnection problem. Pico-Inside concentrated its efforts on electronic interconnects meaning that only metallic electrodes issues are discussed. They also concentrated on the physical and technological aspect of the interconnects and not of the type of information to be exchanged (classical, quantum) nor on the chemical aspect of the interconnection problem.

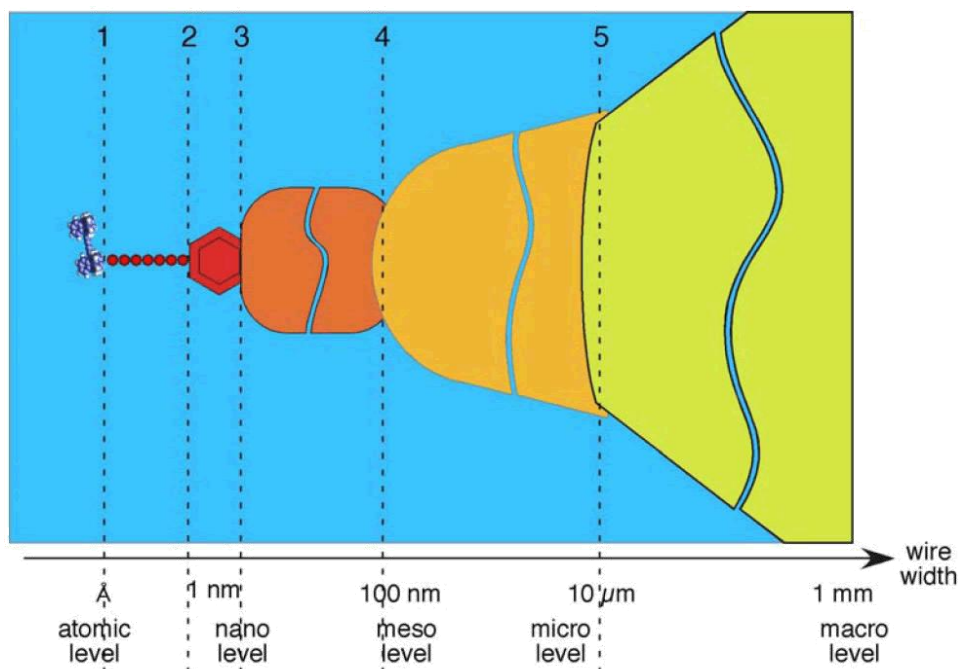


Figure 1: The aim of Pico-Inside was to multiple connect a single molecules to the macro world under ultrahigh vacuum conditions. Different interconnections were studied: 1) molecule to atomic wire (atomic level) 2) atomic wire to a metallic island of a few monolayers high which links the atomic level and the nano level 3) metallic island to a thin metallic ribbon which links the nano level and the meso level 4) thin metallic ribbon to micro-electrode which links the meso level and the micro level 5) microelectrode to macroscopic wiring which links the micro level and the macro level.

In a fully planar technology, a maximum of 5 levels of interconnection is required to pass from the molecule to a macroscopic amperemeter (see Figure 1):

1. From the molecule to the atomic wires. This is the atomic scale level of the interconnects.
2. From the atomic wires to nano metallic islands, only a few mono layers in height. This is the nano scale level of the interconnects.
3. From those nano metallic islands to mesoscopic metallic wires with a width below 100 nm. This is the mesoscale level of the interconnects.
4. From those mesoscopic wires to micron scale metallic pads. This is the microscale level of the interconnects. The lateral size of those pads depending of the next level.
5. From the micropads to macroscopic wiring which links the micro level and the macro level and then to the amperemeter.

At all the levels, a major point is to preserve the cleanness of the others level of the interconnection sequence. This means that the difficult task is to determine a succession of technologies which will preserve the initial atomic scale precision of the atomic scale level of the interconnect. This requires the exploration of fabricating metallic atomic scale mesa islands on semi-conductor and insulating surface, of molecular molding and stabilisation of atomic wires, of self-assembling molecule on an insulator in a systematic way, of developing a nanostencil technique down to 10 nm and of using metallic cantilevers for the interconnect to the macroscopic level. In Pico-Inside, we will also take care of the possibility to suppress one or more of those interconnection levels to increase the reproducibility of the final interconnection chain.

The need for a first atomic scale level of interconnect is explained by a very hard geometric constrain in this multi-interconnection problem. To illustrate this point, let us remind the past tentative in another FET-IST project BUN which ended in year 2003. The problem was to use the ebeam lithography technique for the fabrication of a maximum of nanoscale metallic wires on a circle. A maximum of 20 nanoscale metallic electrodes terminated each by a 20 nm apex diameter were fabricated on a SiO₂ surface.

On this surface, those 20 electrodes open the access to an area of a diameter not smaller than 200 nm. This diameter is clearly too large as compared to the size of conjugate molecules available in our days. This geometrical constrain forces to fabricate local access on the molecule using atomic wires. But this can be considered as positive because it will force the molecular designer to integrate as much as possible the electronic functions to be performed in a small molecule. This part was worked out in the research Unit 1 of Pico-Inside.

The 5 interconnection levels can be separated in two groups. One group for the first and the second interconnect levels is relevant to surface science. The second group for the three last, can be considered as technological interconnects. Notice that these electrical contacts will be used under or near an UHV-STM or NC-UHV AFM head. Therefore, the way to fabricate the second group will depend strongly on the geometrical environment around the local STM or AFM probe. The realization of the first group will depend on the nature of the substrate (semiconductor or insulator) to be used.

4c. From the molecule to the nano-pads on a semi-conductor surface

Constructing interconnection nanostructure on the MoS₂ surface

J.S. Yang¹, Deng Jie¹, C. Troadec¹ and C. Joachim^{1, 2}

¹ *Institute of Materials Research and Engineering, A*STAR
(Agency for Science, Technology and Research), 3 Research Link, Singapore 117602*

² *Centre d'Elaboration de Matériaux et d'Etudes Structurales (CEMES-CNRS)
29, rue Jeanne Marvig, BP 94347, 31055 Toulouse Cedex 4, France*

Introduction

As presented in section 4a, a small electronic gap (below a few eV) of the surface material supporting the interconnection structure leads to only 3 levels of interconnects. Levels (A) and (B) are depending on the mastering of atomic scale surface science phenomena while level (C2) is relying on the ability to fabricate multiple ultra sharp metallic tips to contact each metallic nano-island of level (B). With a multi-access interconnection technology on a small electronic gap surface material, the constraint is to avoid surface leakage current between the electrodes contacting the surface metallic nano-islands. Therefore, it is compulsory to contact them from the top. This constrain has a lot of consequences in the structure of the interconnection machine depicted in section 4a. In particular, a scanning electron microscope is required instead of an optical microscope because the lateral size of the nano-islands is necessary very small to avoid inter nano-island leakage current. In this section, we are presenting the progresses towards the construction of a nano-pads arrangement at the surface of a low gap semi-conductor. This was explored mainly in Singapore under the VIP A*STAR Atom Tech. project where an interconnection machine is under construction at IMRE.

Semi-conductor surface preparation

After an atomic scale UHV surface preparation, not a lot of semiconductor materials are presenting a surface semi-conductor electronic gap in the range of a few eV. Generally, the surface of these materials needs to be saturated by an ultra thin layer in charge of completing the valence of the surface atoms existing after the cleavage operation of the crystal. This is for example the case of the standard Ge and Si surfaces. While for example the native Si(100) surface gap is 1.2 eV, it reaches 2.1 eV with an hydrogen saturation in its 2x1 reconstruction phase [1]. In UHV, the preparation of such a semi-conductor surface is usually following the same procedure. After degassing and destroying the oxide layer, the surface is reconstructed by passing a high intensity current through the sample, between 8 to 12 A depending of the doping level of the bulk material behind [2]. One problem is to prepare large atomically flat terraces in the 50 nm width range with a homogeneous reconstruction all along a terrace. Another problem is that such an open surface is very sensitive to the quality of the vacuum in the preparation chamber. It is often found that without any chemical protection, a very well prepared semi-conductor surface becomes totally polluted by contaminants if the waiting time for working on this surface is too long.

Saturating these surfaces by adsorbing hydrogen, chlorine, sulfur or small molecules is a nice solution to preserve the surface integrity [3]. In many case, it is also a good solution to increase the electronic surface band gap. For example, molecular hydrogen can be cracked in front of Si(100) or Si(111) surfaces to form the hydrogen saturated Si(100)-H or Si(111)-H surfaces. But the rule is not systematic. The saturation of a semi-conductor surface not always leads to a large increase of its surface electronic gap [3]. Furthermore the phase diagram of such surfaces generally presents a surface

reconstruction temperature with the destruction of the saturation layer beginning between 300°C to 400 °C [4]. Notice that the stabilization of nanowires at the surface of an insulator is a very delicate task. With the saturation layer grown on a semi-conductor surface, an atomic surface wire is natively self-stabilized by the surface structure.

There are a few semi-conductor surfaces where this saturation is part of the material structure. This is the case of lamellar semi-conductor like MoS₂. In this case, the sulphur over layer is hardly bond to the underneath Mo atoms. The MoS₂ surface is rather easy to prepare by a very fast UHV cleaning followed by a standard surface preparation temperature in the 300°C range [5]. The extension of the atomically flat surface of lamellar compounds is usually rather large up to a few microns in lateral extension in some cases. MoS₂ is one of the most interesting materials of the lamellar compound series with a bulk gap around 1.3 eV and a surface gap in the 1.0 eV range [6]. The MoS₂ surface remains atomically perfect and flat up to 1100 K. Above 1200 K, a reconstruction of the top layers of MoS₂ to Mo₂S₃ is observed, leading to one-dimensional atomic double rows on the reconstructed surface [7]. Such temperature stability is very important for the fabrication of surface atomic wires by STM extracting rows of S atoms. The drawback is that it is extremely difficult to extract these surface atoms as compared to the surface atoms of the Si(100) 2x1-H surface [8]. There is a crucial need for a material stable enough in temperature and whose surface atom chemical stability is between Si(100)-H and MoS₂.

LT-STM surface atomic scale imaging

There is generally no STM surface imaging problem of low surface gap semi-conductor materials. STM images of the 2 principal surfaces used at IMRE in Singapore to explore atomic scale interconnection are presented in Figure 1 showing each a nice atomic resolution. For lamellar materials and at low temperature, one imaging problem comes from the softness of lamellar semi-conductor materials in the transverse direction. It is usually very difficult to record a nice current distance characteristic on these materials when changing the tip to surface distance. Therefore, this distance is not known with precision. In this condition, adsorbates or metallic nano-islands can be easily brushed away during an STM tip scan because the tip apex to surface distance can be very small during STM imaging [5].

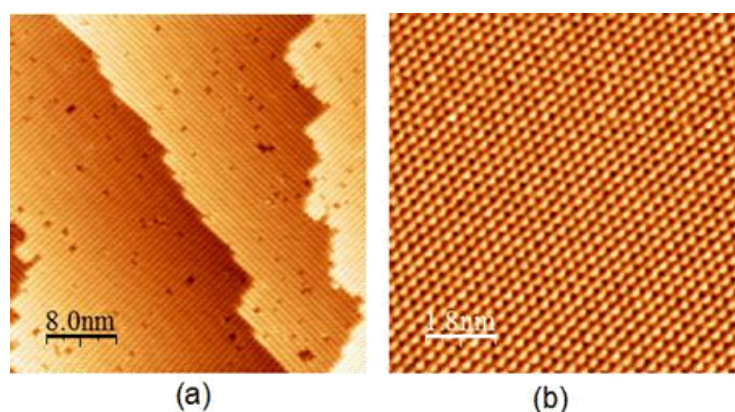


Figure 1: Standard UHV-STM images of an Si(100) 2x1 and an MoS₂ surfaces showing the atomic resolution before the start of any construction or fabrication steps. As described in this section (and in section 3 for large gap surface materials), those construction and fabrication process must be carefully tested in such a way that this atomic resolution is kept up to the multi probes I-V measurements. (a) The Si(100) surface was prepared with the objective to increase the terrace size before the hydrogenation step $V = 2 \text{ V}$ and $I = 10 \text{ pA}$. (b) The MoS₂ surface was prepared to study the conditions to extract the sulphur surface atoms one at a time.

Metallic nanopads fabrication and re-configuration

On a semi-conducting surface, metallic nanopads are necessary to pass from the surface atomic wires made of dangling bond lines to the metallic tip apex. This very local metallization must be practiced directly on the passivated semi-conductor surface. It turns out that there is not a lot of passivated surface whose passivation overlayer can sustain the temperature required for metallization [11]. These temperatures are usually higher than a few hundred degrees which locally destroys the passivation. One solution to this problem is to start with a robust semi-conductor surface like MoS₂ and then to transfer the self assembled metallic nano-islands on another surface by contact printing in UHV [6].

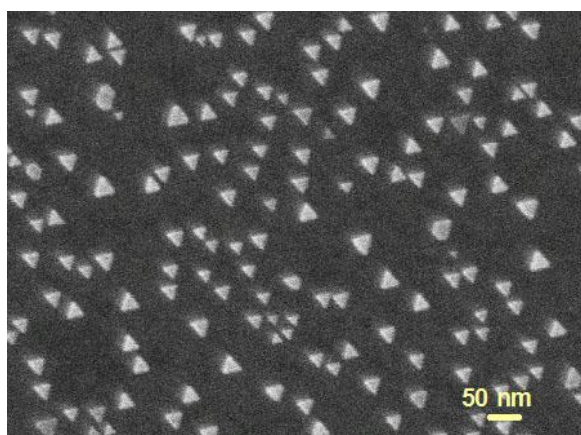


Figure 2: SEM image of the distribution of Au nano-islands on MoS₂ after the fabrication process detailed in section 4.4. Many nano-islands are 30 nm in lateral size. Notice also the very sharp end at each summit of these triangles.

On the MoS₂ surface, gold atoms self-assemble in triangular nano-islands whose lateral dimension can go down to 5 nm for a thickness of a few nm [5]. An optimum of 30 nm lateral and 10 nm in height can be easily obtained by tuning the surface temperature during the metal evaporation [5]. In a standard preparation, MoS₂ wafers are fabricated from bulk molybdenite stones directly mined in Australia. The slides are cut into 10 x 10 mm² pieces. The top surface of a MoS₂ slide is cleaved and immediately loaded in a thermal evaporator. After the sample is outgassed at 400 °C for 3 hours, Au is thermally evaporated onto the MoS₂ surface at 400 °C with a deposition rate of 0.02 nm/sec. The total thickness of

evaporated Au, monitored by a quartz microbalance, can be kept as low as 1 nm. After Au deposition, the sample is maintained at 400 °C for another 1 hour to facilitate the self-assembly of crystalline Au nano-islands on the MoS₂ surface. During processing, the vacuum in the chamber must be better than 2 x 10⁻⁵ Pa. The nano-island growth conditions can be optimized to achieve a majority of nano-islands to be equilateral triangular shape with a 20 to 30 nm lateral size (see Figure 2).

Such a fabrication and self assembly process usually leads to a rather homogeneous distribution of Au nano-islands. In some cases, the apices of 2 nano-islands can be face-to-face at distances as low as a few nanometers, constituting fantastic ultra-clean and atomically well-ordered nano junction to interconnect a single molecule since the background surface has generally kept its atomic scale corrugation. Unfortunately, the MoS₂ electronic surface band gap is too small for the "nano-island - surface - nano-island" conductance to be much smaller than the one of a conjugated molecule to be interconnected. Therefore, we have learnt the conditions to manipulate those nano-islands one by one on the MoS₂ surface [5]. There are 2 modes of manipulation. In the soft one, the tip apex is not mechanically touching the nano-island but is charging it. A large numbers of scans are necessary to charge a nano-island enough for the electrostatic force between the STM tip apex and the nano-island to be large enough for the nano-island to move away but with a precision better than 0.1 nm [5]. In the mechanical mode, the tip apex is simply pushing on a facet of the nano-island. This mode of manipulation is less precise (1 nm or more) but very fast [5]. Figure 3 is

presenting a few examples of Au nano-pads nanostructure arrangements constructed by manipulating the nano-islands one after the other.

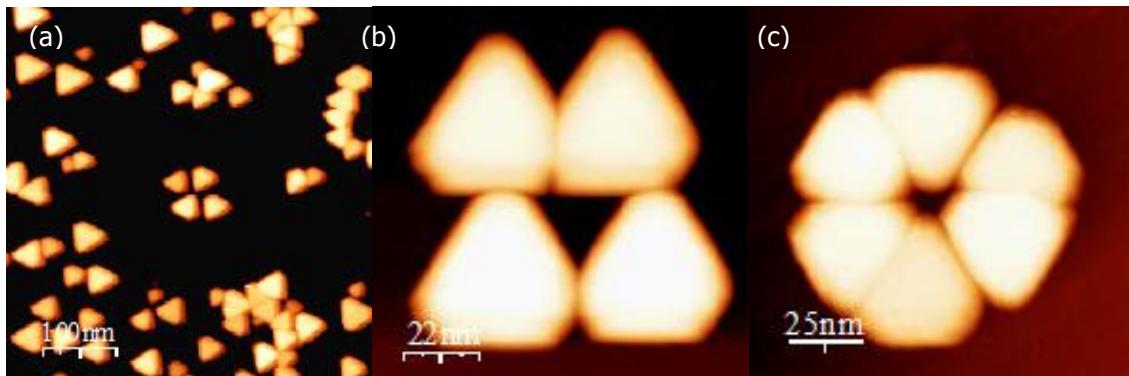


Figure 3: Example of contacting nanostructures constructed by manipulating the nano-islands one after the other in a lateral STM manipulation mode on the MoS₂ surface. (a) More than 50 nano-islands have been manipulated around to assemble the central 4 contacting nanostructure. (b) Zoom on a peculiar construction of 4 nano-islands manipulated in a square. (c) Zoom on a peculiar construction of a 6 nano-islands interconnection structure converging toward a 12 nm central active area where the atomic circuit is supposed to have been atomically fabricated before this construction. (a), (b) and (c) are UHV-STM images recorded on MoS₂ with $V = 0.2$ V and $I = 10$ pA.

These constructed nanostructures cannot be transferred as such by a direct contact printing on a larger gap semi-conductor surface. First, the construction will be deformed during the printing. Secondly, for interconnecting a surface dangling bond interconnecting circuit, it is better to manipulate the nano-islands after the fabrication of the surface atomic wires. In this way, a given metallic nano-island can be manipulated step by step over the corresponding atomic wire up to the point where the contact conductance is lower than the surface leakage conductance. We have recently demonstrated that Au nano-islands can be transferred from the MoS₂ surface to a Si(100)-H surface [12]. For this to occur, the MoS₂ surface must be structured in micron scale pillars creating a matrix of stamps [12]. We have shown that Au nano-islands can be fabricated on the surface of each pillar after changing the characteristic fabrication temperature [12]. A 10 % overall transfer rate to Si Si(100)-H was obtained for 10 to 20 microns lateral size pillars [12]. The experimental conditions remain to be determine to STM manipulate these nano-islands at the Si(100) 2x1 H surface as it was done on the MoS₂ surface. Notice also that the hydrostatic pressure during transfer printing must be optimized to preserve the Si(100)-2x1-H hydrogen passivation layer under the nano-islands.

Conclusion

After preparing an ultra clean MoS₂ semiconducting surface, we have self assembled on this surface a random distribution of metallic nano-islands with an average lateral size in the 30 nm range for a thickness around 10 nm. After the growth and surface diffusion processes of the metal atoms on the MoS₂ surface, the atomic resolution is preserved on the MoS₂ surface. Then, we demonstrated how single gold nano-islands 30 nm in size and 12 nm in height can be manipulated at room temperature with a UHV-STM, on this MoS₂ surface and with an appropriate choice of STM feedback parameters reaching a precision better than 0.5 nm. The precise manipulation of single ultra-flat metallic nano-islands on a semiconductor surface is a new way of constructing planar metallic contact pads to interconnect an atomic wire or a molecule to macroscopic probes, preserving the atomic cleanliness of the surface. Commercially

available UHV compatible multi-STM systems, where each tip apex is positioned independently on a surface using top SEM imaging, provide direct electrical access to the constructed 4-pads nanostructures without the usual nanolithography techniques.

Acknowledgments: We would like to thank A*STAR and IMRE for financial support of this work under the VIP A*STAR Atom Technology for molecule logic gate program in Singapore.

References

- [1] A. Akremi, P. Lacharme and A. Sébenne; 1997 Surf. Sci. 192 377
- [2] A. Bellec, D. Riedel, G. Dujardin, N. Rompotis and L. Kantorovich; 2008 Phys. Rev. B 78 165302
- [3] W. A. Hofer, A. J. Fisher, G. P. Lopinski and R. A. Wolkow; Phys. Rev. B 63 085314
- [4] J. J. Bolland; 1991 Phys. Rev. B 44 1383
- [5] J. S. Yang, Deng Jie, N. Chandrasekhar N. and C. Joachim; 2007 J. Vac. Sci. Technol 25 1694
- [6] K. S. Yong, D. M. Oltavaro, I. Duchemin, M. Saeys and C. Joachim; 2008 Phys. Rev. B 77 205429
- [7] R. K. Kiwari, J. S. Yang, M. Saeys and C. Joachim; 2008 Surf. Sci. 602 2628
- [8] S. Hosoki, S. Hosaka and T. Hasegawa; 1992 Appl. Surf. Sci. 60/61 643
- [9] C. Villagomez, T. Zambelli, S. Gauthier, A. Gourdon, C. Barthes, S. Stojkovic and C. Joachim; 2007, Chem. Phys. Lett. 450 107
- [10] A. Bellec, F. Ample, D. Riedel, G. Dujardin and C. Joachim; 2009 Nanolett. 9 144
- [11] M. Tanaka, F. Chu, M. Shimojo, M. Takegushi, K. Mitsuishi and K. Furuya; 2006, J. Mater. Sci. 41, 2667
- [12] Deng Jie, C. Troadec, H. H. Kim and C. Joachim; 2009 Nanotechnology submitted

Gold-alloy nanowires: a high resolution STM imaging

Grzegorz Goryl, Maria Goryl, Szymon Godlewski, Franciszek Krok, Jacek J. Kolodziej, Piotr Piatkowski, Jakub S. Prauzner-Bechcicki and Marek Szymonski

Research Centre for Nanometer-scale Science and Advanced Materials (NANOSAM), Faculty of Physics, Astronomy and Applied Computer Science, Jagiellonian University, Reymonta 4, 30-059 Krakow, Poland

Keywords: InSb, nanowires, thermally-assisted assembling, high resolution STM imaging

Successful communication between nano- and micro- environment of the molecular electronic device is a crucial ingredient of the future nanoelectronics. One has to interconnect a single molecule, designed to perform particular tasks within a circuit, with other parts of the circuit, especially with a circuit's output interface. Fabrication of gold nanowires on InSb by means of the thermally-assisted assembling process seems to be a promising solution for such a task. Indeed, for specific range of the sample temperatures during gold deposition, micrometer-long conductive nanowires aligned along the surface reconstruction rows of In-terminated (001) $c(8 \times 2)$ face of InSb may be manufactured [1;2].

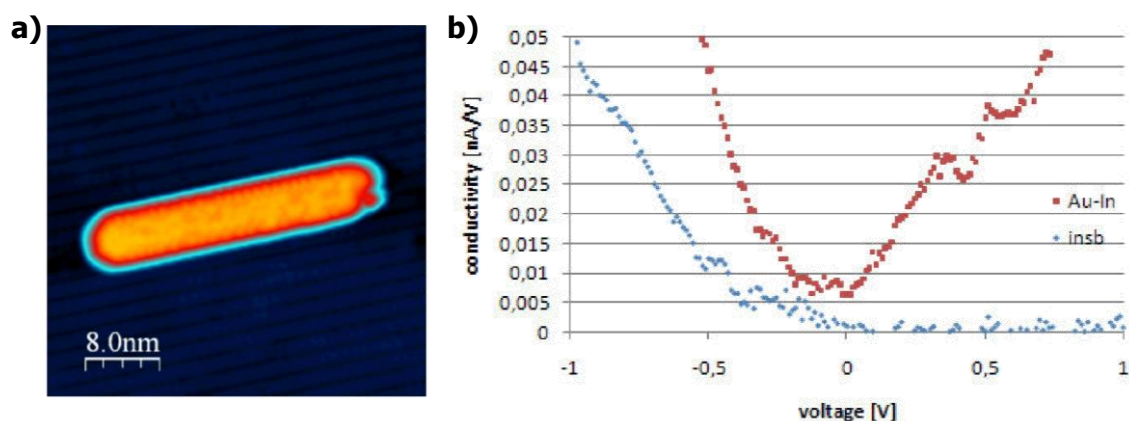


Figure 1: (a) High resolution STM image of gold nanowire formed on InSb(001) surface. Bias voltage: $-0.5V$, tunnelling current: $25pA$. (b) Conductance as a function of bias voltage for gold alloy nanowire (red dots) and InSb substrate (blue dots)

With use of various scanning probe methods (SPM) structural and electronic properties of the nanostructures have been studied in great detail. Experiment was performed in a ultra-high vacuum system equipped with a low temperature scanning tunnelling microscope (LT-STM) commercially designed by Omicron. Gold has been evaporated on atomically flat and clean terraces of (001) reconstructed surface of InSb crystal. Evaporation rate was controlled through a quartz crystal microbalance. InSb samples (Kelpin Crystals) were pre-annealed to 650-750 K and then hot samples were cleaned by ion sputtering with a 700 eV Ar^+ beam [2]. The quality of the surface was controlled with the low energy electron diffraction (LEED) and the STM techniques. During the evaporation several substrate temperatures in the range of 300-700 K were used, as well as, post-deposition thermal annealing. Image processing and analysis was done by means of WSxM software [3].

For a specific sample temperature window, i.e. 600-650 K, narrow, long, with a length up to 800 nm, structures were formed. The height of such nanowires was in the range

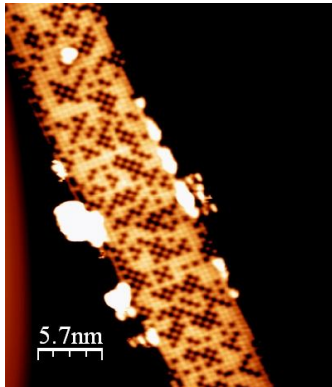


Figure 2: High resolution image of $AuIn_2$ alloy nanowire; bias voltage: $-2V$, tunnelling current: $5pA$.

from 0.8 to 1.5 nm and their width was in the range from 5 to 20 nm. In Figure 1(a) gold nano wire on $InSb(001)$ is presented, its orientation along the $[001]$ direction (atomic troughs of the reconstructed $InSb(001)$ surface) is clearly seen, as well as, atomic resolution on the top of the wire. Spectroscopic data for the gold nanostructure and for the substrate are presented in Figure 1(b). Conductance vs. bias voltage plot indicates different electronic properties of the nanowire with respect to the sample, supporting an earlier conclusion on a metallic character of the former [1;2]. Moreover, detailed analysis of the nanowire structure with atomic resolution suggests, that during gold deposition a gold-indium alloy is created rather than a pure gold structure (see Figure 2).

As already noted, a crucial parameter appears to be the substrate's temperature during gold deposition. However, it was found that also the time of cooling of the sample plays an important role. During the Au deposition the substrate surface undergoes considerable reorganization and if the sample temperature after the evaporation process was quickly decreased, a distorted substrate could be observed (see Figure 3). Further annealing of the sample to the deposition temperature led to reconstruction of the substrate (see Figure 4). It could be noted in Figure 4(b), that lower terrace of the wire exhibits the same structure as the substrate and the upper terrace appearance is significantly different. The upper terrace also includes other than gold atoms as indicated by dark spots in Figure 4 in agreement with previous observation on the alloy nature of the wire (compare with Figure 1) Such an observation suggests, that the lower terrace is created during the reconstruction of the distorted surrounding of the nanowire, while the upper terrace is the intrinsic gold alloy nanowire.

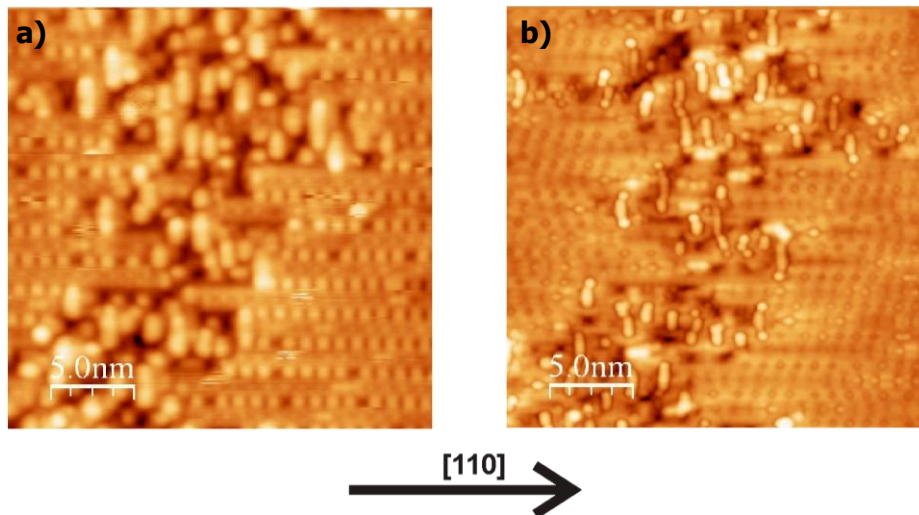


Figure 3: $InSb(001)$ surface distorted during gold deposition. The sample was relatively quickly cooled down after evaporation process was ended. (a) bias voltage: $2V$, tunnelling current: $100pA$; (b) bias voltage: $-0.5V$, tunnelling current: $100pA$.

One could expect similar temperature controlled assembling process for other atomically ordered surfaces of $A_{III}B_V$ semiconductors, such as $InAs(001)$ or $GaAs(001)$. However, gold deposition on $InAs$ and $GaAs$ surfaces under the same condition as for $InSb$ did not lead to formation of wire-like structures. This observation could be attributed to the different reactivity of gold to the respective substrates [2].

Summarising, micrometer long, conducting nanowires could be fabricated via gold deposition on InSb for substrate temperatures during the deposition being in the range 600-650 K. Nanowires are perfectly oriented along the reconstructions troughs of (001) InSb face, as revealed by SPM measurements. Metallic character of the structures is confirmed by spectroscopic data and high resolution STM measurements suggest the gold alloy nature of the wire. During the gold deposition substrate undergoes considerable reorganization leading to the distortion of the surface reconstruction. The latter is restored via post-deposition thermal annealing. Gold nanowires could not be created for InAs and GaAs (001) surfaces.

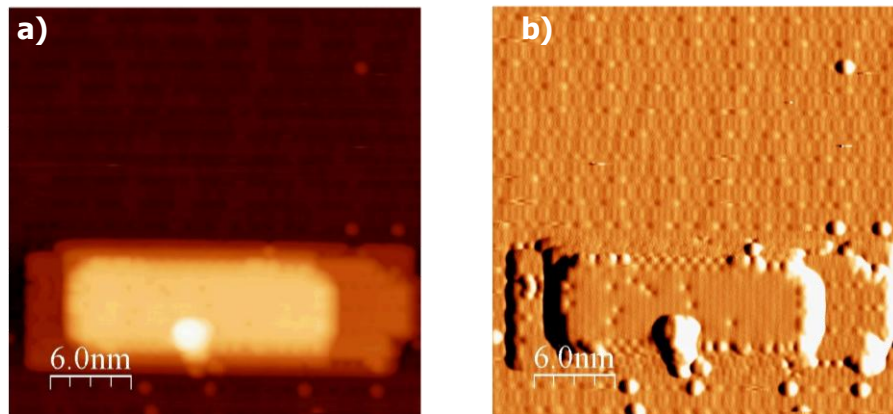


Figure 4: STM scans showing gold alloy nanowire with surrounding substrate surface reconstructed via post-deposition annealing. Bias voltage: $-2V$, tunnelling current: $100pA$. (a) topographic image; (b) error signal.

References

- [1] M. Goryl, et al. *E nano-newsletter*. 2006, 3, 26.
- [2] M. Szymonski, et al. *Nanotechnology*. 2007, 18, 044016.
- [3] I. Horcas, et al. *Rev. Sci. Instrum.* 2007, 78, 013705.

4d. Optic navigation and interconnection

Nano level to macro level interconnects through static and nanostencil techniques

D. Martrou, H. Guo, T. Zambelli, L. Guiraud, S. Gauthier and C. Joachim

GNS, CEMES-CNRS, 29, rue Jeanne Marvig, BP 94347, 31055 Toulouse Cedex 4, France

1-General description of the micro cleanroom for Pico-Inside

The aim of this part is to obtain an electrical contact of low resistance between a thin metallic pad 10 to 100 nm wide and a macroscopic wire. One possibility is to add each interconnect (3 to 5) by different techniques: the micro clean room developed in the Nanoscience Team of the CEMES institute at Toulouse is based on this solution. Indeed the interconnect 3 is obtained by dynamic nanostencil [1], the interconnect 4 by static stencil, and the last one by microcantilever array as shown schematically on the Figure 1. The two last steps 4 and 5 have been already tested in air using e-beam lithography nanowires ending by $2 \times 2 \mu\text{m}^2$ pads which are contacted with a metallic microcantilever array [2].

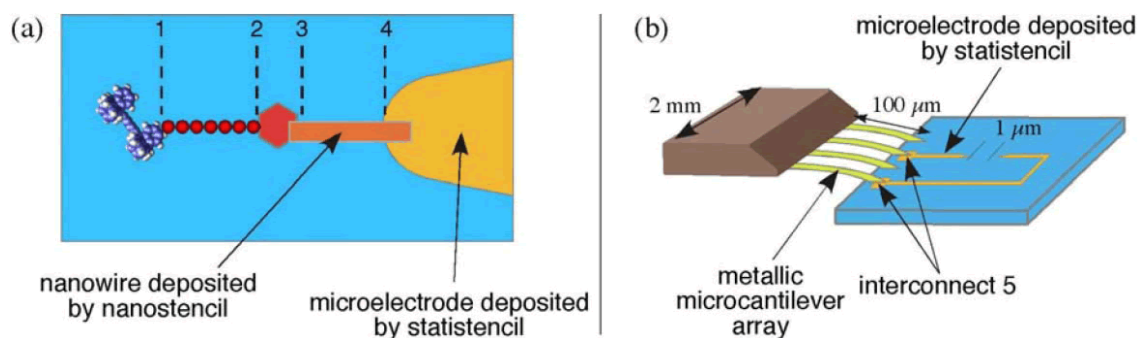


Figure 1: In the GNS group of Toulouse, the interconnects 3 and 4 are made by nanostencil with the micro cleanroom (a), and the interconnect 5 consists of a metallic microcantilever array contacting pads at the end of microelectrodes deposited by the static stencil process.

The first step is the growth of microelectrodes on the substrate by the static stencil process which is evaporation through a thin membrane bored by the desired pattern. Then the interconnects 3 and 4 between the end of one microelectrode and a thin metallic island are made by depositing a small wire with the nanostencil process which consists to use a drilled cantilever as a shadow mask to write on the surface [3]. And the last interconnect 5 is done by positioning the extremities of metallic microcantilevers array (microcomb) on pads at the end of the microelectrodes.

To do successfully all these steps, one needs to 'see' at different scale. For the last interconnect, the microcomb should be positioned at a micrometer scale, so a direct vision of the scene by the way of an optical microscope is sufficient. This optical microscope is also useful to approach the cantilever close to the microelectrodes array. However to find the area between electrodes, it is necessary to see at sub-micrometer scale but on a wide range of several tens of micrometers.

The UHV micro cleanroom developed in the GNS group of Toulouse has all these functionalities. As presented on the Figure 2, it is a commercial VT AFM/STM Omicron head which has been modified.

The first modification was to add a flexural-hinge guided (XY) table ($100 \mu\text{m} \times 100 \mu\text{m}$ with a repeatability of a few nanometers) which carries the Omicron sample plate. With this table, it is possible to do wide scale AFM/STM images, greater than those obtained

with the normal Omicron piezo tube which supports the tip or the cantilever. And the repeatability of a few nm allows a “blind” (ie without AFM imaging) positioning of the cantilever on the surface. Combined with an effusion cell highly collimated on the cantilever, it allows the growth of nanowires (nanostencil process). The positioning of the microcomb is realized by an (XYZ) piezo table under an optical microscope.

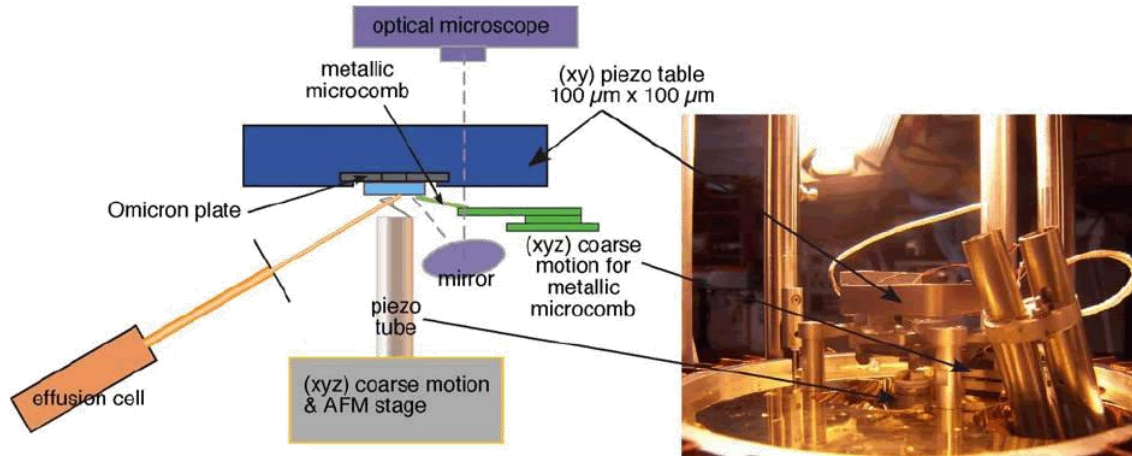


Figure 2: The micro cleanroom developed in the GNS group is based on a VT AFM/STM Omicron head which has been modified: the Omicron plate is now placed on a (XY) piezo table allowing fine motion on a (100 μm x 100 μm) area, an (XYZ) table allows the positioning of the microcomb, and the scene is seen through an optical microscope.

2-Technical description of the nanostencil stage

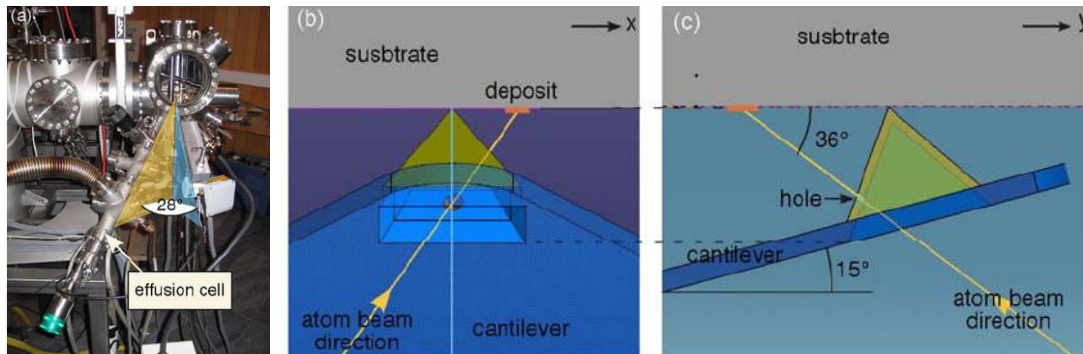


Figure 3: (a) an effusion cell is mounted on the VT AFM/STM; (b) and (c) plane view of the cantilever tip on the surface along the y axis and x axis of scan respectively.

The quality of the nanostencil process depends strongly on the geometrical position of the metal source, the drilled cantilever and the surface. Figure 3 presents our configuration.

The effusion cell is mounted directly on the VT AFM/STM UHV chamber: the geometry of the flange defines two angles for the atom beam direction. The first one is between the two vertical planes passing through the atom beam and the y direction of scan and is equal to 28°. The second one is defined by projection on the vertical plane passing through the y direction and is equal to 36°. This geometrical configuration is reproduced when fabricating the drilled cantilever by FIB. Indeed the

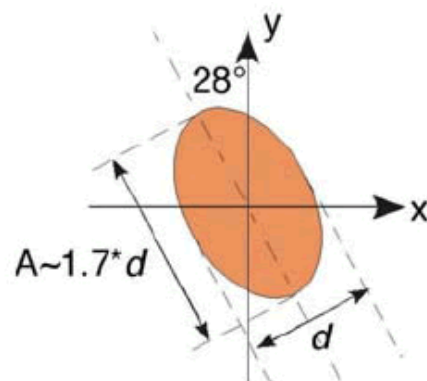


Figure 4: The image of a circular hole made by FIB on the cantilever tip will be an ellipse on the surface sample.

holes of the desired figures are drilled with a focused ion beam oriented in the same direction than the atom beam of the effusion cell. The image of a circular hole made on the cantilever tip will be an ellipse with the main axis oriented at 28° from the y scan axis as shown on Figure 4.

3-Some results obtained by the nanostencil process

To observe the distortion induced by the position of the effusion cell, an experiment was done with a cross drilled on the cantilever tip as presented on Figure 5(a). To decrease the clogging effect during metal evaporation, the first thing done by FIB is to thin the side of the cantilever tip until a thickness of around 100 nm. This leads to the formation of a box where the desired pattern is drilled. Here we choose a cross with eight lines having between them a similar angle of 45° . After deposition of 4 nm of Titanium on a silicon substrate, we evaporated 50 nm of silver through this drilled cantilever. Our (XY) sample table allows us to obtain wide scale STM images of the deposition as presented on Figure 5(b).

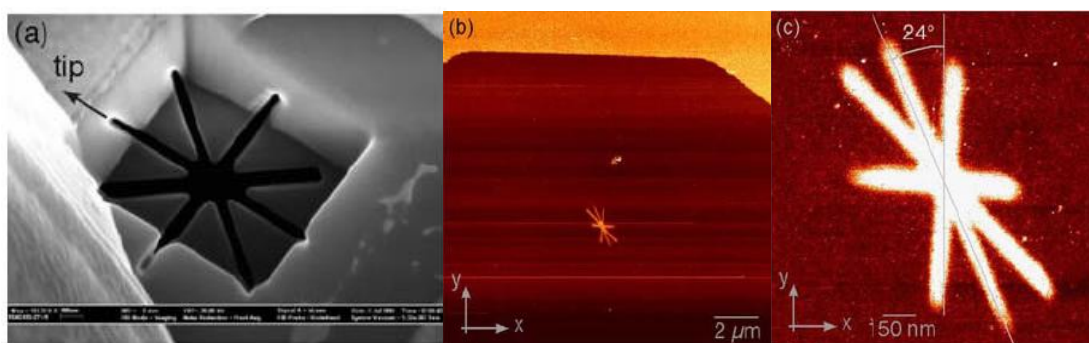


Figure 5: (a) SEM image of the cross drilled by FIB on one side of a cantilever tip ;(b) wide scale STM image ($15 \mu\text{m} \times 15 \mu\text{m}$) obtained by moving the sample with the (XY) table; (c) $1.5 \mu\text{m} \times 1.5 \mu\text{m}$ STM image showing the silver cross deposited.

The ability to do wide scale STM image allowed us to find rapidly the small cross: we can see on this wide scale STM image the shadow of the cantilever, and the silver cross deposited through the drilled pattern. A closer view obtained also by scanning with the (XY) table allows us to determine precisely the distortion induced by our geometrical configuration. For example we can measure the angle between the y scan direction and the line passing through the end of the cantilever tip. As this line should be in a vertical plane parallel to the y scan direction, we should obtain 28° after deposition. We measure only 24° , the difference is probably due to the misorientation of the cantilever during the gluing on the holder. Such a misorientation is observed on the wide scale STM image (see Figure 5(b)) and adds 2° to the measured angle, which gives a value of 26° closer to the 28° expected.

The nanostencil process allows us to deposit a desired pattern directly on a surface without using an etching process. To successfully contact a molecule we need to draw a thin line between a metallic pad and a microelectrode. This means that we will evaporate through a hole drilled in a cantilever tip while moving in the same time the substrate to connect the two objects. However the atoms of the beam stick also on the cantilever and after a while the deposit formed on the edge of the hole will clog it. This well known phenomenon [4] is the main disadvantage of the nanostencil process. To study it we drilled a cantilever tip with five holes of increasing diameter from 32 nm to 200 nm as presented on Figure 6(a).

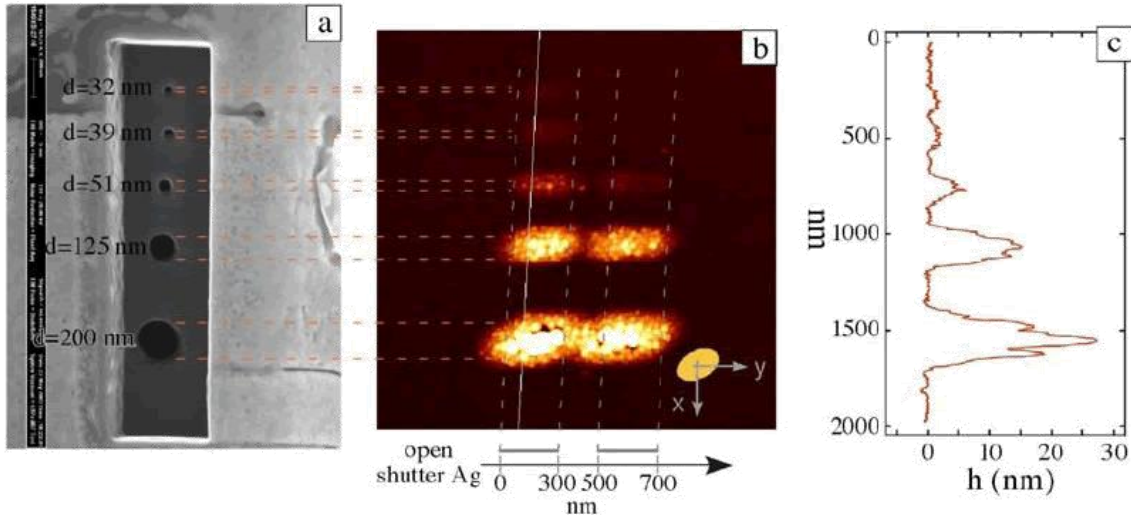


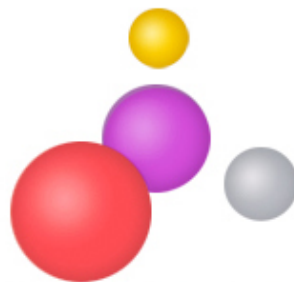
Figure 6: (a) 5 holes of increasing diameter drilled on a cantilever tip; (b) AFM image after deposition of silver ($48 \text{ \AA}/\text{mn}$) while moving the substrate at $20 \text{ nm}/\text{mn}$; (c) cross section along the white line.

We used this drilled cantilever to draw two lines of silver of 300 nm width, and separated by a gap of 200 nm. The silver flux is equal to $48 \text{ \AA}/\text{mn}$ and the sample is moving along the y axis with a speed of $20 \text{ nm}/\text{mn}$. The shutter of the silver cell was open and closed in order to obtain the described pattern. The AFM image presented on Figure 6(b) shows clearly large differences depending on the diameter of the holes. For the two small holes (32 and 39 nm), only the first line is drawn: after the two holes are clogged. The third hole ($\varnothing=51 \text{ nm}$) is clogged at the end of the second line and the two bigger ones are not clogged after the deposit of 120 nm of silver. A careful analysis of the pattern obtained with the smaller holes gives a thickness of clogging equal to three times the diameter of the holes. Another effect observed on the AFM image is the ellipsoidal shape of the lines due to the geometrical configuration of our system.

References

- [1] R. Luthi, R. R. Schlittler, J. Brugger, et al "Parallel nanodevice fabrication using a combination of shadow mask and scanning probe methods", Applied Physics Letters 75 (9): 1314-1316 AUG 30 (1999)
- [2] T. Ondarçuhu, L. Nicu, S. Cholet, C. Bergaud, S. Gerdes and C. Joachim "A metallic microcantilever electric contact probe array incorporated in an atomic force microscope", Review of Scientific Instruments., 71(5) 2087 (2000)
- [3] P. Zahl, M. Bammerlin, G. Meyer, and R. R. Schlittler "All-in-one static and dynamic nanostencil atomic force microscopy/scanning tunnelling microscopy system", Rev. Sci. Instrum. 76, 023707 (2005)
- [4] M. Kolbel, R. W. Tjerkstra, J. Brugger, et al. "Shadow-mask evaporation through monolayermodified nanostencils", Nano Letters 2 (12): 1339-1343 DEC (2002)

5. Conclusion



Mono-molecular electronics on a surface: challenges and opportunities

C. Joachim¹, J. Bonvoisin¹, X. Bouju¹, E. Dujardin¹, A. Gourdon¹, L. Grill², M. Maier³, D. Martrou¹, G. Meyer⁴, J.-P. Poizat⁵, D. Riedel⁶ and M. Szymonski⁷

¹*Nanoscience Group CEMES-CNRS 29, Rue J. Marvig BP 94347, 31055 Toulouse, France*

²*Institut für Experimentalphysik Freie Universität Berlin Arnimallee 14, 14195 Berlin, Germany*

³*Omicron NanoTechnology GmbH Limburger Strasse 75 65232 Taunusstein, Germany*

⁴*IBM Zurich Research Laboratory Säumerstrasse 4 / Postfach, CH-8803 Rüschlikon, Switzerland*

⁵*CEA-CNRS group « Nanophysique et Semi-conducteurs » Institut Néel – CNRS / UJF 25, av des Martyrs BP 166, 38042 Grenoble cedex 9, France*

⁶*Laboratoire de Photophysique Moléculaire CNRS, Bât. 210 Université Paris Sud, 91405 Orsay, France*

⁷*Centre for Nanometer-Scale Science and Advanced Materials, NANOSAM Faculty of Physics, Astronomy, and Applied Computer Science Jagiellonian University ul. Reymonta 4, 30-059 Krakow, Poland*

1. Introduction

Technology continues to produce functioning transistors on ever smaller scales. The day will come soon, however, when there will not be enough atoms on the surface of a semi-conductor to define the structure of a transistor and, consequently, of complex electronic circuits. At this stage, new approaches and new technologies are necessary for building computers, memory or telecommunication devices [1]. Anticipating this challenge, researchers in a few laboratories around the world are now looking for the minimum number of atoms required to fabricate, for example, a calculating unit able to perform a computation by itself. This problem of creating an atom based technology is not limited to electronics or to telecommunication and encompasses all types of devices, including mechanical machines and transducers.

Meeting the atom technology challenge for ICTs requires new understanding in four now well identified fields of science and technology:

1. Learning the kinds of architectures for molecule-machines (or atom surface circuits) which will permit to perform for example complex logic operations stabilized at the surface of a solid where the required interconnection will be constructed.
2. Creating a surface multi-pads interconnection technology with a picometer precision, respecting the atomic order of the surface which is supporting the nano-system assemblage.
3. Cultivating molecular surface science accompanied with molecule synthesis (respectively atom by atom UHV-STM fabrication on a surface).
4. Creating a packaging technology able to protect a functioning atom-technology-based machine, while at the same time insuring its portability.

Those 4 topics were discussed during the 1st nanoICT mono-molecular electronics Working Group meeting in Toulouse, France between the 8th and the 10th of December 2008. Most of the participants of this meeting have worked 3,5 years

together on the Pico-Inside project. So, this meeting was also a conclusion of the Pico-Inside project.

2. The architecture

As recalled in the introduction, Molecular devices i.e. hybrid molecular electronics are on the agenda of the micro-electronics roadmap since the seminal Aviram-Ratner paper in 1974 [2]. Until the turn of the century, such a futurist possibility of using molecules instead of solid state devices for electronics was just considered as a game for exploring the limits of calculating machines and memory devices. Approaching the end of the ITRS roadmap, things are now changing. Thanks to an intense experimental and theoretical effort, molecular electronics has now positively evolved from concepts to the first measurements and comparison with calculations [3]. There is now a real shift towards the full integration of a computing power in a single and the same molecule i.e. the mono-molecular approach [4]. This is now followed by exploring also the possibility of using atomic circuit fabricated on the surface of a passivated semiconductor surface for implementing quantum dot based computer approach [5] and may be one day a mixture of both approaches.

The different possible architectures for a single molecule (or an atomic circuit) to compute include i) the design of single molecule circuits in a standard electrical architecture, ii) electronic wave-like atomic or molecule circuits located on the surface of a semi-conductor and iii) the quantum Hamiltonian like computing architectures. All those approaches are now studied by quantum chemistry software able to take into account the surface electronic structure, the interconnects and the local quantum structure of the computing circuit. Let us take the simple example of a logic gate.

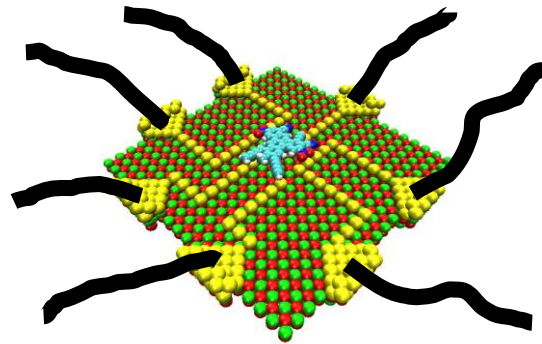


Figure 1: A possible surface implantation of a molecule logic gate. The presented molecule half adder was designed following a Quantum Hamiltonian Computer approach [9]. The interconnection architecture is constructed using metallic atomic wires. The logic inputs are located directly on the molecular board, supposing 2 switchable chemical group current driven inputs.

There are 3 ways of designing a logic gate at the atomic scale:

- (1) The use of surface missing atom to fabricate an atomic scale circuit mimicking the topology of a macroscopic electronic circuit. Those surfaces are generally passivated semi-conductor surface with a relatively large gap. Atoms are extracted one at a time to create a specific surface electronic structure in the electronic surface gap. This new electronic structure will form the surface atomic circuit [6]. The STM vertical manipulation of the single surface atoms can be automated and proceed in parallel.
- (2) The full molecule, instead of the surface can be the electronic circuit. In this case, it is the π system of such an extended molecule which will define the circuit and the σ skeleton will ensure the full chemical stability of the molecular architecture [7]. Such a molecule will have to be directly chemisorbed to the required number of nanometallic pads or in a very dedicated approach to surface atomic wires more able to interact with specific part of the π molecular orbitals.
- (3) Molecular orbitals (from a large molecule or defined from a specific surface atomic circuit) can be manipulated by chemically bonding on the π conjugated computing board specific chemical groups able to shift the corresponding molecular states [8].

Switchable lateral group can be very active playing donor or acceptor group to modify very locally the nodes distribution of a give molecular orbital. Such an effect can be used to design single molecule logic gate (See Figure 1) without forcing the molecule to have the topology of an electrical circuit [9].

Solutions (1) and (2) have been proposed long ago but are not very compatible with the quantum level where those atom circuits or molecule logic gate are supposed to work. For solution (3), a quantum Hamiltonian design of AND, NOR and even halfas adder logic gates have been designed followed by proposal of chemical structure functioning on the manipulation of molecular orbitals [9]. Extreme care has to be taken here for the optimisation of the chemical structure of those molecule-gates taking into account their future adsorption for example on a passivated semi-conductor surface presented above [10]. In particular, the optimisation of the electronic contact between the surface atomic wires and the molecule will be obtained by selecting with care the chemical composition of the end group of the molecule [11] for running current through the gates with the objective to reaching peak values in the range of 10 to 100 nA.

All those architectures provide an indication of the richness of possible quantum behaviours able to be mastered to design a molecule like logic gate up to the complexity of a digital 2 by 2 full adder. At the Working Group meeting, the question was: to what extend the complexity of such a logic function embedded in a single molecule or in a small amount of dangling bond created on purpose on a surface can be increased up for example to a $N \times N$ full adder. There is no theoretical answer yet to this question. But the interesting fact is that a careful quantum design will certainly shift up the elementary physical unit of a logic circuit from the transistor level to a logic function level. For example, no gain at the gate level is required in the Hamiltonian logic gate approach. This will simplify a lot the interconnections and the wiring. But at the same time, cascading the building block at the logic gate level will certainly require some power gain. This will consequently increase the complexity of the interconnection procedure in between the logic gate units. The quantum designer will have to define the most interesting building block complexity (of course beyond the transistor) to find an optimum between the computing power on board of a molecule and the required interconnects. There is no solution yet for designing dynamic memory cell at the atomic scale.

3. N-Interconnects

Creating ultra precise interconnects on a single molecule has often been a bottleneck for molecular electronics [4,12]. But there are now two well-known avenues to realize a full interconnection scheme depending if the supporting surface is a small or large electronic band gap semi-conductor. The first tentative characterization of a single molecule switch was reported already in 1988 using an HV-STM machine [13]. Since then, a lot of progresses have been accomplished using the end atom of the STM tip apex as a pointer to contact one atom [14], one molecule [3,15] and to practice single atom or molecule manipulation [16,17]. The first measurement of the conductance of a single molecule was realized in 1995 with a single C60 molecule using an UHV-STM machine [3].

In parallel, nanolithography has been developed to quit the vertical STM interconnection configuration for a fully planar configuration. In year 2001, what is considered now as the nanolithography limit was reached. The world record of an inter-electrode distance of 2 nm was obtained between 2 metallic nano-electrodes fabricated on a silicon oxide [18]. But this nanotechnology technique was progressively

abandoned because (1) it is limited to a maximum of 2 to 3 electrodes [19] and (2) the use of resists and chemical in the process to define the nano-fabricated pattern is not clean enough with respect to the size of a single molecule and the order of the surface atoms. As a variant, break-junctions are also now used because of the very unique precision in the tuning of inter-electrode distance [12,20]. But it was analysed by the participants of the meeting that this fantastic technique will progressively be abandoned because there is no way to determine the number of molecule in the junction, because the conformation of the molecules located in this junction is unknown and because it is difficult to foresee a multinano-electrodes version of the break junction technique.

In 1999, a new planar nano fabrication technique, the nanostencil was introduced in an attempt to solve the surface cleanness problem [21]. Then, nanostencil was proposed as a new way to interconnect electrically a single molecule. Nanostencil has a great advantage over nanolithography because it is supposed to preserve the atomic cleanness of the surface supporting the planar interconnection electrodes. By varying systematically all the parameter of the nanostencil technique, including the testing of a large variety of surfaces from SiO₂ to NaCl or mica, it was demonstrated that on good surfaces, this technique reaches its limits in the 20 nm range with no possibility to master the atomic structure at the end of the so fabricated nano-pads [22].

Facing this interconnection problem, lab scale experiments were performed: the fabrication of a pseudo-planar interconnection on metal surface taking benefit from native mono atomic step edge and designing specific Lander molecules with legs to level up the molecular wire as compared to the mono atomic step edge [11,15,23]. Those low temperature UHV STM experiments unambiguously demonstrated the need for an ultra clean atomic scale mastered interaction between for example the molecular wire end and the conducting contact entity [24].

It seems that all the standard planar interconnection strategies explored since the end of the 80's like e-beam nano lithography, nano-imprint and Nanostencil will soon be abandoned for mono-molecular electronics. A new surface science approach respecting the exact atomic order of the surface with an interconnection precision better than 0.1 nm between the atomic wire (or the molecular wire) and the atomic scale pads will have to be developed. This challenge triggers a new approach for interconnects, a formal generalization of the technique developed at Bell labs in the 50's to interconnect a bar of a Germanium semiconductor material (See Figure 2). At that time, 4 probes measurement were practiced using 4 metallic tips approaching the semiconductor bar under an optical microscope. The bar was manipulated by micro metric screws together with the tips and stabilized by metallic springs [25].

In our days, atomic scale interconnection machines are starting to be built in a few labs around the world. There are basically low temperature (LT) UHV machines made of 3 LT UHV interconnect separated chambers, one for the atomic scale preparation of the supporting surface, one for single atom or molecule manipulation and one for the atomic scale to mesocale or more interconnection procedure. Depending on the surface, the navigation on the surface is still using an optical microscope completed by a NC-AFM for a large surface electronic gap (See Figure 2). For small gap passivated semiconductor surface, the navigation is ensured by an UHV-SEM with a resolution generally around a few nanometers (See Figure 2). For the nano interconnection step, well faceted and ultra flat metallic nano-island are now in use. Those nano-interconnect pads are positioned at will with a 0.1 nm precision on the surface using the manipulation ability of the STM [26]. For the nano to meso and more interconnection stage, one technique for small gap semiconductor is to use multiple

conducting STM tips in a top or back surface approach. For large gap surfaces, the nanostencil technique can still be used at its 20 nm in width limit and in its dynamic form [27].

Those interconnection machines are so new that it is not clear how one can build up a roadmap to anticipate how many contacts it will be possible to achieve. In the case of multiple STM tips positioned under the SEM, 4 is the actual limit for stability of the interconnects even if system up to 12 STM tips have been proposed (See Figure 2).

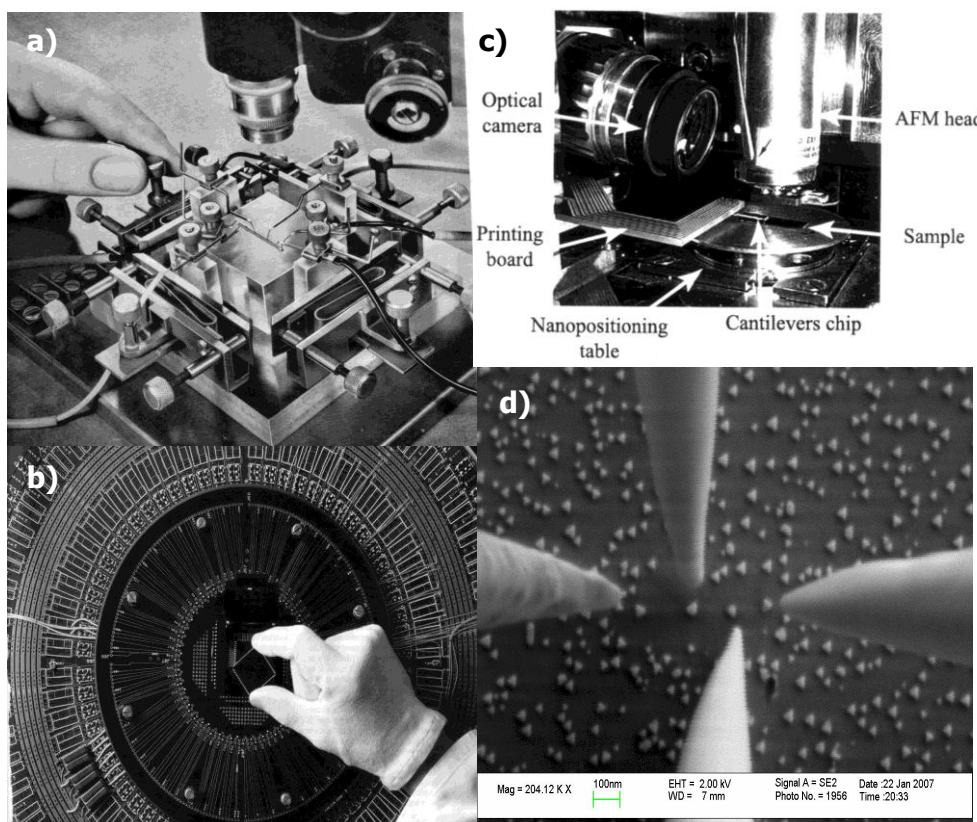


Figure 2: History of planar multi-electrodes interconnects. (a) 1950's Bell Labs system equipped with an optical microscope and 4 electrodes for germanium interconnects [25]. (b) the 20th century multi-probes chip interconnects technology (courtesy of IBM). (c) A new generation of interconnection system involving an optical microscope plus an AFM microscope using 10 metallic cantilever positioned under the AFM head [28]. (d) A more recent version where the optical microscope had been substituted by an UHV scanning electron microscope and the metallic cantilevers substituted by nanoscale apex STM tips [26] (courtesy of the A*STAR VIP Atom tech project, Singapore).

For the optical microscope-NC-AFM case, 10 interconnects seems to be a good number [28]. There is here clearly a need to roadmap the computing power capacity increase embedded in a single molecule or with a surface atomic circuit and the number of possible interconnects converging towards this ultra small computing unit [19]. For example, it may happen that a well designed molecule offers too much computing power locally in regards with the maximum number of interconnects that one can physically be achieved in parallel on a surface. Then, a multiplexing like approach may be more appropriate, asking for more bandwidth and pushing the technology towards optical interconnects. Thus, efforts should be made in the future to extend experiments which aim to combine optics and local probe microscopy in an ultra clean environment with a prospect of a fully planar technology.

4. Atom and Molecule Surface science issues

The stabilization of an atomic scale computing machinery on a surface (be it self stabilized by its chemical structure or by the surface itself) requires a gigantic effort in exploring the properties of a large molecule of a surface at the atomic scale. During the 3 years of Pico-Inside, a lot of questions were discussed in this context starting from the choice of the surface. Of course, those discussions were targeting lab scale logic gate handling and interconnects. For a fully packaged molecule logic gate, a more realistic choice of surfaces is actually out of the range of what can be discussed (see the corresponding section below).

Depending of the atomic scale interconnection machine to be used, a first delicate problem is the choice of the supporting surface. A list of criteria were discussed in Pico-Inside: the electronic surface gap, the stability of the atomic surface structure, the stability of metallic nanoisland on the surface. For example, we know 2 extreme cases of passivated semi-conductor surface: SiH(100) and MoS₂. SiH(100) has a surface gap around 2.1 eV. The surface H atoms can be vertically STM manipulated one at a time to create p dangling bond like surface atomic wires or Hamiltonian computing structures [5,6]. But depending on the bulk doping, those H surface atoms are not so stable with temperature which precludes a thermal growth process to shape the contacting metallic nano-island. The lamellar MoS₂ compound has a self passivated semi conducting surface with a surface gap around 1 eV. The surface S atoms are extremely difficult to vertically STM manipulate [29]. But if manipulated, they also offer the possibility to create surface atomic wires with a band structure much more complicated than the SiH(100) [30]. The surface MoS₂ surface is extremely stable up to 1200 °C [31] and metallic nano-pads can easily be shaped and manipulated to construct any multi-electrode interconnections pattern with an atomic scale precision [26]. But the low surface gap of this material will certainly preclude its direct use as a supporting interconnection surface. A better exploration of the surface properties of diverse semi-conductor surfaces (See for example Figure 3) and their possible passivation is here urgently needed.

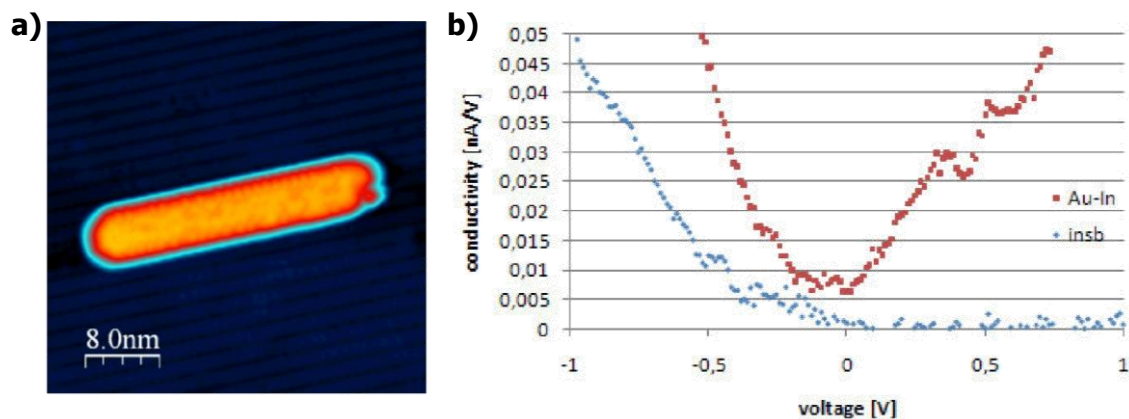


Figure 3: Exploring the surface science of interconnects: fabrication of Au nanowires on the InSb(001) surface in the UHV to be interconnected on a Fig. 2D UHV interconnection machine. (a) High resolution STM image of Au alloy nanowire formed on InSb(001) surface by a good selection of the surface annealing temperature. Bias voltage: -0.5V, tunnelling current: 25pA. (b) STS conductance measured using an STM tip as a function of bias voltage on an Au alloy nanowire (red dots) and directly on the InSb substrate (blue dots) (Courtesy of the Jagiellonian University, Krakow).

Large electronic gap surface are even less explored than their semi-conductor counterparts. The nice property of those surfaces is the fact that leakage surface current

between 2 metallic nano-pads adsorbed on the surface will be very low, well below the fA range, an advantage as compared with the above mentioned semi-conductor surface. The drawback is that there is no easy solution to fabricate or stabilize atomic wire on those surfaces. During the Working Group meeting, two solutions were discussed to bypass this problem: the use of molecular mold to stabilize metallic atomic wires or the use of long molecular wires between the metallic nano-pads and the central computing units. This second solution may be a good way to boost the research on long molecular wires characterized by an extremely small tunneling inverse decay rate [32].

Graphene, the new comer was not on the Pico-Inside agenda and was discussed in Toulouse as a mean to pass directly from the mesoscopic to the atomic scale with a "perfect" chemical like continuity between the 2 scales. This will be another choice of surface self supporting the interconnection and the computing unit. The open question is whether or not progresses in the fabrication techniques will allow an atom by atom fabrication technique respecting the absolute atomic scale precision required for such a circuit [33].

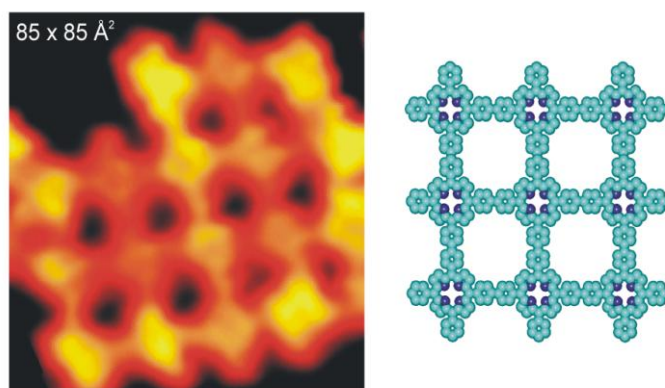


Figure 4: *Playing with single molecules on a surface. Instead of sublimating a large molecule on a surface, it may be better to bring first the monomers and to make them self reacting with each others by controlling the spontaneous 2D diffusion. STM image (left) of a molecular network on a Au(111) surface with the corresponding scheme (right). The network is grown from single porphyrin (TPP) molecules monomers ("on-surface-synthesis") by forming covalent bonds between the individual building blocks [35].*

It is also not clear how far can we go by playing with a single and large molecule adsorbed on a surface be it the one of a semi-conductor or of a bulk insulating materials. There is the difficult challenge of sublimating of a large molecular weight molecule on a surface in an ultra clean manner respecting the integrity of the molecule [34]. May be better to perform the chemistry in situ sublimating only the monomers and playing with them after to construct or assemble the final large molecule (See Figure 4 and [35]). It remains to be explored if such an approach can be performed for example at the surface of a semi-conductor.

Discussions in Toulouse about molecular surface science indicate how far we are from a very good understanding of molecular processes and behaviors of a large molecule on a surface at the atomic scale. There is here a wide range of understanding and know how which need to be acquired before creating a full atomic scale technology for molecular computing.

5. Packaging

In Pico-Inside, packaging was not on the official agenda. Off site discussions about packaging indicate that we are far from being ready to study those questions simply because even the lab scale interconnection machines are just about to be assembled. Packaging is always associated with the number of interconnects which have to be stabilized by the encapsulation technology selected for the circuit [19]. There is not yet

a clear path on how to create a packaging technology for surface mono-molecular electronics. A specific mono-molecular NanoICT seminar may be dedicated in the future to this very strategic problem. But it is so advance and so strategic [36] that it may turn out to be very difficult to trigger an open discussion about packaging.

6. Conclusion

The first mono-molecular nanoICT Working Group seminar was the occasion to cluster in a very Cartesian way all the 4 major issues under grounded in the monomolecular approach of molecular electronics which were worked out during the 42 month of the Pico-Inside project. In all areas of technology, the construction of a complex system by assembling elementary pieces or devices leads to a Moore's law like trend when analyzing the complexity growth of the system per year, a trend which appears threatened in the near future for microelectronics. The mono-molecular approach of molecular electronics with its compulsory atomic scale technology offers way to push past possible limitations in miniaturization, and to gain further increases in computing power by orders of magnitude by relying of a full development of an atom or molecule based technology for both electronics and machines. To reach this stage, each of the 4 issues illustreated in this concluding paper will require a specific discussion and more than that a specific research and technological development program.

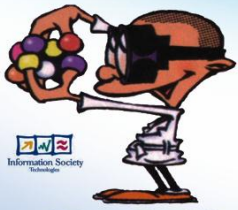
Acknowledgements

The authors would like to acknowledge financial contribution from the European Commission through the Coordination Action NanoICT (ICT-CSA-2007-216165) and through the IST Pico-Inside integrated project.

7. References

- [1] C. Joachim, *Nanotechnology*, 13, R1 (2002)
- [2] A. Aviram and M. Ratner; *Chem. Phys. Lett.*, 29, 277 (1974)
- [3] C. Joachim, J. Gimzewski, R.R. Schlittler and C. Chavy; *Phys. Rev. Lett.*, 74, 2102 (1995)
- [4] C. Joachim, J. K. Gimzewski and A. Aviram, *Nature*, 408, 541 (2000)
- [5] M. B. Haider, J.L.Pitters, G.A. Dilabio, L. Livadaru, J. Y. Mutus and R.A. Wolkow, *Phys. Rev. Lett.*, 102, 046805 (2009)
- [6] A. J. Mayne, D. Reidel, G. Comtet and G. Dujardin, *Prog. Surf. Sci.*, 81, 1 (2006)
- [7] S. Ami, M. Hliwa and C. Joachim, *Chem. Phys. Lett.*, 367, 662 (2003)
- [8] C. Venegas, T. Zambelli, S. Gauthier, A. Gourdon, C. Barthes, S. Stojkovic and C. Joachim, *Chem. Phys. Lett.* 450, 107 (2007). See also: J. Repp, G. Meyer, S. Stojkovic, A. Gourdon and C. Joachim, *Phys. Rev. Lett.*, 94, 026803 (2005)
- [9] I. Duchemin and C. Joachim; *Chem. Phys. Lett.*, 406, 167 (2005)
- [10] P. G. Plva, G. A. Dilabio, J. L. Pitters, J. Zikovsky, M. Rezeq, S. Dogel, W.A.Hofer and B. Wolkow, *Nature*, 435, 658 (2005); M. Lastapis, M. Martin, D. Riedel, L. Hellner, G. Comtet and G. Dujardin *Science*, 308, 1000 (2005)
- [11] L. Grill, F. Moresco, K.H. Rieder, S. Stojkovic, A. Gourdon and C. Joachim, *NanoLett.*, 5, 859 (2005)
- [12] C. Kerguelis, J.P. Bourgoïn, J.P. Pallacin, D. Esteve, C. Urbina, M. Magoga and C. Joachim, *Phys. Rev. B*, 59, 12505 (1999)
- [13] A. Aviram, C. Joachim and M. Pomerantz, *Chem. Phys. Lett.* 146, 490 (1988)
- [14] A. Yazdani, D.M. Eigler and N.D. Lang, *Science*, 272, 1921 (1996)
- [15] V. Langlais, R.R. Schlittler, H. Tang, A. Gourdon, C. Joachim et J.K. Gimzewski *Phys. Rev. Lett.*, 83,2809 (1999)

- [16] D. Eigler and E. Schweizer, *Nature*, 344, 524 (1990)
- [17] T.A. Jung, R.R. Schlittler, J.K. Gimzewski, H. Tang, et C. Joachim *Science*, 271, 181 (1996)
- [18] MSM Saifullah, T. Ondarcuhu, D.F. Koltsov, C. Joachim and M. Welland *Nanotechnology*, 13, 659 (2002)
- [19] O. Cacciolati, C. Joachim, J.P. Martinez and F. Carsenac *Int. Jour. Nanoscience*, 3, 233 (2004)
- [20] S.M. Wu, M.T. Gonzales, R. Huber, S. Grunder, M. Mayor, C. Schonenberger, and M. Calame, *Nature Nano.*, 3, 569 (2008)
- [21] R. Luthi, R.R. Schlittler, R. Berger, P. Vettiger, M. E. Welland and J.K. Gimzewski, *Appl. Phys. Lett.*, 75, 1314 (1999)
- [22] Thet Naing Tun, Ma Han Thu Lwin, Hui Hui Kim, N. Chandrasekhar and C. Joachim, *Nanotechnology*, 18, 335301 (2007)
- [23] F. Moreasco, L. Gross, M. Alemani, K.H. Rieder, H. Tang, A. Research Gourdon and C. Joachim, *Phys. Rev. Lett.*, 91, 036601 (2003)
- [24] S. Stojkovic, C. Joachim, L. Grill and F. Moresco *Chem. Phys. Lett.*, 408, 134 (2005)
- [25] W. Shockley, *Electrons and holes in semiconductors*, (D. Van Nostrand, Princeton, 1950)
- [26] JianShu Yang, Deng Jie, N Chandrasekhar and C. Joachim, *Jour. Vac. Sci. Tech.B*, 25, 1694 (2007)
- [27] H.M. Guo, D. Martrou, T. Zambelli, J. Polesel-Marie, A. Piednoir, E. Dujardin, S. Gauthier, MAF van der Bogeert, L.M. Doeswijk and J. Brugger, *Appl. Phys. Lett.*, 90, 093113 (2007)
- [28] T. Ondarcuhu, L. Nicu, S. Cholet, C. Bergaud, S. Gerdes and C. Joachim *Review of Scientific Instruments*, 71, 2087 (2000)
- [29] S. Hosoki, S. Hosoka and T. Hasegawa, *Appl. Surf. Sci.*, 60/61, 643 (1992)
- [30] K. S. Yong, D.M. Oltavaro, I. Duchemin, M. Saeys and C. Joachim *Phys. Rev. B*, 77, 205429 (2008)
- [31] R. K. Tiwari, J. Yang, M. Saeys and C. Joachim *Surf. Sci.*, 602, 2628 (2008)
- [32] L. Lafferentz, F. Ample, H. Yu, S. Hecht, C. Joachim and L. Grill, *Science*, 323, 1193 (2009)
- [33] J.F. Dayen, A. Mahmoud, D.S. Golubov, I. Roch-Jeune, P. Salles and E. Dujardin, *Small*, 4, 716 (2008)
- [34] T. Zambelli, Y. Boutayeb, F. Gayral, J. Lagoute, N.K. Girdhar, A. Gourdon, S. Gauthier, M.T. Blanco, J.C. Chambon and J.P. Sauvage, *Int. Journ. Nanoscience*, 3, 230 (2004)
- [35] L. Grill, M. Dyer, L. Lafferentz, M. Persson, M.V. Peters and S. Hecht, *Nature Nano*, 2, 687 (2007)
- [36] Thet Naing Tun, C. Joachim, and N. Chandrasekhar IMRE Patent 200630 filled in 2009



Pico-Inside



<http://www.picoinside.org>



Edited by

PHANTOMS
foundation

PCM - Pabellón C - 1ª Planta
Ctra. Colmenar Viejo Km. 15
Campus de Cantoblanco
Universidad Autónoma de Madrid
28049 Madrid, Spain
Fax: +34 91 4973471
WEB: <http://www.phantomsnet.net>

FP6-IST-FET ● Pico-Inside Integrated Project ● Contract nº 015847

